EFFECT OF BORON ADDITIONS ON MICROSTRUCTURE & MECHANICAL PROPERTIES OF TITANIUM ALLOYS PRODUCED BY THE ARMSTRONG PROCESS

DISSERTATION

Presented in Partial Fulfillment of the Requirements for

the Degree Doctor of Philosophy in the Graduate

School of The Ohio State University

By

Jonathan P. Blank, M.S.

* * * * *

The Ohio State University
2008

Dissertation Committee:

Professor James C. Williams, Adviser

Professor Glenn S. Daehn

Professor Hamish L. Fraser

Professor Dan Leavell

Approved by

Adviser
Graduate Program in
Materials Science and Engineering

ABSTRACT

The beneficial influence of boron additions on processing, microstructure, physical and mechanical properties of various titanium alloys has been recognized since 1950's. However, boron additions to titanium alloys to obtain specific microstructures and mechanical properties for several niche applications, including automotive and aerospace, have been actively studied during the past 25 years. The addition of boron concentrations greater than 0.05 wt.% to titanium alloys creates a dispersion of TiB. The presence of TiB enhances the tensile and fatigue strengths as well as the wear resistance as compared to the original titanium alloy. Although these improvements in mechanical properties are attractive, there are still two major obstacles in using these alloys: (1) relationship of microstructure and mechanical properties in Ti-B alloys needs further investigation to optimize the alloys for specific commercial applications; and (2) cost to benefit ratio of producing these alloys is high for a given application(s).

The Armstrong process is a novel process that can produce commercially pure (CP) titanium and titanium alloy powder directly from $TiCl_4$ (and other metal halides or as required, to obtain the desired alloy composition). The Armstrong process uses sodium as a reducing agent, with similar reactions as the Hunter process using sodium as a reducing agent and Kroll process using magnesium as a reducing agent. The Armstrong process forms CP-Ti and titanium alloyed powder, which can be directly consolidated or

melted into the final product. In comparing the downstream processing steps required by the Kroll and Hunter processes with direct consolidation of Armstrong powder, several processing features or steps are eliminated: (1) restriction of batch processing of material, (2) blending of titanium sponge and master alloy material to create titanium alloys, (3) crushing of the sponge product, (4) melting, and (5) several handling steps.

The main objective of this research was to characterize structure and properties of CP-Ti and Ti-B alloys produced by the Armstrong process. Particular emphasis has been placed on improved understanding of the strengthening mechanisms associated with the addition of boron to titanium alloys.

The microstructure and mechanical properties were examined for commercially pure (CP) titanium, Ti-0.8wt.%B and Ti-0.9wt.%B alloy powders produced using the Armstrong process. In order to understand the effects of the boron additions on a range of properties, tensile, notched fatigue, fatigue crack growth and compression testing was performed on the consolidated and heat-treated material made from Armstrong powder. These results were interpreted in the light of microstructural and fractographic characterization also performed during the study.

Dedicated to Heather, Roger and Pat for all their support.

ACKNOWLEDGMENTS

I wish to thank my adviser, Dr. James Williams for his advice on my research. Dr. Williams has provided encouragement, and knowledge on fundamental materials science and titanium metallurgy principles. He has shared many of his experiences and expertise in titanium metallurgy including processing, microstructure development, and properties.

I also would like to acknowledge my co-workers at General Electric (GE) Aviation, specifically the Materials Process Engineering Department (MPED) for their technical support throughout the years. I specifically would like to thank Dr. Robert Schafrik, Dr. David Chang, Dr. Eric Ott, Dr. Kenneth Bain, Mr. Daniel Kruger and Mr. Peter Wayte for their continued support and sharing their knowledge of titanium and powder processing, and microstructure-mechanical property relationships. In addition, I would like to thank Dr. Andrew Woodfield for reviewing my document, Mr. Robert Oligee for discussions on chemical analysis techniques, Mr. William Davis for sharing his knowledge on metallographic evaluation techniques, Mr. Thomas Daniels for discussions with electron microscopy techniques, and Mr. Jeffery Myers for assistance in completion of the compression testing. I am very grateful to have had the chance to work with all the engineers and technicians in the MPED Lab at GE Aviation as without their support, completing this thesis would not have been possible.

I am grateful to Dr. Peter Collins and Dr. Hamish L. Fraser for their discussions and assistance in use of the transmission electron microscopy (TEM) facilities in the Materials Science and Engineering Department at The Ohio State University. I am indebted to Dr. Peter Collins for his support and sharing of his knowledge of titanium-boron alloys and characterization using the TEM.

Financial support from GE Aviation, specifically the Engineering Division and MPED are acknowledged.

VITA

September 7, 1978…….Born in Buffalo, New York

June 2001……...B.S. Materials Science and Engineering
The Ohio State University

August 2000 - June 2002…..……..Graduate Research Associate
The Ohio State University

June 2002…..……..M.S. Materials Science and Engineering
The Ohio State University

June 2002 – Present…….……..Materials Science Engineer
GE Aviation

PUBLICATIONS

Research Publications

1. Gigliotti, J.R., Hardwicke, C.U., Jiang, L., Short, J.W., Lipkin, D.M., Blank, J.P., Anand, K. **Erosion and Wear Resistant Protective Structures For Turbine Engine Components.** *U.S. Patent Office.* Patent No. 2005/0207890 A1. 2005.

2. Wortman D.J., Blank, J.P., Keith, S.R. **Thermal Barrier Coating System and Process Therefor.** *U.S. Patent Office.* Patent No. 2007/0172678 A1. 2007.

FIELD OF STUDY

Major Field: Materials Science and Engineering

Minor Field: Metallurgical Engineering

TABLE OF CONTENTS

LIST OF TABLES

LIST OF FIGURES

CHAPTER 1

LITERATURE REVIEW

1.1 Introduction

In the late 1970s, several groups experimented with the addition of a variety of non-traditional alloying elements to conventional titanium alloys. From these studies it was observed that the addition of boron improved many properties, including strength, of conventional titanium alloys. Unfortunately, at that time, the cost versus benefit analysis was unfavorable, thus the aerospace and automotive industries were not interested in pursuing this process. Recent developments in aerospace and automotive markets have created the need for materials that exceed the capability of current materials, generating a demand for materials that can meet these higher performance requirements. For example, current titanium alloys used in aero-engine applications are approaching their strength and temperature limits, which restricts rotor speeds, and maximum use temperatures. These limits restrict the weight and efficiency of the engine. In addition, the automotive industry would greatly benefit from a weight reduction of their automobiles by selectively using titanium instead of steel, but have been limited by the cost of titanium as compared to steel and aluminum. The desire to improve the properties of

titanium alloys to keep up with rapidly expanding product requirements has led to renewed support of research into the influence of boron additions to titanium alloys using various processing methods. The addition of boron to titanium alloys has been reported to improve the strength, stiffness, wear resistance and microstructural stability over the comparable conventional titanium alloy.[1-4] However, a better understanding of the constitution and microstructure evolution, strengthening mechanisms and reproducible and cost effective processing methods are necessary if these alloys will ever be extensively used. The purpose of this review is to provide a comprehensive summary of the relevant published literature and to assess the current understanding of: (1) conventional titanium alloys including metallurgy, phase transformations, and strengthening mechanisms; and (2) conventional titanium alloys containing boron including metallurgy, phase transformations, processing methods, and mechanical behavior.

1.2 Titanium Metallurgy

To investigate the effect of boron additions on the properties of titanium alloys, it is necessary to first examine conventional titanium metallurgy. In the following sections general titanium physical metallurgy, phase transformations, deformation modes and strengthening mechanisms will be reviewed.

1.2.1 Physical Metallurgy of Titanium Alloys

Pure titanium has a density of 4.57 g/cc and exhibits an allotropic phase transformation at 1620^{o}F (882^{o}C)[5]. Between the melting temperature 3035^{o}F (1668^{o}C)

and 1620°F, titanium forms a stable body-centered cubic (BCC) crystal structure (β phase), while the hexagonal close packed (HCP) crystal structure (α phase) is stable below 1620°F. The α/β transformation temperature is known as the β transus and is strongly influenced by the purity of the alloy, and therefore the transformation temperature is a function of the type and concentration of substitutional and interstitial alloying elements present. The substitutional element Al and interstitial elements O, N, and C raise the transformation temperature and are considered α phase stabilizers. Solute additions of Sn and Zr are considered neutral because they have little to no effect on the transformation temperature. Hydrogen and many substitutional elements including Mo, V, Nb, Cr, Fe, and Si are considered β phase stabilizers because these elements lower the transition temperature.

The transformation from the β phase to the α phase in titanium alloys can occur either by diffusion controlled nucleation and growth, or martensitically by nucleation and shear depending on the alloy composition and cooling rate. The crystallographic orientation relationship between the β phase and α phase (BCC ↔ HCP transformation) for both types of transformations was first studied in the 'sister' element Zr by Burgers[6] and hence has been named the Burgers relationship:

$$\{110\}_{\beta}||\{0002\}_{\alpha}$$

$$<1\bar{1}1>_{\beta}||<11\bar{2}0>_{\alpha} \qquad [1.1]$$

Newkirk and Geisler[7] later confirmed that this relationship holds for titanium alloys for both nucleation and growth, and martensitic transformations.

1.2.2 Titanium Alloy Classification

Titanium alloys are typically classified in three different categories according to their room temperature constitution and the pseudo-binary section through a β isomorphous phase diagram shown in Figure 1.1. The figure shows four distinct alloy categories: α, α+β, metastable β, and stable β. Since α and α+β alloys are of interest for this discussion, no distinction between metastable β and stable β alloys will be made and therefore they will be referred to hereafter as β alloys. A summary of the most important commercial alloys in each of these three categories along with nominal composition, nominal β transus temperature, tensile and fatigue results are shown in Table 1.1.[5,8,9]

The α alloys consist of commercially pure (CP) titanium as well as alloys that retain up to 5 vol.% β phase upon cooling to room temperature. In general, α alloys are lower in strength, more ductile, and more corrosion resistant than α+β and β alloys. The strengthening of these alloys is accomplished by controlling the composition, grain size and texture of the α phase. Strengthening through composition control occurs by causing planar slip in the α phase with the limited addition of Al[10-12] (above ~5 wt.%) or O[10,13] and solid solution strengthening by Al, Sn and Zr[10,14]. The limited amount of β phase (< 5 vol.%) and thermo-mechanical processing is used to control the recrystallized α grain size and the texture of the alloy.[15] It should be noted that α alloys have a lack of response to heat treatment, therefore grain size and texture of the alloys is set by thermo-mechanical processing applied to the alloy. Strengthening mechanisms of these alloys will be discussed in more depth in the strengthening mechanisms section. In summary, these alloys are generally

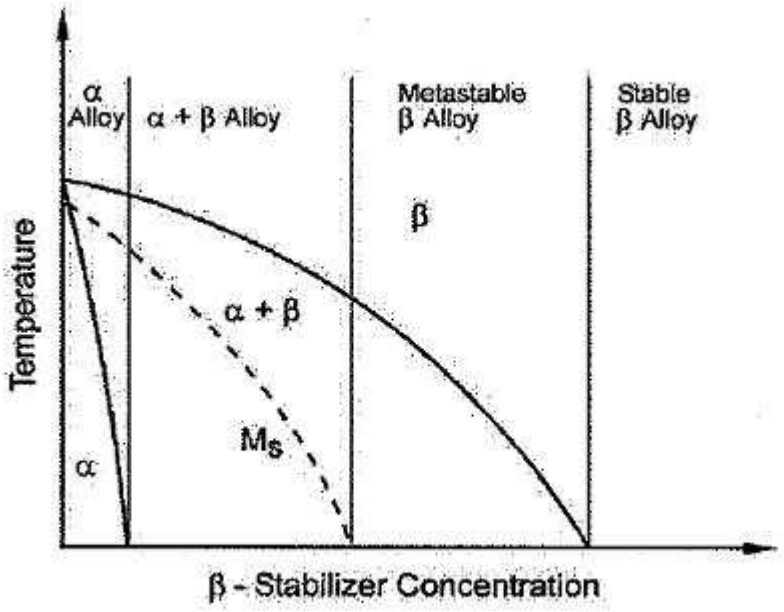

Figure 1.1. Schematic of pseudobinary section through a β isomorphous phase diagram. (cf. ref. 8)

Common Name	Alloy Composition (wt%)	Beta Transus (^{o}F)	UTS (ksi)	0.2% Yield Strength (ksi)	Elongation (%)	Fatigue Strength (10^{7} cycles, R=0.1, smooth bar, ksi)
Grade 1	CP-Ti (0.2Fe, 0.18O)	1635	35	25	24	-
Grade 2	CP-Ti (0.3Fe, 0.25O)	1680	50	40	20	-
Grade 3	CP-Ti (0.3Fe, 0.35O)	1690	65	55	18	-
Grade 4	CP-Ti (0.5Fe, 0.40O)	1740	80	70	15	-
Grade 7	Ti-0.2Pd	1680	50	40	22	-
Ti-5-2.5	Ti-5Al-2.5Sn	1905	120	104	10	80
Ti-811	Ti-8Al-1V-1Mo	1905	120-145	110-135	8-10	80-87
Ti-6242	Ti-6Al-2Sn-4Zr-2Mo-0.1Si	1825	130-172	120-158	7-16	85-91
Ti-6-4	Ti-6Al-4V	1825	120-170	110-160	10-15	71-90
Ti-6246	Ti-6Al-2Sn-4Zr-6Mo	1725	158-184	148-170	6.5-16	90-109
Ti-17	Ti-5Al-2Sn-2Zr-4Mo-4Cr	1635	165-175	155-165	8-15	105-110
Beta-CEZ	Ti-5Al-2Sn-2Cr-4Mo-4Zr-1Fe	1635	177-197	165-172	5-10	123-132
Ti-10-2-3	Ti-10V-2Fe-3Al	1470	160-188	145-160	4-6	120-127
Beta21S	Ti-15Mo-2.7Nb-3Al-0.2Si	1490	180-202	169-192	7.5-10	-
Beta C	Ti-3Al-8V-6Cr-4Mo-4Zr	1345	125-180	120-170	6-10	87-90

Table 1.1. Composition, transformation temperature, room temperature tensile and room temperature fatigue properties of commercial titanium alloys.[5,8,9]

used in applications where factors such as corrosion resistance and weldability are more important than high strength. Typical applications include chemical and petrochemical processing equipment[16] such as heat exchangers and other piping applications[17], and pressure vessels for space craft[8].

The α+β alloys contain one or more α phase stabilizers and one or more β stabilizers. In general, α+β alloys have the most desirable balance of properties: higher strength and comparable ductility to α alloys; and lower strength and significantly better ductility than β alloys. Strengthening is accomplished in these alloys by controlling the composition, microstructural feature size and morphology, and texture of the α phase. Strengthening of the α phase through composition control is the same as with α alloys such that the planar slip in the α phase is caused through the limited additions of Al[10-12] (above ~5 wt.%) or O[10,13] and solid solution strengthening of the α phase by addition of Al, Sn and Zr[10,14]. Thermo-mechanical processing and heat treatment (solution and age) of the alloys are used to control the microstructural feature size and shape, and texture. Strengthening mechanisms of these alloys also will be discussed in more depth in the strengthening mechanisms section. In summary, these alloys are generally used in applications where a good balance of properties is required. Typical applications include aerospace[18], power generation[19], biomedical[20-24], sporting equipment[25-28], and automobiles[29].

The β alloys are sufficiently rich in β stabilizers such that the β phase is retained upon cooling to room temperature. In general, β alloys are higher in strength and less ductile than α and α+β alloys. Strengthening is accomplished in these alloys by

controlling the complex interaction of composition and heat treatment response. Strengthening through composition control is accomplished through solid solution strengthening of the β phase by Fe, Cr, and V[8,30]. Thermo-mechanical processing and heat treatment of the alloys are used to control the microstructural unit size and morphology including the precipitation of α platelets in the β phase upon heat treatment. The strengthening mechanisms are similar between α+β and β alloys except length scale is different between alloys due to the limited amount of α phase that is formed. This is the extent of the discussion of the strengthening mechanisms of these alloys as the focus of this paper is on α and α+β alloys and strengthening of these alloys is primarily due to the α phase (as the primary phase in these alloys is the α phase). In summary, β alloys are generally used in applications where high strengths are desired and good ductility is not as much of a concern. Typical applications for β alloys with higher strength and lower modulus include aerospace[31-33], biomedical[34-36], and automobiles[37,38].

1.2.3 Deformation Modes

Deformation of titanium alloys occurs by conventional dislocation motion in both the α and β phases. Although possible, twinning is not commonly seen in most titanium alloys as it is suppressed as the solute content, particularly α stabilizers, is increased and the phase dimensions are reduced. In commercially pure (CP) titanium alloys and some solute lean α titanium alloys, twinning occurs in conjunction with conventional slip and is responsible for the ductile behavior of these alloys particularly at low temperatures.

1.2.3.1 Commonly Observed Slip Modes

The slip systems and corresponding Burgers vector type for α titanium is shown in the HCP unit cell in Figure 1.2. The combination of $<11\bar{2}0>$ type slip direction ($\vec{a}$ type Burgers vector) on {0002}, $\{10\bar{1}0\}$ and $\{10\bar{1}1\}$ planes total 12 slip systems,[39,40] however, only eight of these slip systems are independent. The number of slip systems can be further reduced to four independent slip systems because the changes of shape that can be produced by combining slip systems on the {0002} and $\{10\bar{1}0\}$ planes are exactly the same as those of the slip systems on the $\{10\bar{1}1\}$ plane. Thus, for the Von Mises criterion of at least 5 independent slip systems for homogeneous plastic deformation of polycrystals to be satisfied, the operation of a non $\vec{a}$ type slip system (either $\vec{c}$ or $\vec{c} + \vec{a}$ type) must be activated. Extension or contraction in the direction of the c-axis requires the movement of $\vec{c} + \vec{a}$ type dislocations to occur to satisfy the Von Mises criterion. Paton et al.[10] and Jones and Hutchinson[14] have observed the presence of such dislocations with a $<11\bar{2}3>$ slip vector typically on the $\{11\bar{2}2\}$ slip plane in a number of titanium alloys.

The slip systems active in the β phase were observed to be in agreement with the generally observed slip systems in BCC metals. Paton and Williams[41] examined a binary Ti-V alloy and observed <111> type slip directions on {110}, {112}, and {123} type planes.

The critical resolved shear stresses (CRSS) for the slip systems in the α phase were obtained using Ti-6.6Al single crystals[42]. Paton et al. determined that the $<11\bar{2}0>\{10\bar{1}0\}$ had the lowest CRSS followed by the $<11\bar{2}0>\{10\bar{1}1\}$ and $<11\bar{2}0>\{0002\}$ slip systems. The CRSS for $\vec{c} + \vec{a}$ slip system was as much as 50% higher than any of the

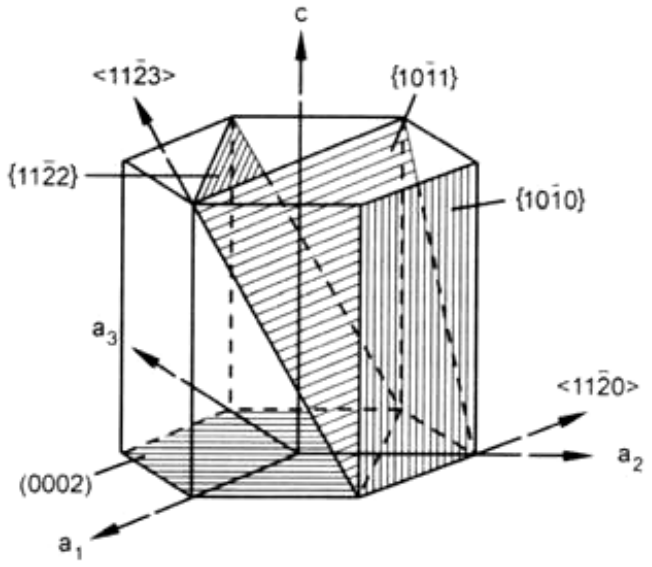

Burgers Vector Type	Slip Direction	Slip System
$\vec{a}$	<11$\bar{2}$0>	(0002)
$\vec{a}$	<11$\bar{2}$0>	(10$\bar{1}$0)
$\vec{a}$	<11$\bar{2}$0>	(10$\bar{1}$1)
$\vec{c} + \vec{a}$	<11$\bar{2}$3>	(11$\bar{2}$2)

Figure 1.2. Slip modes in hexagonal α titanium. (cf. ref. 8)

$\vec{a}$ slip systems. Therefore, it is less common for the α phase to deform extensively by $\vec{c}$ + $\vec{a}$ slip as compared to $\vec{a}$ slip. The CRSS values were observed to be strongly dependent on alloy content and on test temperature. Jones and Hutchinson[14] observed a much smaller difference in CRSS between $\vec{a}$ and $\vec{c}$ + $\vec{a}$ type slip in an α+β alloy than Paton et al.[42] did in their α alloy. The small difference in CRSS between the three $\vec{a}$ type slip systems was observed by Paton et al. to become even smaller at higher temperatures.

1.2.3.2 Deformation Twinning

Deformation twinning occurs in titanium alloys when the stress axis (tension or compression) is parallel to the c-axis and the resolved shear stress is not large enough to activate $\vec{c}$ + $\vec{a}$ type slip. Therefore, specific twinning modes are activated to plastically deform the material and cause extension or contraction of the material along the stress axis. The main twinning modes/planes that have been observed in CP titanium are $\{10\bar{1}2\}$, $\{11\bar{2}1\}$, and $\{11\bar{2}2\}$.[39] All twinning modes have shear directions that include a c-axis component. These three twinning modes are especially important to the alloys ductility and ability to plastically deform at low temperatures, but they have also been observed to occur in pure titanium at higher temperatures typically in response to compression loading.[15] As mention previously, the occurrence of twinning is suppressed as the solute (Al and O especially) concentration is increased. Therefore, the occurrence of twinning is only a major consideration as a deformation mechanism in CP titanium with low oxygen concentrations.[10]

1.2.4 Strengthening Mechanisms

The methods for strengthening titanium alloys are dependent on the class of alloy as previously mentioned. However, the fundamental mechanism behind strengthening all metals and alloys including titanium alloys is the same: impede dislocation motion. Therefore, the sub-ideal c/a ratio of the HCP α phase (1.587 vs. 1.633) significantly influences deformation of the α phase in titanium. This point has been studied extensively and is well understood.[10,13,43-49,52,53,56-59] This review is restricted to α and α+β alloys, thus strengthening of the α phase will be the focus of this section. Strengthening mechanisms associated with the presence of the β phase will be discussed in reference to α/β interfaces or grain boundaries. In titanium alloys, barriers to plastic deformation form based on the alloy's composition, thermo-mechanical processing, and heat treatments (solution and age). The operative strengthening mechanisms are the result of the formation of these barriers and include solid solution, boundary or interface, precipitation, and texture. A summary of titanium strengthening mechanisms is shown in Table 1.2.

1.2.4.1 Solid Solution Strengthening

The α phase is commonly strengthened by the addition of the interstitial element, O, and substitutional elements Al, Sn and Zr. Each of these elements has a large solubility in the α phase, which allows each to contribute to solid solution strengthening

Strengthening Mechanism	Dependence	Examples/Limitations
Substitutional Solid Solution	c	Strain localization >5% Al eq.
Interstitial Solid Solution	$c^{1/2}$	Strain localization >2500 ppm oxygen
Grain Size	$d^{1/2}$	Fine grains limit twinning
Precipitation	$r^{1/2}$, $f^{1/2}$	Occurs >5.5% Al eq.
Texture	c-axis orientation	Max. strength when loaded along c-axis

Table 1.2. Strengthening mechanisms of titanium alloys.[8]

of the α phase. It also is generally accepted that Sn and Zr are less effective as compared to O and Al. It is generally accepted that interstitial and substitutional elements have an additive effect on strengthening α phase titanium. From an atomistic standpoint, the addition of O has been shown to have a stronger effect than Al (~10 times per atom %).[43] In α+β alloys, small concentrations of β stabilizing elements including Mo, V, and Cr are present in the α phase because of limited solubility. The extent to which these elements strengthen the α phase is not well understood, but is thought to be small compared to Al and O.[44]

The addition of O as an interstitial solid solution strengthener significantly increases the strength of the material. The role of O as a barrier to plastic deformation was studied by Williams et al.[13]. At high concentrations of O ($\geq$0.2 wt.%) in an α alloy, they observed a transition in slip modes from wavy to planar slip. This transition in slip mode was attributed to the significant reduction of the resolved shear stress in the active slip planes as a form of strain localization, and not to a reduction of stacking fault energy and subsequent cross-slip as is typically observed in face center cubic (FCC) materials. Based on these observations, strengthening from the addition of O is accompanied by strain localization but the exact mechanism(s) are not clear. There is no doubt that there will be some order of elastic interaction between the interstitial oxygen and dislocations, but this would not be expected to cause a transition in the slip mode. Welsch et al.[45] proposed that this transition is connected to some form of short-range ordering of O in the α lattice. Evidence of such ordering from x-ray diffraction observations has been reported by Weissmann and Shrier[46]. Therefore, the current accepted mechanism for

strengthening by the addition of O is thought to be from short-range ordering of the O in the α lattice.

The addition of Al also significantly increases the strength of α and α+β alloys in a similar manner as O. Paton et al.[10] and Blackburn and Williams[47] studied the role of Al as a strengthening addition and both groups observed the same transition of slip mode from wavy to planar. The addition of Al to the α phase and α+β alloys reduces the 'a' and 'c' lattice parameters of the HCP crystal in the α phase.[44] The reduction in lattice parameters is consistent with a negative misfit that causes elastic interactions with the Al atoms and mobile dislocations. However, as with O, this interaction would not be expected to cause a transition in the slip mode. Experimental evidence has been reported that shows that an additional mechanism for strengthening by Al additions is the short range ordering of the Al in the α lattice which causes a transition from wavy to planar slip as with O additions.[10,47,48] Paton et al.[10] have shown that in dilute Ti-Al alloys (~5 - 9 wt.% Al) a transition in slip was caused from short-range ordering in the α phase. In higher concentration Ti-Al alloys (approximately greater than 6 wt.% Al), the planar slip is more intense due to the presence of small, coherent, ordered Ti_3Al particles (α_2 precipitates) that are sheared during deformation.[47-49] It should be restated that as was true in the case for O, these transitions in slip modes are attributed to the significant reduction of the resolved shear stress in the active slip planes, and not to a reduction of stacking fault energy and subsequent cross-slip as is typically observed in FCC materials.[43]

1.2.4.2 Boundary Strengthening

A variety of boundaries in titanium alloys act as barriers to the motion of dislocations, which strengthens the alloy. The effectiveness of these boundaries to act as barriers to dislocation motion and their spacing has a major effect on the strength of the alloy. For α and $\alpha+\beta$ alloys, there are two common forms of boundary strengthening: grain boundaries, and interphase boundaries. The influence of the first one is important for both α and $\alpha+\beta$ alloys, but the second mainly pertains to $\alpha+\beta$ alloys due to the ability to create a duplex microstructure by the heat treatment. These duplex microstructures consist of some α/α and a high density of α/β interfaces that contribute to strengthening in a similar manner to grain boundaries.

Hall[50] and Petch[51] proposed that the yield strength of most metals is a function of grain size:

$$\sigma_y = \sigma_o + k_y/\sqrt{d} \qquad [1.2]$$

where σ_y is the yield strength, σ_o is the "friction stress" representing the overall resistance of the crystal lattice to dislocation motion, k_y is the "locking parameter" which is a measure of the relative hardening contribution of the grain boundaries, and d is the grain diameter. Terlinde[52] later confirmed this grain size dependence for the grain size of Ti-Al alloys. The grain size sets the slip lengths for dislocations in single phase material. Therefore, as the grain size is decreased, the slip length will be decreased which subsequently reduces the dislocation pile-up length for that grain. Terlinde and Leutjering[53] have shown that the local stress required to initiate a crack in Ti-Al alloys is constant, thus anything that can be done to reduce local stresses also increases the

resistance to crack initiation of the material. As the grain size is decreased, the pile-up length is decreased and the local stresses associated with these pile-ups will be reduced (Figure 1.3). This is the generally accepted grain size effect on fatigue crack initiation for titanium alloys.

In many cases, the literature for α+β alloys refers to the prior β grain size when referencing grain size. This is misleading, as the prior β grain size is typically not the relevant length scale for deformation of the material. The operative length scale changes as a result of the processing of the alloy. It should be noted that "grain sizes" for titanium alloys are typically not those observed in an optical or SEM micrograph showing the microstructure. The grain size is dependent on the crystal structure of each phase, as crystal structures of the α and β phases transform to different variants, sizes and morphologies based on the nucleation and growth of the α phase upon cooling from above the β transus. Above the β transus, the β phase is stable and significant β grain growth occurs. Upon slow cooling through the β transus, grain boundary α forms and α laths will grow from the grain boundaries until they impinge on another α lath or the original β grain boundary. In most cases, the α laths growing from each grain face will grow as a single variant of the Burgers orientation relationship from the prior β grain but, with increased cooling rate, several variants can become active in a single β grain. All the α laths of the same variant have the same crystallographic orientation and are described as a 'colony' consisting of alternating α and β laths. The new "grain size", more aptly called the slip length, of these alloys is then more akin to the colony size than the β grain size. Further reduction of the size of colonies is accomplished by thermo-mechanical

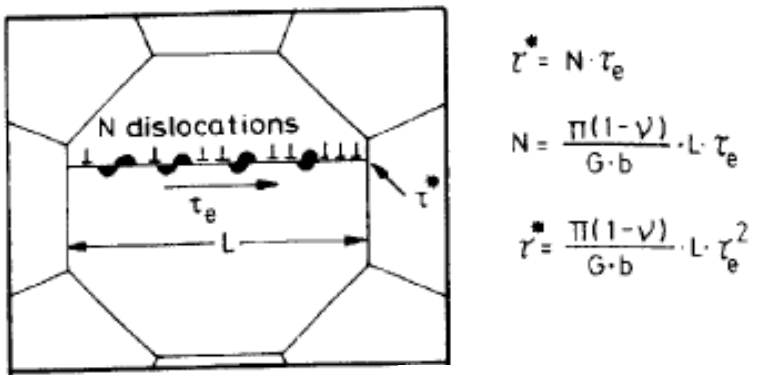

Figure 1.3. Schematic of how grain size sets the slip lengths for dislocations in the material. L is the grain size, N is the number of dislocations, τ_e is the elastic shear stress due to the dislocation pile-up and τ^* is the localized or concentrated shear stress at the grain boundary.[53]

processing below the transformation temperature, which breaks up the coarse colony structure and leads to the formation of equiaxed α grains and β due to recrystallization. Upon cooling to room temperature, the new structure consists of primary α grains (globular α grains) and prior β grains consisting of refined α/β colonies. In this case the primary α grains and the refined colonies are the two microstructural length scales or sizes that need to be considered. The equiaxed grains are formed from individual α plates within a colony. This creates the possibility for formation of aligned α grains. Therefore, special attention needs to be taken to determine the texture prior to indicating the actual grain size of the alloy. Further discussion of texture and texture effects will be presented in later sections.

As shown in the Hall-Petch relationship previously, strengthening of a material is not only dependent on the grain size but also the ability of the boundaries to act as barriers to dislocation motion (k_y term in equation 2). In α+β alloys, these boundaries are grain and interphase boundaries. The strength of a boundary as a barrier to dislocation motion is dependent on the ease at which the dislocations can transfer across the grains or interphase region. Hirth[54] and Hirth and Balluffi[55] proposed that the transfer of slip across a grain boundary requires some adjustment locally so the Burgers vector of the slip directions is conserved between the two structures (regardless if α/α or α/β interface). They also suggest that such dislocations can dissociate into components; some of which stay in the grain boundary and others of which glide out into adjacent grains to sustain the plastic deformation. Although this seems reasonable, little evidence has been presented that confirms this theory. On the other hand, several studies have examined the effect of

crystallographic alignment of slip systems across interphase regions.[56-58] Lin et al.[56] studied the deformation of an α+β alloy (Ti-6211) that consisted of colonies of α and β laths. They observed $\vec{a}$ type slip on $\{10\bar{1}0\}$ planes in the α laths that easily transversed the β laths. Large dislocation pile-ups were observed only at colony interfaces (grain boundary). Therefore, they concluded that α/β interfaces provided little resistance to slip transmission. Several other groups have observed the small misorientation of the Burgers orientation relationship (misorientation angle between HCP and BCC slip directions) reduces the ease of slip transmission from the α to β phase.[57,58] It is clear from the published literature that grain boundaries and interphase regions can be barriers to slip transmission but to what extent and the associated mechanisms are still not well understood.

1.2.4.3 Precipitation Hardening

Precipitation or age hardening occurs as a result of the formation of a second phase that acts as a barrier to motion of dislocations. These second phases are precipitated out of a supersaturated solid solution during aging after solution heat-treating of the alloy. In α and α+β alloys, the most common precipitates are the ordered α_2 phase (mentioned in solid solution strengthening section), Ti_5Si_3 silicides, and various intermetallic compound systems such as Ti-Cu. Limited literature on strengthening due to silicides and intermetallic compounds have been published and are not of significant interest for commercial alloys. The ordered α_2 phase, however, is of great interest as it has been extensively studied in several commercial α and α+β alloys.

As mentioned in the solid solution hardening section, high Al concentration Ti-Al alloys (approximately greater than 5 wt.% Al) have been studied and planar slip was observed due to the presence of small, coherent, ordered Ti_3Al particles (α_2 precipitates).[47,49] When the Al is in excess of 9 wt.%, the alloy has been shown to become brittle possibly due to the further loss of deformation modes from the formation of this ordered phase. The α_2 particles are an ordered hexagonal DO_{19} structure (Mg_3Cd prototype structure). Strengthening of the α phase from α_2 with no other alloying additions is a consequence of the particles having to be sheared (since α_2 is coherent with α phase) by moving dislocations. This results in planar slip and extensive pile-ups at boundaries. Leutjering and Weissmann[49] showed that addition of Si and Zr changes the particle-matrix misfit, which leads to dislocations bypassing the α_2 particles. These additions lowered the strength of the alloy and provided substantial improvements in ductility. Williams and Blackburn[59] have reported that additions of Sn and Ga appreciably increase the strengthening contribution of the α_2 particles, but the mechanism is not fully understood.

1.2.4.4 Texture

The anisotropic behavior of the HCP α phase plays a significant role in the plastic deformation of titanium alloys. This is never more evident then in strengthening due to the presence of texture (preferred crystal orientations) in α and $\alpha+\beta$ alloys. The strengthening of these alloys is based on the deformation modes of titanium and their relative resolved shear stress (RSS) values. Paton et al.[10] tested single crystals of Ti-6Al

oriented with the [0001] direction parallel and normal to the stress axis. They observed that the alloy tested with the [0001] parallel to the stress axis deformed by $\vec{c} + \vec{a}$ slip and had a larger yield stress as compared to the crystals oriented with the [0001] normal to the stress axis that deformed by $\vec{a}$ slip. This difference in yield stress was attributed to the RSS and the variation in critical resolved shear stress (CRSS) for the operative slip systems including correction for the Schmid factor[60]. These observations were in agreement of those by Williams et al.[48]. Therefore, in α and $\alpha+\beta$ alloys with large regions of similarly oriented α phase (heavily textured), the yield strength is highly anisotropic. As mentioned in the boundary strengthening section, the crystal orientations of the α phase are strongly influenced by the processing history of the alloy. The right combination of temperature and severe plastic deformation are necessary during thermo-mechanical processing to break up the large oriented grains and produce a refined, random textured alloy that has more isotropic properties. In addition to reducing the grain size, severe deformation typically creates larger misorientation angles between adjacent phases/grains producing further strengthening (as mentioned in the boundary strengthening section). The importance of texture for an alloy will be dependent on the property requirements for desired application.

1.3 Titanium-Boron Alloys

1.3.1 Physical Metallurgy of Titanium-Boron Alloys

The addition of boron to various titanium alloys has been shown to precipitate a boron containing phase (TiB_x) *in-situ* resulting in a microstructure consisting of the initial alloy as the matrix and the TiB_x as dispersoids.[1-4,61-86] The influence of the addition of

boron to various grades of commercially pure (CP) titanium and to Ti-6Al-4V has been most extensively studied and documented. Therefore, the following discussion is based primarily on the results of CP titanium and Ti-6Al-4V.

The two most relevant TiB_x stochiometries are the metastable TiB_2 and the thermodynamically stable TiB. TiB is one of the most commonly studied boron containing titanium phases due to its thermodynamic stability and cleanliness of the interface formed between matrix and boride (no undesirable phases or elements).[61-68,70] The formation of TiB *in-situ* is primarily due to the low solubility (<0.05 wt%) of boron in both allotropic forms of titanium as shown in the titanium-boron phase diagram (Figure 1.4). Titanium and boron precipitate out of the liquid solution upon cooling and form a TiB phase. Upon further cooling, the titanium alloy matrix phase(s), as predicted from the titanium alloy matrix phase diagram, is formed around the TiB phases. Banerjee et al.[61] have suggested the following hypereutectic equilibrium solidification path for Ti-2wt.%B:

$$\text{Hypereutectic: Liquid} \rightarrow \text{Liquid + Primary TiB} \rightarrow \text{Primary TiB + Eutectic TiB} + \text{Eutectic } \beta \rightarrow \text{Primary TiB + Eutectic TiB + } \alpha \qquad [1.3]$$

Although this seems reasonable based on typical metal eutectic solidification, further study is warranted to elucidate the details. A similar hypoeutectic equilibrium solidification path can be proposed for a Ti-<1.6wt.%B alloy:

$$\text{Hypoeutectic: Liquid} \rightarrow \text{Liquid + Primary } \beta \rightarrow \text{Eutectic TiB} + \beta \rightarrow \text{Eutectic TiB + } \alpha \qquad [1.4]$$

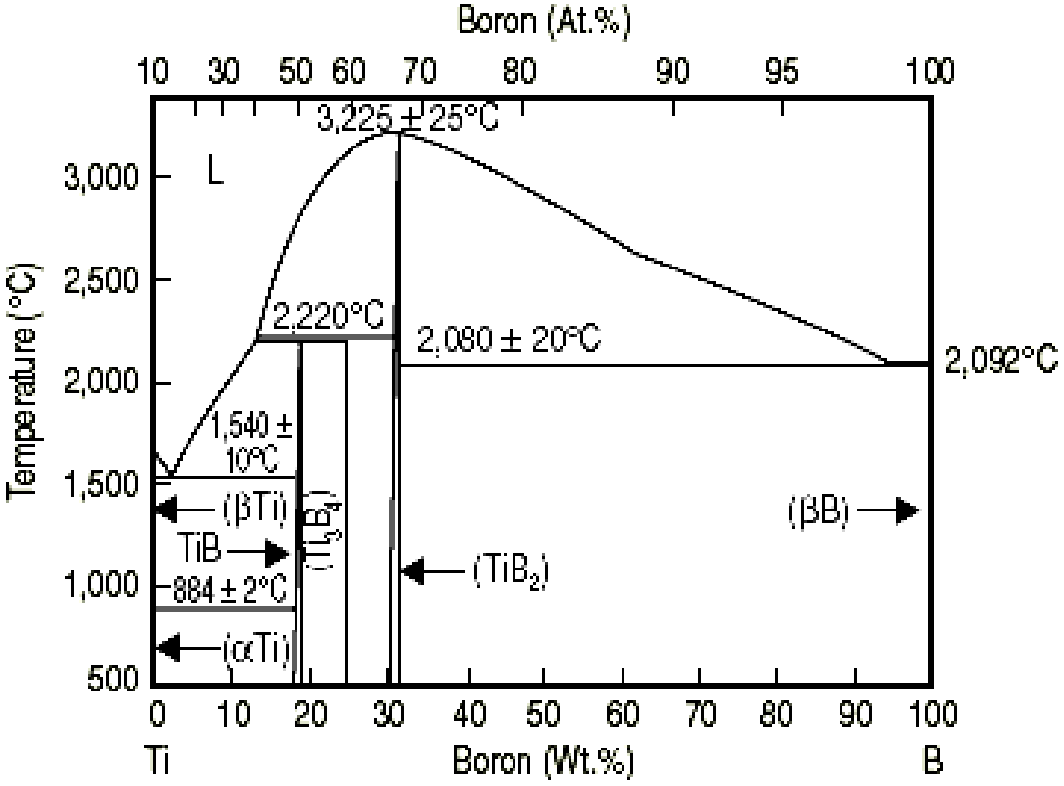

Figure 1.4. Binary Ti-B phase diagram. (cf. ref. 4)

TiB particles are generally equiaxed or needle-like particles, ranging from a few to 100's of μm in size. The morphology has been shown to be dependent on the boron concentration relative to the eutectic (~1.6 wt% boron as shown in Figure 1.4).[61,63,69,71,72,74] For boron composition that is: (1) hypereutectic, the TiB particles have been shown to form as equiaxed (primary TiB) and needle-like particles (eutectic TiB) as shown in Figure 1.5; and if (2) hypoeutectic, the TiB particles are needle-like as shown in Figure 1.6.[61,63,69] The TiB particles are chemically stable within the matrix and can be observed at grain/phase boundaries or within grains/phases of the titanium alloy matrix. The presence of the TiB particles at the grain/phase boundaries as the matrix is formed assists in refining the matrix microstructure. The TiB particles are thought to pin the grain/phase boundaries during processing thus forming a refined matrix microstructure as compared to those observed in the conventional titanium alloy.[1-4,61,63,69,71,72,74] The resulting titanium matrix microstructure is similar to that observed in the conventional titanium alloy except with a finer microstructural scale.

The TiB particles precipitate from the solid solution with an orthorhombic (B27) structure (Figure 1.7).[61-70] Titanium-boron alloys have been observed to have a specific orientation relationship between the α and β phases of α+β and β-titanium alloy matrices and the TiB.[62,63,65,70] For titanium-boron alloys with a Ti-6Al-4V matrix, two orientation relationships between the α phase and TiB have been observed.[63] An arc

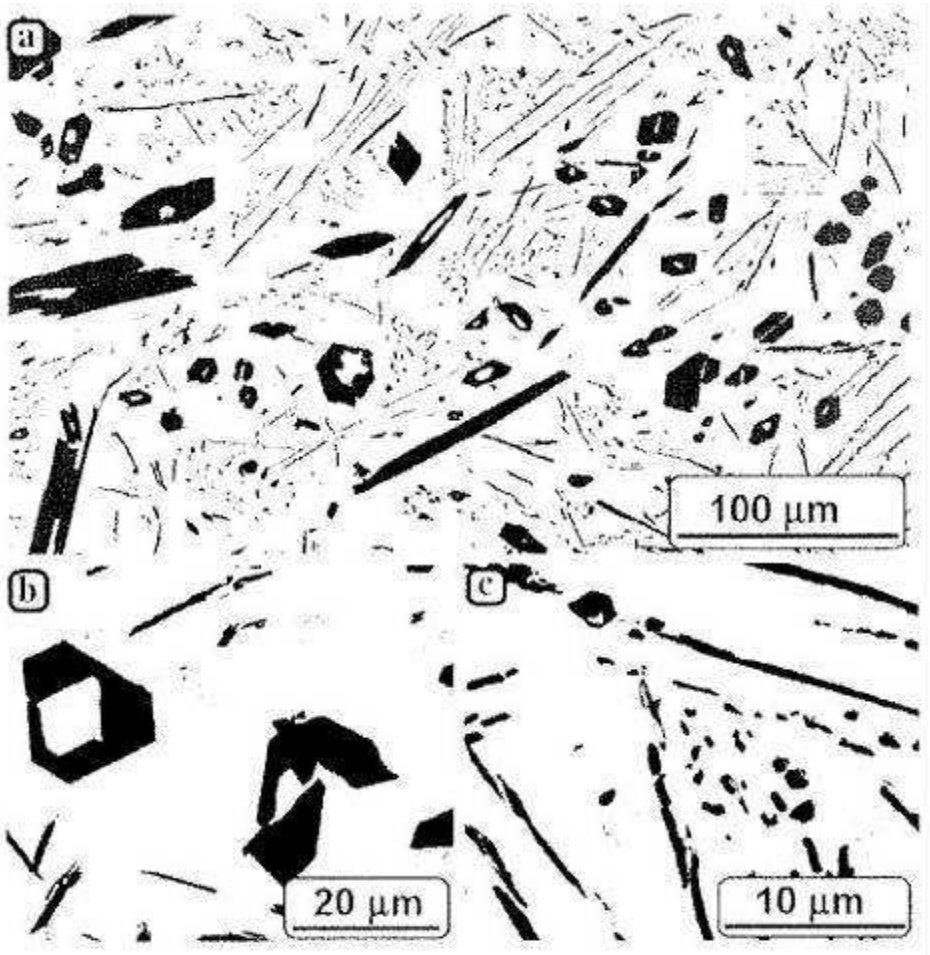

Figure 1.5. Micrographs of arc-melted Ti-2wt%B at (a) low magnification, and (b) and (c) higher magnifications showing the blocky primary TiB precipitates and needle-like eutectic TiB precipitates.[63]

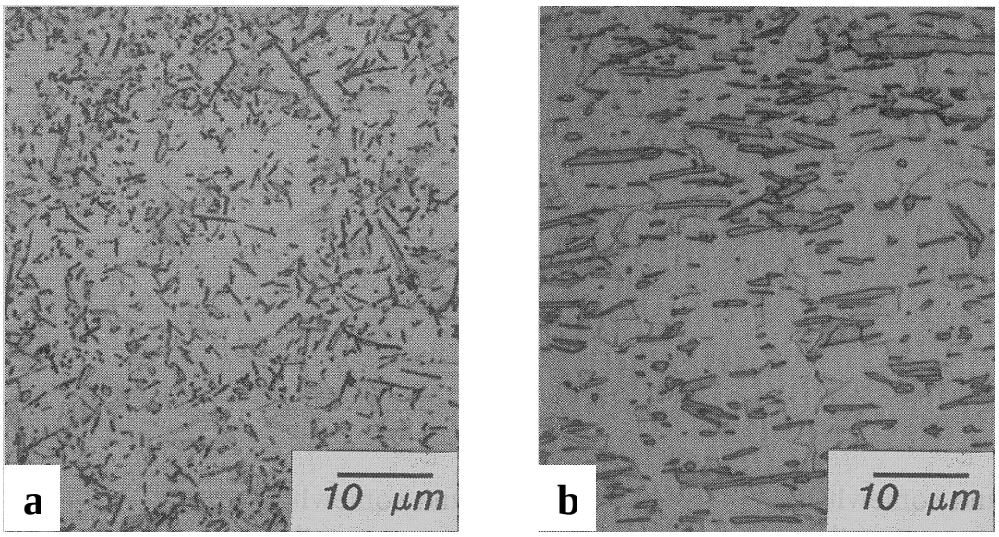

Figure 1.6. Micrographs of powder blended Ti-6Al-4V-1.4wt%B (a) HIPed at 1832^{o}F (1000^{o}C), 103 MPa, 3 hours and heat treated at 1796^{o}F (980^{o}C) for 1 hour furnace cooled; and (b) direct extruded and heat treated at 1796^{o}F (980^{o}C) for 1 hour furnace cooled. Micrographs show needle-like eutectic TiB precipitates.[69]

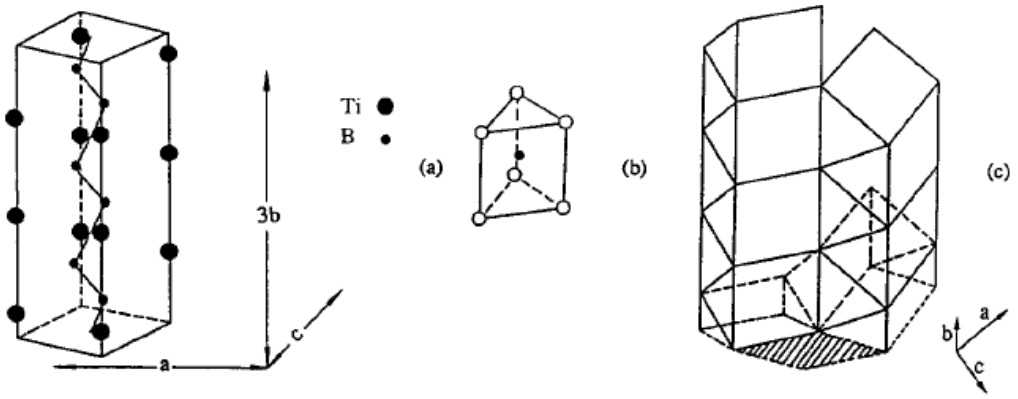

Figure 1.7. Schematic illustration of (a) TiB orthorhombic B27 unit cell; (b) basic trigonal prismatic arrangement of titanium atoms around each B atom; (c) arrangement of basic trigonal prisms to form TiB structure. (cf. ref. 67)

melted Ti-6Al-4V-XB exhibited an orientation relationship as follows:

$$\{010\}_{TiB}||\{11\bar{2}0\}_{\alpha\text{-}Ti}$$

$$\{001\}_{TiB}||\{0001\}_{\alpha\text{-}Ti}$$

$$\{100\}_{TiB}||\{10\bar{1}0\}_{\alpha\text{-}Ti} \quad [1.5]$$

A LENS™ deposited Ti-6Al-4V-XB exhibited an orientation relationship as follows:

$$\{010\}_{TiB}||\{11\bar{2}0\}_{\alpha\text{-}Ti}$$

$$\{001\}_{TiB}||\{1\bar{1}01\}_{\alpha\text{-}Ti}$$

$$\{100\}_{TiB}||\{1\bar{1}0\bar{2}\}_{\alpha\text{-}Ti} \quad [1.6]$$

The orientation relationship between the β phase and TiB was observed for blended elemental powder metal Ti-4.3Fe-7.0Mo-1.4Al-1.4V as follows:[62,65,70]

$$(010)_{TiB}||(001)_{\beta\text{-}Ti}$$

$$\langle 001\rangle_{TiB}||\langle 110\rangle_{\beta\text{-}Ti} \quad [1.7]$$

1.3.2 Processing & Microstructures of Titanium-Boron Alloys

Several boron addition methods have been studied to obtain desirable microstructures and mechanical properties. Typical methods have focused on using conventional powder metallurgy (PM) methods (gas atomization and powder blending), melting methods, and rapid solidification processes (RSP) to incorporate boron in titanium alloys. For most methods, secondary processing (HIP, CIP, working operations) is required to obtain material with a desirable microstructure and properties, as summarized in the following sections.

1.3.2.1 Gas Atomization

Limited studies have been completed using direct inert gas atomization to create titanium-boron alloys.[71-74] Yolton and Moll[71] examined a prealloyed Ti-6Al-4V-XB alloy produced by cold wall induction melting of master alloys and titanium diboride followed by argon gas atomization. The alloys ranged from 0.9 – 2.2 wt.% boron with a mean powder size of ~140 μm and packing density of ~68%. The powder was also HIPed and direct extruded to study the effects of secondary processing on the microstructure. The powder was HIPed for 3 hours at 1832^{o}F (1000^{o}C) and a pressure of 15 ksi (103 MPa); followed by a heat treatment at 1796^{o}F (980^{o}C) for 1 hour, furnace cooled at 131^{o}F (55^{o}C) per hour to 1400^{o}F (760^{o}C) and then air-cooled. The extrusion was completed at 2003^{o}F (1095^{o}C) using a reduction ratio of 9:1 with the same subsequent heat treatment as the HIPed material. The powder, as atomized, consisted of fine TiB particles dispersed uniformly in a Ti-6Al-4V matrix. At higher boron levels, the powder contained a higher density of TiB particles some of which were needle shaped. A small number of relatively coarse (~25 μm) needle shaped particles were observed for the 2.2 wt.% boron alloy. The HIP and heat treatment cycles produced similar microstructures with randomly oriented acicular TiB particles. Extrusion and heat treatment of the consolidated powder produced a microstructure with a mixture of relatively fine (1 - 2 μm) and coarser (~25 μm) TiB particles with high aspect ratios (~15:1). The most notable change in the microstructure after extrusion was that the TiB particles were aligned in the extrusion direction which is consistent to other published work produced using other powder metallurgy methods[75]. Microstructures of as-compacted and extruded materials made from gas atomized powder are shown in Figures 1.8 and 1.9, respectively.

1.3.2.2 Powder Blending

Powder blending methods have been the most popular of the processes to produce titanium-boron alloys as is evident by the large amount of published literature. Some of the most desirable combinations of microstructure(s) and properties have been produced at a reasonable cost using blending methods. The major difference in powder blending methods is the starting titanium and boron powder. Each of the methods produce powders of varying size, morphology and purity, which subsequently influences the density, size, morphology, distribution and composition of the resulting alloy's microstructure.

Several methods have been used to produce the starting powder including, hydrogenation/dehydrogenation (HDH)[62,65,68,76], sponge fines[70], direct gas atomization[71-74], and rotating electrode process (REP) or plasma rotating electrode process (PREP)[77,78]. Saito et al.[70] studied a Ti-4.3Fe-6.8Mo-1.4Al-1.4V-XB alloy produced from sponge fines that were subsequently blended with elemental powder, cold isostatic pressed (CIPed), and sintered. The powder blends were CIPed at 56.8 ksi (392 MPa) and sintered at 2372^{o}F (1300^{o}C) for 100 hours in a vacuum of $1.5x10^{-7}$ psi (10^{-3} Pa). The microstructure consisted of primary TiB and eutectic TiB particles in a $\alpha+\beta$ titanium matrix, mostly the latter. The primary TiB particles were several microns in size and exhibited an equiaxed morphology. The eutectic TiB particles were also several microns in size and exhibited a needle-like morphology. In comparison, Saito et al.[62,65,68] also studied a Ti-4.3Fe-6.8Mo-1.4Al-1.4V-XB alloy produced using the HDH process, blended with alloying elements and subsequent CIPing and sintering at the same

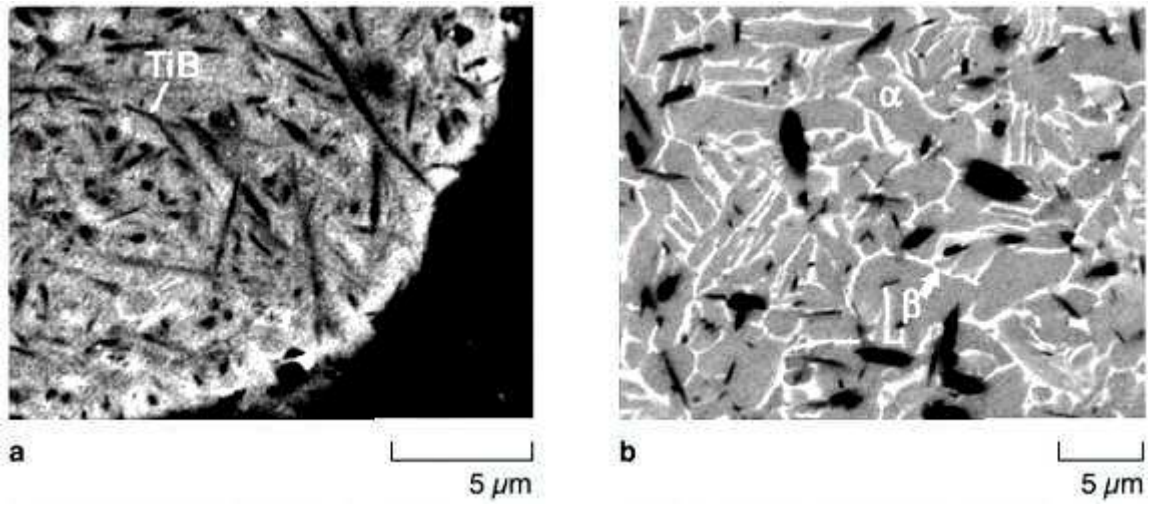

Figure 1.8. Micrographs of Ti-6Al-4V-1.6wt%B produced using gas-atomized, pre-alloyed powder: (a) powder cross-section; (b) blind-die compacted.[74]

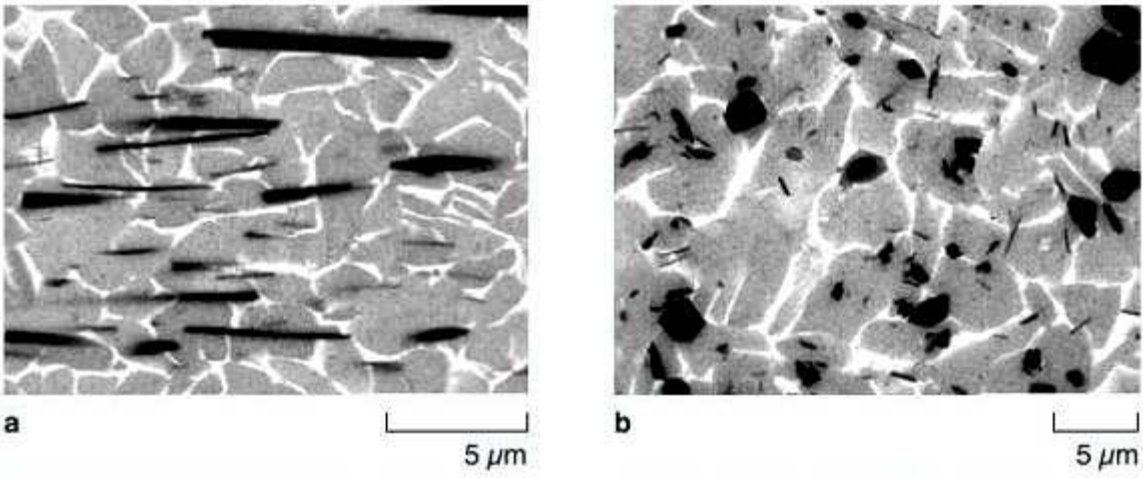

Figure 1.9. Micrographs of Ti-6Al-4V-1.6wt%B produced using gas-atomized, pre-alloyed powder: (a) extruded - longitudinal; (b) extruded – transverse. Extrusion axis is parallel to horizontal axis of micrographs.[74]

conditions as the sponge fine produced alloy. They report similar microstructural results but noted that mechanical properties of the alloy made from sponge fines may be adversely affected by the impurity (namely O) of the starting sponge fines. Microstructures of as-compacted and extruded blended elemental powder are shown in Figures 1.10 and 1.11, respectively.

In comparison to using sponge fines and HDH powder, gas atomized powder particles and powder particles produced by REP or PREP are larger in size (≥150 μm), which raises problems in obtaining a uniform distribution of TiB particles. Godfrey et al.[77] and Goodwin et al.[78] have shown that mechanical milling of the blended powders reduces the size of the powders which obtains a uniform distribution of the TiB particles throughout the alloy. This reduction in powder size should also further refine the TiB particle and matrix alloy size, but neither group considered this in their studies.

1.3.2.3 Melting

The melting methods that have been used include arc melting[63], casting[79-81], and self-sustained high temperature synthesis (SHS)[82,83]. All of these processes can use powder material produced using the previously mentioned methods or conventional processed material. Although melting methods have been shown to be more cost effective than PM, these methods often have produced undesirable microstructures and associated properties for commercial applications. Banerjee et al.[63] examined a Ti-2wt.%B alloy melted and cast in a vacuum arc-melter. The microstructure consisted of large primary and smaller eutectic TiB particles in a α titanium matrix. The primary TiB particles were ~20 - 100 μm in size and exhibited a faceted, equiaxed morphology. The eutectic TiB

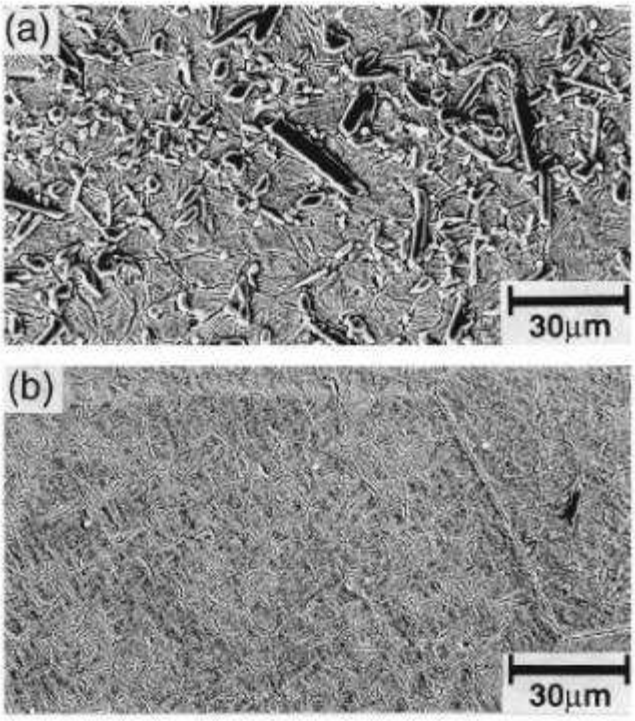

Figure 1.10. Micrographs of as-sintered self-sustained high temperature synthesis (SHS) melted Ti-6.8Mo-4.2Fe-1.4Al-1.4V with (a) 20 vol.% TiB; and (b) matrix alloy only (no TiB present).[68]

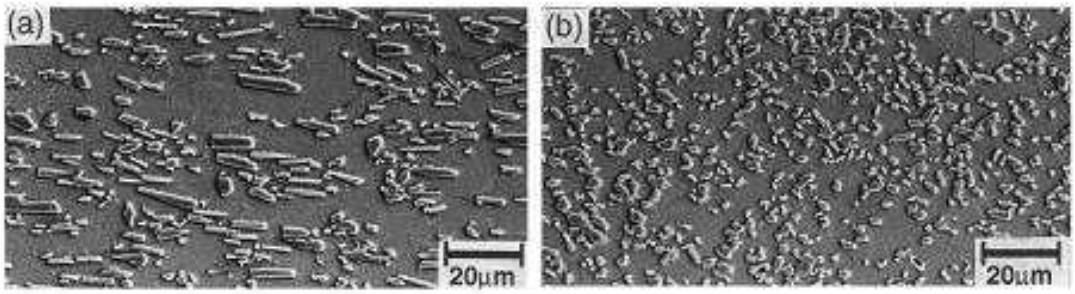

Figure 1.11. Micrographs of as-forged self-sustained high temperature synthesis (SHS) melted Ti-6.8Mo-4.2Fe-1.4Al-1.4V with 20 vol.% TiB: (a) longitudinal cross-section, and (b) transverse cross-section.[68]

particles were smaller and exhibited an acicular morphology with diameters of ~1 μm and lengths of ~10 - 20 μm. Similar results were reported by Philliber et al.[79,81] for a β-titanium alloy, Ti-17Mo, that was arc-melted and heat-treated at 1832°F (1000°C) for 12 hours and water quenched to homogenize the alloys and eliminate the micro-segregation that occurred during solidification. Size, distribution and ratio of the primary and eutectic TiB particles were approximately the same as those reported by Banerjee et al.[63] while the matrix was β titanium stabilized with Mo. Tsang et al.[82] used SHS to melt titanium-boron alloys ranging from 5 – 15 wt.% B and observed similar results as Banerjee et al.[63] and Philliber et al.[79,81]. The microstructure consisted of primary and eutectic TiB particles in an α titanium matrix. The primary TiB particles exhibited a faceted, equiaxed morphology and were smaller than the primary TiB observed by Banerjee et al. and Philliber et al. The eutectic TiB particles exhibited an acicular morphology and were also smaller than the eutectic TiB observed by Banerjee et al. and Philliber et al. (Figure 1.12).

1.3.2.4 Rapid Solidification

Some of the more recent methods for creating titanium-boron alloys include rapid solidification processing (RSP).[61,63,64,66,67,75,84] The microstructures and properties observed from material produced by RSP are equivalent or better to those of powder blending. RSP has been used to melt spin ribbons and flakes of titanium-boron alloys by Fan et al.[64,67] and Sastry et al.[84]. Fan et al.[64,67] studied the influence of pre-consolidation heat treatment at 572 - 1652°F (300 - 900°C) for 4 hours and water

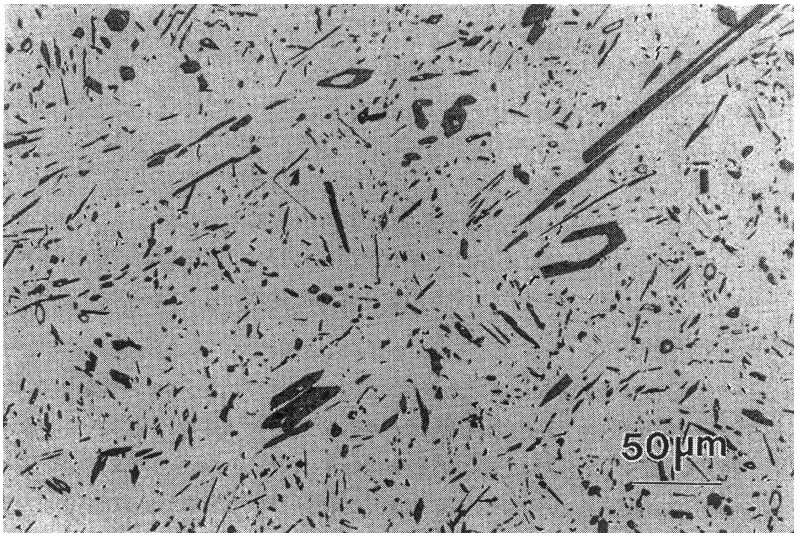

Figure 1.12. Micrographs of cast Ti-15Mo-10B after heat treatment at 1832^{o}F (1000^{o}C) for 12 hours and 1112^{o}F (600^{o}C) for 24 hours.[81]

quenched and secondary processing on melt spun ribbons of Ti-6Al-4V-0.5 wt.%B. The ribbons were HIPed at 1652^{o}F (900^{o}C) and 22 - 44 ksi (150 - 300 MPa) for 2 hours and furnace cooled; and extruded at 1652^{o}F at a 40% reduction. Ribbons without a pre-consolidation heat treatment consisted of a two-zone microstructure: columnar grain zone at the wheel side and equiaxed dendrite zone at the free side. They also observed a region consisting of a eutectic structure of β and TiB between the columnar and dendrite zones. Although no explanation is given, it appears that except for the eutectic region the boron is in solid solution in the α+β matrix since no TiB particles can be observed from their LM and SEM micrographs. Secondary processing of the ribbons without a pre-consolidation heat treatment eliminated the multi-zone/region structure. The microstructure consisted of eutectic TiB with a high aspect ratio needle-like morphology in an α+β matrix. Ribbons with a pre-consolidation heat treatment below 1292^{o}F (700^{o}C) consisted of primary TiB particles in an α+β matrix, while ribbons heat-treated above 1292^{o}F consisted of a large number of primary TiB particles and a small fraction of eutectic TiB particles. In both cases, the primary TiB particles were ~100 nm in size and exhibited an equiaxed morphology while the eutectic TiB particles were smaller and exhibited a needle-like morphology. Secondary processing of the ribbons with a pre-consolidation heat treatment produced a microstructure consisting mainly of primary TiB with an equiaxed morphology and limited eutectic TiB with a needle-like morphology in an α+β matrix.

The results from the Fan et al.[64,67] and the Sastry et al.[84] studies show promise for commercial applications, but scale-up of these processes to the necessary production

quantities has been unsuccessful to date. The only RSP process that currently has shown potential for scale-up is also the most recent RSP that has been developed, the LENS™ (Laser Engineered Net Shaping) process. The LENS™ process entails a metal base plate being moved accordingly under a stationary laser rapidly melting and re-solidifying blended elemental powder that is fed continuously in the laser beam.[61,63,66] The advantage of the LENS™ process is it forms the material into a near net shape unlike the other processes, which require secondary processing steps. As with other RSP methods, the LENS™ process produces material with a desirable microstructure, but property evaluation is still being completed. Banerjee et al.[61,63,66] examined Ti-2wt.%B and Ti-6Al-4V-2wt.%B produced using the LENS™ process. For the Ti-2wt.%B alloy, the microstructure consisted of primary and eutectic TiB particles in a α titanium matrix. The primary TiB particles were ~0.6 μm in size and exhibited an equiaxed morphology. The eutectic TiB particles exhibited an acicular morphology with an average length of ~2.5 μm and aspect ratio of ~7:1. Detailed TEM analysis of the α phase revealed nanoscale TiB particles that were not resolvable using optical or SEM. For the Ti-6Al-4V-2wt.%B alloy (as shown in Figure 1.13), the microstructure consisted of limited primary and mostly eutectic TiB particles in an $\alpha+\beta$ matrix. The primary TiB particles were ~1.0 μm in size and exhibited an equiaxed morphology. The eutectic TiB particles exhibited an acicular morphology with an average length of ~1 - 5 μm and aspect ratio of ~5:1. The thermodynamic stability of this alloy was also examined by heat-treating the alloy at (1) 1292^{o}F (700^{o}C) for 100 hours; and (2) 2012^{o}F (1100^{o}C) for 10 hours. No significant amount of coarsening of the TiB particles was observed for both heat treatments

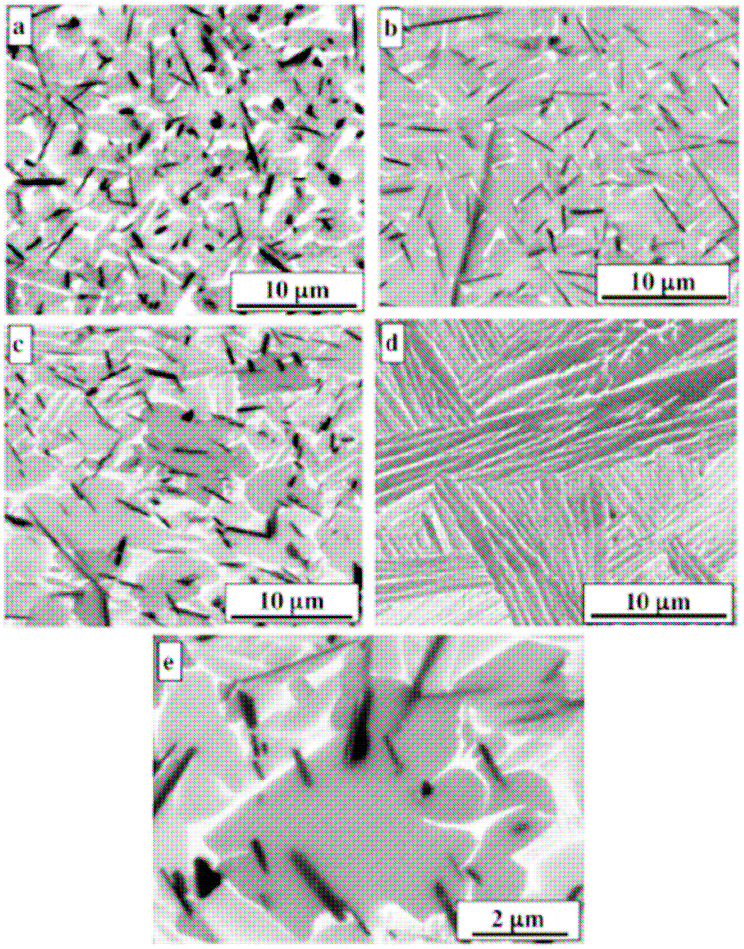

Figure 1.13. Micrographs of LENS™ processed Ti-6Al-4V with TiB: (a) as-deposited (b) heat treated at 1292°F (700°C) for 100 hours; (c) heat treated at 2012°F (1100°C) for 10 hours; (d) and (e) as deposited at higher magnifications.[61]

indicating the microstructure is stable at elevated temperatures.

1.3.3 Mechanical Properties of Titanium-Boron Alloys

As a general rule, the titanium-boron alloy microstructures obtained through the addition of boron exhibit increased RT and high temperature strength[1-4,62,65,68,70-72,74,76,77,79-82,84,85], higher stiffness (elastic modulus)[1,2,71,72,74,84], improved fatigue strength[62,65,68,70,86], creep resistance[2,83,85], hardness[2,65], and wear resistance[1,2,85]. However, the boron addition has also had either no effect or a decrease in ductility[2,62,65,68,70-72,74,82,84], and fracture toughness[1,74] as compared to the same basic titanium alloy without boron additions. The focus of this research is to examine strengthening of titanium alloys due to the addition of boron. Tensile and fatigue testing of the titanium-boron alloys are the main interest. Therefore, the published results of tensile and fatigue testing of titanium-boron alloys will be summarized in this discussion.

Several authors have demonstrated that tensile and fatigue properties of the titanium-boron alloys are influenced not only by the percent addition of boron but also by the form (particles or whiskers), distribution, and orientation of the TiB particles.[1-4,60,63,66,68-70,72,73,75,77-80,82,83,85] The refined microstructure of the matrix phase has also been shown to have an influence on mechanical properties of the titanium-boron alloys. Since the refined microstructure is due in part to the presence of the TiB during transformation of the matrix, the influence of each microstructural feature on mechanical properties is not well understood. The combined influence of TiB particles and fine grain matrix on strengthening mechanisms for various titanium-boron alloy processing methods constitutes the majority of published literature.[1-4,62,65,68,70-72,76,77,79-82,84,85,86]

1.3.3.1 Tensile Properties

The bulk of work related to mechanical properties of titanium-boron alloys deals with influence of boron additions on the tensile properties of titanium alloys. Figures 1.14 - 1.16 show the influence of TiB on 0.2% yield strength, ultimate tensile strength, and ductility, respectively. Since several studies have been completed using different titanium alloys, most commonly CP titanium and Ti-6Al-4V, differentiating the influence of boron on the strengths of the titanium alloys is difficult. Therefore, the strength of the titanium alloys without the boron additions was subtracted from the TiB containing alloys to obtain the increase in strength due to the addition of boron by a variety of processing methods. This increase in strength for the 0.2% yield stress and ultimate tensile strength are plotted in Figures 1.14 and 1.15. As clearly shown in the plots, the amount of strength increase over the conventional titanium alloy increased as the volume percent of TiB was increased.

Several factors that could be a part of the strengthening include the matrix grain size, oxygen concentration, and size, morphology, orientation and distribution of the TiB particles, but there is no clear understanding of the influence of these factors on strengthening titanium alloys. Godfrey et al.[77] studied a Ti-6Al-4V-XB alloy with levels of O ranging from 0.185 – 0.205 wt.% and B ranging from 0 – 2.0 wt.%(volume fraction of TiB was not reported). They observed an increase from 148 – 163 ksi (1020 - 1125 MPa) in the 0.2% yield strength increase and a decrease in ductility from 1.3% to 0%, respectively, for material with an oxygen level of ~1165 ppm as compared to 2050 ppm.

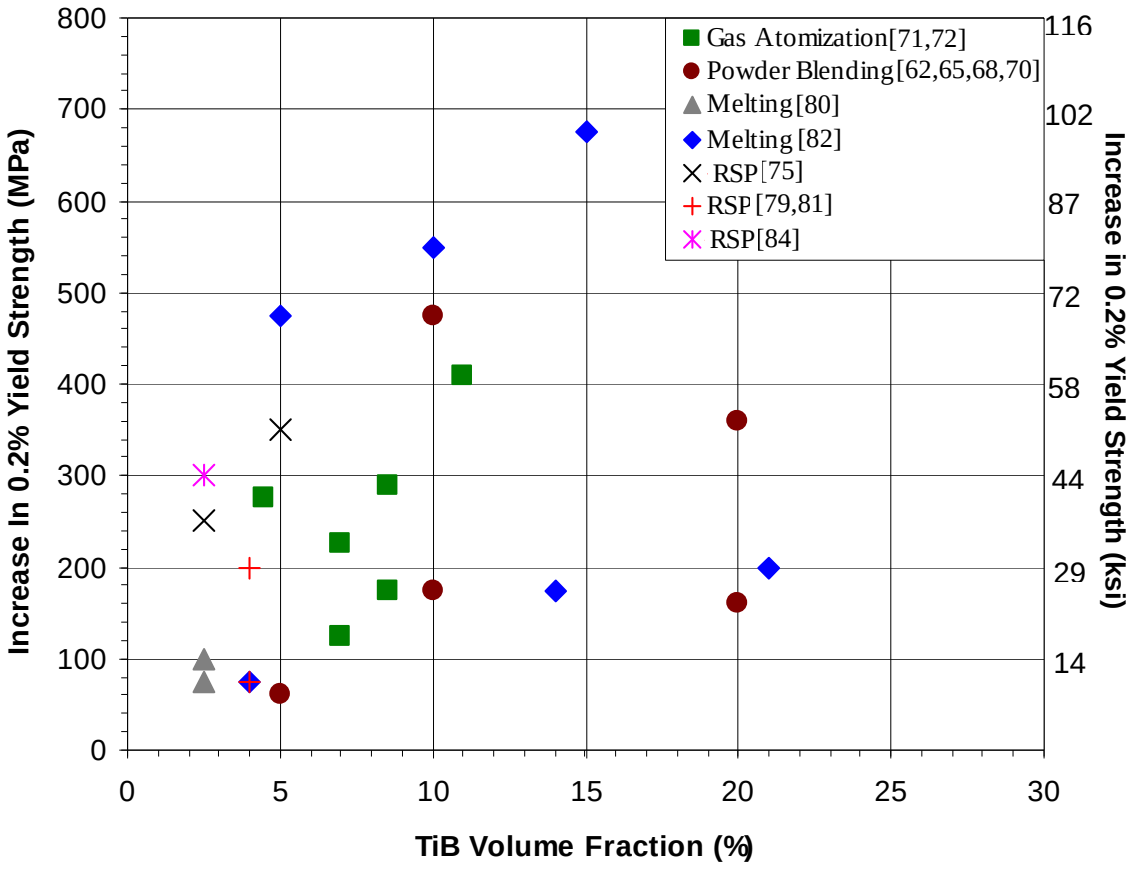

Figure 1.14. Increase of 0.2% yield strength due to addition of boron to titanium alloys via various processing methods. The strength of the titanium alloys without the boron additions was subtracted from the TiB alloys to obtain the increase in strength due to the addition of boron. (Figure modified from Godfrey et al.[77])

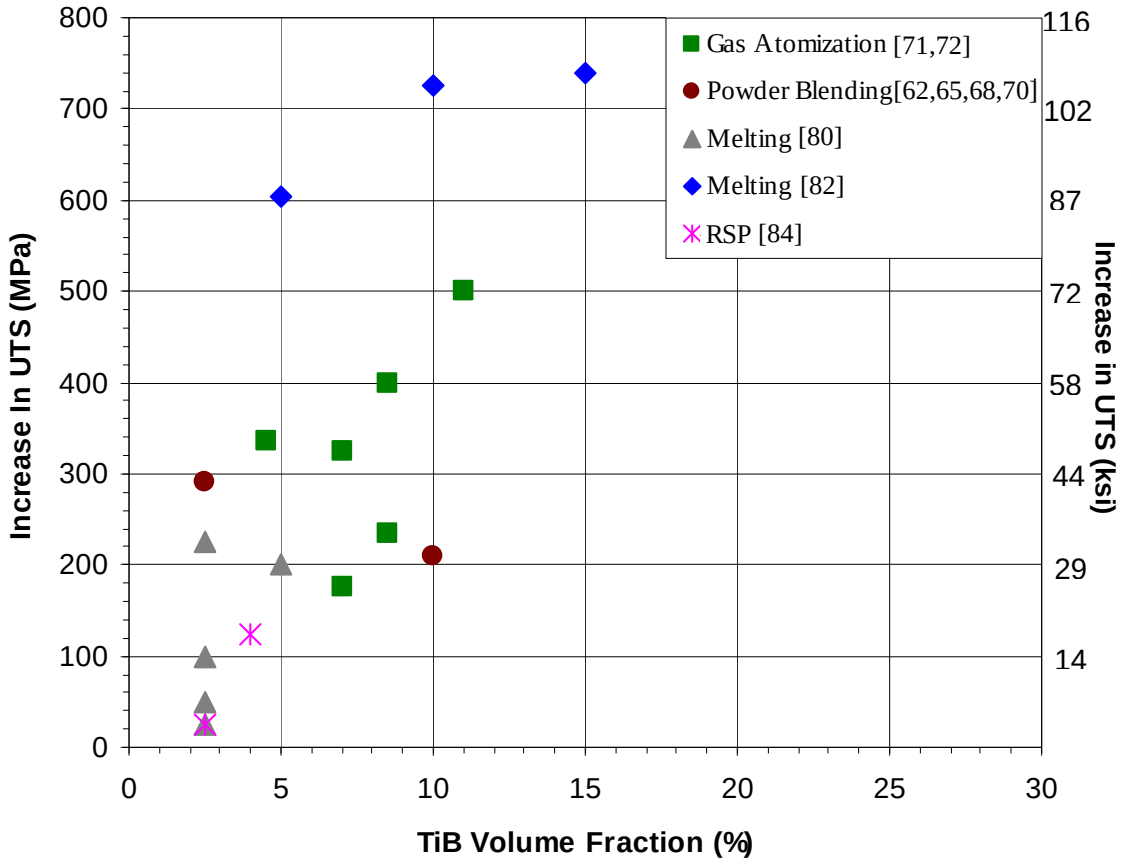

Figure 1.15. Increase of ultimate tensile strength due to addition of boron to titanium alloys via various processing methods. The strength of the titanium alloys without the boron additions was subtracted from the TiB alloys to obtain the increase in strength due to the addition of boron. (Figure modified from Godfrey et al.[77])

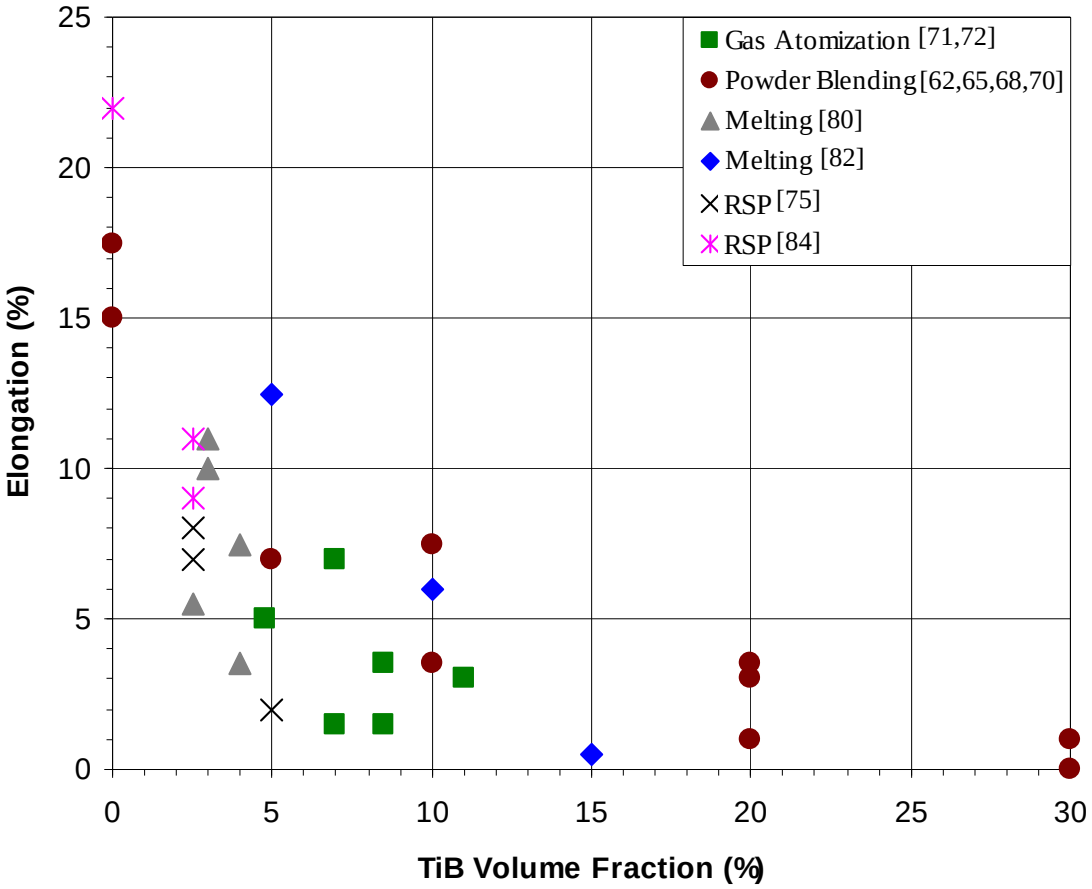

Figure 1.16. Ductility of titanium-boron alloys due to addition of boron to titanium alloys via various processing methods. (Figure modified from Godfrey et al.[77])

This increase in strength and loss of ductility is expected based on the previous discussion of oxygen as a strengthener in titanium. Tsang et al.[81] studied the influence of boron additions on CP titanium and observed that the morphology of the TiB particles plays a role in the tensile was increased, ductility was reported to drastically decrease (~12% decrease over 10 vol.% TiB) while the strength was observed to be unaffected. Several research groups have shown that when titanium-boron alloys are subjected to secondary processing (forging, rolling or extrusion), the TiB particles aligned along the working direction.[64,67,71,72,75] When the TiB particles are aligned, the titanium-boron alloys were shown to have highly anisotropic properties with the highest strength and lowest ductilities obtained along the working direction. Several models have been proposed to explain the tensile trends with TiB particle size and distribution.[3,69,74,79,81] These models are comprised of strengthening due to load sharing, grain size (Hall-Petch), and Orowan (Gb/l) strengthening of varying degrees. All of these models are purely data-fit with no scientific basis explaining the observed relationships.

1.3.3.2 Fatigue Properties

In contrast to tensile properties, only a couple of groups have studied the influence of boron additions on the fatigue properties of titanium alloys.[62,65,68,70,86] As expected based on the tensile results, fatigue strength/life has been observed to increase with the addition of boron to a titanium alloy. It is common in metals that the factors that increase the yield strength also increase the high cycle fatigue strength/life. Therefore, based on the tensile properties of titanium-boron alloys, several factors could influence the fatigue strength/life including the density (porosity), oxygen concentration, matrix

grain size, and the size, morphology, orientation and distribution of the TiB particles. As with tensile properties, though, there presently is no clear understanding of the influence of these factors on fatigue strength/life of titanium-boron alloys.

Saito et al.[62,65,68,70] has studied the influence of boron additions on Ti-6Al-4V and Ti-4.3Fe-6.8Mo-1.4Al-1.4V. In each case, they observed an increase in the fatigue strength at 10^7 cycles. The Ti-6Al-4V-10vol.%B was reported to have a fatigue strength of ~87 ksi (~600 MPa) while the Ti-6Al-4V processed in the same manner but without boron had a fatigue strength of ~65 ksi (~450MPa). The Ti-4.3Fe-6.8Mo-1.4Al-1.4V-XB alloy was reported to have a fatigue strength of ~152 ksi (~1050 MPa) while no fatigue strength was report for this alloy without boron additions. When the failed test bars were examined, it was determined that crack initiation occurred at pores in the material and not at TiB particles or in the matrix alloy. Fatigue cracks propagated through the matrix and were stopped at particles. After a period of time, it appeared the cracks cut through or fracture the particles and continued propagating through the matrix. Srivatsan et al.[86] studied the influence of TiB particle orientation on fatigue strength/life for a Ti-6Al-4V-XB alloy. They observed the fatigue strength/life to be as good or better than Ti-6Al-4V when tested parallel to the extrusion direction. When the failed test bars were examined, it was determined that failure occurred due to a combination of particle pull-out, interface cracking and rapid crack propagation through the matrix. They attributed failure to be due to constraints in deformation induced in the matrix by the particle coupled with local intrinsic concentration effects at the matrix particle interfaces.

1.4 Summary

The influence of boron additions on processing, microstructure, physical and mechanical properties of various titanium alloys has been investigated since 1950's. However, only during the past 25 years has boron been added to titanium alloys to obtain desirable microstructures and mechanical properties for several niche applications. The presence of the boron enhances the tensile and fatigue strengths as well as the wear resistance of the alloy as compared to the conventional titanium alloy. Although these improvements in mechanical properties are attractive, there are still a few major obstacles in using these composites for commercial applications. (1) Microstructural evolution in boron containing titanium alloys is not well understood. Therefore, the relationship between microstructure and mechanical properties in these alloys needs further investigation to optimize the mechanical properties of boron containing titanium alloys for specific commercial applications. (2) Strengthening and deformation mechanisms of titanium–boron containing alloys is not well understood. Therefore, the relationship between microstructure and mechanical behavior of these alloys needs further investigation to understand individual and combined modes of plastic deformation of the titanium alloy matrix and TiB particles. (3) The cost of producing these alloys is too high compared to the specific property benefit over the current materials used for given application(s). Advances in the understanding of phase transformations, mechanical behavior and cost-effective production methods could ultimately lead to the widespread commercial use of titanium-boron alloys.

1.5 References

1. Abkowitz, Stanley, Abkowitz, Susan M., Fisher, Harvey, Schwartz, Patricia J. *JOM.* **56(5).** 2004. pp. 37.

2. Ravi Chandran, K.S., Panda, K.B., Sahay, S.S. *JOM.* **56(5).** 2004. pp. 42.

3. Kumari, Sweety, Prasad, N. Eswara, Chandran, K.S. Ravi, Malakondaiah, G. *JOM.* **56(5).** 2004. pp. 51.

4. Ravi Chandran, K.S., Miracle, Daniel B. *JOM.* **56(5).** 2004. pp. 32.

5. Boyer, R., Welsch, G., Collings, E.W. **ASM Materials Properties Handbook: Titanium Alloys.** *ASM International, Materials Park, OH.* 1994.

6. Burgers, W.G. *Physica 1*. 1934. pp. 561.

7. Newkirk, J.B., Geisler, A.H. *Acta Met. 1*. 1953. pp. 370.

8. Leutjering, G. Williams, J.C. **Titanium (Engineering Materials and Processes).** *Springer-Verlag Publishing*. 2003.

9. Miska, K. *Materials Engineering.* **79-80.** 1974. pp. 61.

10. Paton, N.E., Williams, J.C., Rauscher, G.P. *Titanium Science and Technology.* 1973. pp. 1049.

11. Blackburn, M.J., Williams, J.C. *Trans. ASM*. **62.** 1969. pp. 398.

12. Williams, J.C., Baggerly, R.G., Paton, N.E. *Metall. Trans. A* **33.** 2002. pp. 837.

13. Williams, J.C., Sommer, A.W., Tung, P.P. *Metall. Trans. A.* **3(11).** 1972. pp. 2979.

14. Jones, I.P., Hutchinson, W.B. *Acta Met.* **29.** 1981. pp. 951.

15. Paton, N.E., Backofen, W.A. *Metall. Trans. 1*. 1970. pp. 2839.

16. Schutz, R.W., Thomas, D.E. **Corrosion, Metals Handbook, 9th Edition, Volume 13.** *ASM Metals Park, USA.* 1987. pp. 669.

17. Sakurai, K., Itabashi, Y., Komatsu, A. *Titanium '80: Science and Technology.* AIME, Warrendale, USA. 1980. pp. 299.

18. Helm D. **Fatigue Behavior of Titanium Alloys.** *TMS Warrendale, USA. 1999.* pp. 291.

19. Jaffe, R.I. **Titanium Steam Turbine Blading.** *Pergamon Press, New York, USA.* 1999.

20. Breme, J. *6th World Conference on Titanium.* Les Editions de Physique, Les Ulis, France. 1988. pp. 57.

21. Brunette, D.M., Tengvail, P., Textor, M., Thomsen, M. **Titanium in Medicine.** *Springer-Verlag, Berlin, Germany.* 2001.

22. Hosonuma, M., Shimamune, T. *6th World Conference on Titanium.* Les Editions de Physique, Les Ulis, France. 1988. pp. 495.

23. Breme, J., Biehl, V., Wack, T. Eisenbarth, E. *Titanium '99: Science and Technology.* St. Petersburg, Russia. 2000. pp.1187.

24. Albrecht, J., Leutjering, G. Nicolai, H-P., Liesner, C. **Fatigue 2002**, *EMAS, Warley, UK.* 2002. pp. 2085.

25. Froes, F.H., Allen, P.G., Niinomi, M. **Non-Aerospace Applications of Titanium.** *TMS Warrendale, USA.* 1998. pp. 3.

26. Blenkinsop, P.A. *Titanium '95: Science and Technology.* The University Press, Cambridge, UK. 1996. pp. 1.

27. Boyer, R.R. *Titanium '95: Science and Technology.* The University Press, Cambridge, UK. 1996. pp. 41.

28. Shira, C., Froes, F.H. **Non-Aerospace Applications of Titanium.** *TMS Warrendale, USA.* 1998. pp. 331.

29. Froes, F.H. **Non-Aerospace Applications of Titanium.** *TMS Warrendale, USA.* 1998. pp. 317.

30. Borradaile, J.B., Jeal, R.H. *Titanium Science and Technology*. 1984. pp. 141.

31. Boyer, R.R. *Mat. Sci. & Eng. A.* **(A213).** 1996. pp. 103.

32. Boyer, R.R. **Beta Titanium Alloys in the 1990s.** *TMS Warrendale, USA.* 1993. pp. 335.

33. Boyer, R.R. **Beta Titanium Alloys.** *Societe Francaise de Metallurgie et de Materiaux, Paris, France.* 1994. pp. 253.

34. Wang, K., Gustavson, L., Dumbleton, J. *Titanium '92: Science and Technology.* TMS Warrendale, USA. 1993. pp. 2697.

35. Fanning, J.C. *Titanium '95: Science and Technology.* The University Press, Cambridge, UK. 1996. pp. 1800.

36. Niinomi, M., Kuroda, D., Fukunaga, K., Fukui, H., Kato, Y., Yashiro, T., Suzuki, A., Hasegawa, J. *Titanium '99: Science and Technology.* St. Petersburg, Russia. 2000. pp.1195.

37. Friedrich, H., Kiese, J., Haldenwanger, H-G., Stich, A. *Proceedings of the 10th World Conference on Titanium.* Wiley-VCH, Weinheim, Germany. 2003.

38. Sommer, C., Peacock, D. *Titanium '95: Science and Technology.* The University Press, Cambridge, UK. 1996. pp. 1836.

39. Partridge, P.G. *Met. Rev.* **12.** 1967. pp.169.

40. Yoo, H.M. *Metall. Trans. A.* **12A.** 1981. pp. 409.

41. Paton, N.E., Williams, J.C. *2nd International Conference on the Strength of Metals and Alloys*. 1970. pp. 108.

42. Paton, N.E., Baggerly, R.G., Williams, J.C. Rockwell Report. 1976.

43. Williams, J.C., Leutjering, G. *Titanium Science and Technology*. 1984. pp. 671.

44. Williams, J.C., Thompson, A.W., Rhodes, C.G., Chestnutt, J.C. *Titanium and Titanium Alloys*. 1982. pp. 467.

45. Welsch, G., Leutjering, G., Gazioglu, K., Bunk, W. *Metall. Trans*. **8A.** 1977. pp. 169.

46. Weissmann, S., Shrier, A. **The Science, Technology and Application of Titanium.** *Pergamon Press, Oxford*. 1970. pp. 441.

47. Blackburn, M.J., Williams, J.C. *Trans. ASM*. **62.** 1969. pp. 398.

48. Williams, J.C., Baggerly, R.G., Paton, N.E. *Metall. Trans. A* **33.** 2002. pp. 837.

49. Leutjering, G., Weissmann, S. *Acta. Met.* **18.** 1970. pp. 785.

50. Hall, E.O. *Proceedings of the Physical Society*. London B64. 1951. pp. 747.

51. Petch, N.J. *Journal of the Iron and Steel Institute*. London 174. 1953. pp. 25.

52. Terlinde, G. **PhD Thesis.** *Ruhr-University Bochum.* 1978.

53. Terlinde, G., Leutjering, G. *Metall. Trans. A.* **13(7).** 1982. pp. 1283.

54. Hirth, J.P. *Metall. Trans*. **3.** 1972. pp. 3047.

55. Hirth, J.P., Balluffi, R.W. *Acta Met.* **21.** 1973. pp. 929.

56. Lin, F.S., Starke, E.A. Chakrabortty, S.B., Gylser, A. *Metall. Trans. A.* **15A.** 1984. pp. 1229.

57. Mills, M.J., Hou, D.H., Suri, S., Viswanathan, G.B. *Boundaries and Interfaces in Materials*. TMS Warrendale, PA. 1998. pp. 295.

58. Suri, S., Viswanathan, G.B., Neeraj, T., Hou, D.H., Mills, M.J. *Acta Mater.* **47.** 1999. pp.1019.

59. Williams, J.C., Blackburn, M.J. **Order Alloys**. *Claitors Press.* 1970. pp. 425.

60. Schmid, Z.E. *Elektrochem.* **37.** 1931. pp. 447.

61. Banerjee, R., Collins, P.C., Genc, A., Fraser, H.L. *Mater. Sci. Eng. A.* **A358.** 2003. pp. 343.

62. Saito, T., Takamiya, H ., Furuta, T. *Titanium '95: Science and Technology.* 1995. pp. 2859.

63. Banerjee, R., Genc, A., Collins, P.C., Fraser, H.L. *Met. and Mater. Trans.* **35A.** 2004. pp. 2143.

64. Fan, Z., Chandrasekaran, L., Ward-Close, C.M., Miodownik, P. *Scripta Met.* **32(6).** 1995. pp. 833.

65. Saito, T., Furuta, T., Takamiya, H. *Titanium '95: Science and Technology.* 1995. pp. 2763.

66. Banerjee, R., Collins, P.C., Genc, A., Tiley, J. Fraser, H.L. *Titanium Science and Technology '03*. Munich. 2004. pp. 2547.

67. Fan, Z., Miodownik, P. *Acta Metall.* **44.** 1995. pp. 93.

68. Saito, T., Takamiya, H ., Furuta, T. *Mat. Sci. & Eng. A.* **A243.** 1998. pp. 273.

69. Hanusiak, W., Yolton, C.F., Fields, J., Hammond, V., Grabow, R. *JOM.* **56(5).** 2004. pp. 49.

70. Saito, T., Furuta, F., Yamaguchi, Y. **Recent Advances In Titanium Metal Matrix Composites.** *TMS Warrendale, PA.* 1995. pp. 33.

71. Yolton, C.F., Moll, J.H. *Titanium '95: Science and Technology.* 1996. pp. 2755.

72. Yolton, C.F. *JOM.* **56(5).** 2004. pp. 56.

73. Hu, D., Johnson, T.P., Loretto, M.H. *Advances In Powder Metallurgy and Particulate Materials*. MPFI. 1995. pp. 109.

74. Tamirisakandala, S., Bhat, R.B., Ravi, V.A., Miracle, D.B. *JOM.* **56(5).** 2004. pp. 60.

75. Soboyelo, W.O., Lederich, R.J., Sastry, S.M.L. *Acta Metall.* **42(8).** 1994. pp. 2579.

76. Zhao, F., Fan, Y. *Titanium '95: Science and Technology.* 1996. pp. 2688

77. Godfrey, T.M.T., Wisbey, A., Goodwin, P.S., Bagnall, K., Ward-Close, C.M. *Mater. Sci. Eng. A.* **A282.** 2000. pp. 240.

78. Goodwin, P.S., Wisbey, A., Ubhi, H.S., Kulikowski, Z., Gasson, P., Ward-Close, C.M. *Titanium '95: Science and Technology.* 1995. pp. 2874.

79. Philliber, J.A., Dary, F.C., Zok, F.W., Levi, C.G., Blenkinsop, P.A. *Titanium '95: Science and Technology.* 1995. pp. 2714.

80. Dubey, S., Lederich, R.J., Soboyejo, W.O. *Metall. Trans. A* **28.** 1997.

81. Philliber, J.A., Dary, F.C., Zok, F.W., Levi, C.G. **Recent Advances In Titanium Metal Matrix Composites.** *TMS Warrendale, PA.* 1995. pp. 213.

82. Tsang, H.T., Chao, C.G., Ma, C.Y. *Scripta. Met.* **37(9).** 1997. pp. 1359.

83. Zhang, X., Lu, W., Zhang, D., Wu, R., Bian, Y., Fang, P. *Scripta. Met.* **41(1).** 1999. pp. 39.

84. Sastry, S.M.L., Peng, T.C., O'Neal, J.E. *5th International Conference on Titanium*. Munich. 1984. pp. 397.

85. Saito, Takashi. *JOM.* **56(5).** 2004. pp. 33.

86. Srivatsan, T.S., Soboyejo, W.O., Lederich, R.J. **Recent Advances In Titanium Metal Matrix Composites.** *TMS Warrendale, PA.* 1995. pp. 225.

CHAPTER 2

CP-TI AND TI-B POWDER MATERIAL VIA ARMSTRONG PROCESS

2.1 Introduction

2.1.1 Titanium Processing

All titanium alloys are produced from two natural ores: rutile (TiO_2) and ilmenite ($FeTiO_3$). From these ores, titanium sponge is produced as the input raw material for titanium alloys. Historically, two major processes, the Kroll[1] and Hunter[2] processes, have been used to obtain titanium sponge from these ores. Both of these processes use similar operations for the extraction of titanium: (1) chlorination of the ore to produce $TiCl_4$; (2) purification of $TiCl_4$ by distillation; (3) sodium or magnesium reduction of $TiCl_4$ to produce titanium sponge; (4) purification of titanium sponge to remove by-products of reduction process; and (5) crushing of titanium sponge for use in subsequent melting to create titanium alloys. The Kroll process (Figure 2.1) uses magnesium to reduce $TiCl_4$ while the Hunter process uses molten sodium as the reducing agent. Since the 1940s, very few processing plants have used the Hunter process, as it is less cost effective than using magnesium to reduce $TiCl_4$ as in the Kroll process. Regardless of the process used, producing titanium sponge is costly and time consuming. Although the

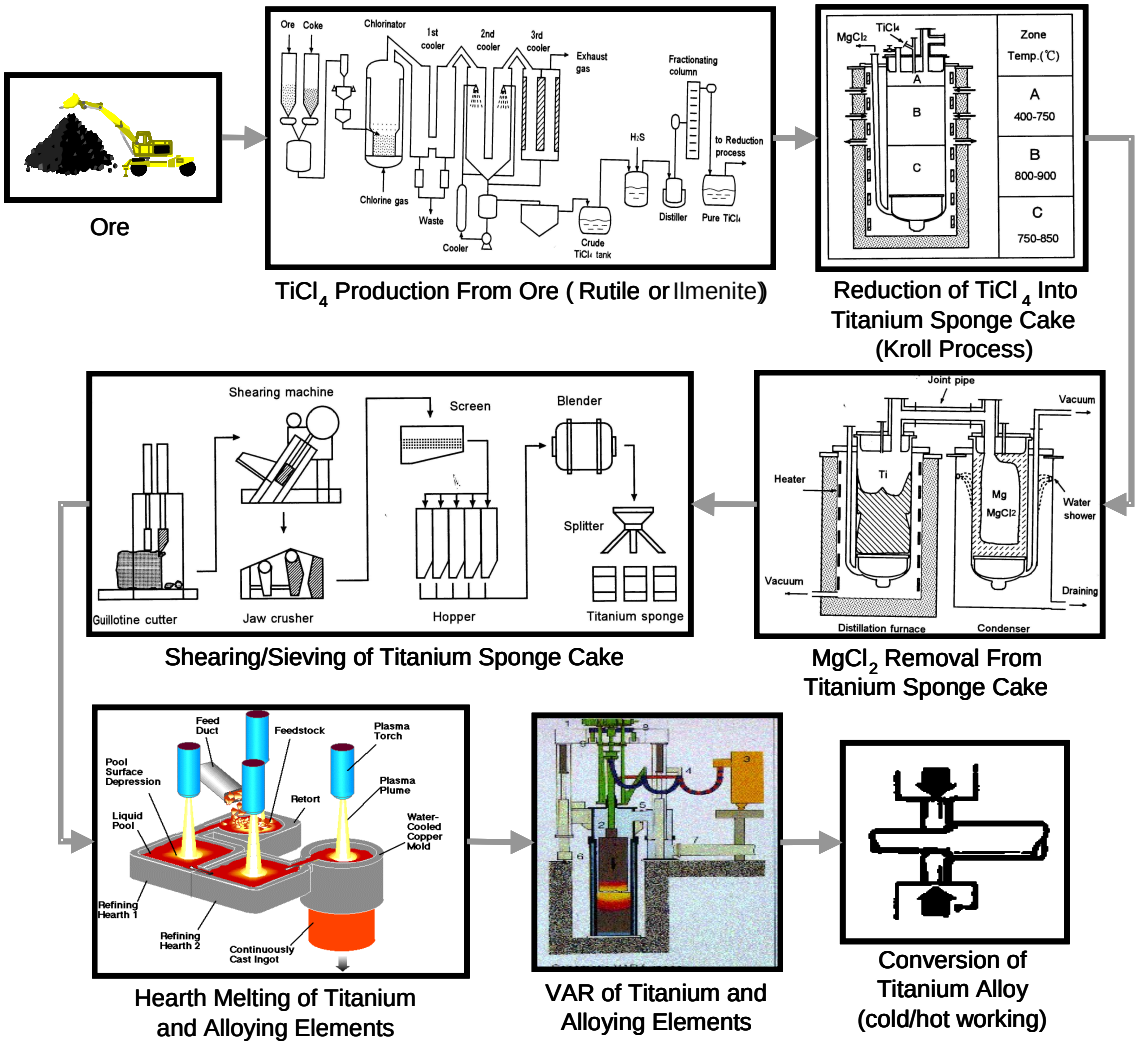

Figure 2.1. Conventional processing of titanium using the Kroll process to reduce $TiCl_4$ to titanium sponge[3,31]

Kroll process is widely used in industry and the Hunter process is used to a much lesser extent, lower cost alternatives to these processing methods are currently being investigated in an effort to reduce the overall cost of titanium alloys. Cost analysis of titanium raw material, regardless of the process used, shows that over 50% of the cost is derived from the production of $TiCl_4$ from rutile and ilmenite.[3] Therefore, great emphasis has been placed on lowering the cost of extracting titanium from ores by alternate means.

In the last 15 years, several new processes have been developed that aim to produce titanium through more cost effective methods. Ginatta[4] and Rio Tinto[5] aimed to produce molten titanium metal directly whereas processes like the Armstrong[6-31] and Idaho Titanium Technologies (ITT) have used sodium and magnesium, respectively, to produce titanium and titanium alloys in particulate/powder form via reduction of $TiCl_4$. Electrolytic reduction of rutile in halide salts has also been used in the FFC-Cambridge process[6] and MER and EMR/MSE processes[32] to produce titanium products which can be used as titanium feedstock. Although all of these processes have successfully demonstrated the ability to produce some form of titanium from rutile (TiO_2) or $TiCl_4$ in a laboratory environment, only the Armstrong process has been scaled-up to produce titanium in significant quantities. The commercialization feasibility of any of these processes is still an open question. In addition, the titanium material from these processes could potentially be used as input material for conventional ingot metallurgy or as titanium powder for direct consolidation.

2.1.2 Titanium-Boron Processing

Several methods for adding boron to titanium alloys have been studied to obtain desirable microstructures and mechanical properties.[33-44] Three standard processes have been used to create titanium alloys with boron: melting, conventional powder metallurgy (PM), and rapid solidification processes (RSP). PM methods have been the most widely utilized as these processes generate the most desirable combination of microstructure and properties albeit at a high cost.

Each PM method produces powders of varying size, morphology and purity, that affects the ability to compact the powder. The downstream processing of the powder, including compaction and working processes, subsequently influence the density, size, morphology and composition of the resulting alloy's microstructure. To alter/control the morphology and chemistry of starting powder product, a wide variety of methods have been used. Direct gas atomization[33-37], rotating electrode (REP) or plasma rotating electrode process (PREP)[35-38], and rapid solidification processes[35-37,45-52]. The direct gas atomization process has several steps: (1) melting input material, virgin raw materials or clean pre-alloyed stock; (2) bottom pouring the melt; (3) atomizing the molten stream with high-pressure argon gas; and (4) cooling the particulate under an argon atmosphere to room temperature (Figure 2.2a). The rotating electrode process (REP) or plasma rotating electrode process (PREP) entails rotating a titanium bar in an inert chamber while a heat source (REP - electric arc; PREP – plasma torch) melts the bar material. The molten material is then expelled from the bar and solidifies into spherical droplets (Figure 2.2b). The only RSP process that currently has shown potential for scale-up is also the most recent rapid solidification process that has been developed, the LENS™ (Laser

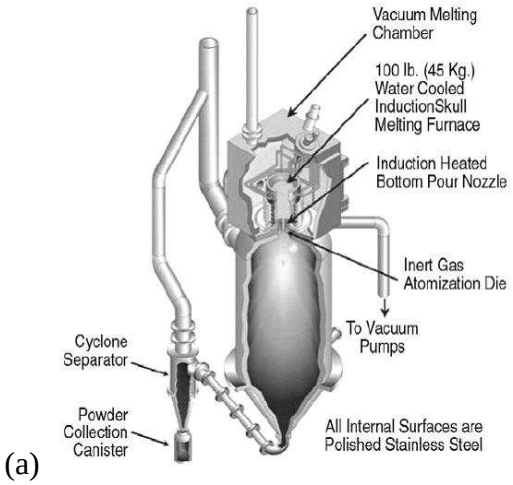

(a)

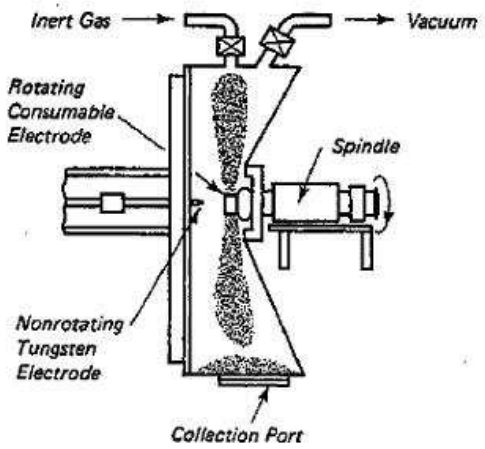

(b)

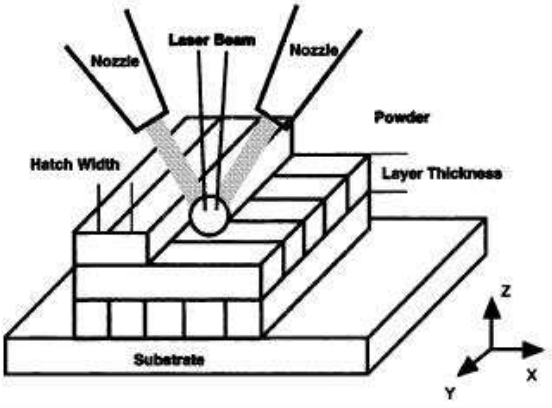

(c)

Figure 2.2. Schematics of (a) gas atomization process (GA)[33-37], (b) REP (rotating electrode process) and PREP (plasma rotating electrode process) process[35-38], and (c) LENS™ (Laser Engineered Net Shaping) method[46] used to produce titanium alloys containing boron in powder form.

Engineered Net Shaping) process[46]. In the LENS™ process, a metal base plate is moved accordingly under a stationary laser rapidly melting and re-solidifying blended elemental powder that is fed continuously into the laser beam (Figure 2.2c).[46]

Although PM methods can produce alloys with homogeneous and stable structures not available using conventional melt methods, these processes area not cost effective methods of manufacturing titanium powder and the probability of creating inclusions and defects in the powder is high. These processes are well-accepted production processes for nickel and iron base alloys; but are more difficult and costly for titanium alloys. Thus, the PM processes are not widely used in lieu of conventional processing.

2.1.3 Armstrong Titanium Processing

The purpose of this research is to examine titanium alloys produced using a novel titanium processing method called the Armstrong process[6-31] (Figure 2.3). This process produces titanium powder (pure titanium or titanium alloys) from $TiCl_4$ (and other metal halides as required to obtain the desired alloy composition) using sodium as a reducing agent. Unlike conventionally processed titanium, the Armstrong reduction of $TiCl_4$ produces pure titanium as a continuous process with the final product in a useable form. The final product of the Armstrong process is titanium powder, which can be directly consolidated without melting, or melted (Figure 2.4). Compared to the Kroll or Hunter processes, the direct consolidation of Armstrong process powder eliminates several processing steps/restrictions including: (1) restriction of batch processing of material (affects downtime of process), (2) multiple cleaning steps, (3) crushing of material,

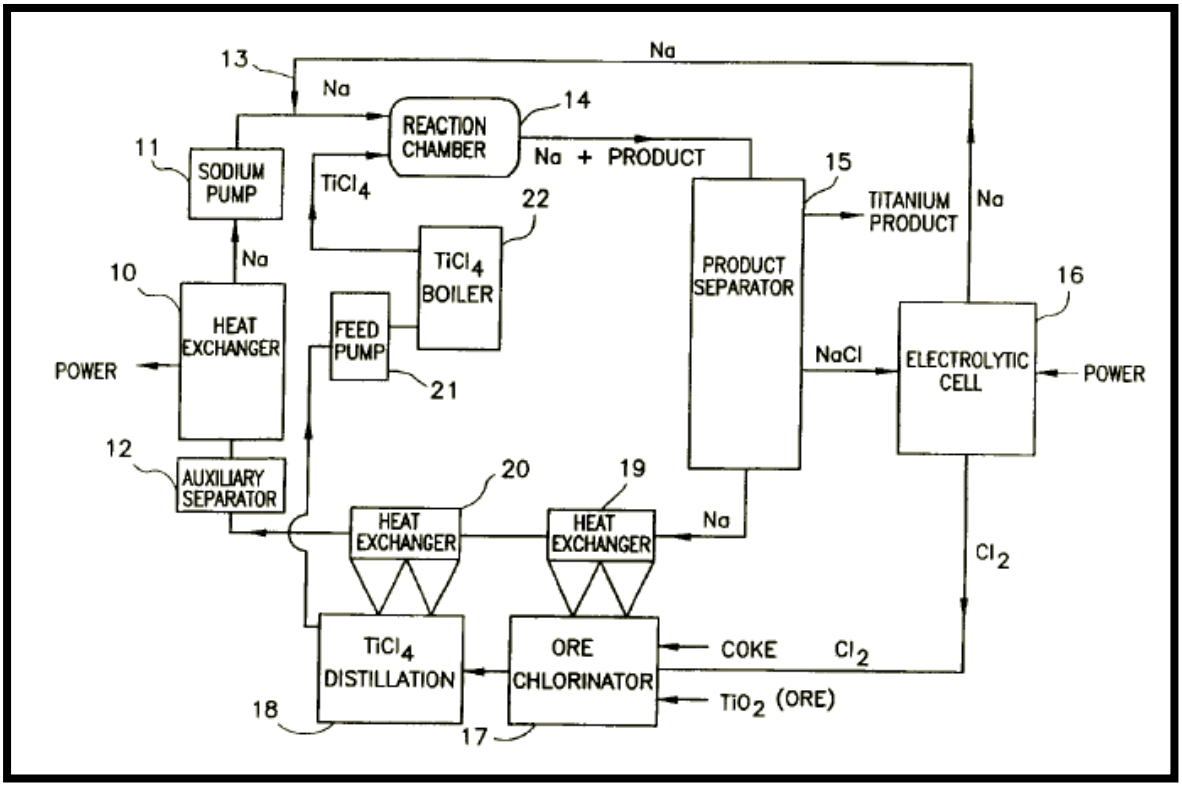

Figure 2.3. Novel processing to reduce $TiCl_4$ (and possibly rutile, TiO_2, in the near future) to titanium powder using the Armstrong process.[15-31]

(a) Novel processing of titanium (with melting):

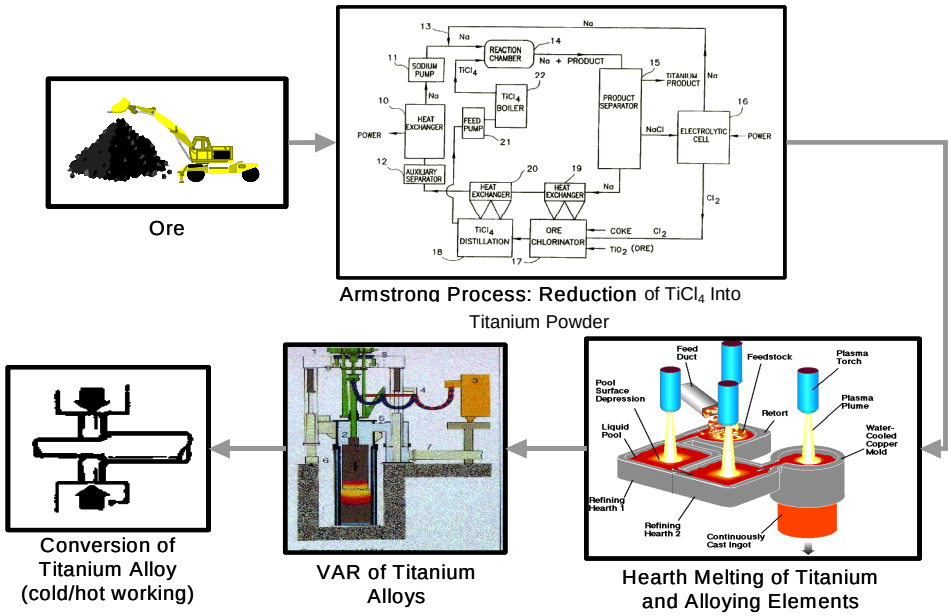

(b) Novel powder processing of titanium:

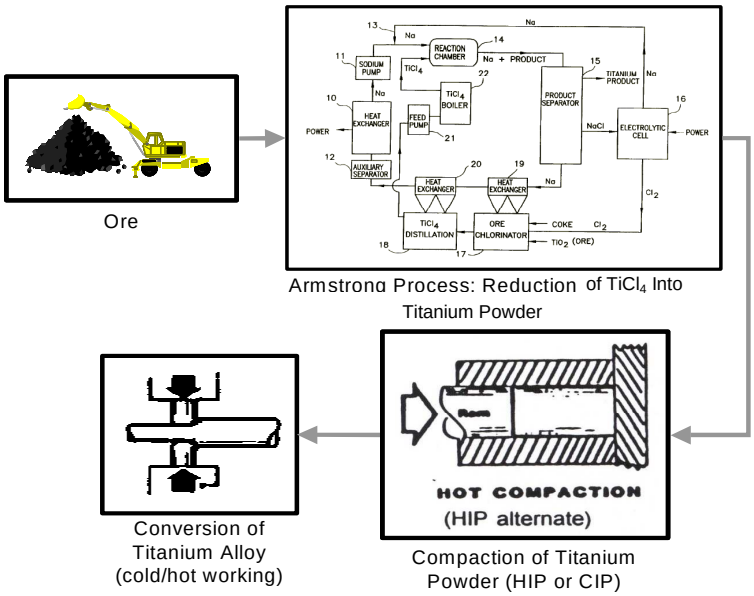

Figure 2.4. Novel processing of titanium using the Armstrong process to reduce $TiCl_4$ to titanium powder. (a) processing using melting; and (b) powder process.[3,15-31]

(4) multiple melting steps, and (5) several handling steps to consolidate the raw material to feed into the melt as well as handling of ingots between melting steps. In principle, the elimination of these processing steps significantly reduces or eliminates capital and labor cost, impurities including iron and nickel that could be picked up from the reduction vessel, and melt-related defects including hard alphas, high density inclusions, beta flecks, and other alpha stabilized defects.[53]

Currently, all of the Ti-B alloy production processes use conventionally processed titanium sponge or ingot metallurgy product as the starting material to produce a titanium alloy with boron. The input titanium material is produced from titanium sponge that was created by the Kroll[1] or Hunter[2] processes and subsequently processed utilizing one of the previously mentioned methods. The titanium powder produced using the Armstrong process does not require titanium sponge or mill product as the input material like the melting, PM or RSP methods. It produces alloyed titanium powder directly from $TiCl_4$ and other chlorides eliminating the process steps in creating titanium sponge and minimizing the opportunity for introduction of inclusions from handling and subsequent processing. The purpose of this research is to examine directly consolidated commercially pure (CP) titanium and Ti-B alloys produced using a novel titanium processing method, the Armstrong process[6-31,54-56].

2.2 Materials and Methods

2.2.1 Powder Processing

Commercially pure (CP) titanium and titanium alloyed powders with 0.8 and 0.9 wt.% (3.4 and 3.9 at.%) boron was procured from International Titanium Powder (ITP)

Company (Lockport, IL). The powder was produced using the Armstrong process in which the initial elements were added in the form of chlorides producing CP-Ti and Ti-B alloys with a desired chemistry as shown in Table 2.1. It should be noted that the boron containing powders were the first process runs to attempt to alloy titanium with boron using the Armstrong process.

2.2.2 Chemical Analysis

Chemical analysis was performed on of the three lots of powder with aim chemistries as shown in Table 2.1. The specification chemistries of Grade 2 and Grade 4 CP-Ti are also shown for comparison purposes. The chemistry of the powder was determined using ICP/MS (Perkin-Elmer Elan 5000 Inductively Coupled Plasma-Mass Spectrometer per NIST, Brammer, and Certified Aqueous standards) for the elements boron, iron, sodium, and nickel; combustion for carbon and inert gas fusion for hydrogen, nitrogen, and oxygen (LECO TC600 and TCH600 instruments per ASTM E 1409 and ASTM E 1447); and GD/MS (ThermoFisher Scientific VG9000 High Resolution Glow Discharge Mass Spectrometer per ASTM F1710-97, F1593-97, and F2405-04) for chlorine. Concentration of titanium was determined from the balance of the other elements. The concentration of each element was determined for one lot of powder for CP-Ti, Ti-0.8B and Ti-0.9B, and reported in weight percent.

2.2.3 Physical Characteristics

The physical characteristics of the CP-Ti, Ti-0.8B and Ti-0.9B lots of powder were characterized by measuring the size of the powder. To quantify the average size and

	CP-Ti[#]	Ti+0.8wt.%B[#]	Ti+0.9wt.%B[#]	CP-Ti Grade 2*	CP-Ti Grade 4**
Ti	Balance	Balance	Balance	Balance	Balance
O	0.4% max.	0.4% max.	0.4% max.	0.2% max.	0.4% max.
B	-	0.800%	0.900%	-	-
Fe	0.5% max.	0.5% max.	0.5% max.	0.3% max.	0.5% max.
Na	0.1% max.	0.1% max.	0.1% max.	0.1% max.	0.1% max.
Cl	0.1% max.	0.1% max.	0.1% max.	0.1% max.	0.1% max.
Ni	0.1% max.	0.1% max.	0.1% max.	0.1% max.	0.1% max.
C	0.08% max.	0.08% max.	0.08% max.	0.08% max.	0.08% max.
H	0.0125% max.	0.0125% max.	0.0125% max.	0.0150% max.	0.0125% max.
N	0.05% max.	0.05% max.	0.05% max.	0.05% max.	0.05% max.

CP-Ti, Ti-0.8B and Ti-0.9B produced using the Armstrong process.
* Grade 2 CP-Ti chemistry per AMS4902.
** Grade 4 CP-Ti chemistry per AMS 4901.

Table 2.1. Target compositions of commercially pure (CP) titanium, Ti-0.8B and Ti-0.9B powder produced using the Armstrong process.

size distribution of the titanium powder, the CP-Ti, Ti-0.8B and Ti-0.9B powder was sieved using ½ inch, 4 (0.187 in.), 10 (0.0787 in.), 25 (0.0278 in.), 50 (0.0117 in.), 100 (0.0059 in.), 150 (0.0041 in.) and 200 (0.0029 in.) mesh sieves. The weight of powder in each size range was measured and the distribution of powder size is reported as percent of total weight.

2.2.4 Metallography

Metallographic mounts containing samples of each of the three lots of powder were used for material characterization. Each lot of powder was mounted in methyl methacrylate epoxy resin set at 330^{o}F (165^{o}C) at a pressure of 4,200 psi (29 MPa) for ~7 minutes. The metallographic mounts were then wet ground and polished as outlined in Table 2.2. After grinding and polishing, the mounts were swab etched at room temperature with a solution of 10% oxalic acid, 1% HF, and 89% H_2O for characterization by scanning electron microscopy.

2.2.5 Light Microscopy (LM)

The CP-Ti, Ti-0.8B and Ti-0.9B lots of powder were characterized using light microscopy (LM). Each lot of powder was characterized as-received in powder form and after being mounted, ground, polished and etched. All analysis was completed using ZeissAxioplan 2, ZeissAxiovert 100A, and 200MAT, and ZeissAxoskop 2 microscopes each equipped with a Zeiss Axiocam MRc/MRc5 camera for direct digital imaging.

2.2.6 Scanning Electron Microscopy (SEM)

The CP-Ti, Ti-0.8B and Ti-0.9B lots of powder were characterized using scanning electron microscopy (SEM). Each lot of powder was characterized as-received in powder form and after being mounted, ground, polished and etched. All SEM analysis was completed using a JEOL field emission microscope with a Tungsten filament and a Sirion field emission microscope, both at 15-20 kV accelerating voltage.

2.3 Results

2.3.1 Chemical Analysis

Chemical analysis was performed on the as-received titanium powder produced using the Armstrong process. The target compositions were commercially pure (CP) Grade 4 titanium material with 0.0, 0.8 and 0.9 wt.% boron. Table 2.3 shows the composition of the three lots of titanium powder produced. The specification compositions for Grade 2 and Grade 4 CP-Ti were also included in Table 2.3 for comparison. The oxygen and iron concentrations for the CP-Ti powder are 0.13 wt.% and <0.001 wt.%, respectively. The CP-Ti powder has 0.27 wt.% less oxygen and 0.50 wt.% less iron than specification maximum for Grade 4 CP-Ti material. The oxygen and iron concentrations for the Ti-0.8B and Ti-0.9B powder range from 0.58 – 0.61 wt.% and ~0.02 wt.%, respectively. The Ti-0.8B powder has 0.18 wt.% more oxygen and 0.48 wt.% less iron than specification maximum for Grade 4 CP-Ti. The Ti-0.9B powder has 0.21 wt.% more oxygen and 0.48 wt.% less iron than specification maximum for Grade 4 CP-Ti. The three lots of titanium powder also contain trace amounts of sodium, chlorine, nickel, hydrogen and carbon, which were significantly less then the maximum allowed in

Procedure Step	Grit/Abrasive	RPM	Pressure per mount (lbs.)	Time (sec.)
1	120	300	5	30-50
2	180	300	5	30-50
3	240	300	5	30-50
4	320	300	5	30-50
5	400	300	5	30-50
6	600	300	5	30-50
7	800	300	5	30-50
8	Colloidal Silica & Hydrogen Peroxide solution	150	5	120-180

Table 2.2. Standard metallographic grinding and polishing procedure.

in Grade 2 and Grade 4 CP-Ti specifications.

2.3.2 Physical Characteristics

The typical size distribution of the CP-Ti , Ti-0.8B and Ti-0.9B powder was measured using various sieves. The CP-Ti powder typical size distribution is ~75% at 4 mesh (0.185 in) and the remaining 25% at or below ½ inch mesh. The Ti-0.8B powder typical size distribution is: ~10% between 150 mesh (0.0041 in) to 50 mesh (0.0117 in); ~43% between 50 mesh (0.0117 in) to 25 mesh (0.0278 in); and the remaining 47% at or below 25 mesh (0.0278 in). For the Ti-0.9B powder, the typical size distribution is: ~38% between 50 mesh (0.0117 in) to 25 mesh (0.0278 in); and the remaining 62% at or below 25 mesh (0.0278 in). It should be noted that the abnormal morphology of the powder made the sieving more difficult. Since the powder was not spherical, the dimensions of the powder are not equivalent in all directions. Therefore, some powder could pass through some of the smaller sieve openings even though the powder larger in all other dimensions, thus producing a small error in the true measure of the powder size.

2.3.3 Light Microscopy (LM)

The CP-Ti, Ti-0.8B and Ti-0.9B powder is shown in the as-received condition in Figures 2.5, 2.6 and 2.7, respectively. The CP-Ti, Ti-0.8B and Ti-0.9B powder is an irregular shaped aggregate with a porous and friable appearance. The finer CP-Ti particles or aggregates are more equiaxed in shape while the larger CP-Ti particles are elongated in shape. The Ti-B particles or aggregates are predominately flat and elongated in shape with some finer, more equiaxed particles.

	CP-Ti[#]	Ti+0.8wt.%B[#]	Ti+0.9wt.%B[#]	CP-Ti Grade 2*	CP-Ti Grade 4**
Ti	Balance	Balance	Balance	Balance	Balance
O	0.130%	0.581%	0.606%	0.2% max.	0.4% max.
B	-	0.820%	0.900%	-	-
Fe	<0.001%	0.018%	0.019%	0.3% max.	0.5% max.
Na	0.049%	0.003%	0.005%	0.1% max.	0.1% max.
Cl	0.012%	0.002%	0.002%	0.1% max.	0.1% max.
Ni	<0.001%	<0.001%	<0.001%	0.1% max.	0.1% max.
C	0.006%	0.019%	0.015%	0.08% max.	0.08% max.
H	0.002%	0.005%	0.008%	0.0150% max.	0.0125% max.
N	0.002%	0.001%	0.007%	0.05% max.	0.05% max.

CP-Ti, Ti-0.8B and Ti-0.9B produced using the Armstrong process.
* Grade 2 CP-Ti chemistry per AMS4902.
** Grade 4 CP-Ti chemistry per AMS 4901.

Table 2.3. Comparison of chemical compositions of commercially pure (CP) titanium, Ti-0.8B and Ti-0.9B powder produced using the Armstrong process and typical Grade 2 and Grade 4 CP-Ti.

2.3.4 Scanning Electron Microscopy (SEM)

The CP-Ti, Ti-0.8B and Ti-0.9B powder is shown in the as-received condition in Figures 2.8 - 2.13. As observed with light microscopy, the powder is an irregular shaped aggregate with a sponge-like and friable appearance at lower magnifications (Figures 2.8 - 2.10). The finer CP-Ti particles or aggregates are more equiaxed in shape while the larger CP-Ti particles are more elongated in shape. The finer Ti-B particles or aggregates are more equiaxed in shape while the larger Ti-B particles are more similar to elongated in shape. At higher magnifications, the CP-Ti, Ti-0.8B and Ti-0.9B powder appears to be an aggregate of fine powder particles that have agglomerated (Figures 2.11 - 2.13).

CP-Ti, Ti-0.8B and Ti-0.9B powder in cross-section is shown in Figures 2.14 - 2.16, respectively. The cross-section of the CP-Ti and Ti-B powder shows again that the powder appears to be an aggregate of fine powder particles that have sintered together. The powder does not exhibit any microstructural features including second phases or grains. X-ray diffraction (XRD) or transmission electron microscopy (TEM) was not performed to validate whether α grains or TiB were present in the as-received powder and not observable using SEM. The fine CP-Ti particles that make up the aggregate are predominately cylindrical in shape with some spherical. The fine Ti-B particles that make up the aggregate are predominately cylindrical in shape with some spherical particles.

2.4 Discussion

2.4.1 Commercially Pure (CP) Titanium Powder Processing

The CP-Ti powder produced using the Armstrong process is similar in morphology to that of titanium sponge except on a finer scale. The Armstrong process

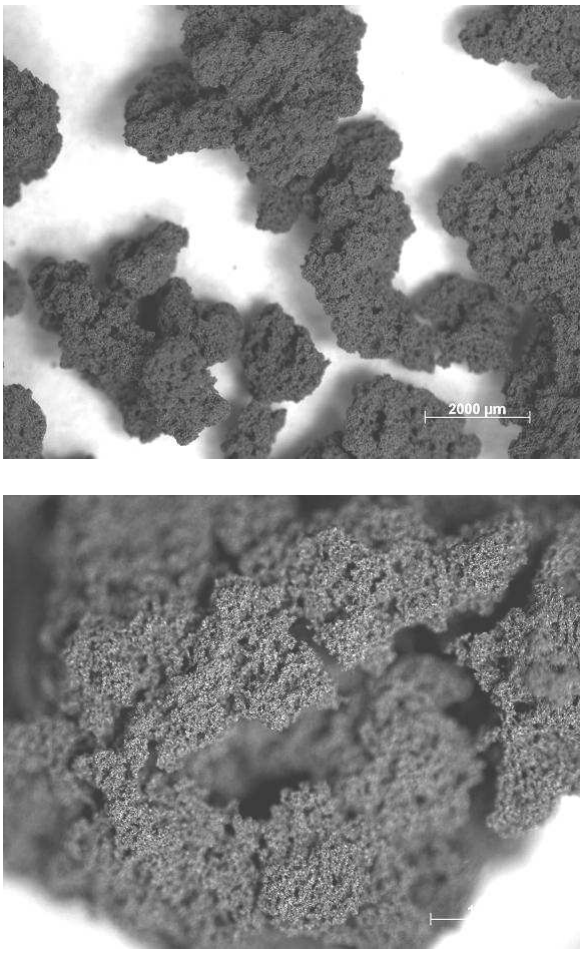

Figure 2.5. Macrographs of commercially pure (CP) titanium powder produced using the Armstrong process.

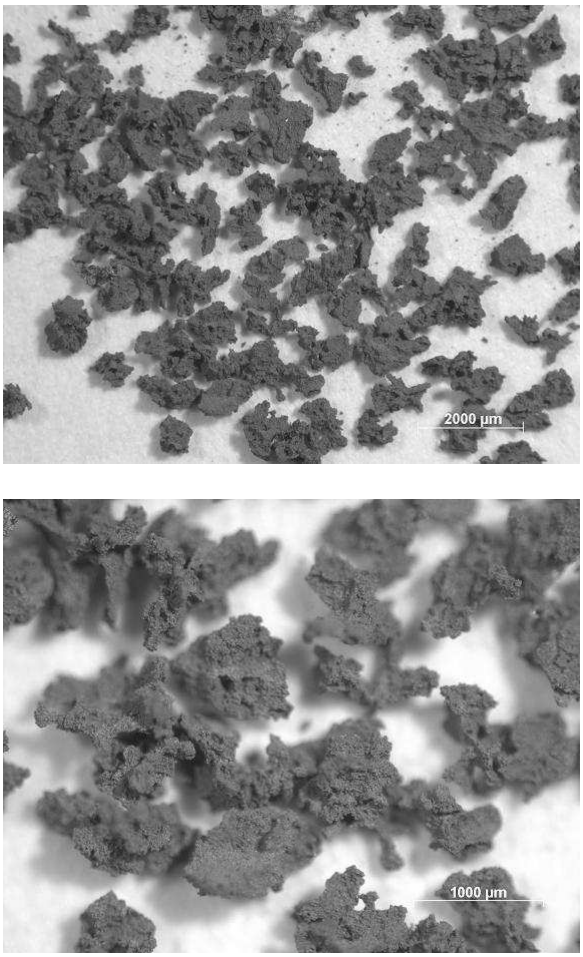

Figure 2.6. Macrographs of Ti-0.8B powder produced using the Armstrong process.

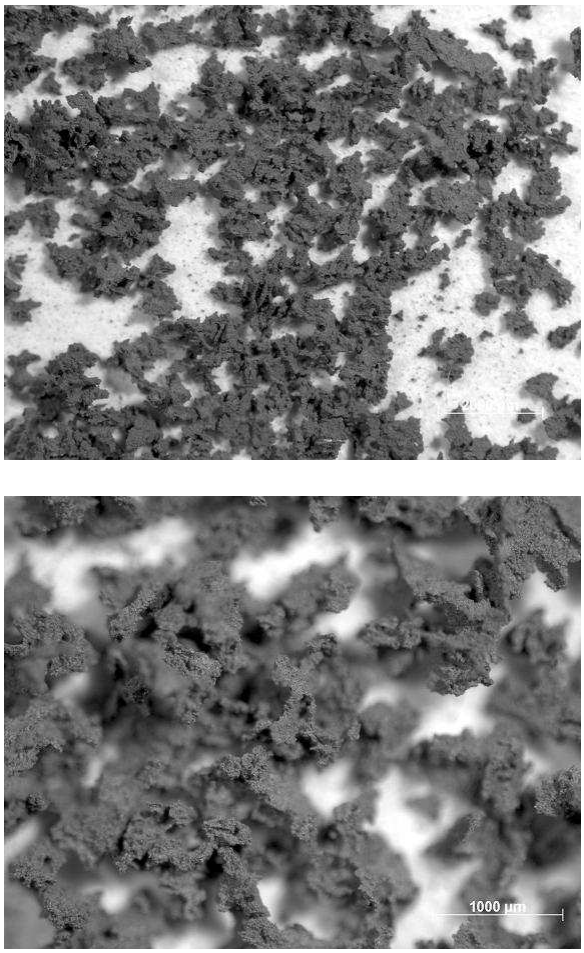

Figure 2.7. Macrographs of Ti-0.9B powder produced using the Armstrong process.

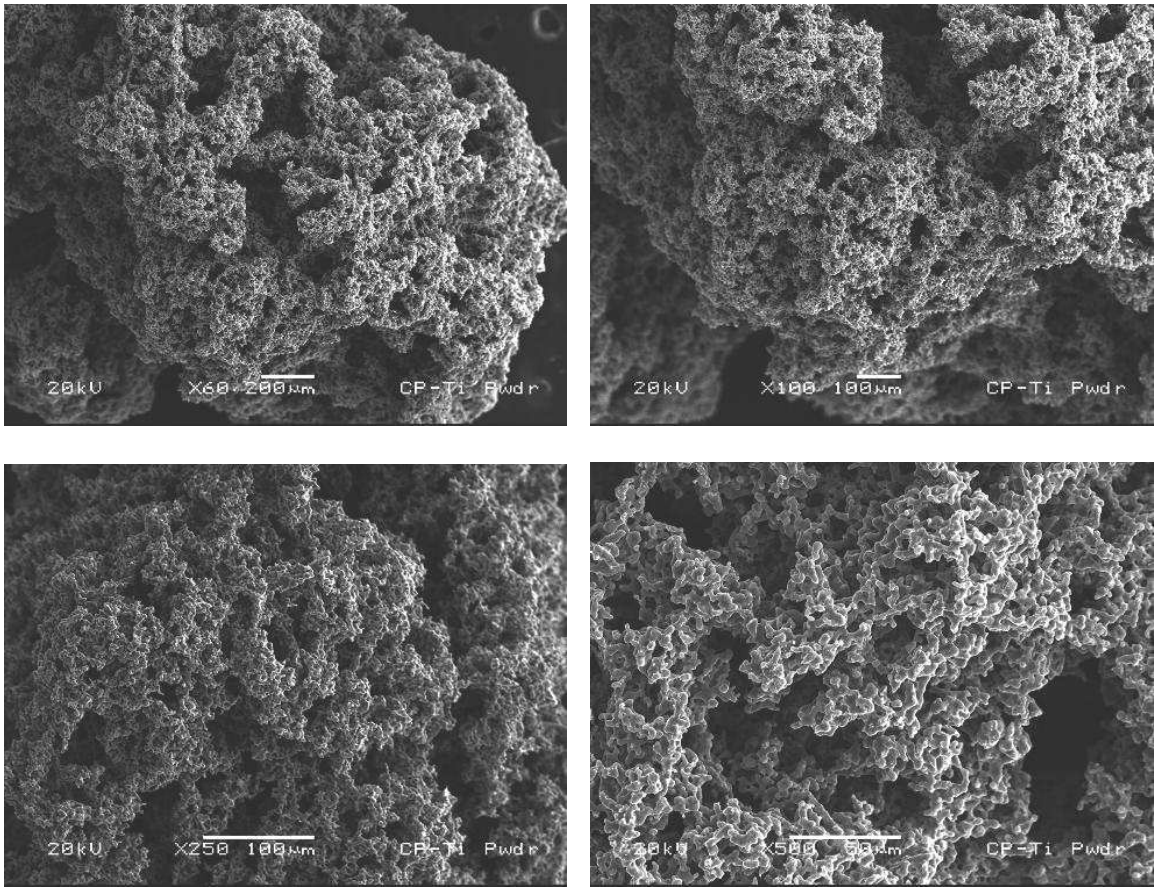

Figure 2.8. Low magnification micrographs of commercially pure (CP) titanium powder produced using the Armstrong process.

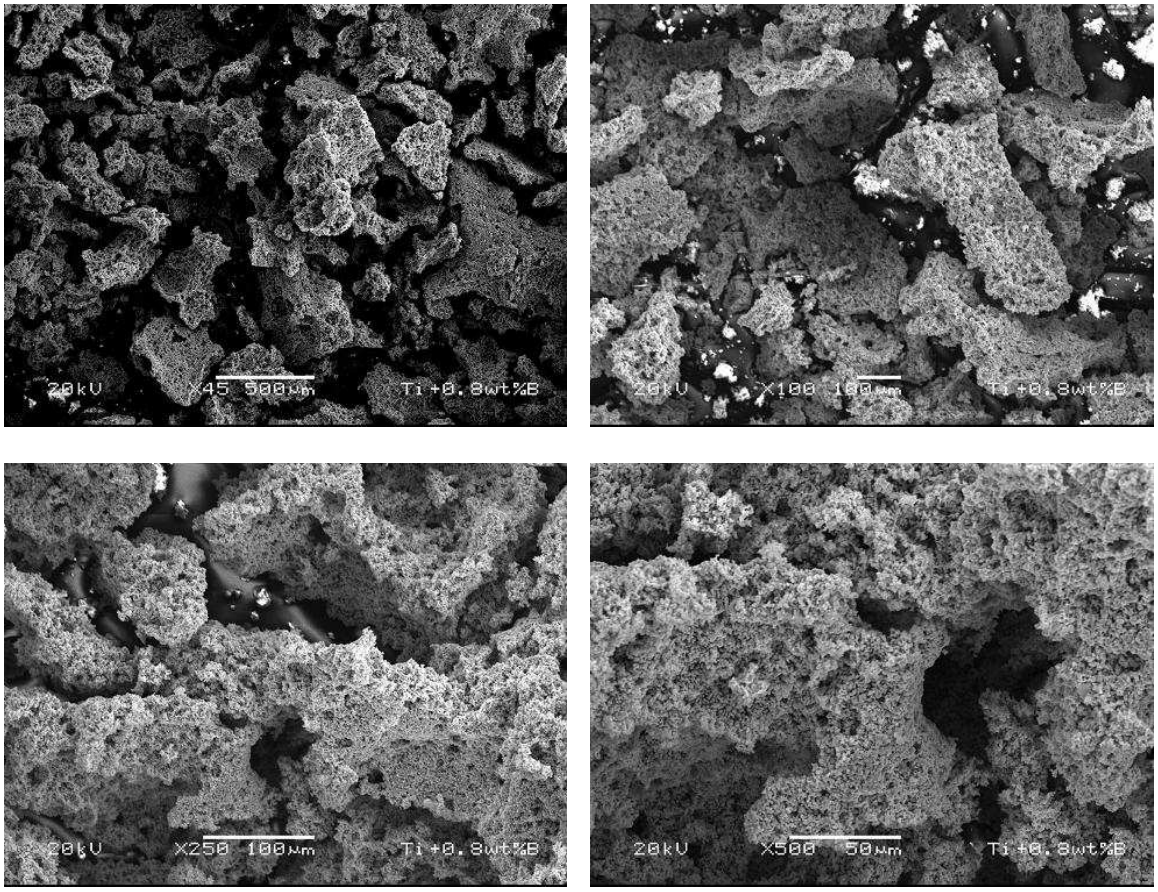

Figure 2.9. Low magnification micrographs of Ti-0.8B powder produced using the Armstrong process.

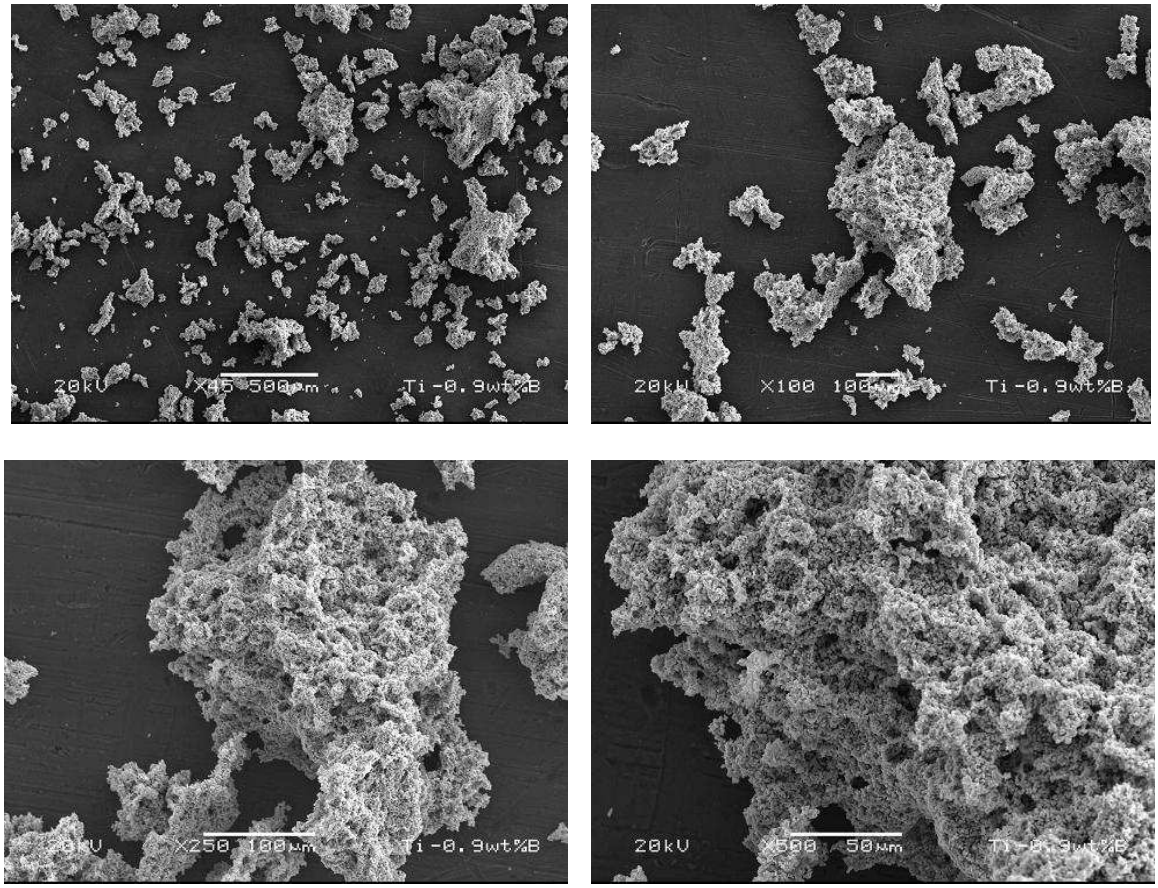

Figure 2.10. Low magnification micrographs of Ti-0.9B powder produced using the Armstrong process.

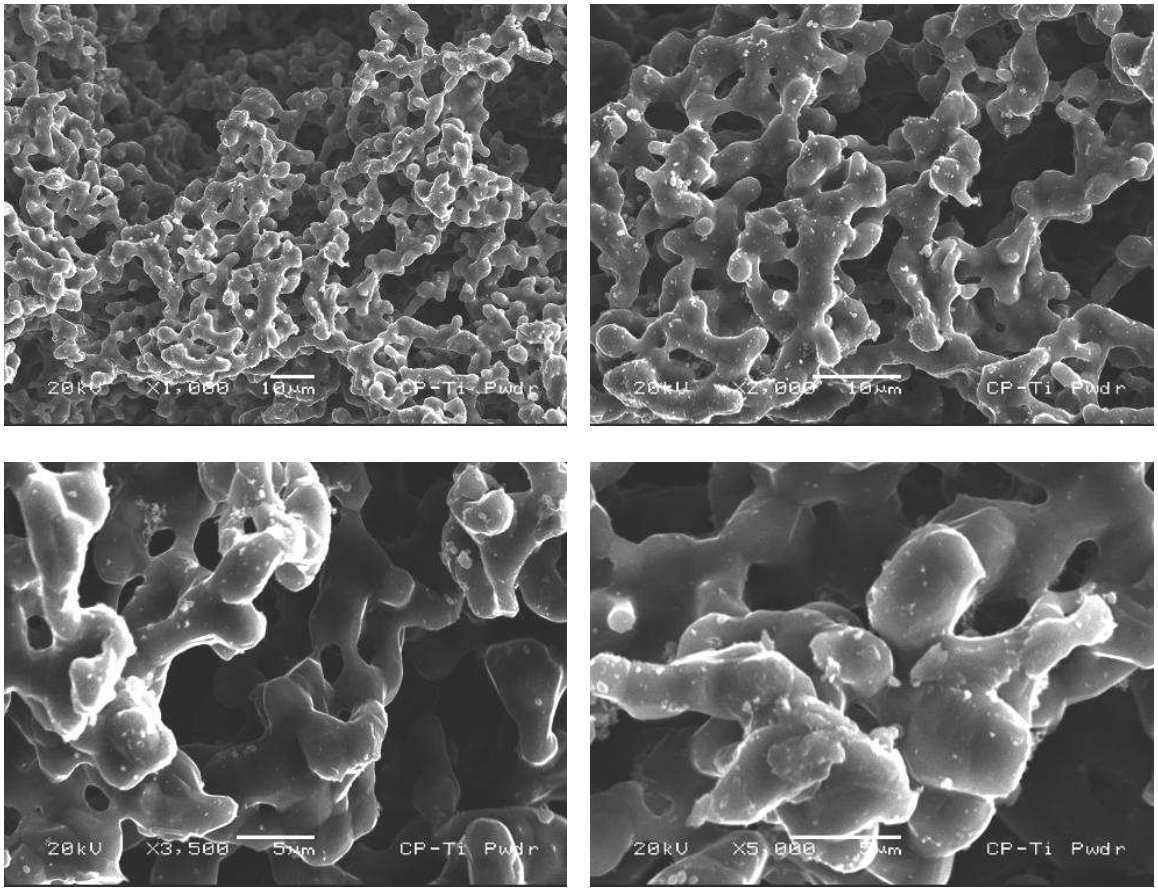

Figure 2.11. High magnification micrographs of commercially pure (CP) titanium powder produced using the Armstrong process.

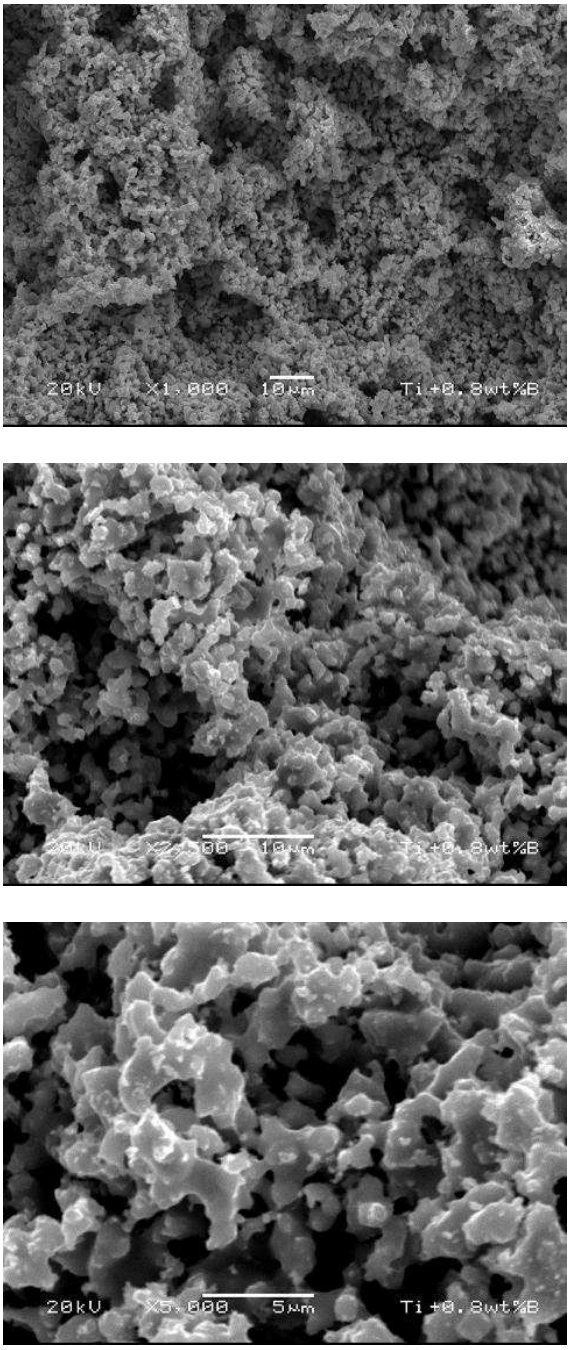

Figure 2.12. High magnification micrographs of Ti-0.8B powder produced using the Armstrong process.

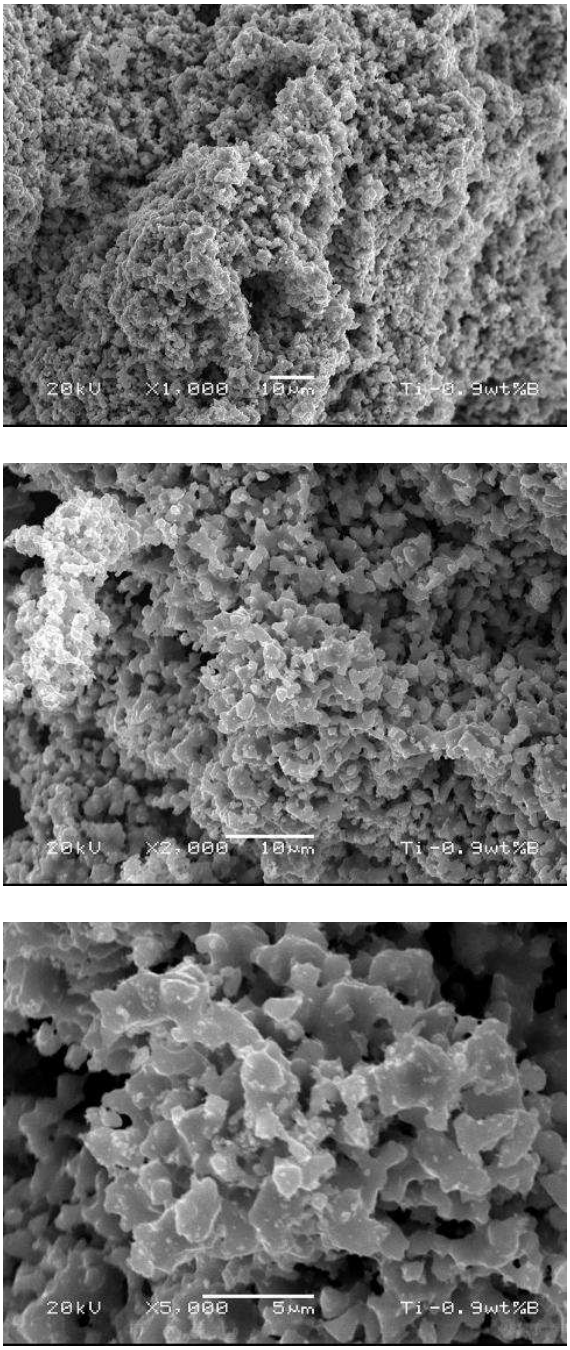

Figure 2.13. High magnification micrographs of Ti-0.9B powder produced using the Armstrong process.

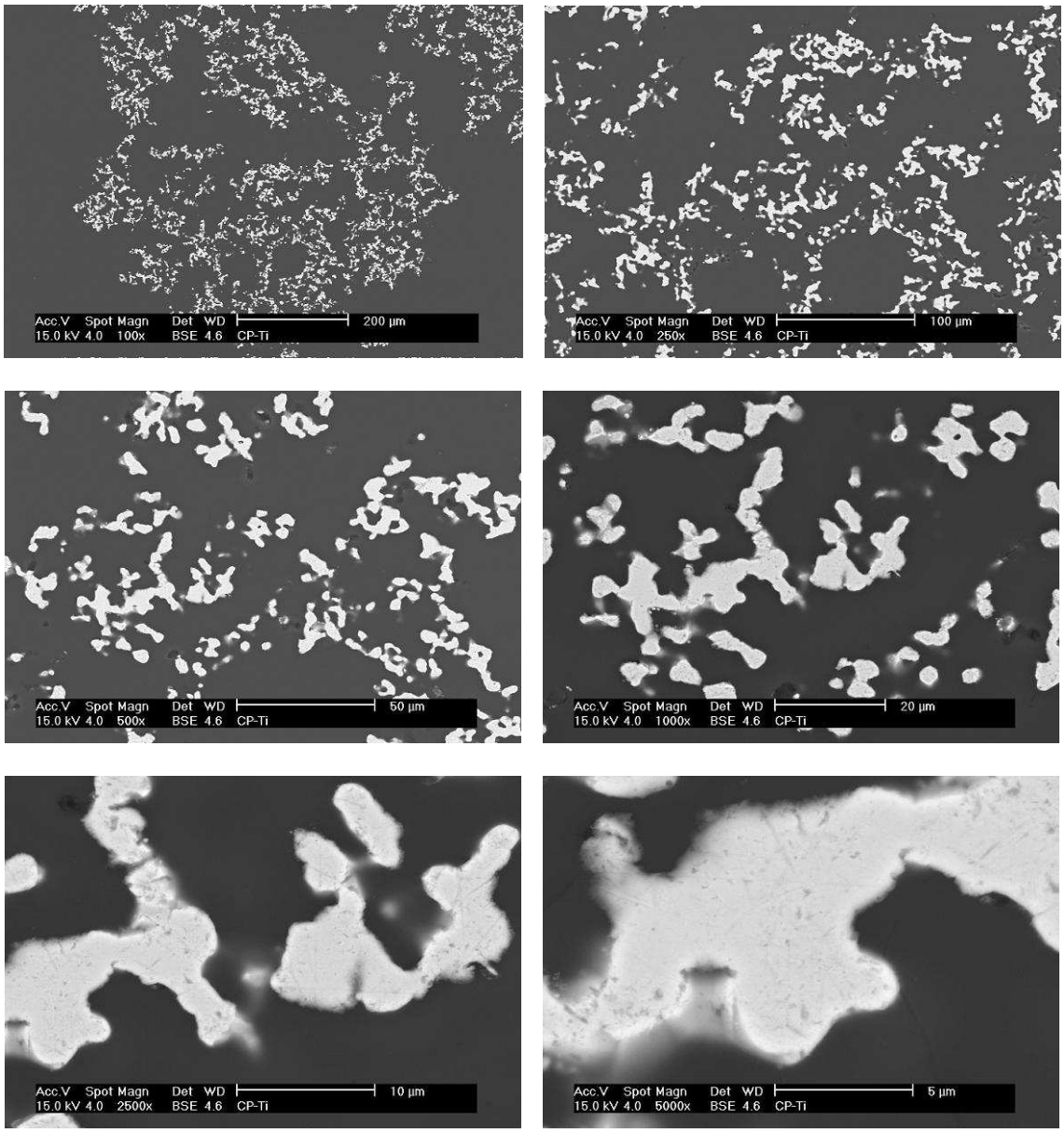

Figure 2.14. Micrographs of cross-sections of commercially pure (CP) titanium powder produced using the Armstrong process.

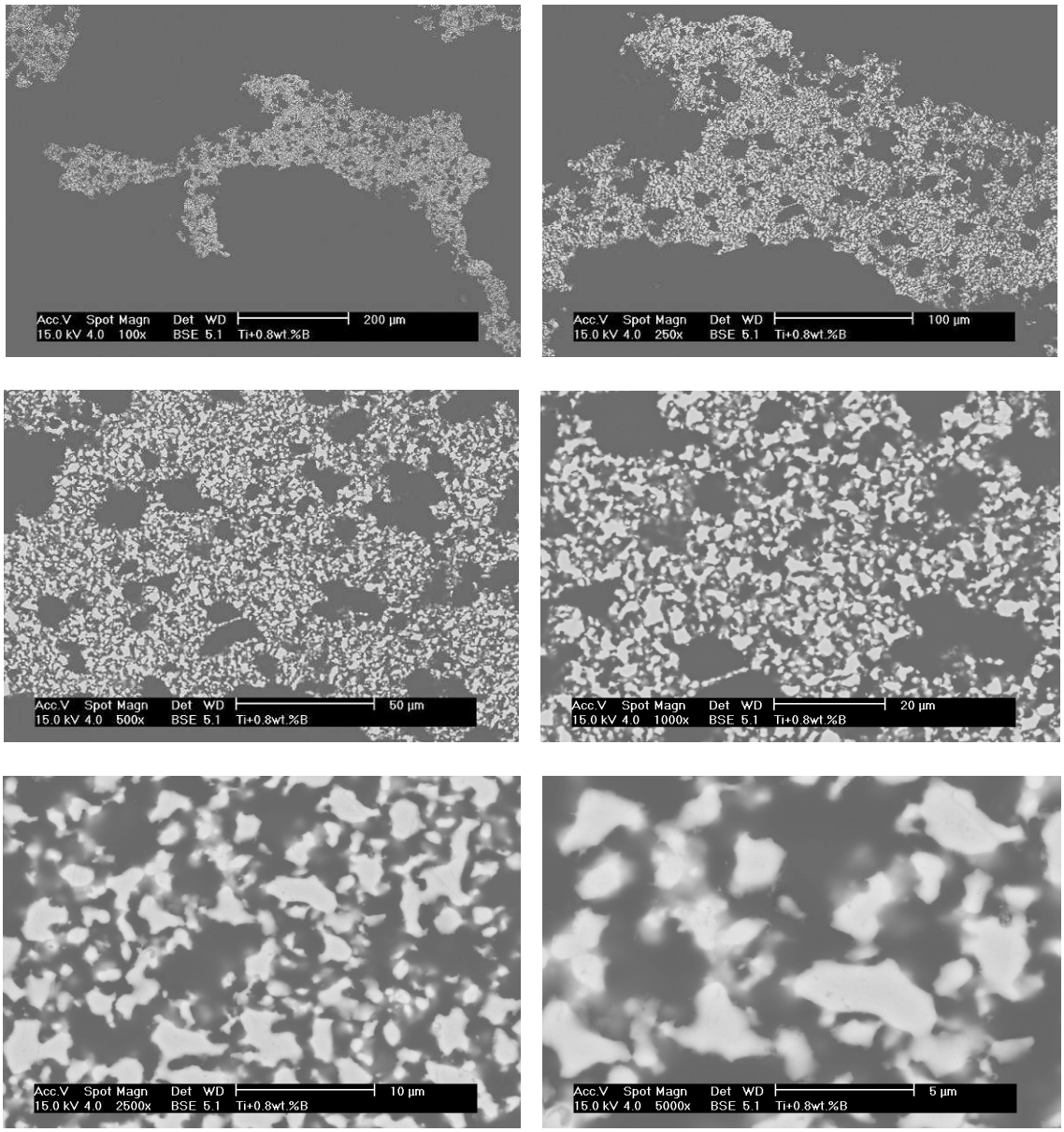

Figure 2.15. Micrographs of cross-sections of Ti-0.8B powder produced using the Armstrong process.

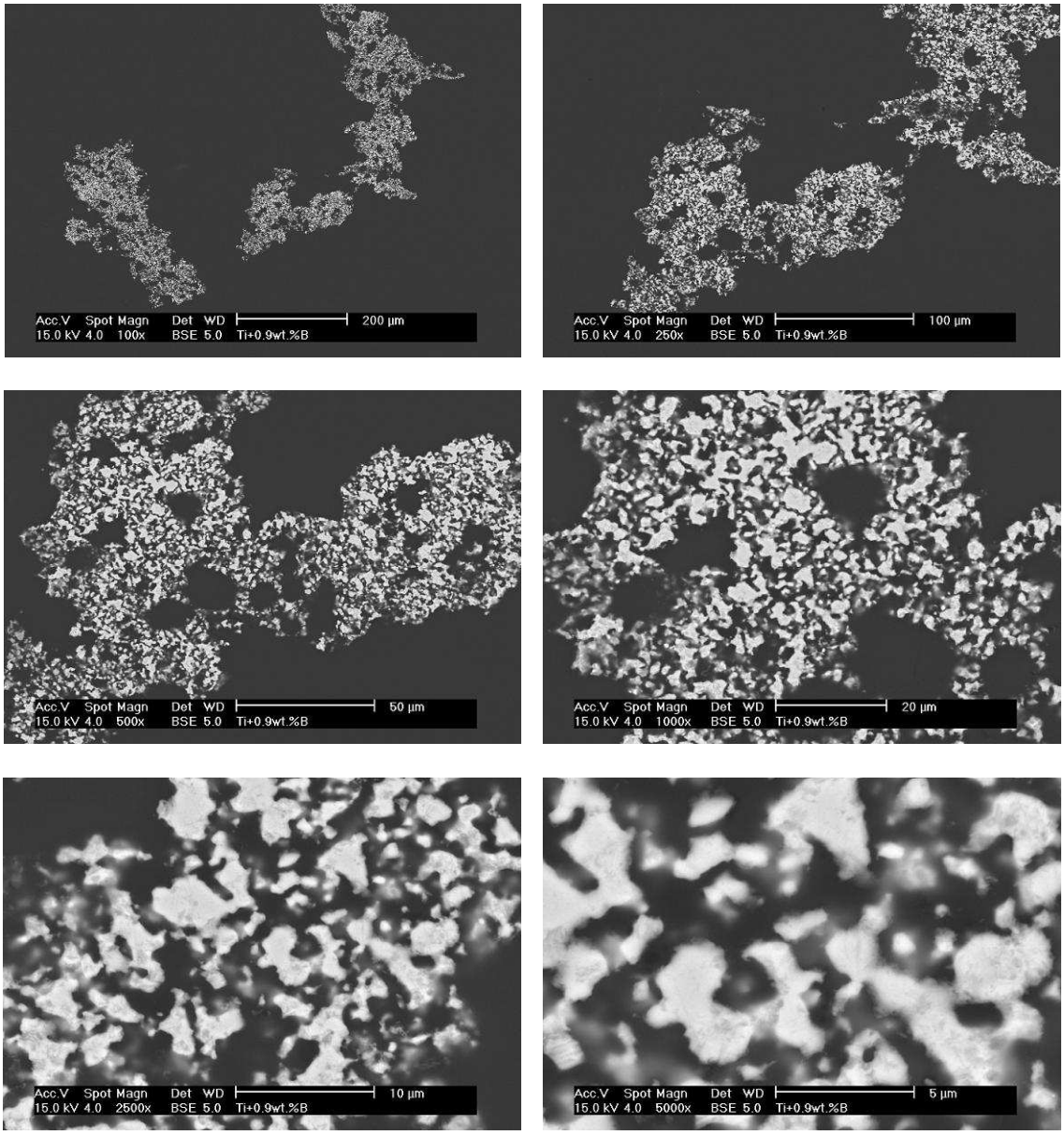

Figure 2.16. Micrographs of cross-sections of Ti-0.9B powder produced using the Armstrong process.

produces titanium powder that is an irregular shaped aggregate with a coarse, sponge-like appearance. Titanium sponge and Armstrong titanium powder are shown in Figure 2.17 for comparison. As mentioned previously, the traditional methods for producing titanium are the Kroll and Hunter processes. In these processes, $TiCl_4$ is reduced using either magnesium for the Kroll process or sodium for the Hunter process to create titanium sponge. Based on all published literature on the Armstrong process, it is essentially a continuous version of the Hunter process, where $TiCl_4$ vapor is reduced as it is injected into a flowing stream of molten sodium. As chemical reactions for the Hunter and Armstrong processes are similar and produce material in a similar appearance, it is expected that the mechanism of titanium sponge or powder formation would be similar. It should be noted that all discussion of the Armstrong process is based on published literature including the patents describing this process. Therefore, all conclusions on the Armstrong process itself are based on comparisons of the open literature on Armstrong process to that of other known processes such as the Kroll and Hunter processes.

Although many studies have been conducted on the Kroll and Hunter processes[57–63], there is no consensus on the relationship between the chemical reactions of the processes and titanium sponge formation. Nagesh et al.[58] have proposed that the $TiCl_4$ vapor becomes reduced to titanium sponge in a two stage process as shown in Figure 2.18.[58] As $TiCl_4$ is fed into the reactor containing molten magnesium or sodium, it vaporizes and is transported to the liquid surface. Reaction of $TiCl_4$ with sodium liquid gives rise to the formation of tiny droplets consisting of NaCl or a solution of $NaCl/TiCl_2$. Significant further reduction of $TiCl_4$ can only take place by the dissolution of sodium in the salt droplets and its transport to the salt/gas interface (Figure 2.18a). Titanium forms

(a)

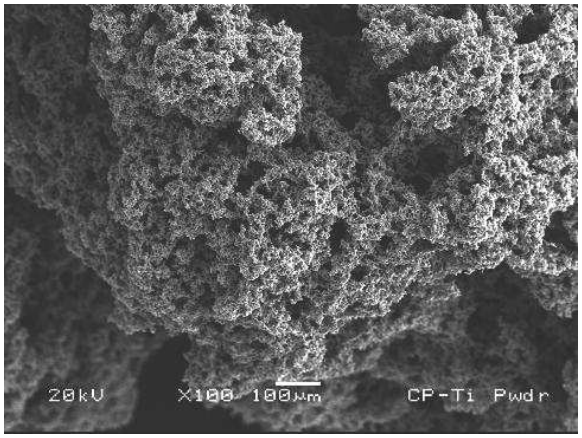

(b)

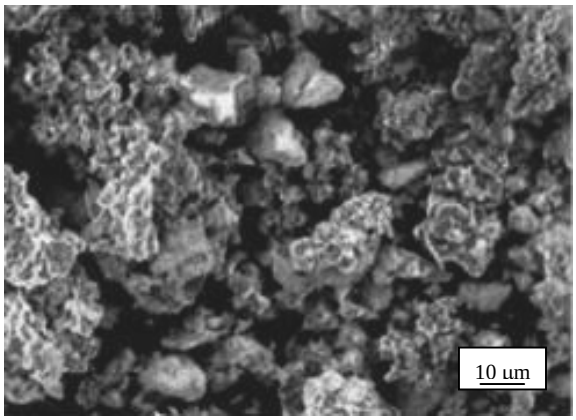

Figure 2.17. Micrographs of commercially pure (CP) titanium powder produced using the Armstrong process in comparison to Ti sponge: (a) CP-Ti powder; (b) Ti sponge[57].

when the NaCl droplet reaches a surface where the nucleation and growth of titanium metal is favored. Sponge formation advances by the dissolution of sodium in the salt and its diffusion through the salt at the crucible wall or the titanium surface (Figures 2.18b and c). This sponge-formation reaction can also take place by an electrochemical mechanism of charge transfer through the chloride at the reactor wall, as proposed by Okabe and Waseda[59], according to which the physical contact of sodium and the intermediate $TiCl_2$ product is not necessary.

Based on these proposed mechanisms, the titanium powder produced with the Armstrong process should form spherical shapes (due to surface tension). However, the data presented currently indicate the powder consists of elongated and equiaxed particles (Figure 2.17). The titanium particulate morphologies shown in Figure 2.17a are analogous to those of the titanium powder produced by the Armstrong process (Figure 2.17b). Fuwa et al.[57] suggested that the key factor controlling the morphology is the reduction temperature, where higher temperatures generate columnar morphologies indicating titanium crystalline growth and partial sintering of grain aggregates during reduction. Fuwa et al. reported results that titanium products at higher reduction-reaction temperatures have a mixed morphology of columns and grain aggregates while those at lower temperatures have mostly grain aggregates as shown in Figure 2.19. The Armstrong titanium powder is consistent with the morphologies observed at the lower reduction-reaction temperatures (~1830°F). Therefore, this would suggest that the titanium powder produced using the Armstrong process was completed at temperatures around those for sintering of titanium (~1830°F), producing more equiaxed aggregates.

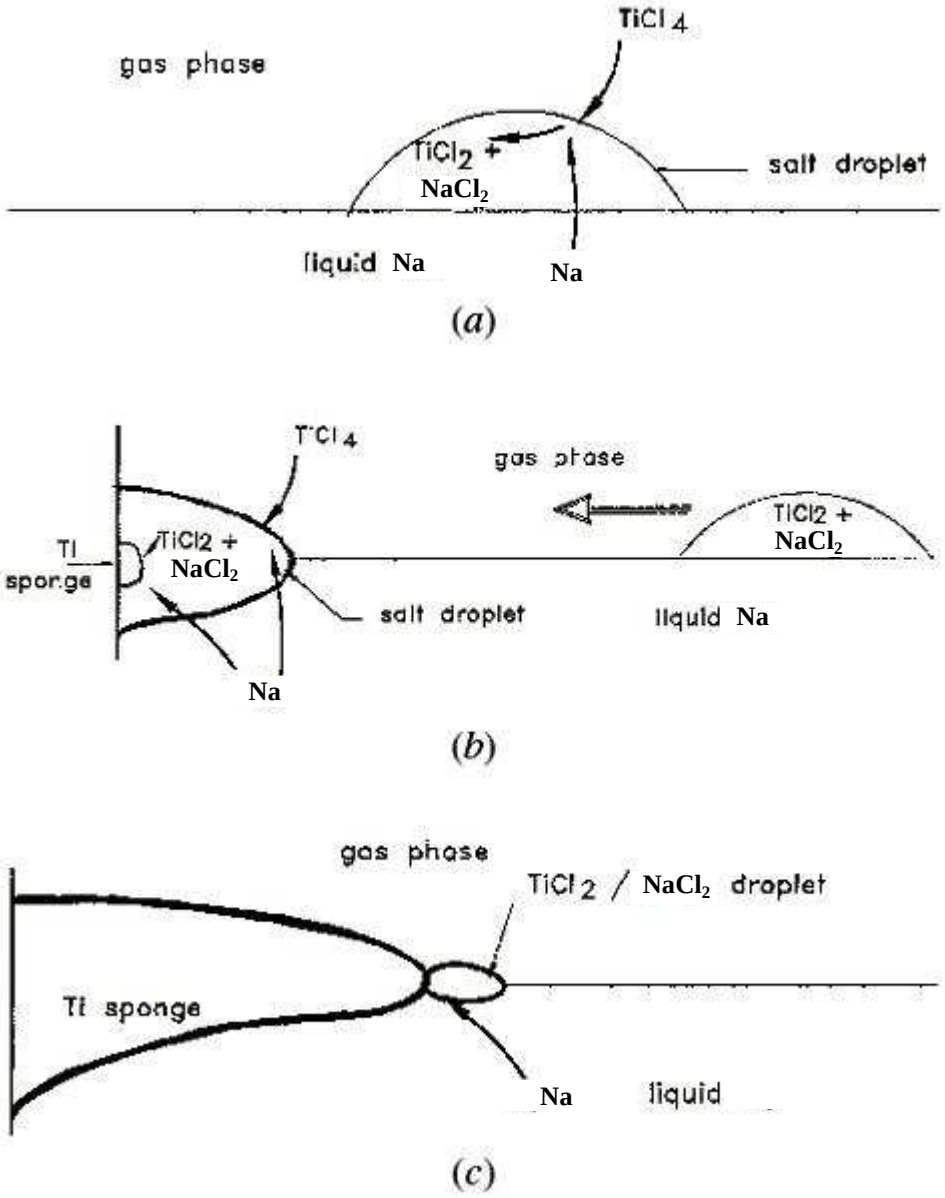

Figure 2.18. Proposed mechanism for commercially pure (CP) Ti powder formation using the Armstrong process. (modified from ref. [58])

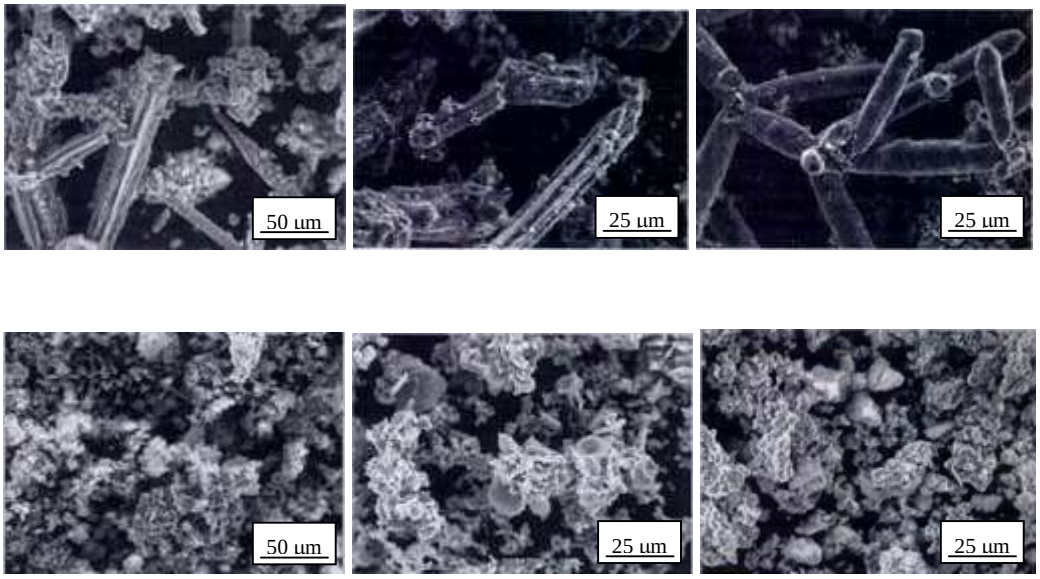

Figure 2.19. Titanium sponge produced at higher reduction-reaction temperatures showing mixed morphology of (a) columns and grain aggregates while those at lower temperatures have mostly (b) grain aggregates.[57]

The current literature on the Armstrong process states the reactions in the process are completed at temperatures less than the published sintering temperature of titanium producing spherical powders.[15-31] However, the results from the first experimental runs (of Ti-B powders) were more equiaxed and elongated in shape suggesting that if spherical powders were formed, then they sinter together during the process to form the aggregates. If this is the case, then the sintering reaction of the material may not be consistent with that published.[15-31]

Several factors, in addition to temperature, must be considered to further explain the Armstrong powder morphology. Time and temperature are significant factors that affect the sintering of materials with particle size and pre-alloying to a lesser extent. Several studies have been completed in an attempt to demonstrate the relationship between these factors and sintering[64-69]. All of these studies show that sintering is a diffusion-based process that is in a form similar to the follow:

$$\frac{d\rho}{dt} = \frac{CD\gamma_s V_m}{RTG^x} \qquad [2.1]$$

where $d\rho/dt$ is the sintering or densification rate, C is a constant, D is the diffusion coefficient, γ_s is the surface energy, V_m is the molar volume, R is the gas constant, T is the absolute temperature, G is the particle size, and x is some value experimentally determined. As is shown by equation 2.1, when particle size is decreased, the rate of sintering increases by a power of 'x' with temperature and all other factors held constant. If temperature was allowed to decrease, the sintering rate could be held constant by increasing the particle size accordingly. Based on the particle sizes shown in Figures 2.17 and 2.19, the particles produced by the Armstrong process are finer in morphology to

those in the Kroll and Hunter process. Therefore, the temperature at which sintering could occur in the Armstrong process reaction chamber would be higher than that of the Kroll and Hunter process. However, this longer reaction time at temperature is a trade-off as the same effect can be obtained at either higher temperatures and shorter times (Armstrong process) or lower temperatures and longer times (Kroll and Hunter processes). The combination of higher temperatures and shorter times is most likely the reason why the Armstrong product is sintered together in aggregates rather than spherical powders as expected.[6-31]

The pre-alloying aspect is another factor that needs to be taken into account when discussing the Armstrong process. In the Kroll and Hunter processes, only titanium sponge is made along with some residuals of iron and nickel from the crucible. An advantage of the Armstrong process is the ability to produce alloy powders by mixing other metal chlorides with $TiCl_4$. The powder in this study was targeted to be Grade 4 CP-Ti, but as shown in Table 2.3 the oxygen and iron were lower than the maximum levels in the specification. Liu et al.[70,71] and others[72-74] have observed that as the amount of iron in titanium powder is increased, the sintering rates increased by 2 – 4 times at sintering temperatures ranging from 1830°F to 2192°F (1000°C to 1200°C) for times ranging from 25 to 350 minutes. This increase in sintering rate was attributed to the high diffusivity of iron in titanium, especially in the β-phase. Although the concentration of iron is small, there still could be a minimal effect that would explain the formation of the aggregates in the Armstrong processed titanium powder.

2.4.2 Titanium-Boron Alloy Powder Processing

The most widely used titanium powder processing methods are gas atomized (GA)[33-37,42,75,76], plasma rotating electrode process (PREP) and rotating electrode process (REP)[35-38,77]. Typical structures of the titanium powder produced by GA, PREP, and REP powders are shown in Figure 2.20(a,b). Using these powder metallurgy (PM) methods to produce Ti-B alloys allows for a more chemically homogeneous final material. The major obstacle for the wide spread use of PM methods in lieu of conventional processing methods is the cost of the powder. The upfront cost of powder processing is potentially lower and is one of the advantages of the Armstrong process compared to the other powder metallurgy methods.[54-56] The powder produced using the Armstrong process is very different than the powder produced using any of the other PM methods. Figure 2.20 shows titanium powder produced by GA, PREP, REP and the Armstrong process. The GA, PREP, and REP processes produce titanium powder that is spherical or near spherical with finer satellite particles attached.[3,78] The Armstrong process produces titanium powder that is a porous, irregular shaped aggregate that is comprised of particles that are sintered together during processing. Although the powders in Figure 2.20 show varying sizes depending on the process, it should be noted it is difficult to compare the effect of process method on powder size and morphology. A change in one of the parameters in the Armstrong process could change the powder size and morphology, but not for GA as this would only affect the size. For example, the powder size will decrease when increasing the pressure of the argon gas used to atomize the material in the GA process.

(a)

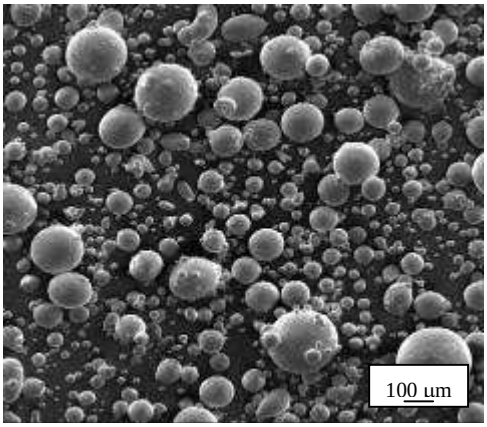

(b)

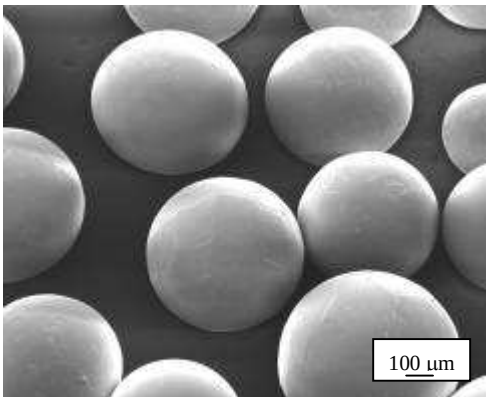

(c)

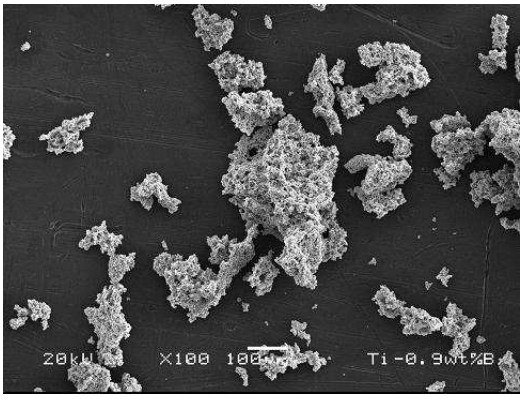

Figure 2.20. Micrographs of titanium powder produced using (a) rotating electrode process[3], (b) gas atomization[78], and (c) Armstrong process.

The titanium powders produced using conventional PM processes and the Armstrong process are not similar in appearance, but the addition of boron has a similar effect on the powders produced by all of the processes. The addition of boron to the titanium powder refines the microstructural features of the powders regardless of the process. Yolton and Moll[34] examined a prealloyed Ti-6Al-4V-XB alloy produced by cold wall induction melting of master alloys and titanium diboride, and argon gas atomization. The powder, as atomized, consisted of fine TiB particles dispersed uniformly in a Ti-6Al-4V matrix. At higher boron levels, the powder had a finer morphology with a higher density of TiB particles some of which were needle shaped (Figure 2.21). The Armstrong process, however, produced powder with no microstructural features. There were no grain boundaries or titanium-borides observed when the cross-sections of the Ti-B powders examined. It is likely the there was titanium present in the form of α grains, but X-ray diffraction (XRD) or transmission electron microscopy (TEM) was not used to assess whether α grains was present. In addition, it is most likely that the boron is in solution with the titanium and TiB does not form until during subsequent processing.

In addition to having no microstructural features, the size of the powder is also reduced using the Armstrong process. It is difficult to determine if the addition of boron affects the size of the powder produced using other processes as the effect can be confounded with process parameters used in the study. The addition of boron in the Armstrong process produced powder with a finer morphology as compared to the CP-Ti powder. The reduction in size of the powder assists in obtaining a uniform distribution of the TiB particles throughout the final consolidated titanium alloy.

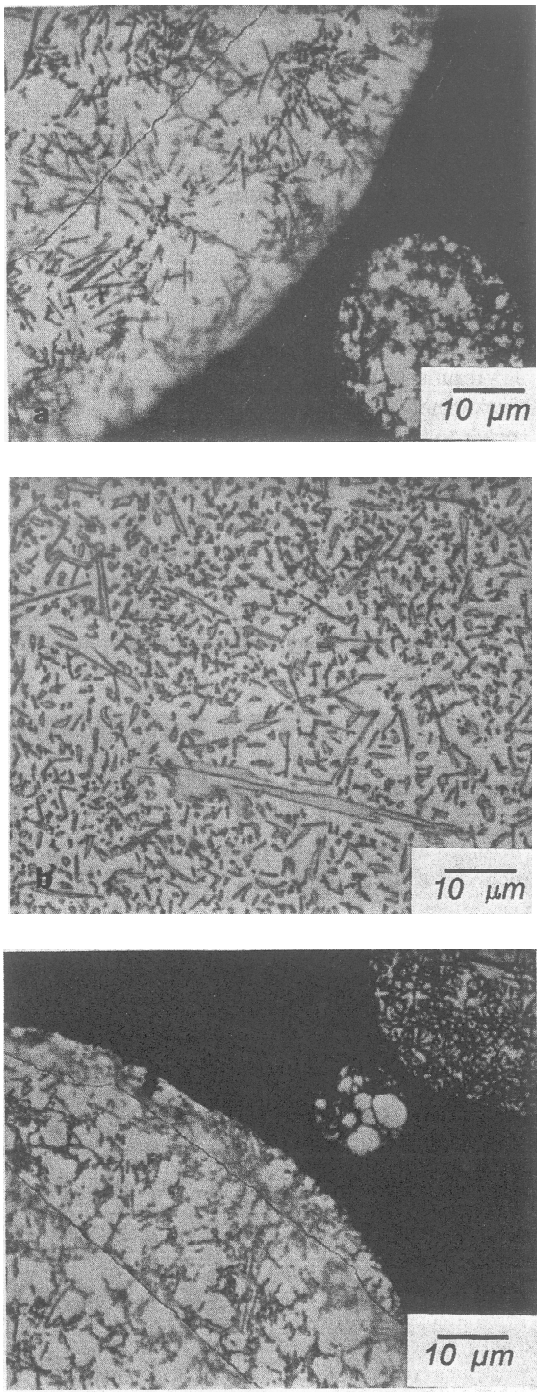

Figure 2.21. Micrographs of Ti-6Al-4V-XB powder produced using gas atomization.[34]

Currently, all of the conventional PM processes use conventionally produced titanium (either sponge or mill product) as the starting material prior to consolidation or solidification with boron to produce Ti-B powder or the consolidated Ti-B alloy. The input titanium material is produced from titanium sponge that was created by the Kroll or Hunter process and either blended or melted with other powders/raw materials of the desired alloying elements to form the titanium powder. The morphology of the Ti-B powder produced using the Armstrong process is analogous to that of the CP-Ti powder and titanium sponge (Figures 2.21 and 2.22). The lots of powder with and without boron are aggregates of smaller particles that appear to have been sintered together during processing. In the case of the Ti-B powder, the aggregates have two size distributions: smaller aggregates that are more spherical in shape while the larger ones are more similar to cylindrical in shape. The larger aggregates with boron are similar to that of the aggregates without boron.

Unlike the Kroll and Hunter processes discussed previously, the mechanism(s) for the formation of Ti-B powder produced using the Armstrong process has not been thoroughly studied with results published in open literature. However, there have been several studies published on the mechanism(s) and reaction(s) associated with the reduction of $TiCl_4$ and BCl_3 to titanium, boron, TiB, and TiB_2 using sodium as the reducing agent.[79-83] Since this is the same reduction process that occurs in the Armstrong process, understanding and applying these mechanism(s) to the Armstrong process could assist in optimizing the powder to obtain the microstructure, and properties required for a particular application.

(a)

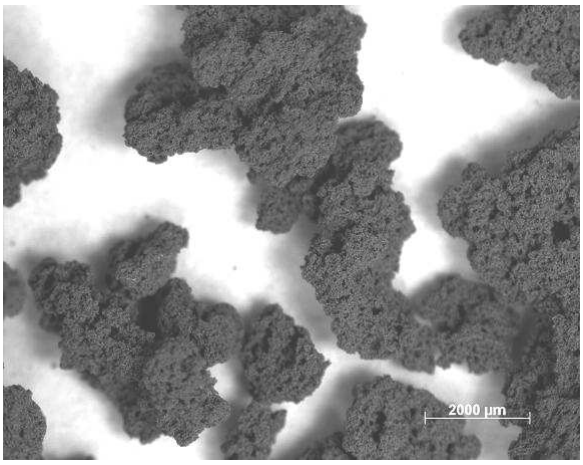

(b)

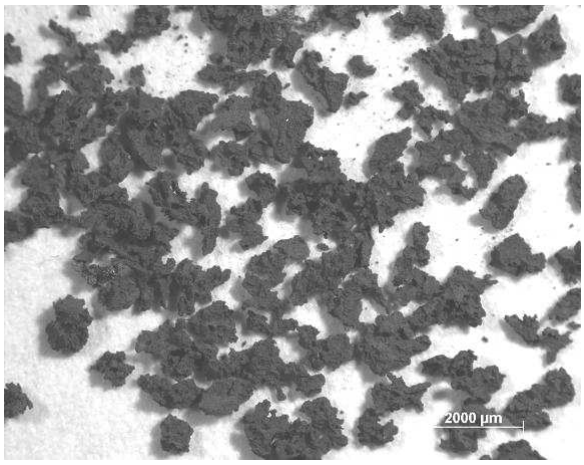

(c)

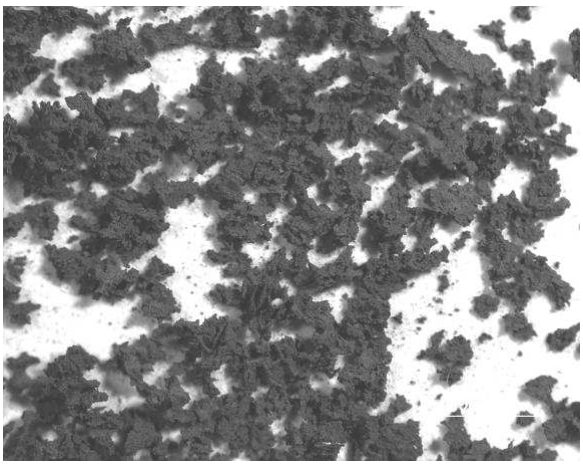

Figure 2.22. Micrographs of (a) commercially pure (CP) titanium, (b) Ti-0.8B, and (c) Ti-0.9B powder produced using the Armstrong process.

(a)

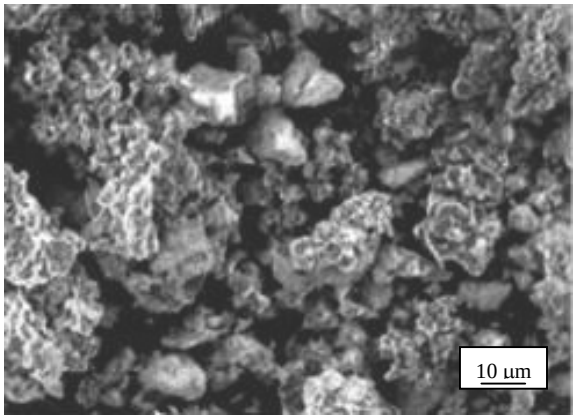

(b)

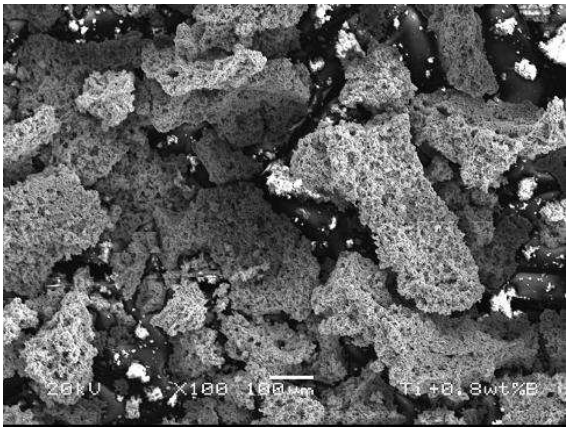

(c)

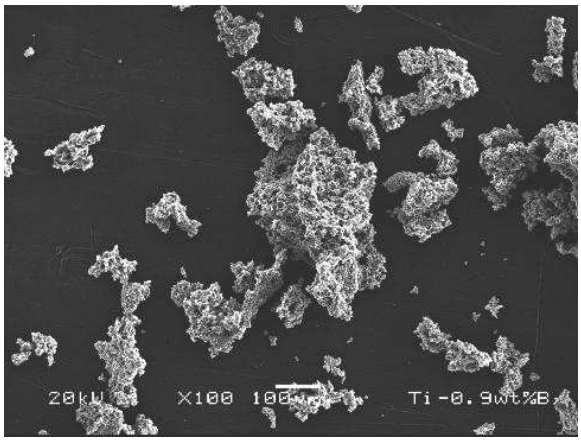

Figure 2.23. Micrographs of (a) titanium sponge[35], (b) Ti-0.8B, and (c) Ti-0.9B powder. Ti-0.8B and Ti-0.9B powder was produced using the Armstrong process.

Axelbaum et al.[80-82] and Steffens et al.[83] have both proposed a mechanism such that $TiCl_4$ and BCl_3 vapor is reduced to titanium, boron, TiB, and/or TiB_2 in a similar way as titanium sponge is produced. As with the reduction of $TiCl_4$ to titanium sponge, the particle formation begins with a gas-phase clustering of reactions rather than nucleation of one component followed by gas-cluster reaction between the two components.[83] Unlike the titanium sponge mechanism/process, the addition of BCl_3 complicates the mechanism/process such that the reduction product is strongly dependent on the chloride ratio. Axelbaum et. al.[80-82] have shown that the yield of the product is a function of chloride ratio (R_{Cl}) as follows:

$$R_{Cl} = \frac{X_{BCl3}}{X_{TiCl4}} \qquad [2.2]$$

where X is the mole fraction of the species. For $R_{Cl} = 0$, that is, for no BCl_3, the yield is 100% titanium (as shown for Armstrong processed CP-Ti powder). For $0 < R_{Cl} < 1$, the product consists of TiB and titanium; $1 < R_{Cl} < 2$, the product is TiB and TiB_2, and for $RCl > 2$ the product is TiB_2 and boron.[80] Notably, for $R_{Cl} = 2$ the yield is 100% TiB_2.[81] The yield increases with chloride vapor pressure because the vapor-phase reactants are converted to solid-phase products. Conversely, decreasing the concentrations of reactants (lowering partial pressures) will reduce yield. Therefore, in principle, by controlling stoichiometry, pressure, and temperature the yields of titanium, boron, TiB, and TiB_2 can be controlled to obtain a variety of useful products including that used in this study. The Ti-B powder produced using the Armstrong process did not show any microstructural features. This may be due to the small amount of powder examined in cross-section or the microstructural features were not resolvable using the SEM. However, the boron was

most likely in solution with the titanium in the powder, as after subsequent processing TiB was observed throughout the material.

This particle formation mechanism/process produces powder that is typically equiaxed in shape. As mentioned previously, the titanium powder with boron produced with the Armstrong process is an aggregate of finer particles. It is believed that the particles are formed by the gas-phase mechanism mentioned previously and while the particles are still in the reactor they sinter to form the aggregates. The sintering of the particles is time, temperature, chemistry and particle size dependent, and as shown previously explains the formation of aggregates from smaller particles in the Armstrong titanium powder.

2.4.3 Commercially Pure (CP) Titanium and Titanium-Boron Powder Metallurgy

The irregular, aggregate shape of the powder will have an effect on the microstructure and properties of the final product. The morphology of the powder will determine the ease with which the powder can be consolidated to obtain the final product.[84] The flowability and packing density of a powder are measures of the ease with which powder can be compacted. If the powder has a good flowability, it can be easily compacted with less pressure and temperature. The packing density is a measure of how tightly the powder can be compacted with respect to a fully dense product. Typical packing densities reported for PREP, REP and GA titanium powder with boron is ~65%.[33-38,42-44,74-77,85-92] The CP-Ti, Ti-0.8B and Ti-0.9B, produced using the Armstrong process, has poor flowability and a low packing density (<20%) in comparison to spherical powder. This is due to the irregular shape of the Armstrong process powder

making it difficult to tightly compact the powder without additional pressure or processing. The lower flow rate and packing density of the powder could lead to additional processing being required to fully consolidate the powder.

The irregular shape and porosity of the CP-Ti powder aggregate that is produced also leaves questions on how well the residual sodium and chlorine can be removed. Residual chloride can cause porosity in the consolidated powder metallurgy alloy which often results in a degradation of the mechanical properties especially fatigue.[54,70] The reduced amounts of sodium and chlorine in both the CP-Ti and Ti-B should have a positive influence on the microstructure and properties of the final product (Table 2.3). A couple of possible reasons for the cleaner powder is: (1) since the powder is fine and so porous, it has less cavities or crevices for the sodium and chlorine to get trapped thus allows for a more effective cleaning, and (2) the cleaning methods used providing a more thorough cleaning of the powder. The powder was washed water to remove the sodium chloride by-product before being shipped in an argon filled container.

The cleanliness of the powder and final product is also dependent on foreign particles in a similar manner as residual chloride. Foreign particles can be introduced when this powder is exposed/transported from the reduction reactor to storage containers, and handled during post processing such as sintering or HIPing. Powder cleanliness is one of the main factors governing the quality of powder metallurgy alloys, because even low levels of contamination from foreign particles may lead to a substantial loss of inherent properties such as with fatigue strength. This is a bigger concern for titanium alloys in comparison to that of nickel and iron alloys as inclusions are not currently a

concern in industry standard material processed using vacuum arc remelting (VAR) and hearth melting.

The fine size of the powder particles will also have an effect on the microstructure and properties of the final product. The Armstrong powder is immediately quenched upon becoming a solid producing a very fast cooling rate. The fine size of the powder allows for the material on the surface and interior of the powder to have the same fast cooling rate, and subsequently reduce the spacing between and increase the number of grain nucleation sites. In other powder metallurgy (PM) methods like gas atomization, the cooling rates of the powder will not be as quick due to the process and, size of the powder. This will lead to a lower number of and spacing between nucleation sites. The larger number of nucleation sites will allow for more grain to nucleate and grow in comparison to gas atomized powder. The larger number of grains growing will impinge on each other limiting the final grain size of the consolidated material. Therefore, it is more likely that the Armstrong powder should produce a finer structure in the consolidated material as compared to other PM methods. In addition, the fine particle size will result in a finer structure and better control of the local chemistry in the final product.

The particle size will have a downstream effect on the consolidated products grain size and subsequently the properties. A fine starting powder size tends to lead to a finer grain size for products consolidated without additional plastic work[93] and should lead to increased strength in the final product based on the Hall-Petch relationship[94,95]. The grain size of powder materials, that are consolidated without plastic work, tend to stay finer than conventional products as the driving force for recrystallization is small. In

conventional products, severe plastic deformation is used to reduce the grain size and there exists a large driving force for recrystallization (reduction in dislocation density). Since the powder is already fine and there is not a large dislocation density from additional plastic work, the microstructure of the consolidated material is relatively stable. Grain growth could occur depending on the subsequent processing like extrusion or isothermal forging, but typically the grain size of the final product is analogous to the starting powder size when consolidation occurs without additional plastic work.[93,96,97] The addition of boron into the titanium powder refines the powder size produced using the Armstrong process. This reduced size should have a downstream effect by refining the grain size and increase the strength of the final product compared to the CP-Ti material.

The chemistry of CP-Ti and other non-heat treatable grade titanium alloys is as important as any other factor including processing method on the microstructure and properties of the final product. Table 2.3 shows a comparison of the chemistries between the CP-Ti powder, Ti-0.8B, Ti-0.9B, and specification Grade 2 and Grade 4 CP-Ti. The Ti-B powder had higher amounts of oxygen, iron, and carbon with lower amounts of sodium and chlorine in comparison to the CP-Ti material. The higher amounts of oxygen, iron and carbon will provide a significant amount of strengthening in addition to that associated with boron.[98-104] The oxygen and carbon are interstitial elements that provide solid solution strengthening of the final product.[98-104] Jaffe et al.[101,102] derived an equation that determines the oxygen equivalence in an attempt to quantify the contributions of oxygen, nitrogen and carbon in strengthening of CP-Ti. Their work shows that the order of interstitial strengthening is nitrogen > oxygen > carbon. Simbi

and Scully[104], on the other hand, have shown that oxygen is a far more potent strengthener than nitrogen and carbon combined. They have shown that the amount of iron present in the alloy needs to also be taken into account as it has confounding effects on the strengthening, and thus oxygen can be a much more potent strengthener (up to ~0.4 wt.% oxygen) than nitrogen and carbon depending on the amount of iron present in the alloy.

The observations by Jaffe et al.[101,102] and Simbi and Scully[104] would suggest that the low oxygen levels in the CP-Ti powder should significantly reduce the strength of the consolidated product. Since Grade 4 CP-Ti conventional material used in industry is typically at or near the maximum levels of oxygen, this would suggest that the consolidated CP-Ti powder would be expected to have lower strength in comparison to that of a conventional product. The Ti-B powder had significantly higher oxygen levels than CP-Ti and conventional Grade 4 CP-Ti, which would likely lead to additional strengthening over that in typical Grade 4 CP-Ti. The higher amount of oxygen in the Ti-B powder in comparison to CP-Ti powder is likely due to the higher surface area to volume ratio of the fine Ti-B powder. In addition, special attention is needed in the further handling and processing of the powder to not introduce additional oxygen, which could reduce the ductility of the final product.

The increased amount of iron in the Ti-B powder in comparison to the CP-Ti powder, is believed to refine the α grain size by forming some β phase mainly at the α grain boundary triple points preventing grain growth and subsequently strengthens the final product.[103,104] The lower iron level in the Armstrong processed CP-Ti and Ti-B powder is expected to have a minimal, if any, effect on the grain size and strength of the

consolidated product as the amount of iron in the powder is less than the solubility of iron in titanium. Therefore, the iron should not form any β phase and stay in solution in the α phase.

2.5 Conclusions

A novel titanium reduction method called the Armstrong process was used to produce commercially pure (CP) titanium, Ti-0.8B and Ti-0.9B powder. The powder was analogous to titanium sponge in that it was an irregular shaped aggregate with a rough, porous and friable appearance. The mechanism(s) of formation of the CP-Ti and Ti-B powder produced using the Armstrong process are analogous to that of the Kroll and Hunter processes. The two major exceptions are the Armstrong process produces finer particles and alloyed products. The morphology and bimodal size distribution of the titanium powder produced by the Armstrong process had a much lower packing density than powder produced using other traditional powder metallurgy methods. When compared to CP-Ti, the morphology of the Ti-B powder had a finer morphology, which is believed to provide a finer grain size in the final product providing for higher strength.

The fine size and porous nature of the Armstrong processed titanium powder makes it is easier to remove the sodium chloride from the reduction step in the Armstrong process. This is important to prevent detrimental effects on the density and properties of the final product. The finer morphology of the powder is also believed to provide a finer grain size in the final product providing for higher strength. The chemistry of the CP-Ti powder could offset this increase in strength from the fine morphology, as the oxygen, nitrogen, carbon and iron are all low in concentration providing only a small amount of

strengthening. The chemistry of the Ti-B powder, however, had higher levels of oxygen and carbon, which should provide solid solution strengthening.

2.6 References

1. Kroll W. J. *Trans El. Soc.* **78**. 1940. pp. 35.

2. Hunter M.A. *J. Amer. Chem. Soc.* **32**. 1910. pp. 330.

3. Leutjering, G. Williams, J.C. **Titanium (Engineering Materials and Processes).** *Springer-Verlag Publishing.* 2003.

4. Giantta; M.V. **2003 Hamburg Titanium Conference: Vol. 1.** 2003. pp. 237.

5. F. Cardarelli, "A Method for Electrowinning of Titanium Metal or Alloy from Titanium Oxide Containing Compound in the Liquid State", WO 03/046258 A2, June 5 2003.

6. Moxson, V., Froes, F.H. *JOM.* **52(5).** 2000. pp. 24.

7. Rivard, J.D.K., Blue, C.A., Harper, D.C., Kiggans, J.O., Menchhofer, P.A., Mayotte, J.R., Jacobsen, L., Kogut, D. *JOM.* **57(11).** 2005. pp. 58.

8. Crowley, G. *Advanced Materials & Processes.* **161(11).** 2003. pp. 25.

9. Benish, A.J., Sathaye, A., Nash, P., Anderson, R., Zwitter, T. **International Conference on Powder Metallurgy & Particulate Materials.** 2005. pp. 61.

10. Anderson, R.P., Ernst, W., Jacobsen, L., Kogut, D., Steed, J.M. **Cost-Affordable Titanium: A Symposium Dedicated to Professor Harvey Flower as held at the 2004 TMS Annual Meeting.** 2004. pp. 121.

11. Gerdemann, S.J., Alman, D.E. **International Conference on Powder Metallurgy & Particulate Materials.** 2000. pp. 12.41.

12. Jacobsen, L.. *Advanced Materials & Processes.* **160(8).** 2002. pp. 25.

13. Lavender, C.A., Carpenter, J.A. **2004 Annual Progress Report for Automotive Lightweighting Materials.** 2005.

14. Shigeta, M., Watanabe, T. **Bulletin of the Research Laboratory for Nuclear Reactors. Volume 28(I/II).** 2004. pp. 108.

15. Armstrong, D.R., Borys, S.S., Anderson, R.P. **Method of Making Metals and Other Elements.** *U.S. Patent Office.* Patent No. 5,779,761. 1998.

16. Armstrong, D.R., Borys, S.S., Anderson, R.P. **Method of Making Metals and Other Elements from the Halide Vapor of the Metal.** *U.S. Patent Office.* Patent No. 5,958,106. 1999.

17. Armstrong, D.R., Borys, S.S., Anderson, R.P. **Method of Making Metals and Other Elements from the Halide Vapor of the Metal.** *U.S. Patent Office.* Patent No. 6,409,797 B2. 2002.

18. Armstrong, D.R., Borys, S.S., Anderson, R.P. **Ceramics and method of producing ceramics.** *U.S. Patent Office.* Patent No. 6,861,038. 2005.

19. Armstrong, D.R., Borys, S.S., Anderson, R.P. **Method of making metals and other elements from the halide vapor of the metal.** *U.S. Patent Office.* Patent No. 2002005090 A1. 2002.

20. Armstrong, D.R., Borys, S.S., Anderson, R.P. **Elemental material and alloy.** *U.S. Patent Office.* Patent No. 2002148327 A1. 2002.

21. Armstrong, D.R., Borys, S.S., Anderson, R.P. **Elemental material and alloy.** *U.S. Patent Office.* Patent No. 2002152844 A1. 2002.

22. Armstrong, D.R., Anderson, R.P., Jacobsen, L.E. **Method and apparatus for controlling the size of powder produced by the Armstrong Process.** *U.S. Patent Office.* Patent No. 2004079196 A1. 2004.

23. Armstrong, D.R., Anderson, R.P., Jacobsen, L.E. **Preparation of alloys by the armstrong method.** *U.S. Patent Office.* Patent No. 2004079197 A1. 2004.

24. Armstrong, D.R., Anderson, R.P., Jacobsen, L.E. **Method and apparatus for controlling the size of powder produced by the Armstrong Process.** *U.S. Patent Office.* Patent No. 2005081682 A1. 2005.

25. Armstrong, D.R., Anderson, R.P., Jacobsen, L.E. **Filter extraction mechanism.** *U.S. Patent Office.* Patent No. 2005225014 A1. 2005.

26. Armstrong, D.R., Anderson, R.P., Jacobsen, L.E. **Preparation of alloys by the armstrong method.** *U.S. Patent Office.* Patent No. 2006150769 A1. 2006.

27. Anderson, R.P., Armstrong, D.R., Jacobsen, L.E. **Filter cake treatment apparatus and method.** *U.S. Patent Office.* Patent No. 2005284824 A1. 2005.

28. Anderson, R.P., Armstrong, D.R., Jacobsen, L.E. **System and method of producing metals and alloys.** *U.S. Patent Office.* Patent No. 2006107790 A1. 2006.

29. Anderson, R.P., Jacobsen, L.E. **Separation system of metal powder from slurry and process.** *U.S. Patent Office.* Patent No. 2006086435 A1. 2006.

30. Jacobsen, L.E., Benish, A.J. **Titanium alloy.** *U.S. Patent Office.* Patent No. 2007017319 A1. 2007.

31. Jacobsen, L.E., Benish, A.J. **Titanium boride.** *U.S. Patent Office.* Patent No. 2007079908 A1. 2007.

32. Suzuki, R.O. **2003 Hamburg Titanium Conference: Vol. 1.** 2003. pp. 245.

33. Yolton, C.F. *JOM.* **56(5).** 2004. pp. 56.

34. Yolton, C.F., Moll, J.H. **Titanium '95: Science and Technology.** 1996. pp. 2755.

35. Froes, F.H., Suryanarayana, C. **Powder Processing of Titanium Alloys.** 1993. pp. 223.

36. Savage, S.J, Froes, F.H. **Titanium Technology: Present Status and Future Trends.** 1985. pp. 60.

37. Froes, F.H., Eylon, D. **Titanium Technology: Present Status and Future Trends.** 1985. pp. 49.

38. Godfrey, T.M.T., Wisbey, A., Goodwin, P.S., Bagnall, K., Ward-Close, C.M. *Mater. Sci. Eng. A.* **A282.** 2000. pp. 240.

39. Yinjiang W., Qingwen, D. **Study of Motive Hydrogenate/Dehydrogenate. Titanium Alloy Powders & Development For Automotive Parts (I).** 2002.

40. Yinjiang W., Qingwen, D. **Metal Powder Design and Fabrication For Laser Forming. Titanium Alloy Powders & Development For Automotive Parts (I).** 2002.

41. Zhao, F., Fan, Y. **Titanium '95: Science and Technology.** 1996. pp. 2688.

42. Tamirisakandala, S., Bhat, R.B., Ravi, V.A., Miracle, D.B. *JOM.* **56(5).** 2004. pp. 60.

43. Saito, T. *JOM.* **56(5).** 2004. pp. 33.

44. Abkowitz, S., Abkowitz, S.M., Fisher, H., Schwartz, P.J. *JOM.* **56(5).** 2004. pp. 37.

45. Chandran, K.S. Ravi, Miracle, Daniel B. *JOM.* **56(5).** 2004. pp. 32.

46. Banerjee, R., Genc, A., Collins, P.C., Fraser, H.L. *Met. and Mater. Trans.* **35A.** 2004. pp. 2143.

47. Fan, Z., Chandrasekaran, L., Ward-Close, C.M., Miodownik, P. *Scripta Met.* **32(6).** 1995. pp. 833.

48. Suryanarayana, C., Froes, F.H., Rowe, R.G. *International Materials Reviews.* **36(3).** 1991.

49. Keicher, D.M., Miller, W.D. *Metal Powder Report.* **53.** 1998. pp. 26.

50. Snow, D.B., Breinan, E.M., Kear, B.H. *Superalloys.* **189.** 1980. pp. 1980.

51. Brooks, J., Robino, C., Headley, T., Goods, S., Griffith, M. **Proceedings of the Solid Freeform Fabrication.** 1999. pp. 375.

52. Brice, C.A., Schwendner, K.I., Mahaffey, D.W., Moore, E.H., Fraser, H.I. **Proceedings of the Solid Freeform Fabrication.** 1999. pp. 369.

53. Adams, R.T., Rosenberg, H.W. **Titanium and Titanium Alloys—Scientific and Technological Aspects.** *Plenum Press Publishing.* 1982. pp. 127.

54. Jackson, M., Dring., K. *Materials Science and Technology.* **22(8).** 2006. pp. 881.

55. Gerdemann, S.J. *Advanced Materials & Processes.* July 2001. pp. 41.

56. Crowley, G. *Advanced Materials & Processes.* November 2003. pp. 25.

57. Fuwa, A. Takaya, S. *JOM*. **57(10).** 2005. pp.56.

58. Nagesh, CH.R.V.S., Sridhar Rao, CH., Ballal, N.B., Krishna Rao, P. *Metallurgical and Materials Transactions B.* **35B.** 2004. pp. 65.

59. Okabe, H.T., Waseda, Y. *JOM.* **49(6).** 1997. pp. 28.

60. Wartman, F.S., Baker, D.H., Nettle, J.R., Homme, V.F. *J. Electrochem. Soc.* **101.** 1954. pp. 507.

61. Petrunko, A.N., Galitsky, N.V., Pampooshko, N.A., Denisov, S.I., Andeev, A.E. **Titanium and Titanium Alloys—Scientific and Technological Aspects.** *Plenum Press Publishing.* 1982. pp. 101.

62. Ogurtsov, S.V. **Titanium and Titanium Alloys—Scientific and Technological Aspects.** *Plenum Press Publishing.* 1982. pp. 41.

63. Reznichenko, V.A. **Titanium and Titanium Alloys—Scientific and Technological Aspects.** *Plenum Press Publishing.* 1982. pp. 63.

64. Coble, R.L. *Journal of Applied Physics.* **32.** 1961. pp. 789.

65. Zhao, J., Harmer, M.P. *Philos. Mag. Letters.* **63.** 1991. pp. 7.

66. Thompson, A.M., Harmer, M.P. *J. Amer. Chem. Soc.* **76.** 1993. pp. 2248.

67. Su, H., Jouhnson, D.L. *J. Amer. Chem. Soc.* **79.** 1996. pp. 3211.

68. Hansen, D., Rusin, R.P., Teng, M.H., Johnson, D.L. *J. Amer. Chem. Soc.* **75.** 1992. pp. 1129.

69. Kang, S-K.L., Jung, Y-L. *Acta Materialia.* **52.** 2004. pp. 4573.

70. Liu, Y., Chen, L.F., Tang, H.P., Liu, C.T., Liu, B., Huang, B.Y. *Materials Science and Engineering.* **A418.** 2006. pp. 25.

71. Wei, W.F., Liu, Y., Tang, H.P., Huang, B.Y. *Powder Metallurgy.* **46.** 2003. pp. 246.

72. Fujita, T., Agawa, A., Ouchi, C., Tajima, H. *Materials Science and Engineering.* **A213.** 1996. pp. 148.

73. Koike, J. Shimoyama, Y., Fujii, H., Maruyama, K. *Scripta Materialia.* **39.** 1998. pp. 1009.

74. Saito, T., Takamiya, H., Furuta, T. *Materials Science and Engineering.* **A243.** 1998. pp. 273.

75. Hu, D., Johnson, T.P., Loretto, M.H. **Advances In Powder Metallurgy and Particulate Materials.** *MPFI.* 1995. pp. 109.

76. Radhakrishna Bhat, R.V., Tamirisakandala, S., Miracle, D. *Metallurgical and Materials Transactions A.* **36(3).** 2005. pp. 845.

77. Goodwin, P.S., Wisbey, A., Ubhi, H.S., Kulikowski, Z., Gasson, P., Ward-Close, C.M. **Titanium '95: Science and Technology.** 1995. pp. 2874.

78. Boyer, R., Welsch, G., Collings, E.W. **ASM Materials Properties Handbook: Titanium Alloys.** *ASM International, Materials Park, OH.* 1994.

79. Chen, L., Gu, Y., Qian, Y. Shi, L., Yang, Z., Ma, J. *Materials Research Bulletin.* **39.** 2004. pp. 609.

80. Axelbaum, R.L., DuFaux, D.P., Frey, C.A., Kelton, K.F., Lawton, S.A., Rosen, L.J., Sastry, S.M.L. *Journal of Materials Research.* **11(4).** 1996. pp. 948.

81. Axelbaum, R.L., Bates, S.E., Buhro, W.E., Frey, C.A., Kelton, K.F., Lawton, S.A., Rosen, L.J., Sastry, S.M.L. *Nanostructured Materials.* **2.** 1993. pp. 139.

82. Axelbaum, R.L., DuFaux, D.P., Frey, C.A., Sastry, S.M.L. *Metallurgical and Materials Transactions.* **B28.** 1997. pp. 1199.

83. Steffens, K.L., Zachariah, M.R., DuFaux, D.P., Axelbaum, R.L. *Chemical Materials.* **8.** 1996. pp. 1871.

84. Carneiro Ueta, M.C., Fracote, C.A., Rodrigues Henriques, V.A., Alencastro Graca, M.L., Alves Cairo, C.A. *Materials Science Forum*. **498-499.** 2005. pp. 211.

85. Kobayashi, M., Funami, K., Suzuki, S., Ouchi, C. *Materials Science & Engineering.* **A243.** 1998. pp. 279.

86. Radhakrishna Bhat, R.V., Tamirisakandala, S., Miracle, D. *Journal of Materials Engineering and Performance.* **13(6).** pp. 653.

87. Saito, T., Takamiya, H ., Furuta, T. **Titanium '95: Science and Technology.** 1995. pp. 2859.

88. Saito, T., Furuta, T., Takamiya, H. **Titanium '95: Science and Technology.** 1995. pp. 2763.

89. Zhao, F., Fan, Y. **Titanium '95: Science and Technology.** 1996. pp. 2688.

90. Saito, T., Furuta, F., Yamaguchi, Y. **Recent Advances In Titanium Metal Matrix Composites.** *TMS Warrendale, PA.* 1995. pp. 33.

91. Fan, Z., Niu, H.J., Miodownik, A.P., Saito, T., Cantor, B. *Key Engineering Materials.* **127-131.** 1997. pp. 423.

92. Feng, H.B., Jia, D.C., Zhou, Y., Huo, J. *Materials Science and Technology.* **20.** 2004. pp. 1205.

93. Hirschhorn, J.S. **Introduction to Powder Metallurgy.** *American Powder Metallurgy Institute.* 1976.

94. Hall, E.O. *Proceedings of the Physical Society*. London B64. 1951. pp. 747.

95. Petch, N.J. *Journal of the Iron and Steel Institute*. London 174. 1953. pp. 25.

96. Cadle, R.D. **Particle Size: Theory and Industrial Applications.** *Reinhold Publishing.* 1965.

97. Irani, R.R., Callis, C.F. **Particle Size: Measurement, Intrepretation and Application.** *Wiley Publishing.* 1963.

98. Ouchi, C., Iizumi, H., Mitao, S. *Materials Science and Engineering.* **A243.** 1998. pp. 186.

99. Finlay, W.L., Snyder, J.A. *Trans. AIME.* **188.** 1950. pp. 277.

100. Barth, W.J., Field, A.L. *Metal Progr.* **64.** 1953. pp. 74.

101. Jaffe, R.I., Campbell, I.E. *Trans. AIME.* **185.** 1949. pp. 646.

102. Jaffe, R.I. *Titanium '80, Science and Technology.* **Vol. 4.** 1980. pp. 1665.

103. Jaffe, R.I. *Progr. Metal Phys.* **7.** 1958. pp. 65.

104. Simbi, D.J., Scully, J.C. *Materials Letters.* **26.** 1996. pp. 35.

CHAPTER 3

MICROSTRUCTURAL DEVELOPMENT OF CP-TI AND TI-B MATERIAL

3.1 Introduction

Over the past 25 years, the price and demand of titanium, not withstanding short - term price/availability perturbations, has risen and continues to rise. For less critical applications, novel, cost-effective titanium processing methods need to evolve to meet the rising demands of the automotive, sports equipment, chemical and petrochemical industries. New processes have recently been developed to produce high quality titanium and titanium alloy powder to meet the increasing demands of these diverse markets. In addition, titanium powder metallurgy (PM) methods could potentially reduce the concerns of elemental segregation and non-uniform dispersion of insoluble second phases allowing the development of new alloys not previously possible using ingot metallurgy methods. In addition, near net shape parts can be produced with PM methods, which reduce the amount of input titanium material and final machining required. As a result, the total cost of producing parts is reduced.

Although titanium PM processing may provide many advantages, significant secondary processing is required to consolidate the powder into the desired shape. These secondary processes include, but are not limited to, hot isostatic pressing (HIP)[1-5],

vacuum hot pressing (VHP)[6,7], mechanical pressing[8-11], cold isostatic pressing (CIP)[12-17], sintering and other hot working operations[3,12,13,18]. As with any production process, choice of the secondary process used to consolidate titanium powder depends on desired mechanical properties (i.e. tensile, fatigue, and fatigue crack growth) and cost. In turn, the mechanical properties depend on cleanliness, density, and microstructure. The final cost depends on cycle time, and production level.

The most common method for consolidating powder metal is hot isostatic processing (HIP). The titanium powder is placed into an oversized metallic container and the gas is evacuated from the container prior to hermetically sealing it. The container is then placed into a pressure vessel in which isostatic pressure is imposed on the powder container while it is heated to the desired temperature. The combination of the pressure and temperature collapses the container onto the powder. The resulting stress state is isostatic. The HIPing process forms a nominally fully dense material that closely resembles the shape of the original container except smaller because of densification. HIPing is the most widely used process to consolidate powder material despite its cost because it produces the cleanest, fully dense product in a mass production environment.

A number of other secondary processing methods utilize pressure with or without heat to consolidate Ti powder. In vacuum hot pressing (VHP), a cavity set typically of Mo alloy dies are filled with titanium powder in a vacuum container and heated to the desired temperature as a vacuum is applied and a hydraulic press exerts consolidation pressure. All of the variables are held until the powder is consolidated into the desired shape. This process produces a product that has similar properties to wrought products, but is more costly than HIPing. Cold isostatic pressing (CIP) is also very similar to HIP

as they both utilize isostatic pressure to consolidate a powder that is in an evacuated and sealed container. However, CIP, as the name implies, is carried out at room temperature and uses a soft plastic or elastomeric container. Although CIP has a lower cost, the inability to obtain full dense and tightly dimensioned products has limited the opportunities for this process. In mechanical pressing, pressure is applied to the powder within the dies using hydraulic presses. As mechanical pressing is carried out at room temperature it does not require expensive Mo alloy die material like VHP requires; however the product formed is not as dense as VHP but has good dimensional control. Thus, an additional processing step is required to improve the density. Although VHP, CIP and mechanical pressing are similar to HIP, none possess the combination of high density and good dimensional control.

In order to obtain higher densities in PM material, subsequent hot working operations are used. The most common hot working operations are rolling, extrusion and closed die forging. The hot working of material after it has been compacted with one of the before mentioned processes, produces a more dense material for applications where porosity must be minimized or eliminated. In addition to minimizing porosity, these working operations put varying amounts of plastic deformation into the material, which affect the final microstructure and mechanical properties of the material. Therefore, the hot working operation that is used is strongly dependent on the mechanical properties required for the final application.

The purpose of this research is to examine titanium alloys produced with boron using the novel titanium production method called the Armstrong process[19-44], as discussed in Chapter 2. The material that is characterized in this study was consolidated

using a HIP, extrude and heat-treat process sequence similar to the processing protocol for nickel powder alloys. Consolidated commercially pure (CP) titanium, Ti-0.8B and Ti-0.9B material was characterized in this study.

3.2 Materials and Methods

The commercially pure (CP) titanium, Ti-0.8B and Ti-0.9B powder mentioned in Chapter 2 was the starting powder material for this part of the study. As mentioned in Chapter 2, the boron containing powders used in this study were the first process runs to attempt to alloy titanium with boron using the Armstrong process.

3.2.1 Consolidation and Heat Treatment Processing

The lots of CP-Ti, Ti-0.8B, and Ti-0.9B powder shown in Table 2.3 were consolidated by HIPing, extrusion, and subsequent heat treatment, in order to characterize the material in a condition similar to that in which it would be used. Each of the powder lots were placed in three different HIP cans in an inert environment glove box. The glove box was equipped with scrubbers for oxygen, nitrogen and hydrogen contaminants for inert handling to minimize the potential for contamination of the powder. Each HIP can was ~6 in. in length by ~2 in. in diameter and made of Ti-6Al-4V. The HIP cans were backfilled with argon, evacuated and closed by electron beam welding. Each HIP can was then placed in a Flow-Autoclave Mini-Hipper (Model QIH9) one at a time. The cans were HIPed at a pressure of 30 ksi (207 MPa) and a temperature of 1700^{o}F (926^{o}C) for 4 hours.

Upon completion of HIPing, the cans were machined round and placed "cold" into a furnace with a hydrogen environment for two and a half hours at 1650^{o}F (900^{o}C). After two and a half hours, the cans were taken one at a time from the furnace and immediately extruded in a 1250-ton hydraulic extrusion press and air-cooled. The extrusions were performed with a ram speed of 50 in./min. and an extrusion ratio of 10 to 1. The length and diameter of each of the three extrusions were then ~45 in. and ~0.665 in., respectively. The three extrusions were heat-treated in a Lindberg air furnace at 1300^{o}F (704^{o}C) for 2 hours and air-cooled.

3.2.2 Chemical Analysis

Chemical analysis was performed on the three lots of powder discussed in Chapter 2 (powder chemistries shown in Table 2.3) after consolidation. The chemical analysis of the consolidated material was performed using the same methods as discussed in section 2.2.2.

3.2.3 X-Ray Diffraction

X-ray diffraction qualitative phase analysis of the consolidated Ti-0.8B and Ti-0.9B material was completed to confirm the crystal structure(s) of all phases in the material. The structure(s) present in the consolidated material was determined using a Bruker-AXS General Area-Detector Diffraction System (GADDS) with a 0.02 in. incidence beam collimator and area detector. The GADDS was equipped with a copper target and a beam size of 0.02 in. x 0.04 in. Diffraction results were compared to known

standards to confirm the crystal structure(s) of the phase(s) present in the consolidated Ti-0.8B and Ti-0.9B material.

3.2.4 Metallography

3.2.4.1 Metallography - Scanning Electron Microscopy

Metallographic mounts were made from each of the lots of consolidated and heat-treated CP-Ti, Ti-0.8B and Ti-0.9B material for characterization. The three lots of material were mounted after being HIPed, extruded and heat-treated. Each lot of material was sectioned using a Struers Labotom-3 SiC cutting wheel. The material was removed from the center of the extrusion and mounted in Konductomet® such that the longitudinal and transverse directions of the material could be characterized. The metallographic mounts were then wet ground and polished as outlined in Table 2.2. After grinding and polishing, the mounts were etched in a solution with 10% oxalic acid, 1% HF, and 89% H_2O for characterization by scanning electron microscopy.

3.2.4.2 Metallography - Transmission Electron Microscopy

Transmission electron microscopy (TEM) foils were made from each of the three lots of consolidated and heat-treated CP-Ti, Ti-0.8B and Ti-0.9B material for characterization. The three lots of material were created into foils after being HIPed, extruded and heat-treated. Each lot of material was drilled using an electrodischarge machine to create cylinders with a diameter of ~3 mm. The cylinders were then sectioned into ~1.25 mm thick disks. Each disk was mechanically ground using 600 grit abrasive to

a thickness of ~100 μm. A Gatan dimple grinder was then used to thin the center of the disks creating a dimple. The dimple was created by dimple grinding to ~20 μm thickness in the center using 6 μm diamond polishing paste to a thickness of 60 μm and down to ~20 μm using 1 μm diamond polishing paste. The dimpled samples were then ion milled to electron transparency using a Gatan Duo Ion Mill. The samples were milled using 6 keV Argon ions at an incidence angle of 10 degrees until the center of the sample was perforated. Once perforated, the foils were then suitable for characterization by TEM.

3.2.5 Scanning Electron Microscopy (SEM)

The lots of consolidated and heat-treated CP-Ti, Ti-0.8B and Ti-0.9B material were characterized using scanning electron microscopy (SEM). The three lots of material were characterized after being HIPed, extruded and heat-treated. Each lot of material was characterized after being mounted, ground, polished and etched. All SEM analysis was completed using a JEOL field emission microscope with a Tungsten filament, and a Sirion field emission microscope, both at 15-20 kV accelerating voltage. Qualitative analysis was completed using a Clemex Vision 3t/JS--2000 image analysis system.

3.2.6 Transmission Electron Microscopy (TEM)

The lots of consolidated and heat-treated CP-Ti, Ti-0.8B and Ti-0.9B material were characterized using transmission electron microscopy (TEM). The three lots of material were characterized after being HIPed, extruded and heat-treated. Each lot of material was characterized after being mechanically ground, dimple ground and ion

milled. All TEM analysis was completed using a PHILIPS CM200 microscope with a LaB6 filament and Tecnai TF-20 field emission S/TEM with an X-TWIN lens, both operating at 200 keV accelerating voltage.

3.3 Results

3.3.1 Chemical Analysis

Chemical analysis was performed on the consolidated commercially pure (CP) titanium, Ti-0.8B and Ti-0.9B material. The target compositions were Grade 4 CP-Ti material with 0.0, 0.8, and 0.9 wt.% boron. Table 3.1 shows the composition of the three lots of consolidated material. The specification composition maximums for Grade 2 and Grade 4 CP-Ti are also included in Table 3.1 for comparison. The oxygen and iron concentrations for the consolidated CP-Ti were 0.25 wt.% and less than 0.01 wt.%, respectively. The oxygen and iron concentrations for the consolidated Ti-0.8B and Ti-0.9B ranged from 0.61 – 0.66 wt.% and less than 0.01 wt.%, respectively. The consolidated Ti-B material had 0.36 – 0.42 wt.% more oxygen and the same amount of iron than the CP-Ti. It was observed that as the boron levels were increased, the oxygen levels increased. The consolidated Ti-B material also had increased levels of chlorine ranging from 0.04 – 0.05 wt.% in comparison to 0.01 wt.% for the CP-Ti material. The two lots of consolidated Ti-B material also contained trace amounts of sodium, nickel, hydrogen and carbon, which are all below maximum for typical Grade 4 CP-Ti material. The concentrations of nickel, hydrogen and nitrogen were comparable for all three lots of consolidated material.

	CP-Ti[#]	Ti+0.8wt.%B[#]	Ti+0.9wt.%B[#]	CP-Ti Grade 2*	CP-Ti Grade 4**
Ti	Balance	Balance	Balance	Balance	Balance
O	0.250%	0.615%	0.665%	0.2% max.	0.4% max.
B	-	0.725%	0.765%	-	-
Fe	0.003%	0.002%	0.003%	0.3% max.	0.5% max.
Na	0.055%	0.006%	0.007%	0.1% max.	0.1% max.
Cl	0.012%	0.040%	0.049%	0.1% max.	0.1% max.
Ni	0.002%	<0.001%	0.002%	0.1% max.	0.1% max.
C	0.021%	<0.005%	<0.005%	0.08% max.	0.08% max.
H	0.007%	0.008%	0.009%	0.0150% max.	0.0125% max.
N	0.007%	0.006%	0.008%	0.05% max.	0.05% max.

Consolidated CP-Ti, Ti-0.8B and Ti-0.9B produced from the Armstrong process powder.
* Grade 2 CP-Ti chemistry per AMS4902.
** Grade 4 CP-Ti chemistry per AMS 4901.

Table 3.1. Chemical composition of commercially pure (CP) titanium, Ti-0.8B and Ti-0.9B consolidated material. Chemistry of typical conventional Grade 2 and Grade 4 CP-Ti are also included for comparison.

3.3.2 X-Ray Diffraction

X-ray qualitative phase analysis was performed on the consolidated Ti-0.8B and Ti-0.9B material. Figures 3.1(a) and (b) shows the intensity versus phase angle from the diffraction scans for the Ti-0.8B and Ti-0.9B material, respectively. The crystal structure(s) of the phases in the Ti-0.8B and Ti-0.9B material were identified as hexagonal close packed (HCP) and orthorhombic. X-ray diffraction confirmed the crystal structures of the α (HCP) phase and TiB (orthorhombic) phase.

3.3.3 Scanning Electron Microscopy (SEM)

CP-Ti, Ti-0.8B and Ti-0.9B material are shown in Figures 3.2 - 3.7 after being HIPed, extruded and heat-treated. The CP-Ti had a microstructure consisting of α grains slightly elongated in the extrusion direction (Figure 3.2 - 3.3). The average α grain size was ~5.0 μm with an aspect ratio of ~1.3 to 1. In addition, a lath-like substructure was observed within ~20% of the α grains as shown in Figures 3.2 and 3.3. A limited amount, less than 5%, of porosity was observed in the consolidated material.

The Ti-0.8B and Ti0.9B had a microstructure consisting of α grains slightly elongated in the extrusion direction with TiB located at α/α grain boundaries and within α grains (Figures 3.4 - 3.7a - c). The average α grain size for Ti-0.8B and Ti-0.9B was ~2.0 μm with an aspect ratio of ~2 to 1, and ~1.5 μm with an aspect ratio of ~1.5 to 1, respectively. The TiB was observed to be either blocky or rod-shaped and was located at both α/α grain boundaries and within the α grains. The blocky TiB at the grain boundaries had an average size of (~2.0 μm and 1.5 μm) for Ti-0.8B and Ti-0.9B, both

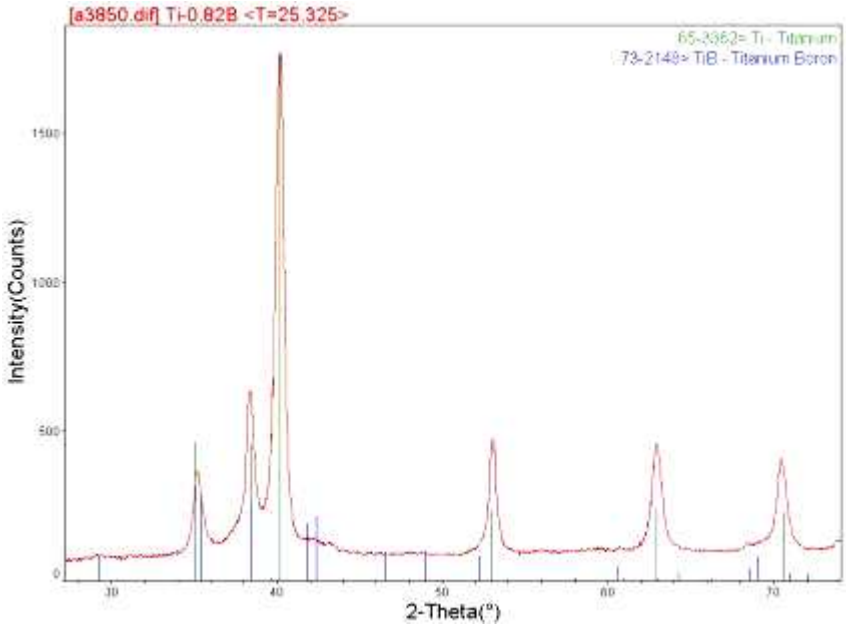

(a)

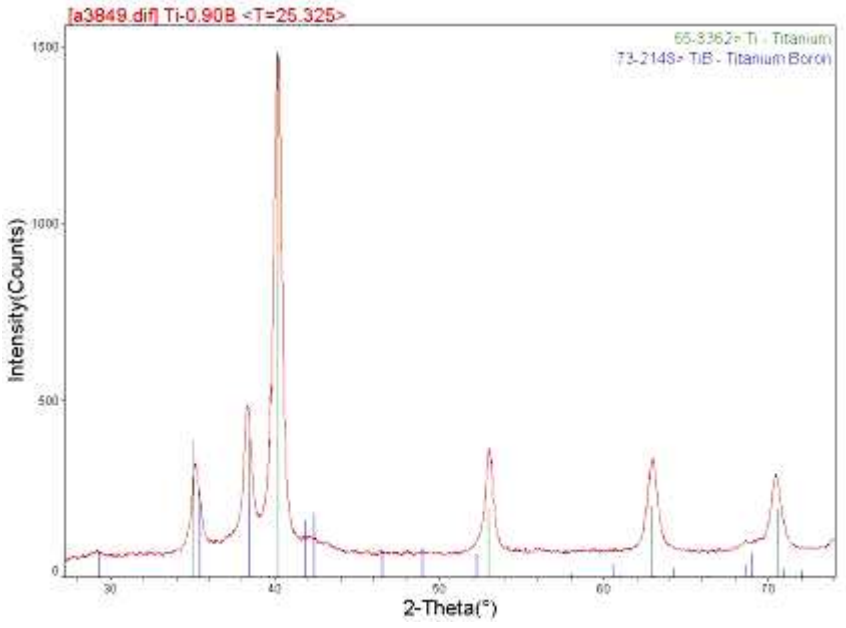

(b)

Figure 3.1. X-ray qualitative phase analysis of consolidated (a) Ti-0.8B, and (b) Ti-0.9B material.

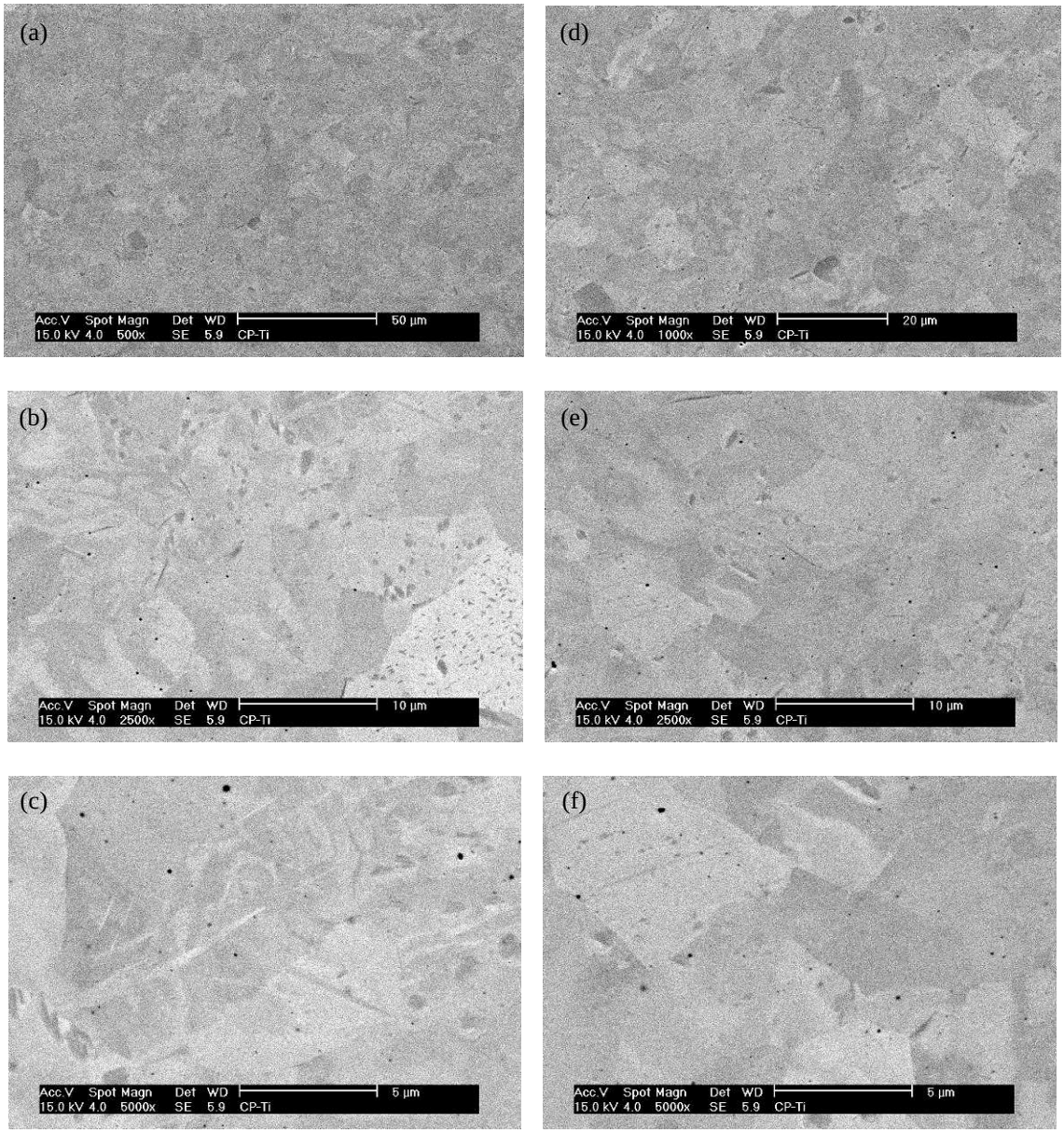

Figure 3.2. Micrographs of transverse cross-section of consolidated and heat-treated commercially pure (CP) titanium.

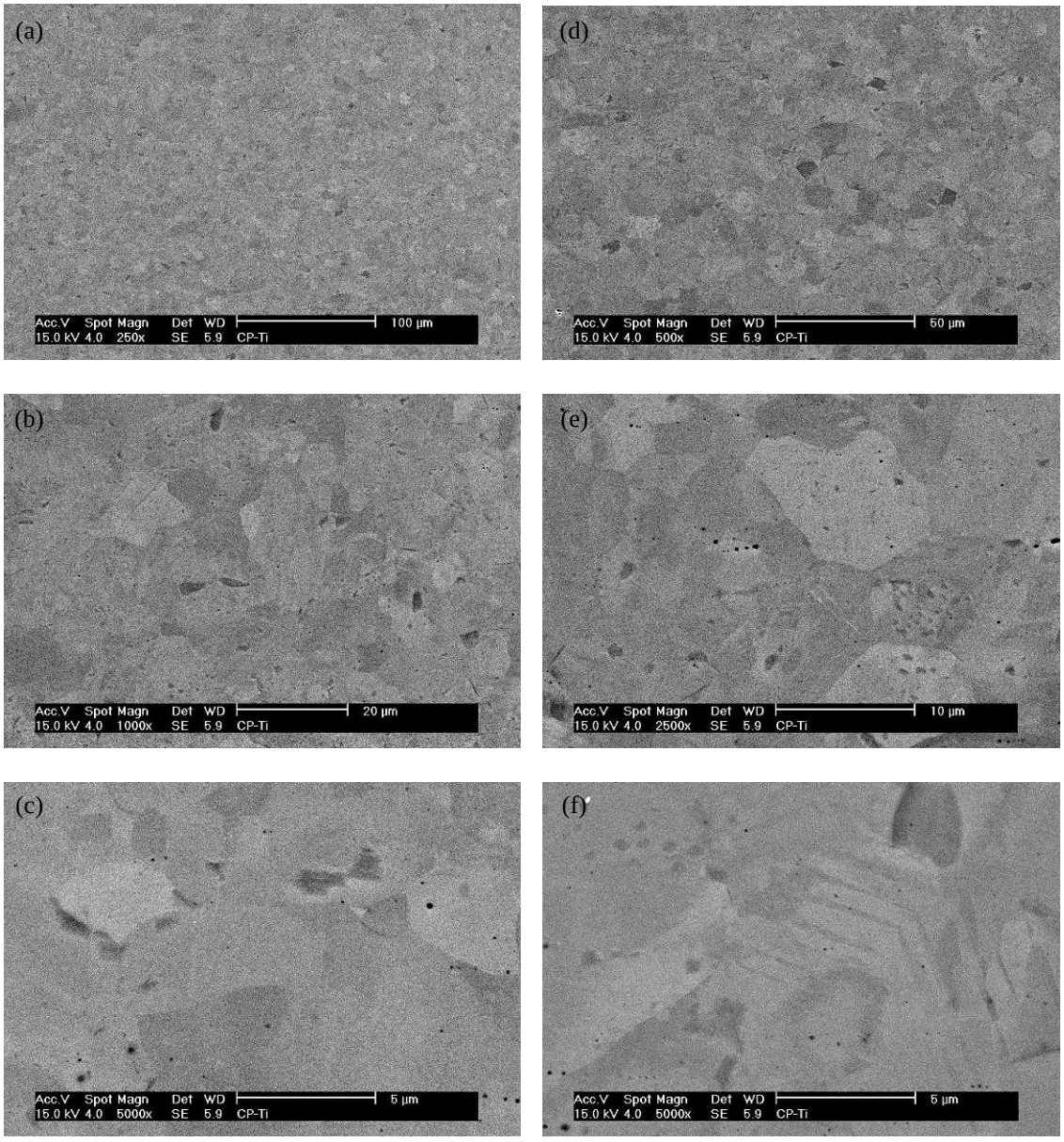

Figure 3.3. Micrographs of longitudinal cross-section of consolidated and heat-treated commercially pure (CP) titanium.

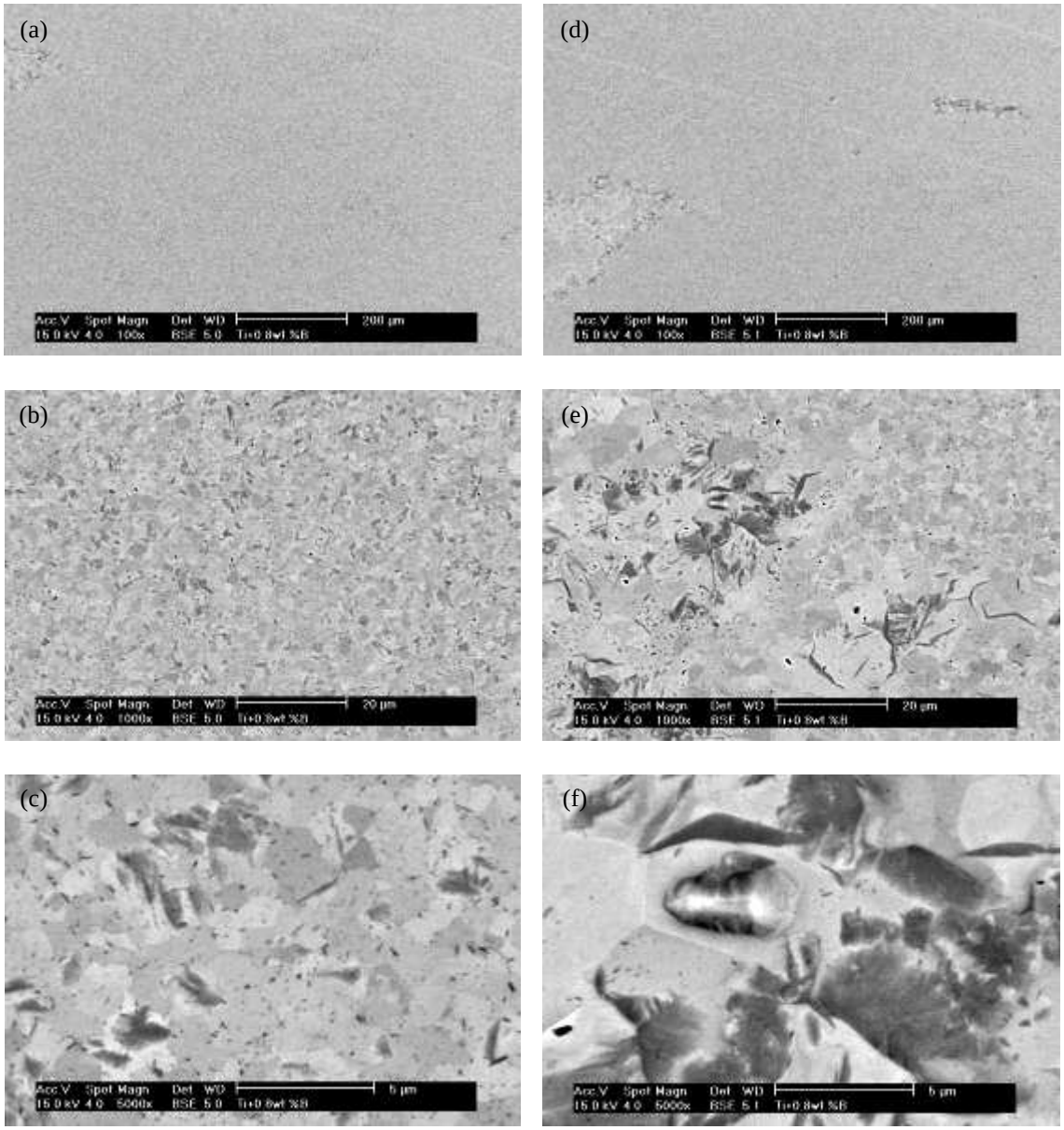

Figure 3.4. Micrographs of transverse cross-section of consolidated and heat-treated Ti-0.8B. Extrusion direction is into plane of paper.

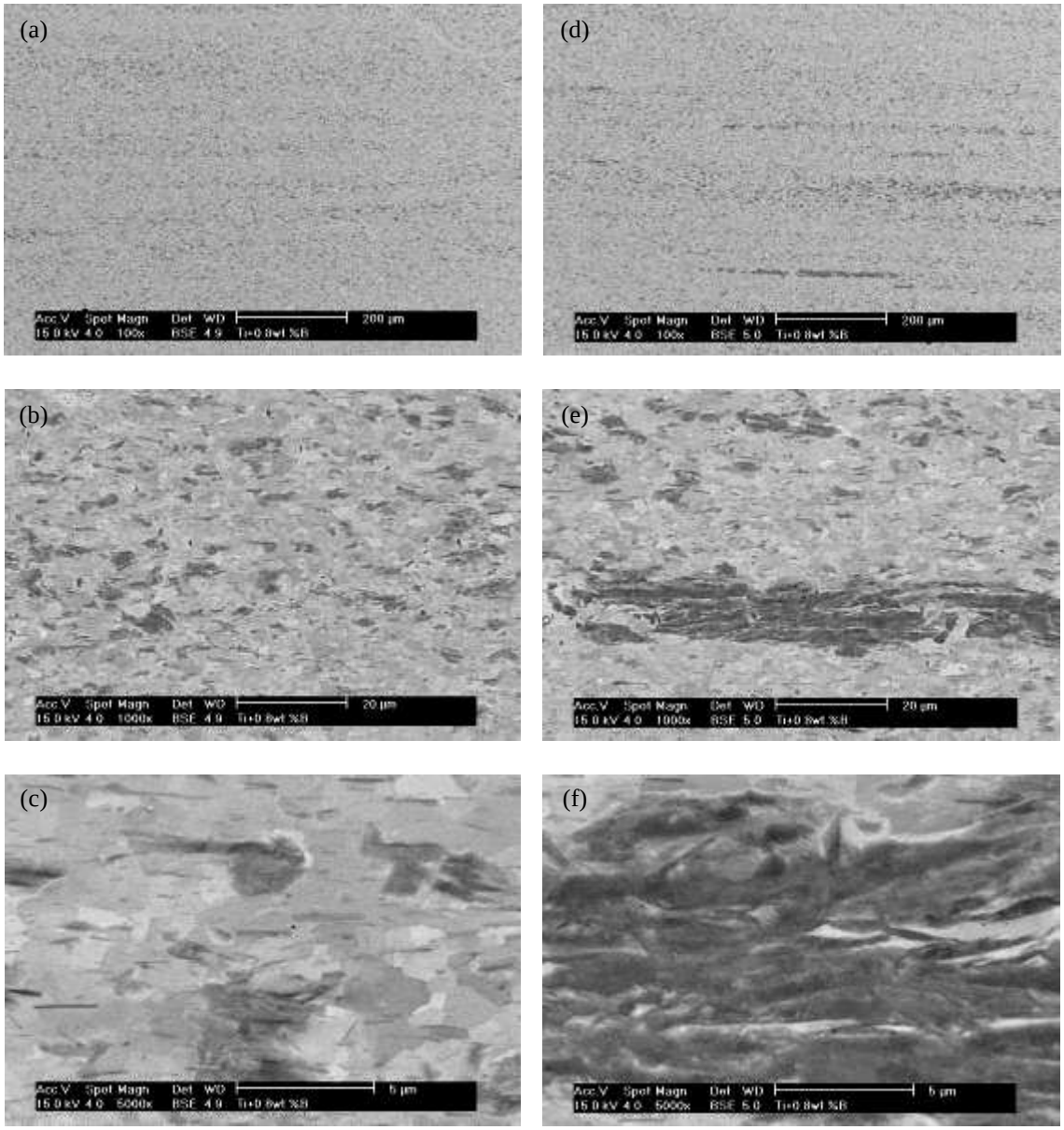

Figure 3.5. Micrographs of longitudinal cross-section of consolidated and heat-treated Ti-0.8B. Extrusion direction is parallel to width of paper.

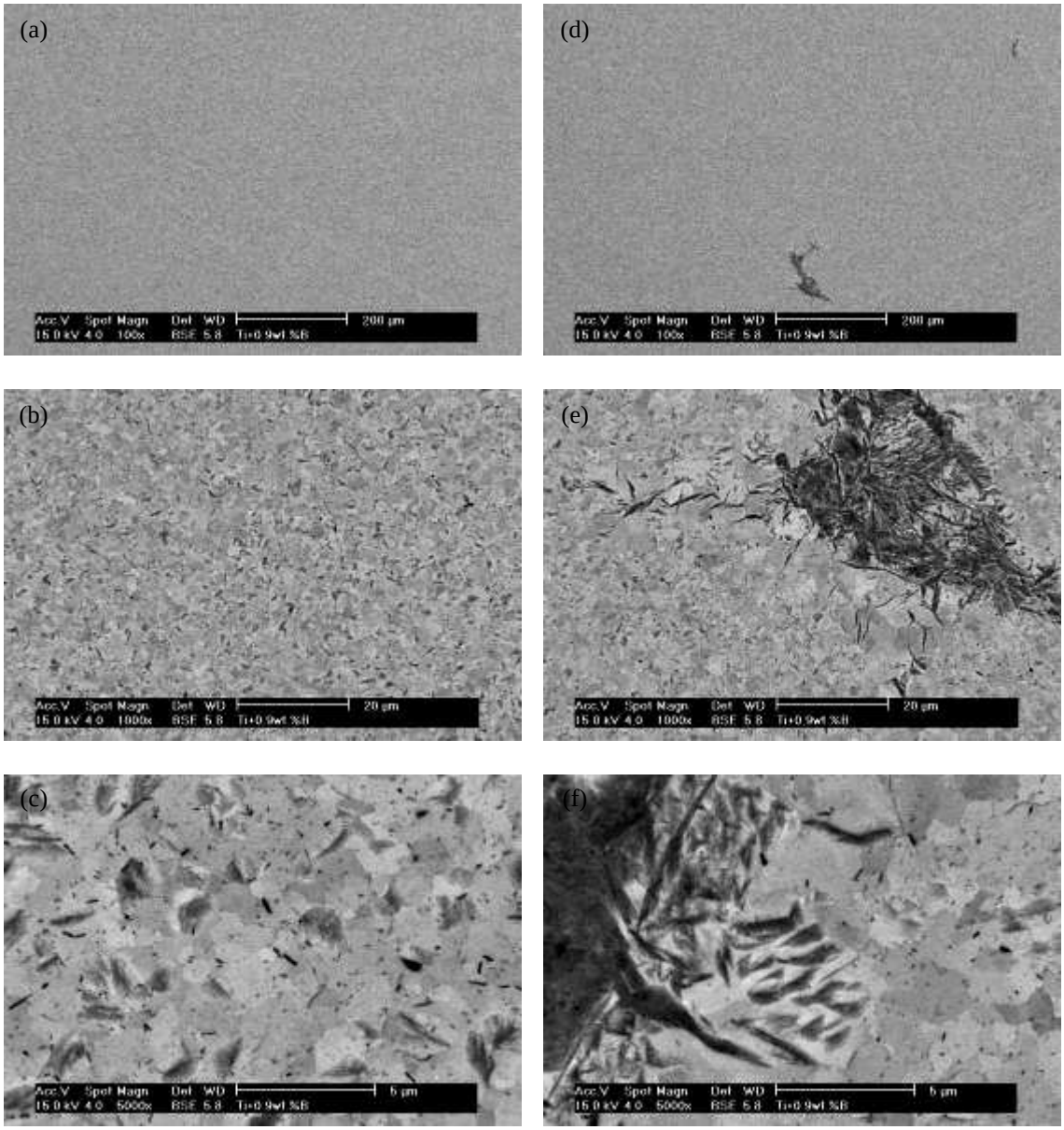

Figure 3.6. Micrographs of transverse cross-section of consolidated and heat-treated Ti-0.9B. Extrusion direction is into plane of paper.

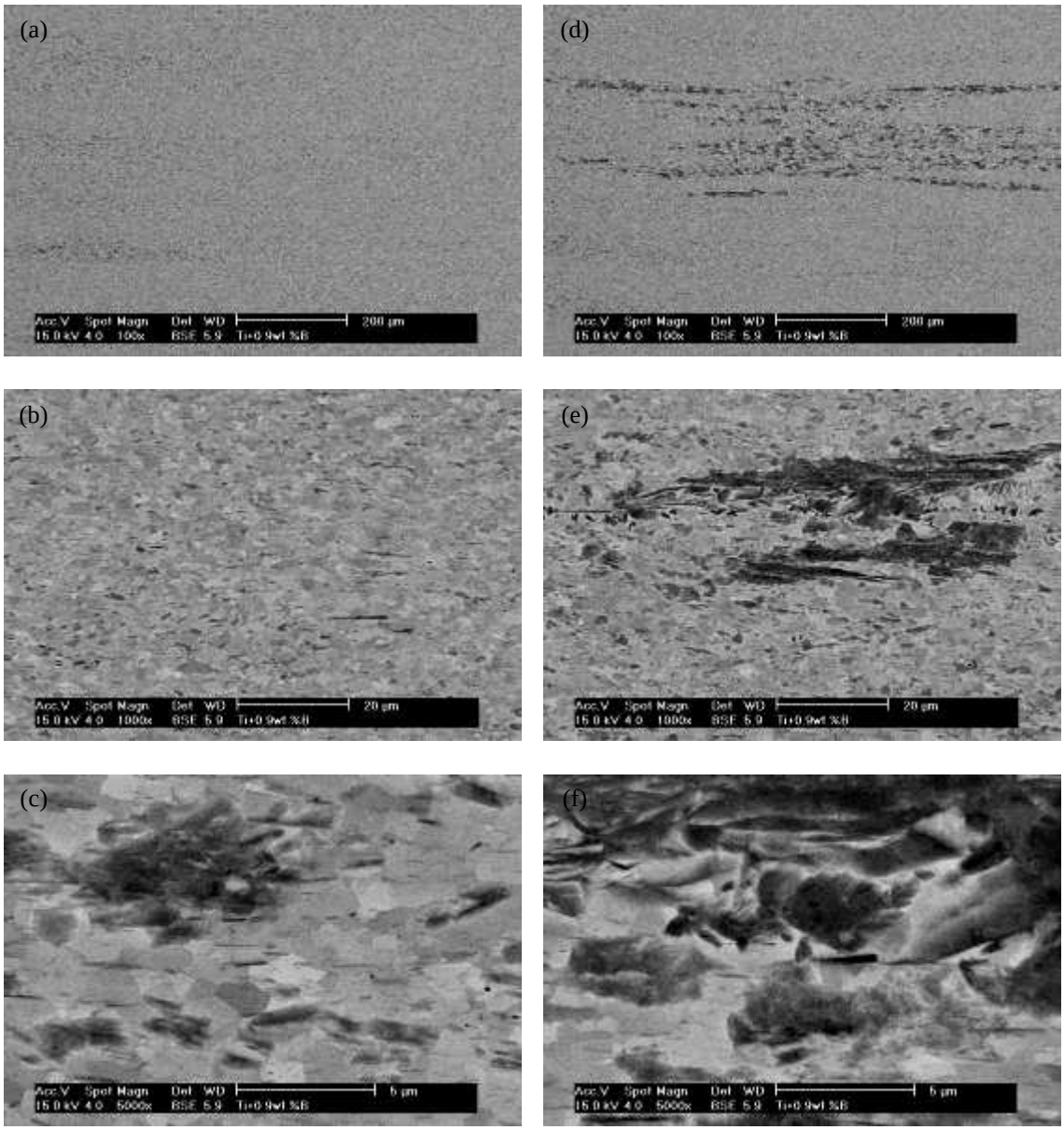

Figure 3.7. Micrographs of longitudinal cross-section of consolidated and heat-treated Ti-0.9B. Extrusion direction is parallel to width of paper.

with an aspect ratio of ~1 to 1. The rod-shaped TiB particles at the α/α grain boundaries and within the α grains for the Ti-0.8B and Ti-0.9B material were ~0.50 - 2.00 μm in length and ~0.05 - 0.20 μm in width; and ~0.50 - 1.00 μm in length, ~0.10 - 0.20 μm in width, respectively. Unlike the CP-Ti material, no porosity was observed in the Ti-0.8B and Ti-0.9B material. The total volume fraction of blocky and rod-shaped TiB in the Ti-0.8B and Ti-0.9B material was ~10% and ~15%, respectively.

In addition to the finer TiB distributed throughout the Ti-B materials, there were randomly distributed areas similar in contrast to TiB (Figures 3.4 - 3.7d - f). These areas, however, were determined to have titanium and not any boron present. Therefore, these regions were not TiB stringers. These regions were aligned along the extrusion direction with coarse α grains adjacent to the stringers. The size of the regions for the Ti-0.8B and Ti-0.9B material were 20 - 430 μm in length and 5 - 40 μm in width, and 50 - 535 μm in length and ~5 - 60 μm in width, respectively. The α grains adjacent to these regions for Ti-0.8B and Ti-0.9B were ~8.0 μm with an aspect ratio of ~1.2 to 1, and ~5.0 μm with an aspect ratio of ~1.2 to 1, respectively.

3.3.4 Transmission Electron Microscopy (TEM)

The CP-Ti, Ti-0.8B and Ti-0.9B material was characterized after being HIPed, extruded and heat-treated (Figures 3.8 - 3.13). The CP-Ti material consisted of α grains slightly elongated in the extrusion direction. In addition, an α lath substructure was observed within the α grains as shown in the bright field micrographs in Figure 3.8. The grains were confirmed to be the α (HCP) phase based on the electron diffraction patterns

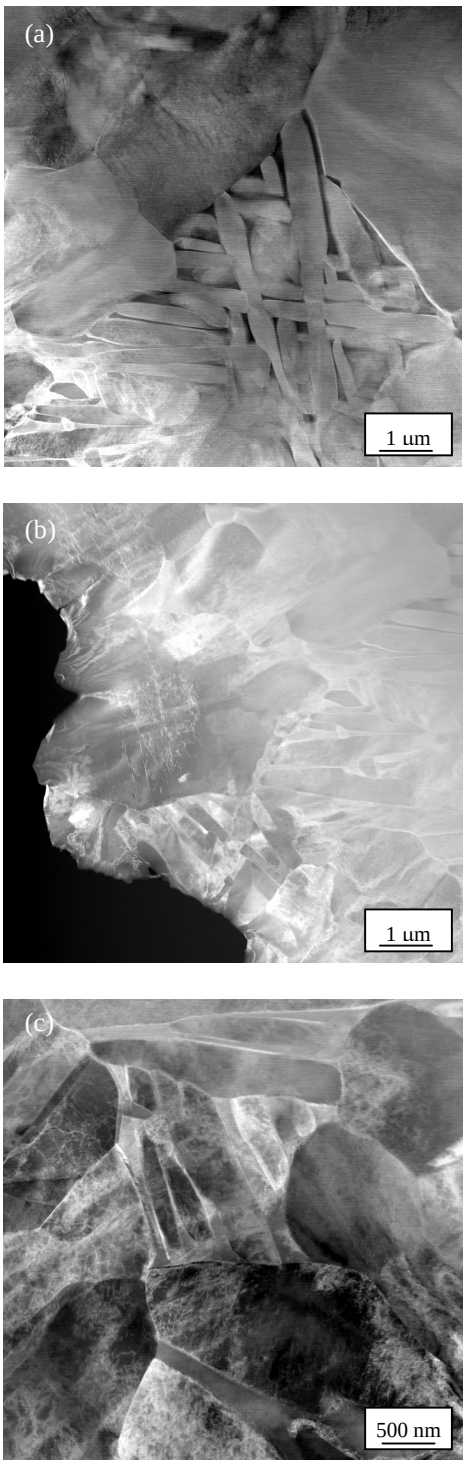

Figure 3.8. Bright field scanning transmission electron microscopy (STEM) micrographs of cross-section of consolidated and heat-treated commercially pure (CP) titanium.

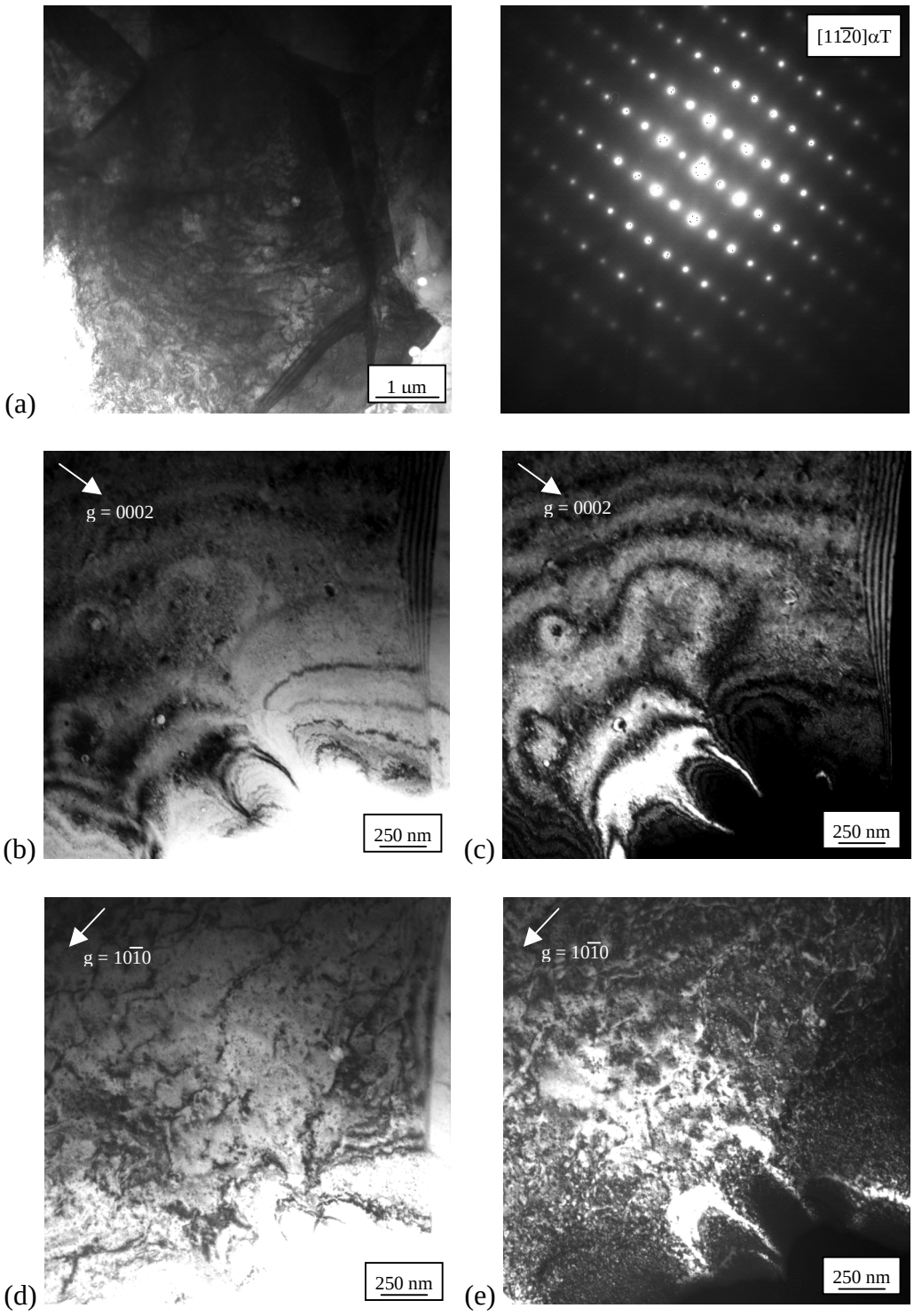

Figure 3.9. Bright field transmission electron microscopy (TEM) micrographs showing (a) HCP crystal structure of α grains, and overall dislocation structure of consolidated and heat-treated commercially pure (CP) titanium: g = 0002 (b) bright field, (c) dark field; g = 10$\bar{1}$0 (d) bright field, (e) dark field.

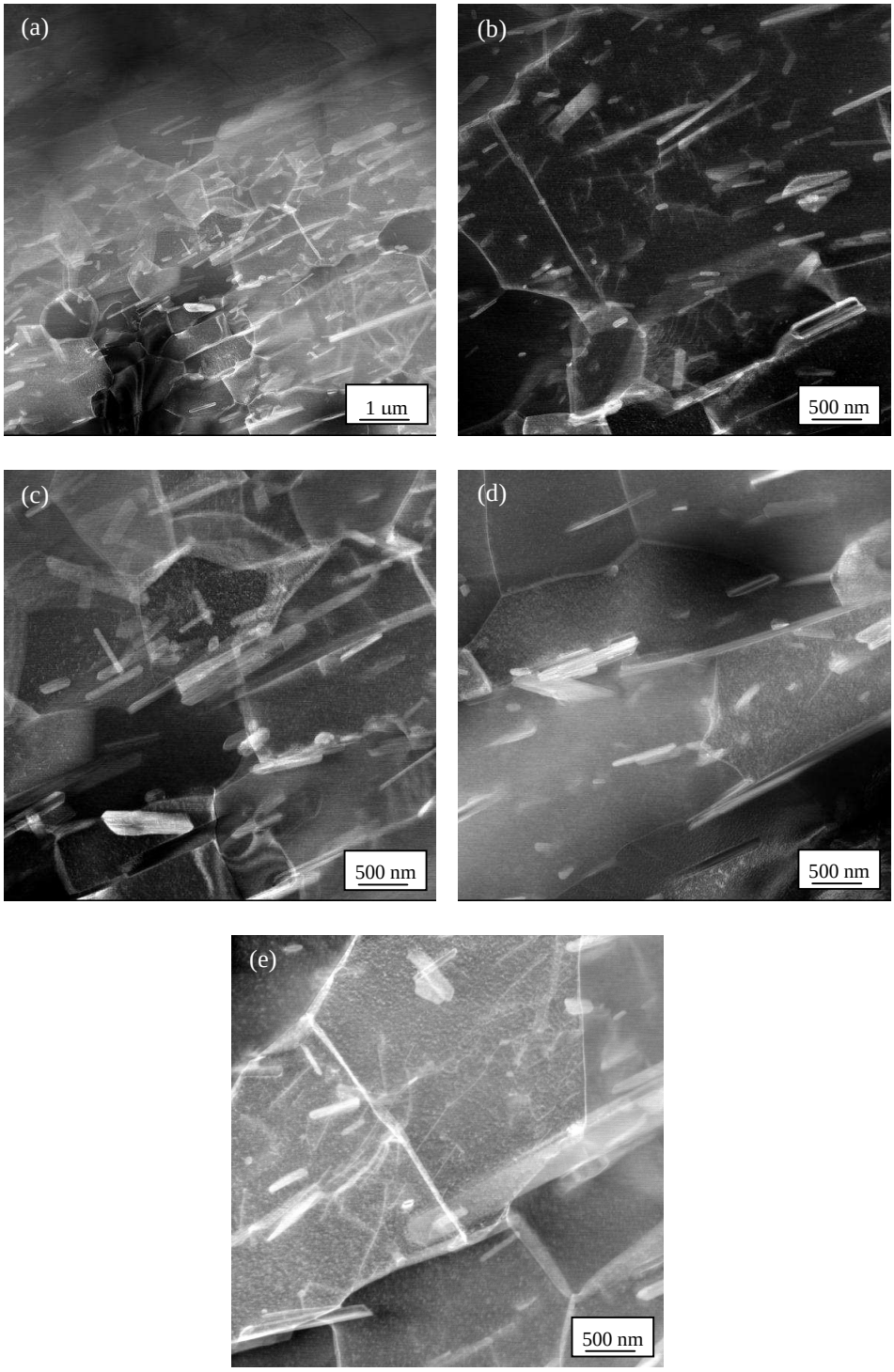

Figure 3.10. Bright field scanning transmission electron microscopy (STEM) micrographs of cross-section of consolidated and heat-treated Ti-0.8B. Micrographs show TiB in longitudinal direction.

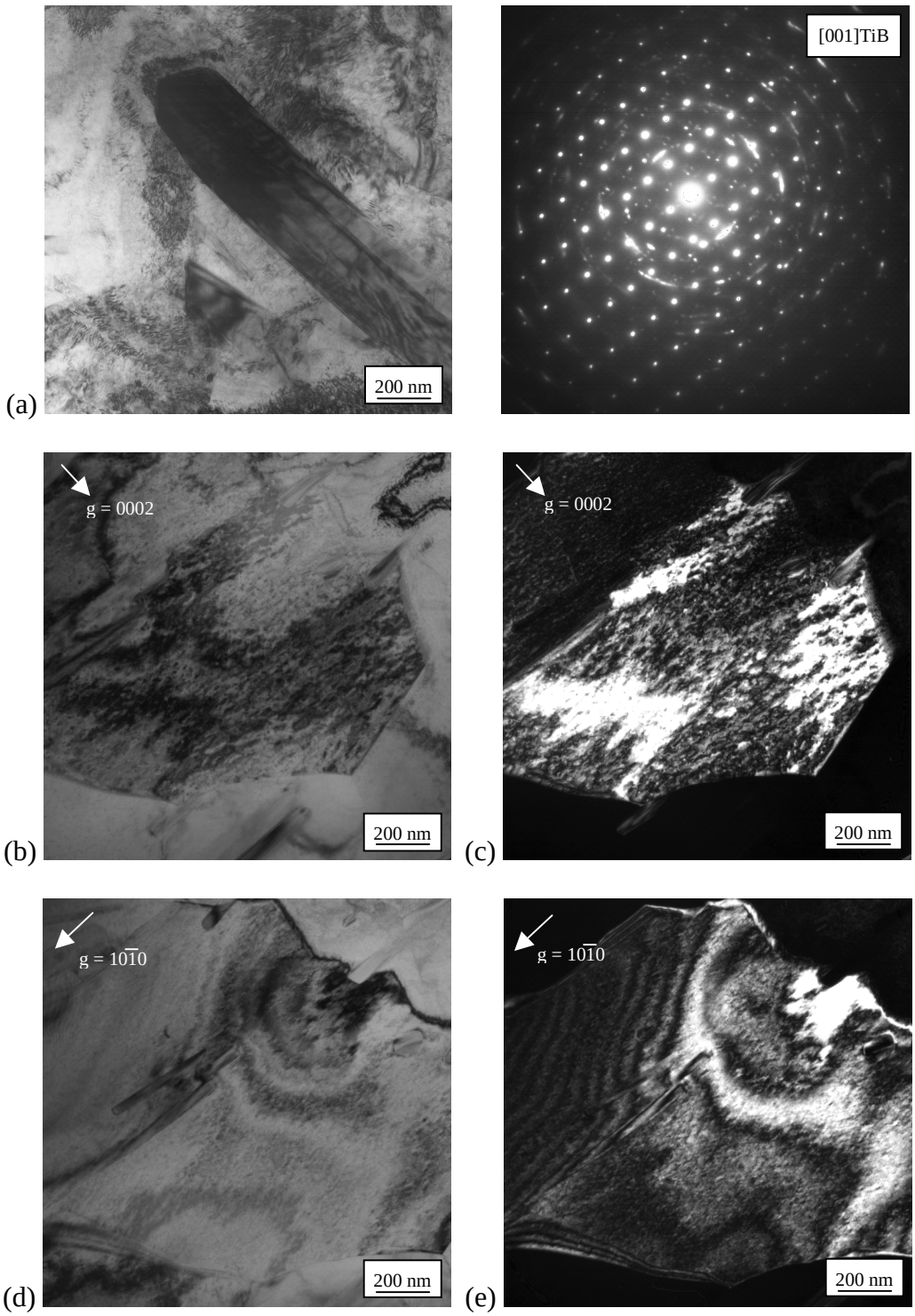

Figure 3.11. Bright field transmission electron microscopy (TEM) micrographs showing (a) orthorhombic structure of TiB, and overall dislocation structure of consolidated and heat-treated Ti-0.8B: g = 0002 (b) bright field, (c) dark field; g = 10$\bar{1}$0 (d) bright field, (e) dark field. Micrographs show TiB in longitudinal direction.

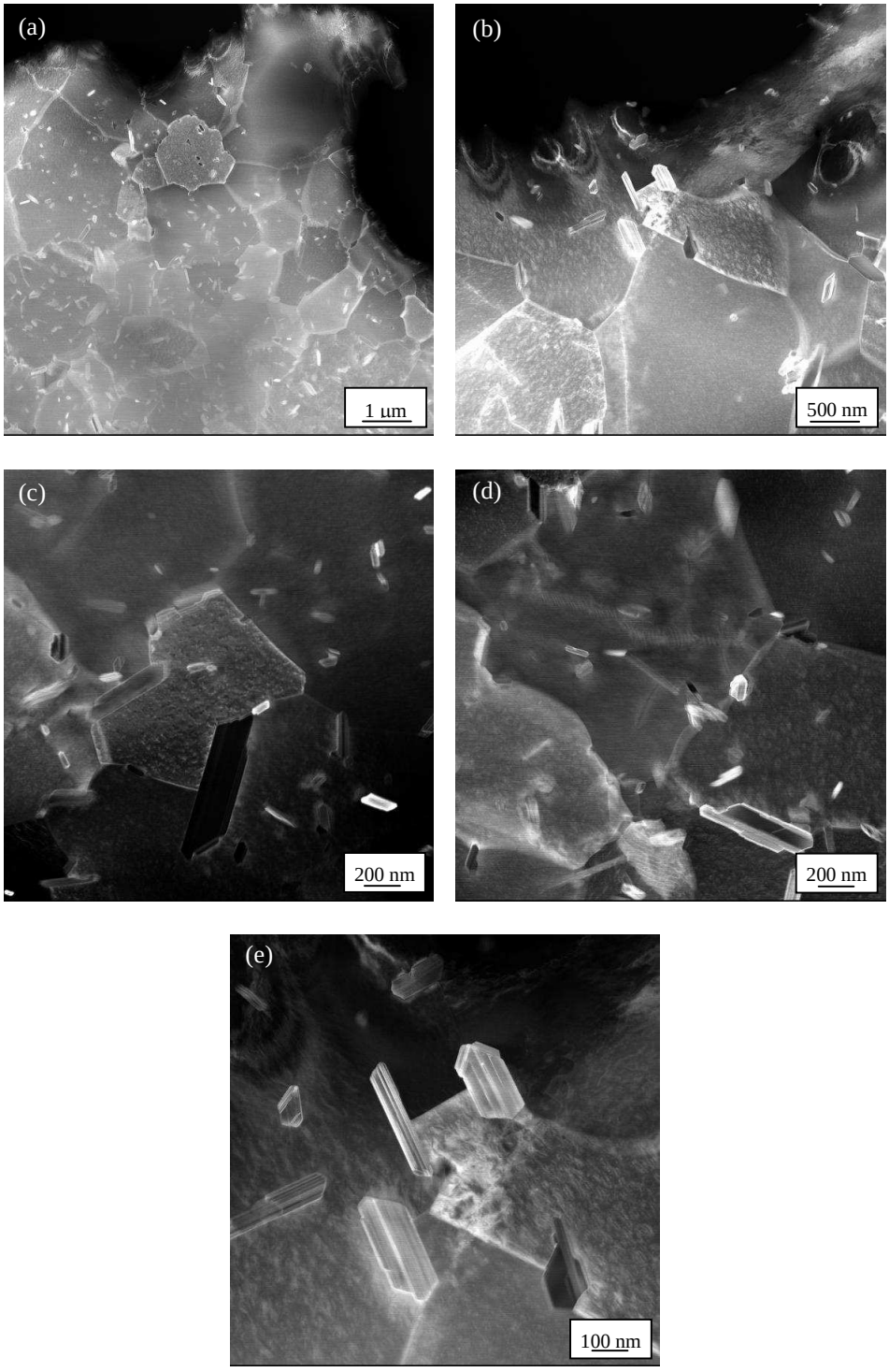

Figure 3.12. Bright field scanning transmission electron microscopy (STEM) micrographs of cross-section of consolidated and heat-treated Ti-0.9B. Micrographs show TiB in transverse direction.

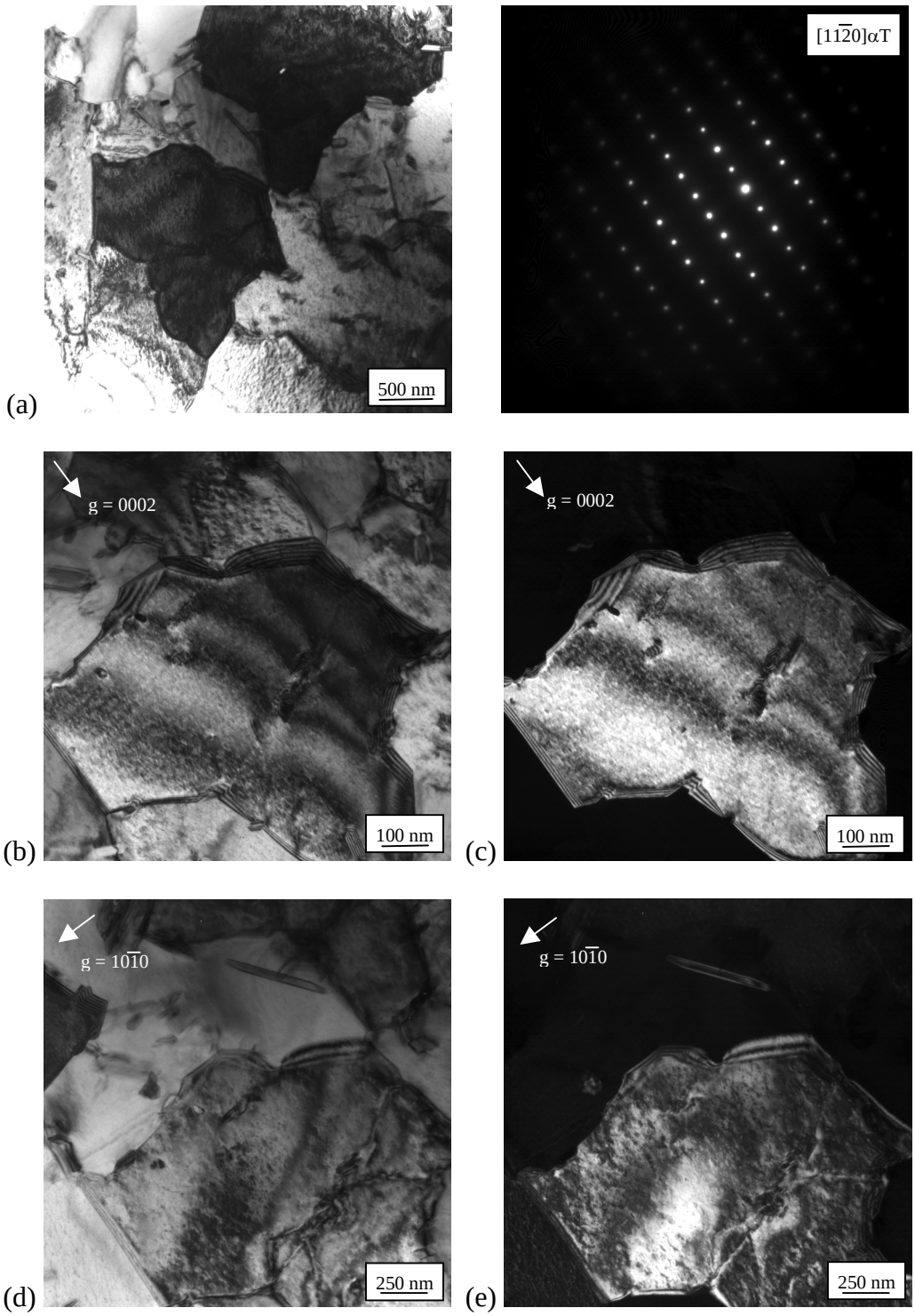

Figure 3.13. Bright field transmission electron microscopy (TEM) micrographs showing (a) HCP crystal structure of α grains, and overall dislocation structure of consolidated and heat-treated Ti-0.9B: g = 0002 (b) bright field, (c) dark field; g = 10$\bar{1}$0 (d) bright field, (e) dark field. Micrographs show TiB in transverse direction.

(Figure 3.9). Even with a high extrusion ratio, the α grains had a very low dislocation density due to the post-extrusion heat treatment annealing out most of the dislocations. The dislocations were observed to be $\vec{a}$ type and wavy in appearance.

The Ti-0.8B and Ti-0.9B material consisted of α grains slightly elongated in the extrusion direction with TiB located at α/α grain boundaries and within α grains (Figures 3.10 - 3.13). As with the CP-Ti material, a very low dislocation density was observed in the α grains from plastic deformation during the extrusion process. The dislocations were observed to have $\vec{a}$ and $\vec{c}$ type slip character and wavy in appearance. Based on the published literature and morphology of the dislocations, they are most likely $\vec{a}$ and $\vec{c} + \vec{a}$ type. The TiB was blocky at α/α grain boundaries, specifically the triple points, and rod-shaped at both α/α grain boundaries and within α grains. The blocky and rod-shaped TiB varied in size with fine intergranular rod-shaped TiB that was not resolvable with the SEM, but was observed using the TEM. Electron diffraction pattern analysis confirmed the crystal structures of the α (HCP) phase and TiB (orthorhombic) phase (Figures 3.11a,b and 3.13a,b for 0.8 and 0.9 wt.% boron, respectively). The TiB exhibited a heavy degree of faulting which is not unexpected as it is a topologically close-packed structure.[45] No reaction products were observed at the α to TiB interfaces.

3.4 Discussion

3.4.1 Commercially Pure (CP) Titanium Microstructure

The commercially pure (CP) titanium, Ti-0.8B and Ti-0.9B powder produced using the Armstrong process was subsequently HIPed, extruded and annealed.

(a)

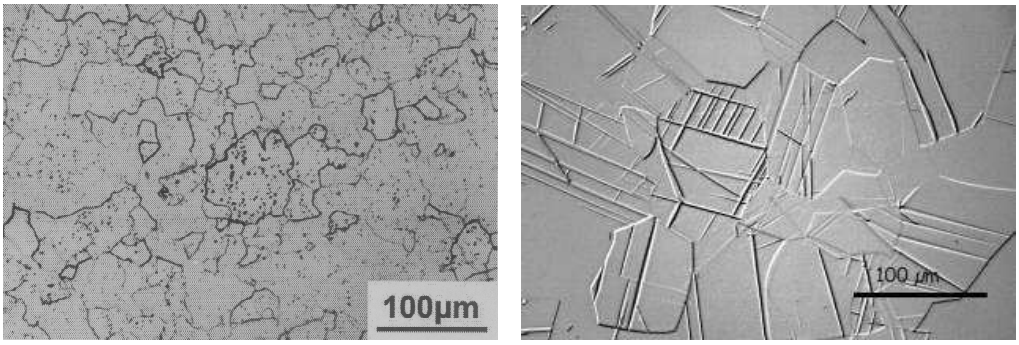

(b)

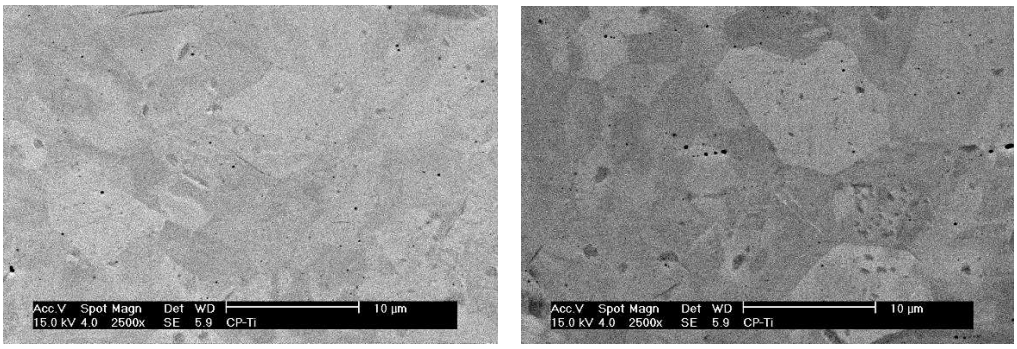

Figure 3.14. Comparison of microstructures observed for (a) conventionally processed commercially pure (CP) titanium[18], and (b) CP-Ti from consolidated and heat-treated Armstrong powder.

Figure 3.14 shows a comparison of a typical microstructure observed for CP-Ti along with CP-Ti material produced from Armstrong powder. The microstructure of the CP-Ti material, from consolidated and heat-treated Armstrong powder, exhibits slightly elongated α grains with ~20% of those grains having an α lath substructure. The elongated grains and substructure are believed to have formed as part of the extrusion process. The powder was consolidated and worked below the β transus in the HIP and extrusion processes. The HIPing process produces an essentially fully dense product with an equiaxed α grains. The material was then extruded at a ratio of 10 to 1. The unidirectional structure deformation during extrusion caused the α grains to become elongated in the extrusion direction.

In CP-Ti, the ductile behavior of the α phase is the result of twinning deformation in addition to conventional slip by dislocations. However, oxygen has been reported to suppress the propensity for twinning.[46,47] Since the oxygen concentration is 0.25 wt.% in the material being studied here, it is not surprising that twinning was not observed. In addition, an α lath substructure was observed in a low volume fraction of the α grains. The formation of this substructure has not been reported before. The substructure is considered not to influence the mechanical behavior of the material due to the low volume fraction, non-uniform and widely spaced. Therefore, detailed analysis of this feature is not germane to the main objectives of this study.

3.4.2 Titanium-Boron Alloy Microstructure

The Ti-B material was similar to that of CP-Ti with the exception of the dispersion of TiB. The Ti-B material also did not have the α lath substructure within the α grains, and no twinning was observed as would be expected with oxygen concentrations greater than 0.6 wt.%. The Ti-B material had elongated α grains with rod-shaped and blocky TiB at the α/α grain boundaries and within the α grains. The volume fraction of TiB in the Ti-B material was ~10% and ~15% TiB for 0.8 wt.% and 0.9 wt.% boron, respectively. These values disagree with the lever rule and titanium-boron phase diagram, as they are 2 times that which is predicted. This difference is believed to be due to the high oxygen concentrations possibly influencing the lever rule with respect to the published phase diagram or making the alloys more of a ternary system rather than a binary system.

As with the CP-Ti material, the Ti-B powder was consolidated and worked below the β-transus in the HIP and extrusion processes. The HIPing process produces a consolidated product with a microstructure consisting of TiB particles and equiaxed α grains, which were finer in grain size than the CP-Ti. All processes mentioned in literature follow the Ti-B phase diagram such that TiB forms during solidification from liquid to solid. The Armstrong process does not create molten titanium or titanium alloy. Instead, the Ti-B alloy rapidly forms from the vapor phase with the boron in solution in the α phase. During the HIPing process, the powder material had TiB precipitate out from the supersaturated solution creating a non-uniform distribution of TiB in the α matrix. The formation of the TiB directly from the α phase is a unique and interesting

result. This has only been reported in literature by Banerjee et al[45,48] in producing Ti-B alloys using the LENS™ process. They observed that the TiB precipitated out of the α phase forming nano-TiB from the supersaturated solution. The nano-TiB precipitated out during the subsequent passes of the laser over the consolidated powder after the prior formation of coarser TiB and the titanium matrix alloy on prior passes of the laser. Therefore, it is unlikely that the material produced by the Armstrong process will exhibit the same mechanisms for formation of TiB in the titanium matrix as those in published literature. This makes direct comparisons between the present results and those in the literature difficult.

The non-uniform distribution of TiB is believed to be due to the inhomogeneous distribution of boron in the titanium powder in the experimental runs using the Armstrong process. In these experimental runs, it appears that the titanium and boron chlorides may not have been completely mixed. Even so, the mixing is likely better than that produced by mechanically alloyed powders[49-51] or in blended elemental powders[49-51]. In those processes, the amount and size distribution of titanium and TiB_2 powder can be controlled to ensure that titanium and diboride are in contact to ensure sufficient amounts of each for diffusion to create a uniform distribution of TiB. The Armstrong process entails the mixing of titanium and boron chlorides in the vapor form in a reactor. If the mixing were not completely homogeneous, then a non-uniform distribution of TiB particles would be expected. Unlike other powder processes, the local concentration of boride is set during the formation of the powder and not controlled during the packing of powders as in mechanically alloyed or blended elementals. The combination of the inhomogeneous concentrations of boron, and the limited diffusion rate of boron in α

titanium, leads to the non-uniform distribution of boron and subsequently TiB in the consolidated material.

The morphologies of the TiB observed in the Ti-B material can also be explained based on the difference in local concentrations of boron along with the crystal structure of the TiB. Bhat et al.[52] and Sahay et al.[53] have shown the morphology of the TiB depends on the local boron concentration or volume fraction of TiB. They have shown that if the boron concentration is hypereutectic with respect to the Ti-B phase diagram, than the TiB morphology tended to be rounded, blocky and close to equiaxed while hypoeutectic TiB morphology tended to have a higher aspect ratio and needle-like in appearance.

The TiB morphology in the Ti-B material, from the Armstrong powder, was attributed to the diffusion rates, local concentration of boron and titanium, and grain and crystallographic restrictions in α titanium. The TiB in the Ti-B material was confirmed to have an orthorhombic crystal structure, which is consistent with other published work.[54,55] The TiB orthorhombic structure is formed by close packing of trigonal prisms only in one direction, forming columns with a rectangular base with the central chain of boron atoms oriented in the [010] direction of the crystal.[53] The rate of the one-way diffusion of boron along the [010] direction has been reported as being much higher than that of the opposite diffusion of titanium in TiB.[54,56] This enhanced diffusion rate as well as the arrangement of the boron atoms in the [010] direction would suggest that the growth rates of the TiB in the [010] are larger, relative to the [100], [101], and [001] directions. [54,56] The growth rate of TiB in the axial direction being higher than that in the transverse direction(s) of the TiB explains the typical high aspect ratio of the TiB. This accounts for the formation of the rod-shaped TiB observed along the α/α grain

boundaries and within the α grains. The different size scales for the rod-shaped TiB are most likely related to the local concentration of boron (from the original powder aggregate boron concentration), and grain and crystallographic restrictions. The local concentration of boron is essentially the only boron present for the formation of TiB in the α grains since the diffusion of boron in α titanium is limited. In addition, since the TiB precipitates out of the α phase, there will be crystallographic restrictions based on the orientation relationships between the TiB and α phase (like that between the α and β phases in α+β and β titanium alloys). For the rod-shaped TiB at α/α grain boundaries, the enhanced diffusion rates along the grain boundaries assist in providing additional boron thus forming coarser TiB at the grain boundaries, which is consistent with that reported by Feng et al.[57] The grain boundary rod-shaped TiB will also be restricted by the α grains already present and crystallographic relationship of the TiB and α phase. The presence of the α grains likely limits the available area for the TiB to form at the α/α grain boundaries. Therefore, the size and morphology of TiB at the grain boundaries is dependant on the grain structure. As with the intragranular TiB, the grain boundary TiB size and morphology of TiB will also be dependent on the crystallographic restrictions from the orientation relationships possible between the TiB and α phase.

The blocky morphology of the TiB at the α/α grain boundaries, including the grain boundary triple points, would likely be due to the increased diffusion rates of boron to the TiB along the α/α grain boundaries[57] , and grain restrictions. The higher diffusion rates along the α/α grain boundaries would allow for more diffusion of boron to the TiB and in the axial and transverse directions of the TiB. Thus, forming blocky TiB with a

lower aspect ratio than the rod-shaped TiB. In addition, the size and morphology of the TiB will also be restricted by the α grains, especially at grain boundary triple points, and by crystallographic relationships as with the rod-shaped TiB at grain boundaries.

There were regions in the material that had a similar contrast to that of the blocky and rod shaped TiB. These regions were originally believed to be TiB stringers but after Gatan image filtering transmission electron (FTEM) analysis was completed on the Ti-B material it was determined there was no boron present in these regions. Titanium was observed in these regions with the regions being randomly distributed. These boron lean regions are most likely due to non-uniform chemical distribution in the powder. These regions are believed to have elongated or aligned parallel to the extrusion direction in a similar manner as the α grains were elongated. In addition to the regions being elongated or aligned, the extrusion process caused the rod-shaped TiB to become aligned parallel to the extrusion direction. This alignment of constituent phases due to extrusion is similar to that in aluminum alloys where iron-manganese and iron-chromium-manganese phases are aligned in the extrusion direction.[58]

Several other processes have been used to produce titanium alloys with boron and have shown similar results to that of the Armstrong product.[59-63] Yolton and Moll[59] examined a prealloyed Ti-6Al-4V-XB alloy with 0.9 – 2.2 wt.% boron produced by gas atomization. The material, after HIP, extrusion and heat treatment, produced a microstructure with a mixture of relatively fine (~1 - 2 μm) and coarser (~25 μm) TiB with high aspect ratios (~15 to 1) and the TiB aligned parallel to the extrusion direction. This work is also consistent to other published work produced using other powder metallurgy methods[60]. Banerjee et al.[48] examined a Ti-2B alloy melted and cast in a

laboratory arc-melter and also produced using the LENS™ process. The arc-melted material had primary TiB particles that were ~20 - 100 μm in size and exhibited a faceted, equiaxed morphology. The eutectic TiB particles were smaller and exhibited an acicular morphology with diameters of ~1 μm and lengths of ~10 - 20 μm. Similar results were reported by Philliber et al.[61,62] for a β-titanium alloy, Ti-17Mo, that was arc-melted and heat-treated, and by Tsang et al.[63] using self-sustained high temperature synthesis (SHS) to melt titanium-boron alloys ranging from 5 – 15 wt.% boron. The LENS™ process produced primary TiB particles that were ~0.6 μm in size and exhibited an equiaxed morphology. The eutectic TiB particles exhibited an acicular morphology with an average length of ~2.5 μm and aspect ratio of ~7 to 1. The α grain size for all of these works was not published and therefore no comparison could be made.

The major difference between the Armstrong product and all other processes discussed in the published literature is the presence of the TiB stringers. The rod-shaped and blocky TiB obtained in the Armstrong product was equivalent to or finer than the primary and eutectic TiB produced by all other processes. The microstructure of the Armstrong product is most similar to that of the LENS™ product as the morphologies of the TiB are very similar, which suggests that the mechanisms of formation may be similar. One major difference though is the LENS™ process melts the powder and rapidly solidifies from liquid to solid while the Armstrong process does not melt the powder but the titanium and boron rapidly forms from the vapor phase. Therefore, it is unlikely that these processes will have the same mechanisms for formation of TiB and the titanium matrix. A review of all the processes used to create titanium alloys containing boron

show there is no published work on producing these alloys from a vapor to a solid (powder in this case) with a supersaturated solution of boron.

3.4.3 Commercially Pure (CP) Titanium and Titanium-Boron Alloy Strengthening

The CP-Ti, Ti-0.8B and Ti-0.9B have a finer α grain size than typical CP-Ti material. The increase in boron concentrations shows a further decrease in the α grain size of the material. The fine dispersion of TiB makes the alloy more resistant to recrystallization and α grain growth than CP-Ti. According to the Hall-Petch relationship[64,65], the finer α grain size in the Armstrong product will increase the yield strength of the final product. The CP-Ti material showed some porosity which most likely is due to the higher levels of sodium as the elements are known to cause porosity in material produced from consolidated powder[66,67]. The limited porosity in this material could lead to a reduction in the mechanical properties, especially the fatigue strength of the material.[66,67] No porosity was observed in the Ti-B material, which is consistent with the sodium and chlorine levels being lower than the CP-Ti material.

The TiB in the titanium matrix is intended to be a source for dispersion strengthening. The TiB will act as barriers impeding the motion of dislocations through the α titanium matrix. The motion of the dislocations will be impeded thus producing a large amount of strain hardening of the material until the dislocations either bypass or cut through the TiB. Estimates of the amount of strengthening due to the fine dispersion of the TiB can be obtained using the Orowan equation[68] as follows:

$$\Delta\tau = \frac{G\boldsymbol{b}}{l} \qquad [4.1]$$

where G is the shear modulus, b is the burgers vector, and l is the spacing between TiB. This relationship assumes the TiB are spherical but in the case of the Armstrong product, the TiB is more rod shaped. These morphologies have been found to provide twice the amount of strengthening in comparison to spherical particles.[69]

The chemistry of CP-Ti, Ti-0.8B and Ti-0.9B material, as with other non-heat treatable grade titanium alloys, is an important factor on the microstructure and subsequently the properties of the final product. The Ti-B material had higher amounts of oxygen and chlorine with lower amounts of sodium and carbon. The higher amounts of oxygen will provide a significant amount of strengthening in addition to that from the addition of boron.[70-76] At oxygen concentrations greater than 0.25 wt.% in CP-Ti, the slip mode has been shown to be planar rather than wavy.[46,47] This transition in slip mode has been attributed to the significant reduction of the resolved shear stress in the active slip planes as a form of strain localization. Welsch et al.[77] proposed, and Weissmann and Shrier[78] have shown evidence that this transition is connected to some form of short-range ordering of oxygen in the α lattice which provides strengthening of the CP-Ti material. The concentrations of iron, nickel, hydrogen and nitrogen were similar between the material with and without boron. Therefore, any difference in the microstructure or properties between the CP-Ti, Ti-0.8B and Ti-0.9B material would not be due to these elements.

3.5 Conclusions

The Armstrong process was used to produce commercially pure (CP) titanium, Ti-0.8B and Ti-0.9B powder. The powder was HIPed, extruded and annealed in order to understand the effect of boron additions on the microstructure of the final product. The microstructures of the consolidated and heat-treated CP-Ti and Ti-B material was analogous to that observed by other processes used to create CP-Ti and Ti-B alloys. The CP-Ti material had a finer α grain size elongated in the extrusion direction along with an α lath substructure, which has not been reported in published literature. The Ti-B material had a finer α grain size than CP-Ti and had rod shaped TiB at α/α grain boundaries and within the α grains, blocky TiB at α/α grain boundaries and TiB stringers randomly distributed. The microstructure of the Ti-B material was believed to have the TiB formed first, based on the limited solubility of boron in titanium, and the α grains forming there after. The morphologies and distribution of the TiB was attributed to the inhomogeneous concentrations of boron from the experimental runs of Armstrong processed powder, the limited diffusion of boron in α titanium and the orthorhombic structure of the TiB. The TiB particles located at α/α grain boundaries were observed to be coarser and in some cases blocky due to the enhanced diffusion rates of boron along the α/α grain boundaries. The chemistry of the consolidated and heat-treated Ti-0.8B and Ti-0.9B material was found to have high levels of oxygen while the CP-Ti material had an oxygen concentration similar to that of typical Grade 2 CP-Ti material. The oxygen levels should provide all three materials solid solution strengthening. The TiB produced a finer α grain size that should provide additional strengthening over that of the already

fine α grains for the CP-Ti material. In addition, the rod shaped TiB are intended to provide dispersion strengthening in addition to the solid solution and grain size strengthening. The non-uniform distribution of the TiB was likely due to incomplete mixing of the chlorides during the experimental runs to produce the powder. Improvements in the chloride mixing will likely lend to a more homogeneous distribution of TiB.

3.6 References

1. Dulis, E.J., Chandhok, V.K., Froes, F.H., Clark, L.P. *Proceedings of the 10th National SAMPE Technical Conference*. 1978. pp.316.

2. Eylon, D., Kerr, W.R. *STP 645: Fractography in Failure Analysis.* 1978. pp. 235.

3. Hu, D., Johnson, T.P., Loretto, M.H. *Advances In Powder Metallurgy and Particulate Materials*. MPFI. 1995. pp. 109.

4. Banerjee, R., Collins, P.C., Genc, A., Tiley, J. Fraser, H.L. *Titanium Science and Technology '03*. Munich. 2004. pp. 2547.

5. Hanusiak, W., Yolton, C.F., Fields, J., Hammond, V., Grabow, R. *JOM.* **56(5).** 2004. pp. 49.

6. Kao, W.H., Orsborn, L.M. *Powder Metallurgy of Titanium Alloys.* 1980.

7. Kao, W.H. *AFML Contract F33615-77-C-5173, Semi-annual Report.* 1979.

8. Miller, J.A., Brodi, G. *AFML-TR-79-4028.* 1979.

9. Andersen, P.J., Eloff, P.C. *Powder Metallurgy of Titanium Alloys.* 1980.

10. Philliber, J.A., Dary, F.C., Zok, F.W., Levi, C.G., Blenkinsop, P.A. *Titanium '95: Science and Technology.* 1995. pp. 2714.

11. Dubey, S., Lederich, R.J., Soboyejo, W.O. *Metall. Trans. A* **28.** 1997.

12. Garriott, R.E., Thellman, E.L. *Proceedings of the 1976 International Powder Metallurgy Conference.* 1976.

13. Abkowitz, S. *Powder Metallurgy of Titanium Alloys.* 1980.

14. Yolton, C.F. *JOM.* **56(5).** 2004. pp. 56.

15. Fan, Z., Chandrasekaran, L., Ward-Close, C.M., Miodownik, P. *Scripta Met.* **32(6).** 1995. pp. 833.

16. Fan, Z., Miodownik, P. *Acta Metall.* **44.** 1995. pp. 93.

17. Saito, T., Furuta, F., Yamaguchi, Y. **Recent Advances In Titanium Metal Matrix Composites.** *TMS Warrendale, PA.* 1995. pp. 33.

18. Leutjering, G. Williams, J.C. **Titanium (Engineering Materials and Processes).** *Springer-Verlag Publishing*. 2003.

19. Moxson, V., Froes, F.H. *JOM.* **52(5).** 2000. pp. 24.

20. Rivard, J.D.K., Blue, C.A., Harper, D.C., Kiggans, J.O., Menchhofer, P.A., Mayotte, J.R., Jacobsen, L., Kogut, D. *JOM.* **57(11).** 2005. pp. 58.

21. Crowley, G. *Advanced Materials & Processes.* **161(11).** 2003. pp. 25.

22. Benish, A.J., Sathaye, A., Nash, P., Anderson, R., Zwitter, T. **International Conference on Powder Metallurgy & Particulate Materials.** 2005. pp. 61.

23. Anderson, R.P., Ernst, W., Jacobsen, L., Kogut, D., Steed, J.M. **Cost-Affordable Titanium: A Symposium Dedicated to Professor Harvey Flower as held at the 2004 TMS Annual Meeting.** 2004. pp. 121.

24. Gerdemann, S.J., Alman, D.E. **International Conference on Powder Metallurgy & Particulate Materials.** 2000. pp. 12.41.

25. Jacobsen, L.. *Advanced Materials & Processes.* **160(8).** 2002. pp. 25.

26. Lavender, C.A., Carpenter, J.A. **2004 Annual Progress Report for Automotive Lightweighting Materials.** 2005.

27. Shigeta, M., Watanabe, T. **Bulletin of the Research Laboratory for Nuclear Reactors. Volume 28(I/II).** 2004. pp. 108.

28. Armstrong, D.R., Borys, S.S., Anderson, R.P. **Method of Making Metals and Other Elements.** *U.S. Patent Office.* Patent No. 5,779,761. 1998.

29. Armstrong, D.R., Borys, S.S., Anderson, R.P. **Method of Making Metals and Other Elements from the Halide Vapor of the Metal.** *U.S. Patent Office.* Patent No. 5,958,106. 1999.

30. Armstrong, D.R., Borys, S.S., Anderson, R.P. **Method of Making Metals and Other Elements from the Halide Vapor of the Metal.** *U.S. Patent Office.* Patent No. 6,409,797 B2. 2002.

31. Armstrong, D.R., Borys, S.S., Anderson, R.P. **Ceramics and method of producing ceramics.** *U.S. Patent Office.* Patent No. 6,861,038. 2005.

32. Armstrong, D.R., Borys, S.S., Anderson, R.P. **Method of making metals and other elements from the halide vapor of the metal.** *U.S. Patent Office.* Patent No. 2002005090 A1. 2002.

33. Armstrong, D.R., Borys, S.S., Anderson, R.P. **Elemental material and alloy.** *U.S. Patent Office.* Patent No. 2002148327 A1. 2002.

34. Armstrong, D.R., Borys, S.S., Anderson, R.P. **Elemental material and alloy.** *U.S. Patent Office.* Patent No. 2002152844 A1. 2002.

35. Armstrong, D.R., Anderson, R.P., Jacobsen, L.E. **Method and apparatus for controlling the size of powder produced by the Armstrong Process.** *U.S. Patent Office.* Patent No. 2004079196 A1. 2004.

36. Armstrong, D.R., Anderson, R.P., Jacobsen, L.E. **Preparation of alloys by the armstrong method.** *U.S. Patent Office.* Patent No. 2004079197 A1. 2004.

37. Armstrong, D.R., Anderson, R.P., Jacobsen, L.E. **Method and apparatus for controlling the size of powder produced by the Armstrong Process.** *U.S. Patent Office.* Patent No. 2005081682 A1. 2005.

38. Armstrong, D.R., Anderson, R.P., Jacobsen, L.E. **Filter extraction mechanism.** *U.S. Patent Office.* Patent No. 2005225014 A1. 2005.

39. Armstrong, D.R., Anderson, R.P., Jacobsen, L.E. **Preparation of alloys by the armstrong method.** *U.S. Patent Office.* Patent No. 2006150769 A1. 2006.

40. Anderson, R.P., Armstrong, D.R., Jacobsen, L.E. **Filter cake treatment apparatus and method.** *U.S. Patent Office.* Patent No. 2005284824 A1. 2005.

41. Anderson, R.P., Armstrong, D.R., Jacobsen, L.E. **System and method of producing metals and alloys.** *U.S. Patent Office.* Patent No. 2006107790 A1. 2006.

42. Anderson, R.P., Jacobsen, L.E. **Separation system of metal powder from slurry and process.** *U.S. Patent Office.* Patent No. 2006086435 A1. 2006.

43. Jacobsen, L.E., Benish, A.J. **Titanium alloy.** *U.S. Patent Office.* Patent No. 2007017319 A1. 2007.

44. Jacobsen, L.E., Benish, A.J. **Titanium boride.** *U.S. Patent Office.* Patent No. 2007079908 A1. 2007.

45. Banerjee, R., Collins, P.C., Genc, A., Fraser, H.L. *Mater. Sci. Eng. A.* **A358.** 2003. pp. 343.

46. Paton, N.E., Williams, J.C., Rauscher, G.P. *Titanium Science and Technology.* 1973. pp. 1049.

47. Williams, J.C., Sommer, A.W., Tung, P.P. *Metall. Trans. A.* **3(11).** 1972. pp. 2979.

48. Banerjee, R., Genc, A., Collins, P.C., Fraser, H.L. *Met. and Mater. Trans.* **35A.** 2004. pp. 2143.

49. Froes, F.H., Suryanarayana, C. *Powder Processing of Titanium Alloys.* 1993. pp. 223.

50. Savage, S.J, Froes, F.H. *Titanium Technology: Present Status and Future Trends.* 1985. pp. 60.

51. Froes, F.H., Eylon, D. *Titanium Technology: Present Status and Future Trends.* 1985. pp. 49.

52. Radhakrishna Bhat, B.V., Subramanyam J., Bhanu Prasad, V.V. *Materials Science & Engineering A.* **325(1-2).** 2002. pp. 126.

53. Sahay, S.S., Ravichandran, K.S., Atri, R., Chen, B., Rubin, J. *Journal of Materials Research.* **14(11).** 1999. pp. 4214.

54. Hyman, M.E., McCullough, C., Valencia, J.J., Levi, C.G., Mehrabian, R. *Metall. Trans.* **22A.** 1991. pp. 1647.

55. Decker, B.F., Kasper, R. *Acta Crystallogr.* **7.** 1954. pp. 77.

56. Fan, Z., Guo Z.X., Cantor, B. *Composites.* **28A.** 1997. pp. 131.

57. Feng, H.B., Jia, D.C., Zhou, Y., Hou, J. *Materials Science & Technology.* **20(9).** 2004. pp. 1205.

58. Williams, J.C., Starke, E.A. **1982 ASM Seminar: Deformation, Processing, and Structure.** 1982. p. 284.

59. Yolton, C.F., Moll, J.H. *Titanium '95: Science and Technology.* 1996. pp. 2755.

60. Soboyelo, W.O., Lederich, R.J., Sastry, S.M.L. *Acta Metall.* **42(8).** 1994. pp. 2579.

61. Philliber, J.A., Dary, F.C., Zok, F.W., Levi, C.G., Blenkinsop, P.A. *Titanium '95: Science and Technology.* 1995. pp. 2714.

62. Philliber, J.A., Dary, F.C., Zok, F.W., Levi, C.G. **Recent Advances In Titanium Metal Matrix Composites.** *TMS Warrendale, PA.* 1995. pp. 213.

63. Tsang, H.T., Chao, C.G., Ma, C.Y. *Scripta. Met.* **37(9).** 1997. pp. 1359.

64. Hall, E.O. *Proceedings of the Physical Society*. London B64. 1951. pp. 747.

65. Petch, N.J. *Journal of the Iron and Steel Institute*. London 174. 1953. pp. 25.

66. Jackson, M., Dring., K. *Materials Science and Technology.* **22(8).** 2006. pp. 881.

67. Liu, Y., Chen, L.F., Tang, H.P., Liu, C.T., Liu, B., Huang, B.Y. *Materials Science & Engineering A.* **418.** 2006. pp. 25.

68. Orowan, E. *Discussion in "Symposium on Internal Stresses"*. London. 1947. pp. 451.

69. Kelly, P.M. *Scripta. Metall.* **6.** 1972. pp. 647.

70. Ouchi, C., Iizumi, H., Mitao, S. *Materials Science and Engineering.* **A243.** 1998. pp. 186.

71. Barth, W.J., Field, A.L. *Metal Progr.* **64.** 1953. pp. 74.

72. Jaffe, R.I., Campbell, I.E. *Trans. AIME.* **185.** 1949. pp. 646.

73. Jaffe, R.I. **Titanium '80, Science and Technology. Vol. 4.** 1980. pp. 1665.

74. Jaffe, R.I. *Progr. Metal Phys.* **7.** 1958. pp. 65.

75. Simbi, D.J., Scully, J.C. *Materials Letters.* **26.** 1996. pp. 35.

76. Finlay, W.L., Snyder, J.A. *Trans. AIME.* **188.** 1950. pp. 277.

77. Welsch, G., Leutjering, G., Gazioglu, K., Bunk, W. *Metall. Trans.* **8A.** 1977. pp. 169.

78. Weissmann, S., Shrier, A. **The Science, Technology and Application of Titanium.** *Pergamon Press, Oxford*. 1970. pp. 441.

CHAPTER 4

STRENGTHENING OF CP-TI DUE TO THE ADDITION OF BORON

4.1 Introduction

The influence of boron additions on processing, microstructure, physical and mechanical properties of various titanium alloys has been investigated since the 1950's. However, only during the past 25 years has boron been added to titanium alloys with the intent of creating specific microstructures and mechanical properties for several niche applications. The addition of significant concentrations of boron to titanium alloys can create a stronger alloy with the original titanium alloy as the matrix phase and TiB_x as a dispersed phase.[1-19] The presence of the dispersed phase enhances the physical and mechanical properties including the tensile and fatigue strengths as well as the wear resistance of the boron containing alloys with a reduction in the ductility as compared to the original titanium alloy.[4-9,12,14,15,17-19]

Physical properties are often called structure insensitive because they depend on composition, temperature and crystal structure but not on grain size, hot or cold working and heat treatment history of the material. This is in sharp contrast to mechanical properties.[20] The TiB particles have a similar coefficients of thermal expansion but different elastic modulus as the titanium alloy matrix reducing the potential for

undesirable interfacial stresses or strains due to differences in the elastic modulus, but that could cause early failure of the alloy (Table 4.1). Also, since the interfaces between the TiB and titanium matrix are “clean” and thermodynamically stable upon formation of the TiB, the potential for undesirable interfacial stresses or strains are eliminated. The refined microstructure also has little to no effect on physical properties, as grain size has not been shown to have an influence on physical properties.[20] Therefore, the presence of the TiB and refined microstructures have a negligible effect on the physical properties of the titanium alloy with boron except with elastic modulus[3,5], which increases because of the stiffer TiB particles.

As a general rule, the microstructures obtained through the addition of boron to titanium alloys increase room and elevated temperature strength[1-6,14,15,17], stiffness (elastic modulus)[1-5,14], fatigue strength[3], creep resistance[3,5,15], hardness[3,5], and wear resistance[3-5] while having a decrease in ductility[1-3,5,14] as compared to the titanium alloy without boron additions. Table 4.1 shows a sampling of room temperature tensile, wear and physical properties of commercially pure (CP) titanium, TiB, Ti-6Al-4V and Ti-6Al-4V with boron. Several authors have demonstrated that mechanical properties, including tensile and fatigue strengths, of these alloys are influenced not only by the percent addition of boron but also by the form (equiaxed particles or continuous and discontinuous needlike particles), distribution, and orientation of the TiB formed in the material.[1-6] The refined microstructure of the matrix phase has also been shown to increase the yield strength and fatigue strength of the Ti-B. However, the traditional trade-off between yield strength and ductility is also observed such that the

	Density (lb/in^3)	Coefficient of Thermal Expansion (1/K)	Elastic Modulus (Msi)	0.2% Yield Strength (ksi)	Ultimate Tensile Strength (ksi)	Elongation (%)	Wear Loss (lb/in)
α Titanium	0.165	8.6×10^{-6}	15.9	69.6	79.7	15	-----
TiB compound	0.164	7.15×10^{-6}	52.8 - 79.8	-----	-----	-----	-----
Ti-6Al-4V	-----	-----	16.8	129.1	139.9	14	0.0062
Ti-6Al-4V/TiB	-----	-----	18.6	156.6	175.4	1.3	$<5.6 \times 10^{-5}$

Table 4.1. Room temperature tensile, wear, and physical properties of commercially pure (CP) titanium, TiB, Ti-6Al-4V, and Ti-6Al-4V with boron.[2-5,14]

ductility is decreased with an increase in yield strength. Since the refined microstructure is due in part to the presence of the TiB during transformation of the matrix, the influence of each microstructural feature on mechanical properties is not well understood. The combined influence of TiB particles, fine grain matrix and alloy composition on strengthening and deformation mechanisms for various processing methods constitutes the majority of published literature.[1-6]

The addition of boron to titanium alloys has been well documented to increase the tensile and fatigue strength. The detailed origins of this strengthening have not been identified. The main objective of this research is to better understand the strengthening mechanisms associated with the addition of boron to titanium alloys. The microstructure and mechanical properties are examined using CP-Ti, Ti-0.8wt.%B and Ti-0.9wt.%B alloy powders produced using the Armstrong process. The composition, constitution, and phase morphology of the constituents will be examined to determine the strengthening associated with each.

4.2 Materials and Methods

The consolidated and heat-treated commercially pure (CP) titanium, Ti-0.8B and Ti-0.9B powder mentioned in Chapter 3 was the starting material for this part of the study. As mentioned in Chapter 2 and 3, the boron containing powders that were consolidated and heat-treated and used in this study were the first process runs to attempt to alloy titanium with boron using the Armstrong process.

All test specimens were made from each of the three lots of consolidated and heat-treated material for tensile, notched fatigue, and fatigue crack growth property

measurement except Grade 4 CP-Ti was used in the notched fatigue testing. The Grade 4 CP-Ti material used in the notch fatigue testing was conventional bar stock Grade 4 CP-Ti material. Each lot of material was sectioned using a Struers Labotom-3 SiC cutting wheel. The Ti-6-4 can material was removed using an electro-discharge machining (EDM). Sections were removed from the longitudinal center of the consolidated and heat-treated material with the test specimen bars being taken along the cross-sectional center. The specimens were machined with the loading axis parallel to the extrusion direction. After final machining, all specimens were low stress ground to eliminate any surface residual stresses due to material processes and machining.

4.2.1 Tensile Testing

Tensile specimens were made and tested from each of the three lots of consolidated and heat-treated material for tensile property measurement. The tensile bar specimen geometry is shown in Figure 4.1. The specimens were nominally 2 in. in length with a gage diameter of 0.160 in. Tensile testing was completed at room temperature in accordance with ASTM E8 (Tension testing of Metallic Materials). According to ASTM specifications, once the 0.2% yield strength is reached the extensometer may be removed and the test switched from strain control to crosshead displacement control. This was the procedure followed for all tensile tests reported in this study. The strain rate up to around 2% total strain was 0.005 in./in./min., and the crosshead displacement rate after the extensometer removal was 0.03 in./min. All specimens were tested using servo-hydraulic Instron test machines.

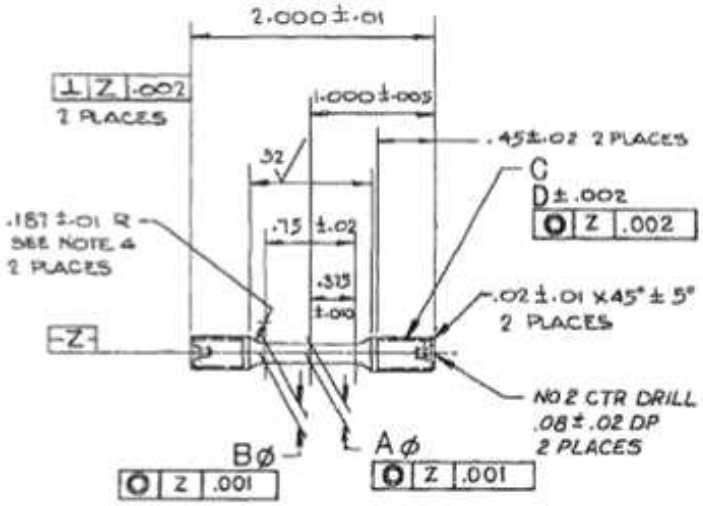

A dia. (±0.001)	B dia. (±0.001)	C thread size	D root rad.
0.160	0.163	0.250-20UNC 2A	0.010

Figure 4.1. Room temperature tensile test bar geometry.

The hardening rates and strength coefficients (equation 4.1) for the consolidated material was determined from the strain levels at 0.2% yield strength to ~2% total strain. This was because the strain rate for these tests from the strain levels at 0.2% yield strength to ~2% total strain was 0.005 in./in./min. and was changed to 0.03 in./min. from ~2% total strain until failure. The hardening rates of the consolidated material were determined by linearly fitting a line to the log true stress – log true strain curve with the slope being the strain hardening rate.

$$\text{Strength coefficient: } \sigma_{True} \text{ at } \varepsilon_{true} = 1.0\% \qquad [4.1]$$

4.2.2 Fatigue Testing

Notched fatigue specimens were made and tested from each of the two lots of consolidated and heat-treated Ti-B material and conventional Grade 4 CP-Ti bar stock for fatigue property measurement. The fatigue specimen geometry is shown in Figure 4.2. The specimens were nominally 2 in. in length with a gage diameter of 0.226 in. Fatigue testing was completed at room temperature, R-ratio = 0.05 (A-ratio = 0.90), and a frequency of 30 hertz in accordance with ASTM E466 (Constant Amplitude Axial Fatigue Test of Metallic Materials). The fatigue test bars had a notch in the gage section creating a K_t = 1.70 such that any contaminants from the processing would not cause a low failure and allowing for a true test of the materials fatigue capability. All specimens were tested using servo-hydraulic Instron test machines operating in load control.

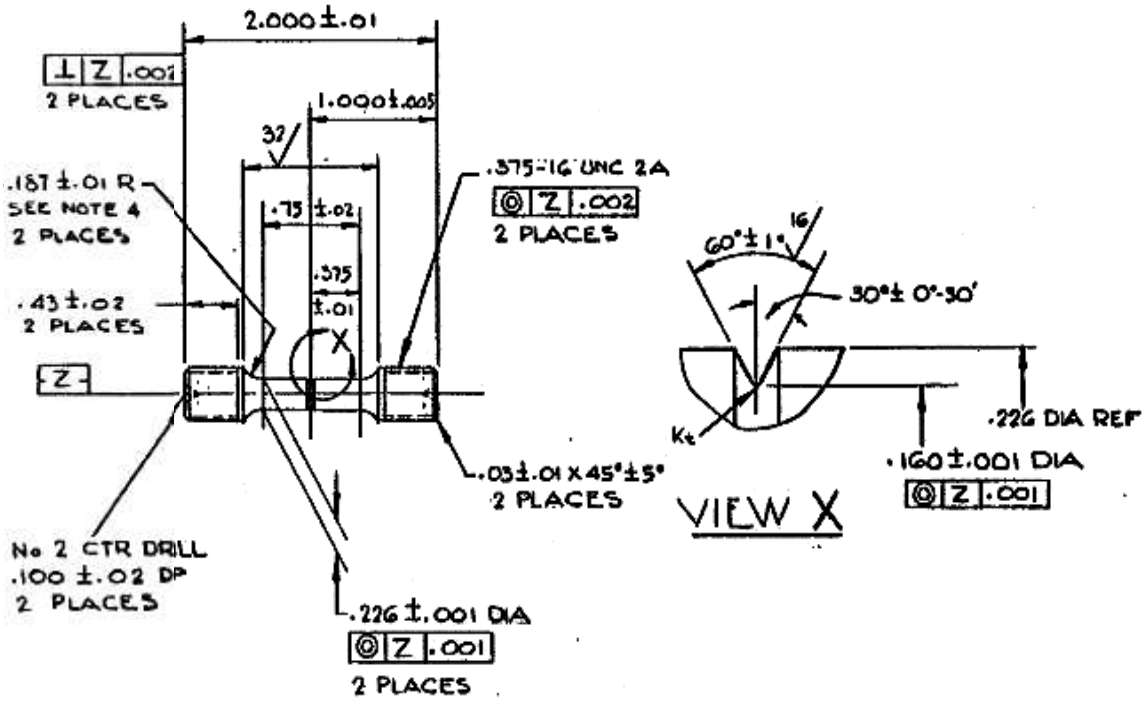

Figure 4.2. Room temperature notched fatigue test bar geometry.

4.2.3 Fatigue Crack Growth Testing

Crack growth specimens were made and tested from each of the three lots of consolidated and heat-treated material for crack growth testing. The fatigue specimen geometry is shown in Figure 4.3. The specimens were nominally 1.78 in. in length with a gage section width and thickness of 0.180 in. and 0.025 in., respectively. Crack growth testing was completed at room temperature, R-ratio = 0.05 (A-ratio = 0.90), and a frequency of 20 cycles/min. in accordance with ASTM E647 (Constant Load Amplitude Fatigue Crack Growth Rates above 10^{-8} m/cycle). The fatigue test bars had a 0.01 in. crack starter notch in the gage section. All specimens were tested using servo-hydraulic Instron test machines.

4.2.4 Compression Testing

Compression specimens were made and tested from each of the three lots of consolidated and heat-treated material for characterization of material deformation. The compression specimen geometry is shown in Figure 4.4. The specimens were nominally 0.80 in. in length with a hexagonal cross- section with a total diameter of 0.40 in. Compression testing was completed at room temperature to a total strain ranging from 5% to 10%. All specimens were tested using servo-hydraulic Instron test machines. Each compressed specimen was then sectioned, ground and ion milled to create transmission electron microscopy (TEM) foils for deformation characterization.

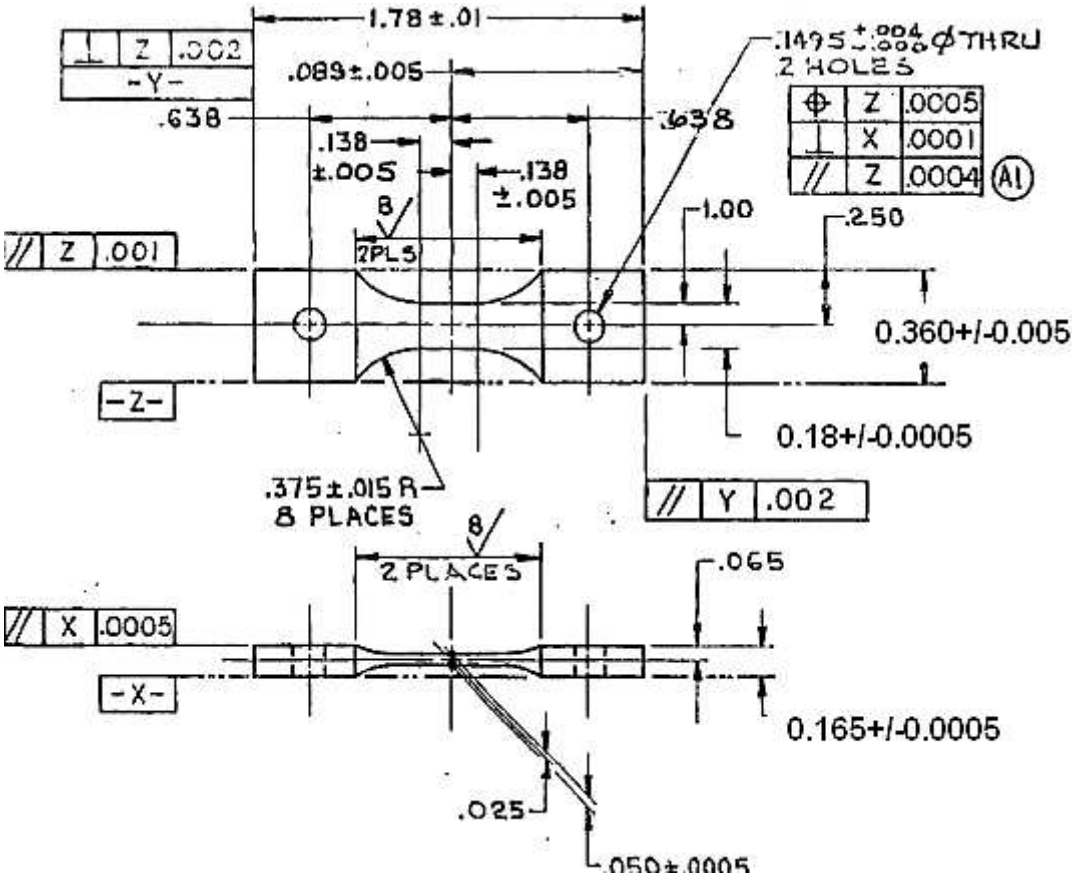

Figure 4.3. Room temperature notched fatigue crack growth test bar geometry.

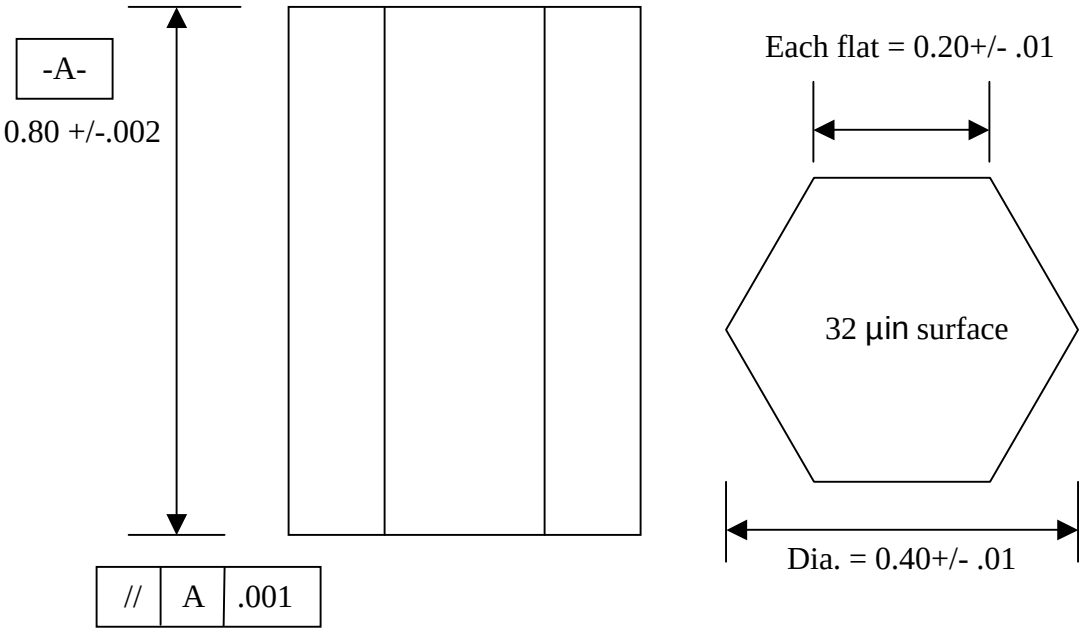

*BREAK ALL EDGES WITH .015 +/-.005 RADIUS OR CHAMFER

Figure 4.4. Room temperature compression test bar geometry.

4.2.5 Scanning Electron Microscopy (SEM)

Fractures of the tensile, fatigue and crack growth bars for the three lots of material were characterized using scanning electron microscopy (SEM). All SEM analysis was completed using a JEOL field emission microscope with a Tungsten filament at 20 kV accelerating voltage.

4.2.6 Transmission Electron Microscopy (TEM) Metallography

Transmission electron microscopy (TEM) foils were made from each of the three lots of consolidated and heat-treated material compression tested for characterization of material deformation. Each tested specimen was drilled using an EDM to create cylinders with a diameter of ~3 mm and subsequently sectioned into ~1.25 mm thick disks. Each disk was mechanically ground using 600 grit abrasive to a thickness of ~100 μm. A Gatan dimple grinder was then used to thin the center of the disks creating a dimple. The dimple was created by dimple grinding to ~20 μm thickness in the center using 6 μm diamond polishing paste to a thickness of 60 μm and down to ~20 μm using 1 μm diamond polishing paste. The dimpled samples were then ion milled to electron transparency using a Gatan Duo Ion Mill. The samples were milled using 6 keV Argon ions at an incidence angle of 10 degrees until the center of the sample was perforated. Once perforated, the foils were suitable for characterizing the deformation structures by TEM.

4.2.7 Transmission Electron Microscopy (TEM)

The three lots of consolidated and heat-treated material that were compression tested were characterized using transmission electron microscopy (TEM). The three lots of material were characterized after being HIPed, extruded, heat-treated, and compression tested. Each specimen was characterized after being mechanically ground, dimple ground and ion milled. All TEM analysis was completed using a PHILIPS CM200 microscope with a LaB6 filament and a Tecnai TF-20 field emission S/TEM with an X-TWIN lens, both operating at 200 keV accelerating voltage.

4.3 Results

4.3.1 Tensile

Room temperature tensile testing was performed on the consolidated and heat-treated commercially pure (CP) titanium, Ti-0.8B and Ti-0.9B material. The 0.2% yield strength, ultimate tensile strength, ductility, reduction of area, and stress-strain curves were obtained for CP-Ti, Ti-0.8B and Ti-0.9B material.

4.3.1.1 Tensile Testing

Figure 4.6 shows the 0.2% yield strength and ultimate tensile strength (UTS) as a function of boron concentration. The minimum strengths for Grade 2 and Grade 4 CP-Ti in conventional form are also included in Figure 4.5 for comparison. The UTS and 0.2% yield strength for the consolidated and heat-treated CP-Ti, Ti-0.8B and Ti-0.9B material, ranges from 88.5 – 170.5 ksi (610 – 1175 MPa) and 65.3 – 148.0 ksi (450 - 1020 MPa), respectively. An increase of 11% in UTS and decrease of 6% in 0.2% yield strength was

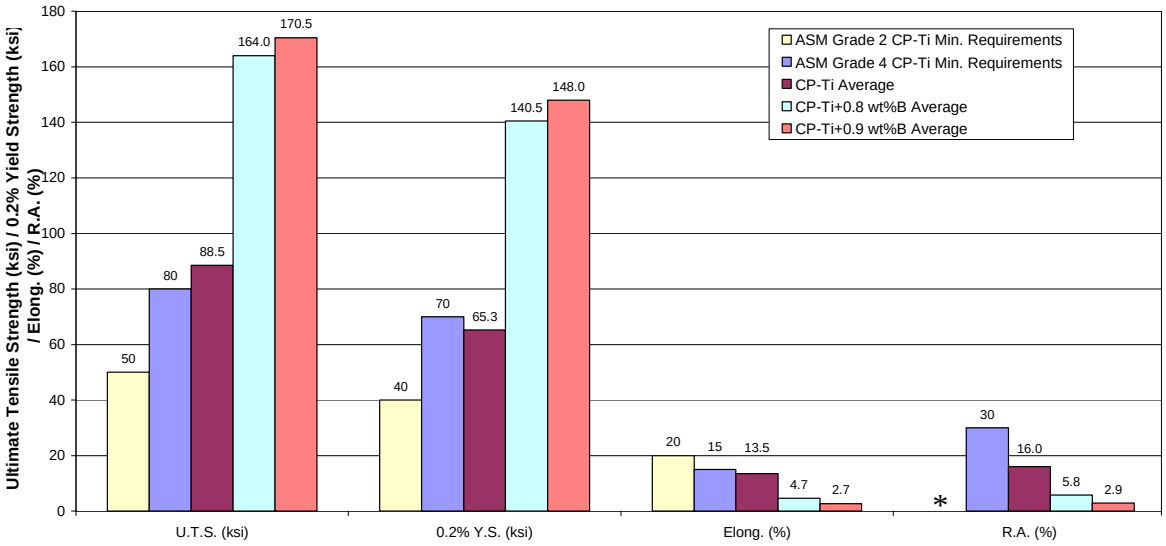

Figure 4.5. Room temperature ultimate tensile strength, 0.2% yield strength, elongation, and reduction of area for consolidated and heat-treated commercially pure (CP) titanium, Ti-0.8B and Ti-0.9B powder. *No published Grade 2 CP-Ti minimum reduction of area requirement.

observed between typical Grade 4 CP-Ti and the lot of Armstrong CP-Ti material. UTS increased up to ~90% with the addition of up to 0.9 wt.% boron to titanium material. An increase in 0.2% yield strength of ~125% was obtained with increasing boron addition up to 0.9 wt.% boron. A linear fit was made through the UTS and 0.2% yield strength to obtain an experimental relationship between the tensile strengths and the concentration of boron added to consolidated and heat-treated CP-Ti. These experimental relationships are:

$$0.2\%\ \text{Yield Strength (ksi)} = (92.757 * \text{wt.\% Boron}) + 65.354 \qquad [4.2]$$

$$\text{UTS (ksi)} = (92.363 * \text{wt.\% Boron}) + 88.661 \qquad [4.3]$$

These relationships were linear fits of the data with R^2 values of 0.99 for both the 0.2% yield strength and UTS relationships.

Figure 4.5 also shows the elongation and reduction of area as a function of boron concentrations. Minimum ductility values for Grade 2 and Grade 4 CP-Ti in conventional form is also included in Figure 4.5 for comparison. The elongation and reduction of area for the consolidated and heat-treated CP-Ti, Ti-0.8B and Ti0.9B material ranges from 13.5% – 2.7% and 16.0% – 2.9%, respectively. A decrease of 10% in elongation and 46% in reduction of area was observed between minimum Grade 4 CP-Ti and the lot of CP-Ti material. Elongation decreased up to ~80% with an increase in boron concentration up 0.9 wt.%. Reduction of area decreased up to ~80% with an increase in boron concentration up to 0.9 wt.%. A linear fit was made through the elongation and reduction of area to obtain an experimental relationship between ductility and the concentration of

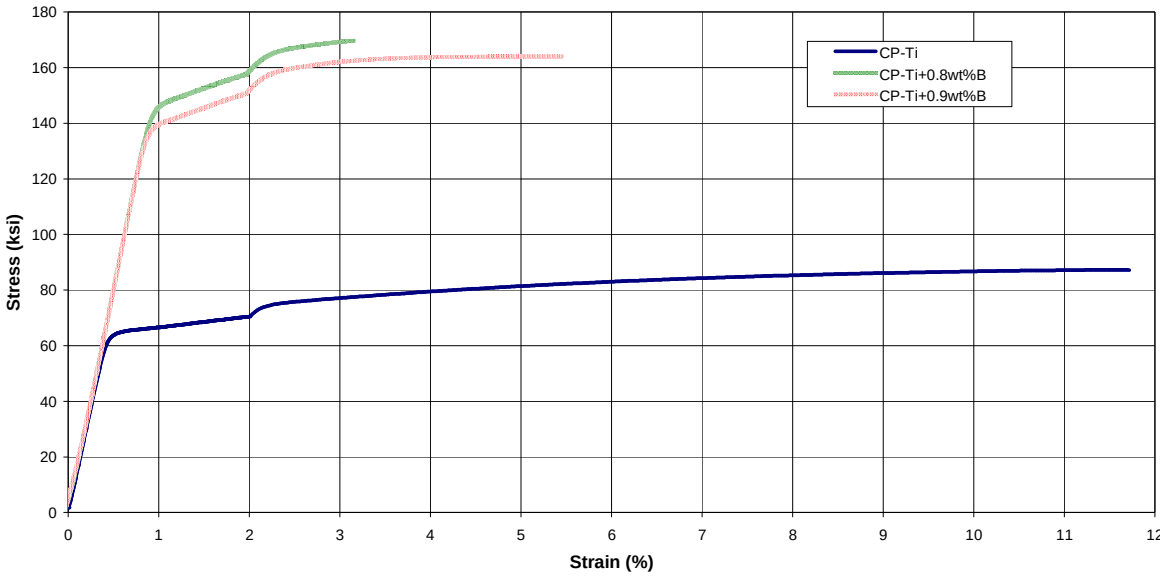

Figure 4.6. Room temperature tensile true stress – true strain curves of consolidated and heat-treated commercially pure (CP) titanium, Ti-0.8B and Ti-0.9B powder.

boron added to consolidated and heat-treated CP-Ti. These experimental relationships are:

$$\text{Elongation}(\%) = (-11.651 * \text{wt.\% Boron}) + 13.552 \quad [4.4]$$

$$\text{Reduction of Area}(\%) = (-13.887 * \text{wt.\% Boron}) + 16.086 \quad [4.5]$$

These relationships were linear fits of the data with R^2 values of 0.97 and 0.94 for the elongation and reduction of area relationships, respectively.

The true stress – true strain curves as a function of boron concentration are shown in Figure 4.6. An increase of ~10% in stiffness was observed for the consolidated and heat-treated Ti-B material in comparison to the CP-Ti material. The hardening rates and strength coefficients were determined from the strain levels at 0.2% yield strength to ~2% total strain. The strain hardening rates were 0.06, 0.10, and 0.17 for consolidated CP-Ti, Ti-0.8B and Ti-0.9B material, respectively. The strength coefficients were 66.6 ksi (460 MPa), 139.6 ksi (963 MPa), and 145.8 ksi (1005 MPa) for consolidated CP-Ti, Ti-0.8B and Ti-0.9B material, respectively.

4.3.1.2 Fractography

Typical fracture surfaces of the room temperature tensile test bars of CP-Ti, Ti-0.8B and Ti-0.9B material are shown in Figures 4.7 - 4.9, respectively. The fracture surfaces of the CP-Ti showed evidence of ductility with shear lips formed with elongated fracture features. The elongated fracture features are most likely from voids that form at α/α grain boundaries and grow by plastic stretching. The voids ultimately coalesce by ductile tearing of the ligaments between the voids forming the elongated features. The crack origin (Figure 4.7a - b) is flat and shows less local ductility than that of the

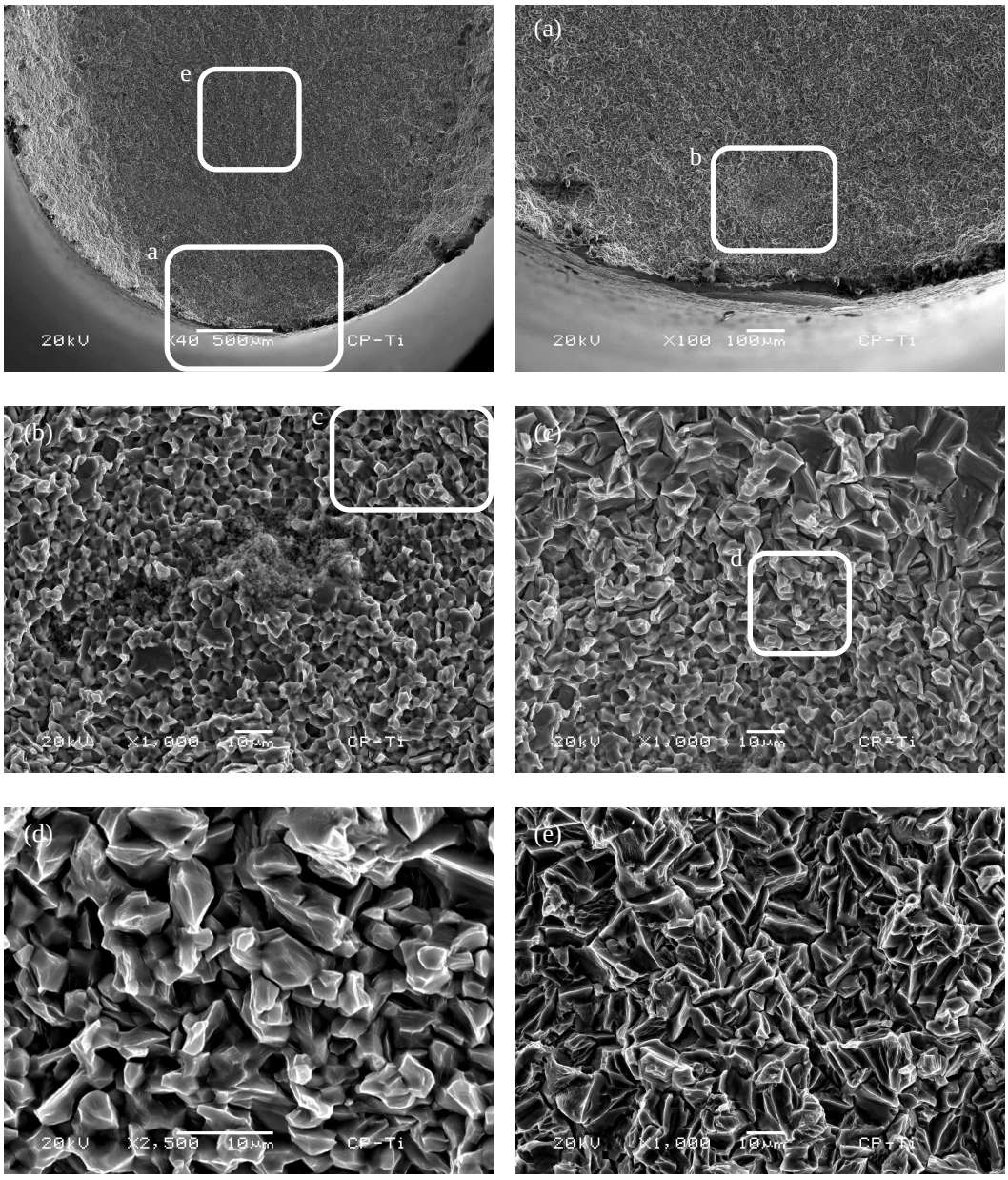

Figure 4.7. Micrographs of tensile fracture surfaces of consolidated and heat-treated commercially pure (CP) titanium powder.

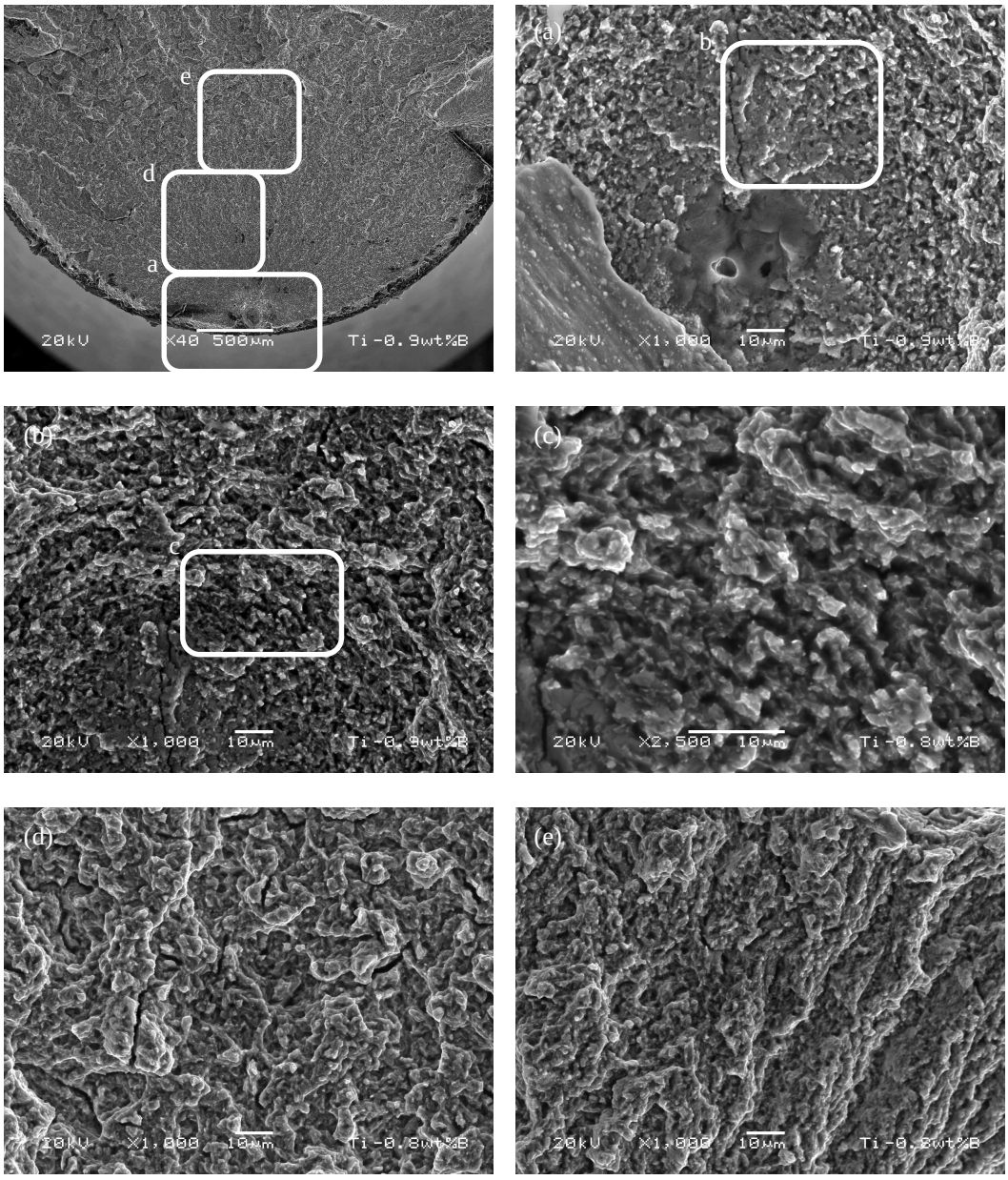

Figure 4.8. Micrographs of tensile fracture surfaces of consolidated and heat-treated Ti-0.8B powder.

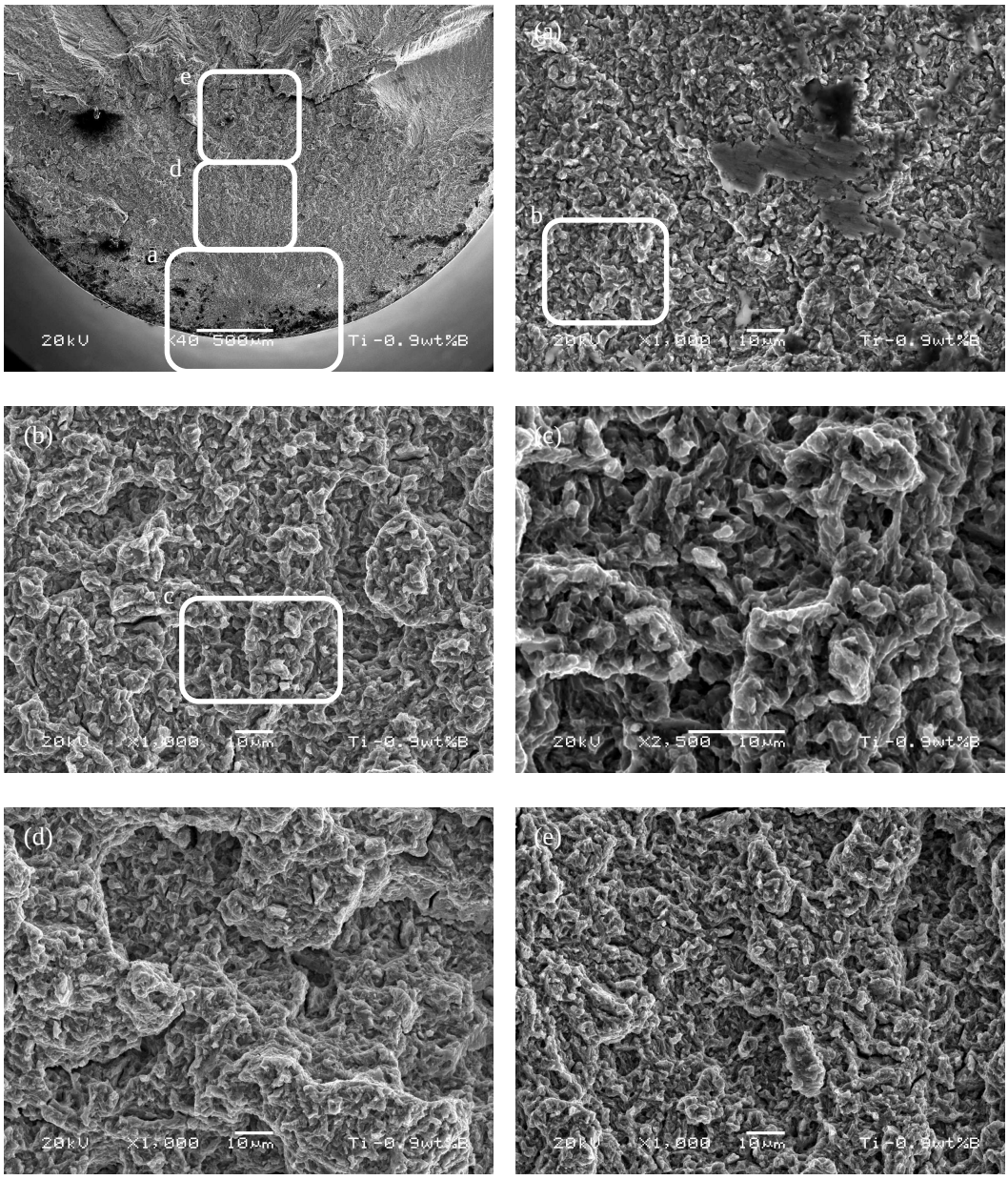

Figure 4.9. Micrographs of tensile fracture surfaces of consolidated and heat-treated Ti-0.9B powder.

propagation area (Figure 4.7c - e), which shows extensive local plastic tearing as described else where as flutes or void tubes[11]. The reason for the flat fracture features is due to a lower stress intensity at the crack origin. Secondary cracking was observed along α/α grain boundaries of the fracture surface.

The fracture surfaces of the Ti-B material were consistent and showed evidence of limited amount of ductility with a flatter fracture surface and smaller elongated fracture features in comparison to the CP-Ti material. As with the CP-Ti material, the elongated features are most likely due to void coalescence. The finer fracture features are consistent with the finer α grain size of the Ti-B material. The Ti-B material has a crack origin (Figure 4.8a – b) that was flat and showed less local ductility than the propagation area (Figure 4.9c - e), which shows local plastic tearing. Secondary cracking was also observed along α/α grain boundaries of the fracture surface as was in the CP-Ti material.

4.3.2 Fatigue

Room temperature notched fatigue testing was performed on the consolidated and heat-treated Ti-0.8B and Ti-0.9B material. Fatigue strength as a function of net section and concentrated alternating pseudostress was obtained for CP-Ti, Ti-0.8B and Ti-0.9B.

4.3.2.1 Fatigue Testing

Figure 4.10 shows the net section alternating stress versus life as a function of boron concentration. Figure 4.11 shows the concentrated alternating stress versus life as a function of boron concentration. Grade 4 CP-Ti in conventional form was also tested and included in Figure 4.10 and Figure 4.11 for comparison. The fatigue strength at 10^7

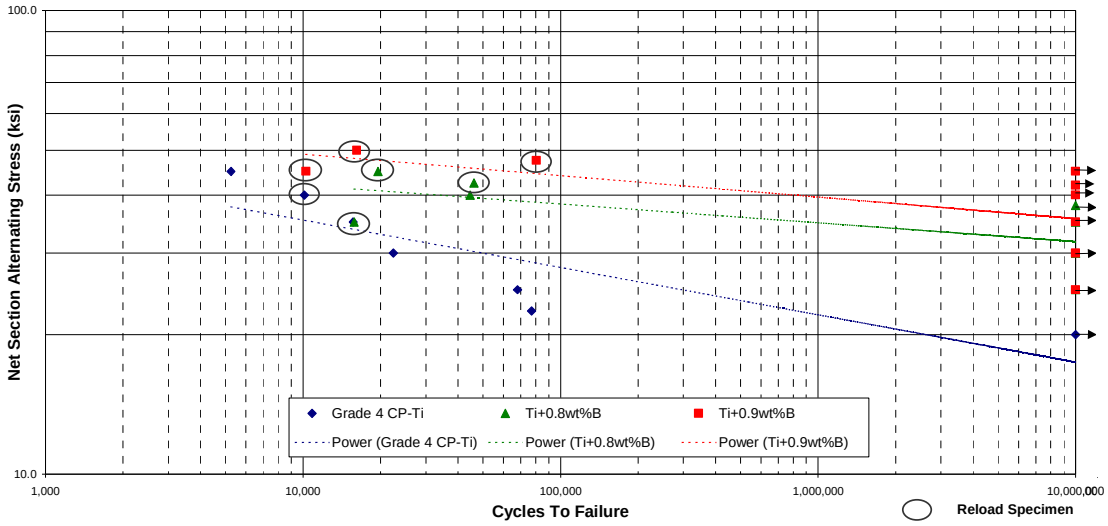

Figure 4.10. Room temperature net section alternating stress versus life of commercially pure (CP) Grade 4 titanium conventional material, and consolidated and heat-treated Ti-0.8B and Ti-0.9B material produced using the Armstrong process.

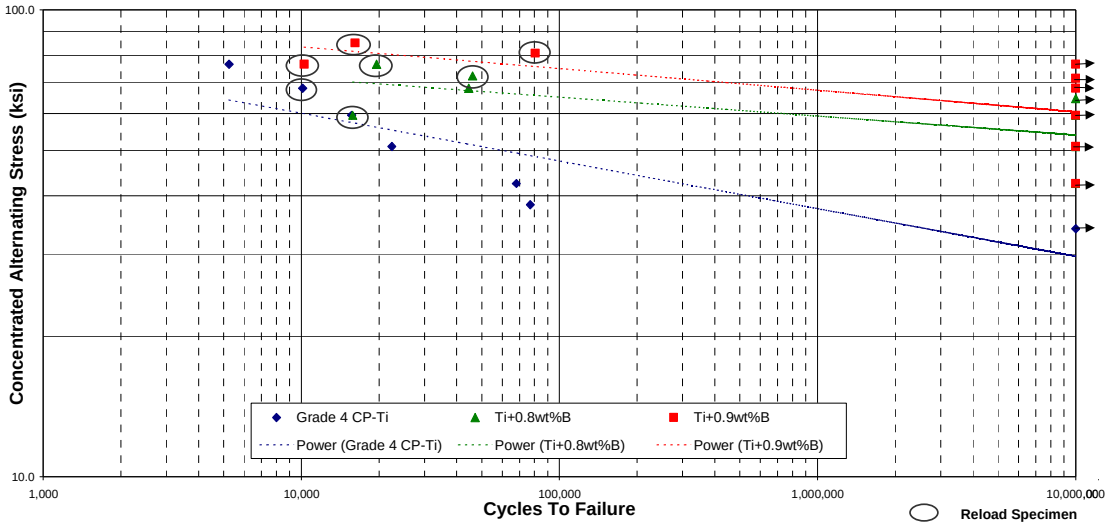

Figure 4.11. Room temperature concentrated alternating stress versus life of commercially pure (CP) Grade 4 titanium conventional material, and consolidated and heat-treated Ti-0.8B and Ti-0.9B material produced using the Armstrong process.

cycles for the Ti-0.8B and Ti-0.9B material is both greater than 30 ksi (207 MPa) net section alternating and 50 ksi (345 MPa) concentrated alternating, respectively. Fatigue life of Ti-0.8B material was 5 times greater than typical Grade 4 CP-Ti at higher stresses and over 100 times greater at lower stresses. Fatigue life of Ti-0.9B material was ~35 times greater than typical Grade 4 CP-Ti at higher stresses and over 300 times greater at lower stresses. A linear fit was made through the fatigue data to obtain an experimental relationship between the net section and concentrated alternating stresses versus life as a function of boron concentration added to consolidated and heat-treated Armstrong processed CP-Ti. These experimental relationships are:

Grade 4 CP-Ti (conventional form):

$$\text{Log } N_f = [\text{Log}(\sigma_{\text{Net Section Alt.}}/393.9)]/(-0.2519) \quad [4.6]$$

$$\text{Log } N_f = [\text{Log}(\sigma_{\text{Concentrated Alt.}}/669.64)]/(-0.2519) \quad [4.7]$$

Consolidated and heat-treated Ti+0.8wt.% Boron:

$$\text{Log } N_f = [\text{Log}(\sigma_{\text{Net Section Alt.}}/95.415)]/(-0.0775) \quad [4.8]$$

$$\text{Log } N_f = [\text{Log}(\sigma_{\text{Concentrated Alt.}}/162.21)]/(-0.0775) \quad [4.9]$$

Consolidated and heat-treated Ti+0.9wt.% Boron:

$$\text{Log } N_f = [\text{Log}(\sigma_{\text{Net Section Alt.}}/67.35)]/(-0.0308) \quad [4.10]$$

$$\text{Log } N_f = [\text{Log}(\sigma_{\text{Concentrated Alt.}}/114.50)]/(-0.0308) \quad [4.11]$$

4.3.2.2 Fractography

Typical fracture surfaces of the room temperature fatigue test bars of conventional Grade 4 CP-Ti and Armstrong consolidated and heat-treated Ti-0.8B and Ti-0.9B

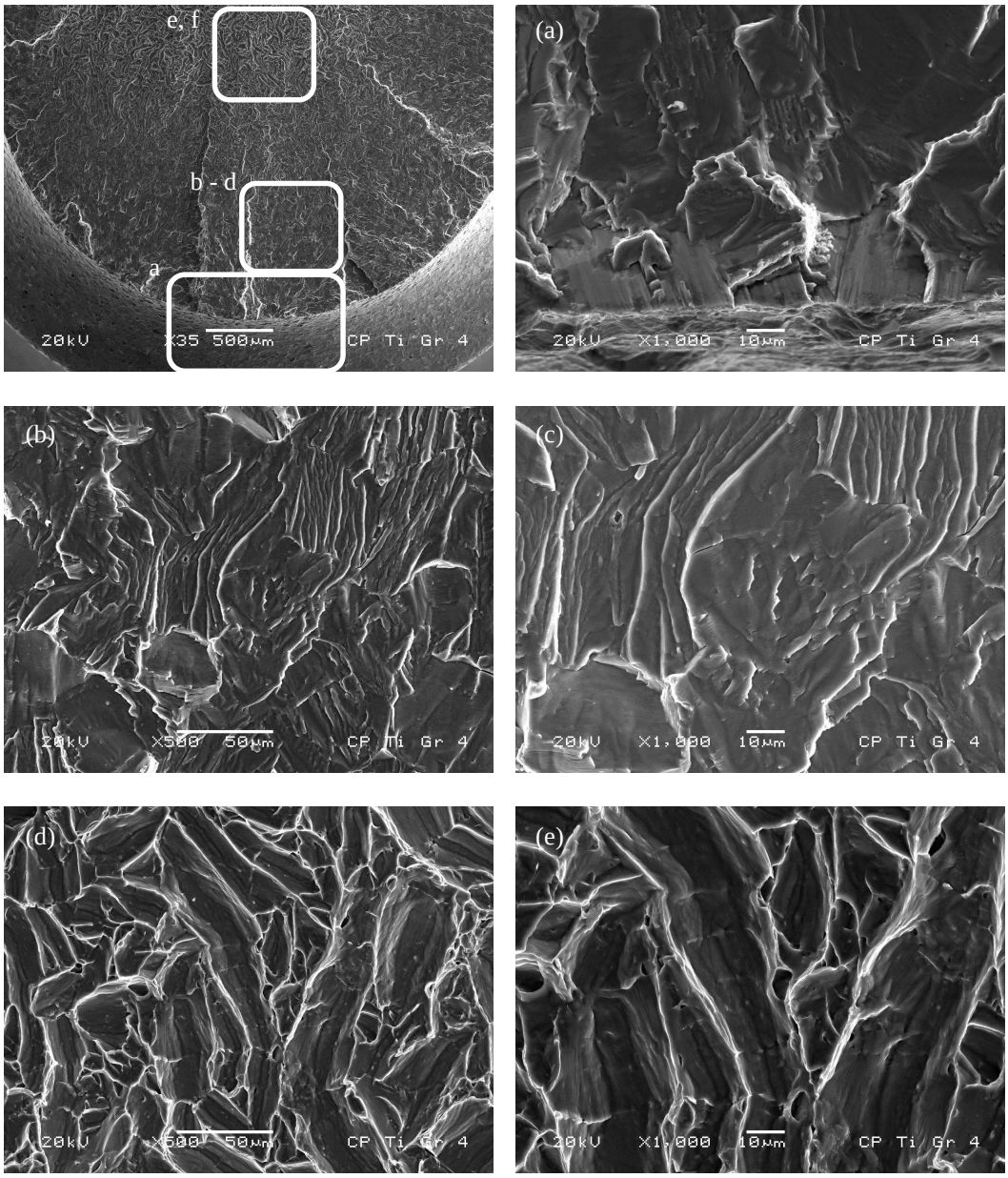

Figure 4.12. Micrographs of fatigue fracture surfaces of conventional Grade 4 commercially pure (CP) titanium.

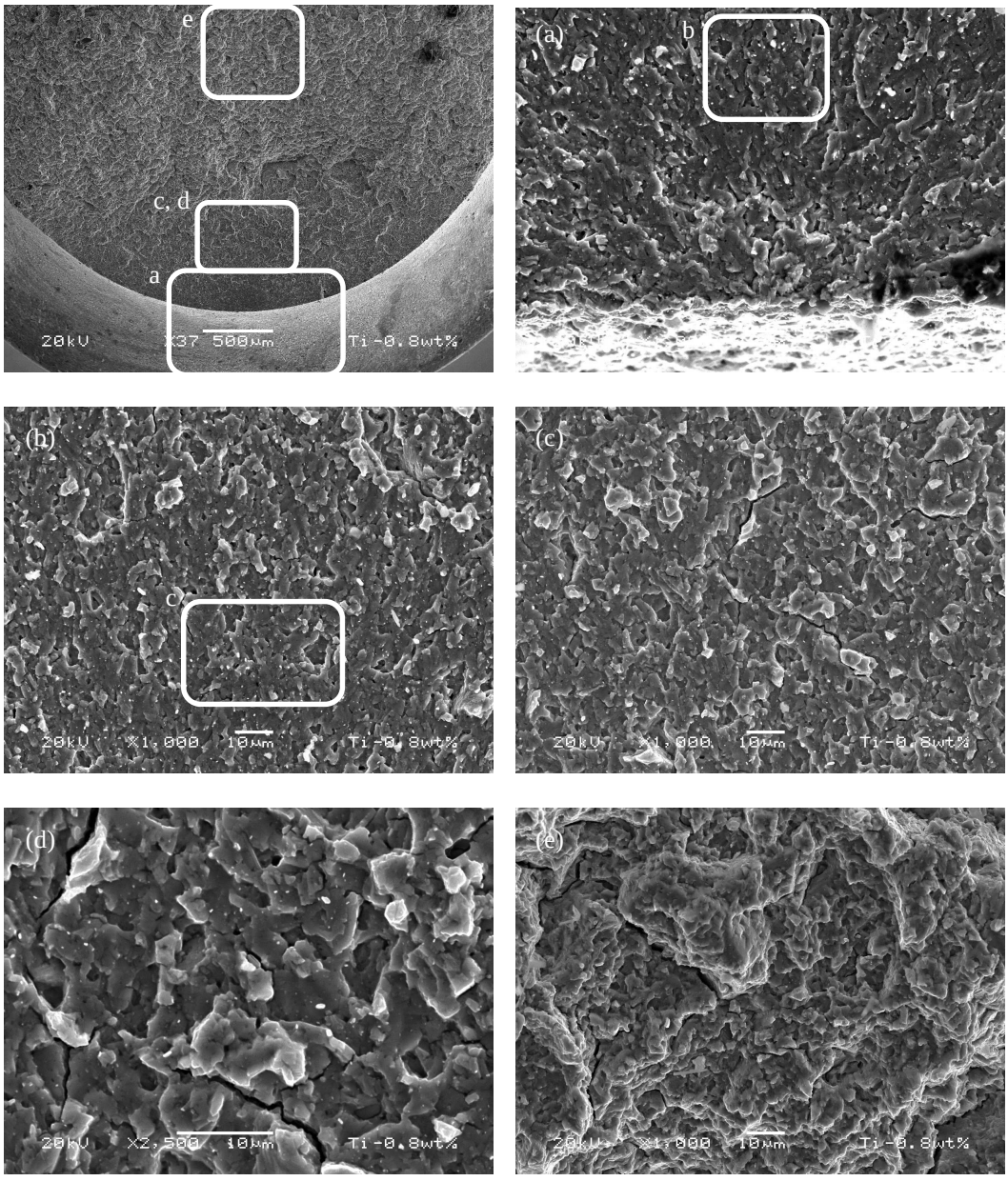

Figure 4.13. Micrographs of fatigue fracture surfaces of consolidated and heat-treated Ti-0.8B powder.

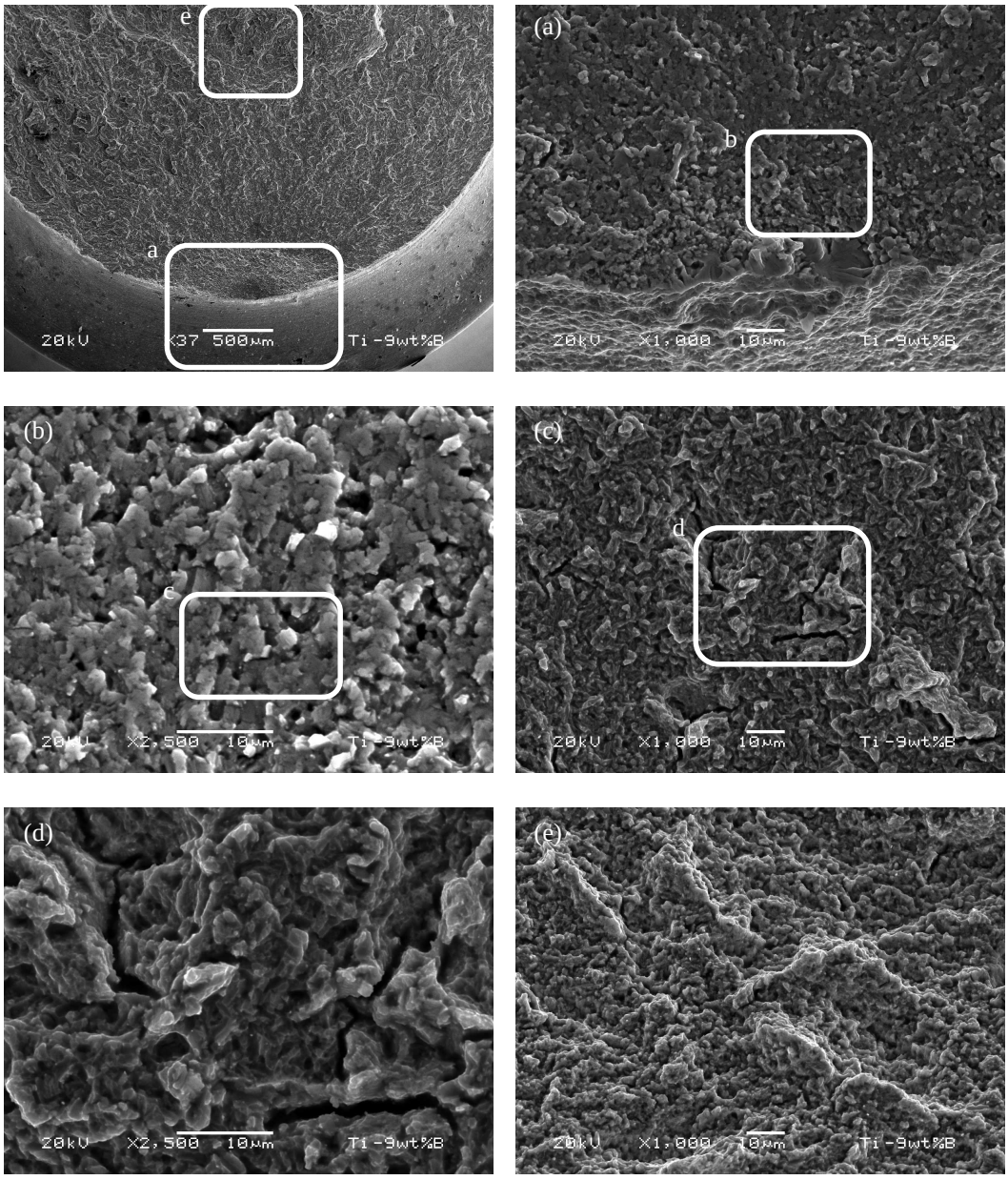

Figure 4.14. Micrographs of fatigue fracture surfaces of consolidated and heat-treated Ti-0.9B powder.

material are shown in Figures 4.12 - 4.14, respectively. The fracture surfaces of the conventional Grade 4 CP-Ti had the primary crack initiating from the notch root in a rough and transgranular mode. The primary crack propagated in a smooth and transgranular mode with serpentine glide marks observed on the faceted surfaces. Secondary cracking was observed along the α/α grain boundaries of the fracture surface. This propagation mode was consistent over half the fracture surface with a transition to tensile overload for the remainder of the fracture surface.

The fracture surfaces of the TiB material were consistent and had the primary crack initiating from the test bar surface at the notch root in a flat and transgranular mode. Unlike the CP-Ti material, there were no striations or serpentine glide marks observed most likely due to the fine grain size being the same size as the propagating cracks plastic zone size. Secondary cracking was observed along α/α grain boundaries of the fracture surface. It is logical to conclude the light speckles shown in Figures 4.13 – 4.14 are most likely TiB particles, but there is no method to identify them in the SEM. There was no evidence of TiB cracking for any of the test specimens. The mode of propagation transited to ductile tearing consistent with higher stress intensity in the finer α grain material.

4.3.3 Fatigue Crack Growth

Room temperature fatigue crack growth testing was performed on the consolidated and heat-treated Ti-0.8B and Ti-0.9B. Cyclic crack growth rate as a function of stress intensity were obtained for CP-Ti, Ti-0.8B and Ti-0.9B material.

4.3.3.1 Fatigue Crack Growth Testing

Figure 4.15 shows the fatigue crack growth rate as a function of stress intensity for the Ti-B materials. Grade 2 CP-Ti in conventional form from Adib & Baptista[21] was also included in Figure 4.15 for comparison. The fatigue crack growth rate for the Ti-0.9B material is 3.5 - 10 times greater than Ti-0.8B, over the range of stress intensities evaluated. Fatigue crack growth rate of the Ti-0.8B material was 1.5 - 14 times greater than typical Grade 2 CP-Ti at stress intensities ranging from 10-20 ksi√in, respectively. Fatigue crack growth rate of the Ti-0.9B material was 15 - 50 times greater than typical Grade 2 CP-Ti at stress intensities ranging from 10-20 ksi√in, respectively. The Paris law exponents calculated from the fatigue crack growth curves were ~5 and ~4 for the Ti-0.8B and Ti-0.9B material, respectively. It should be noted that the Ti-0.9B material had a larger crack growth rate in comparison to that of Ti-0.8B material, but with a smaller Paris law exponent. This was an unusual observation as when a titanium alloy has an increased crack growth rate in comparison to another titanium alloy, it typically has the same or greater Paris law exponent as the other titanium alloy.

4.3.3.2 Fractography

The fracture surfaces of the room temperature fatigue crack growth test bars of Ti-0.8B and Ti-0.9B material are shown in Figures 4.16 and 4.17, respectively. The fracture surfaces of the Ti-B material were consistent and had the primary crack propagating from the starter notch in a flat and transgranular mode. Secondary cracking was observed along α/α grain boundaries of the fracture surface. The dark areas on the

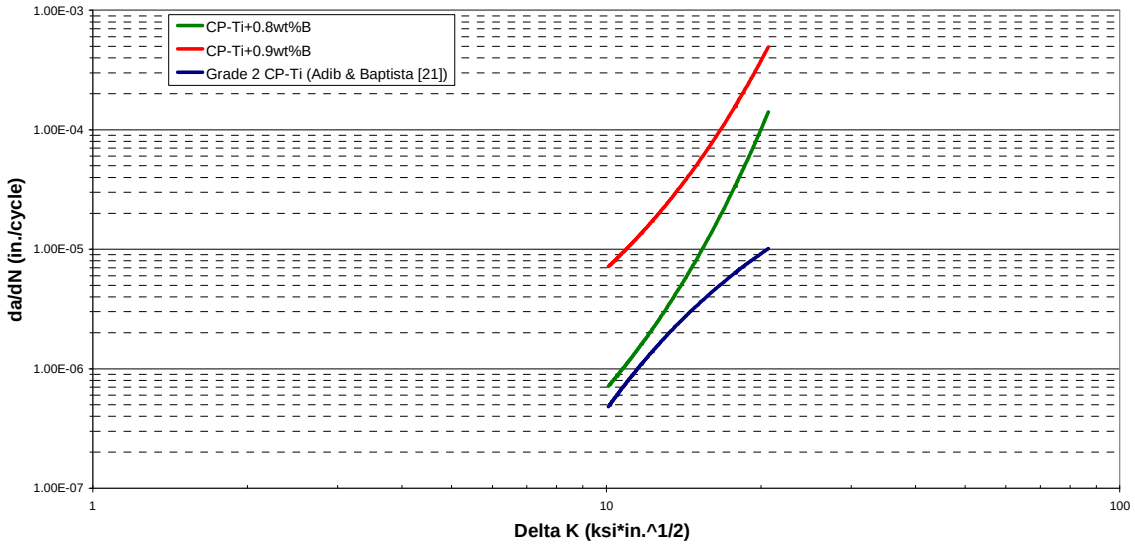

Figure 4.15. Room temperature fatigue crack growth of consolidated and heat-treated Ti-0.8B and Ti-0.9B powder, in comparison to published results for conventional commercially pure (CP) Grade 2 titanium material.

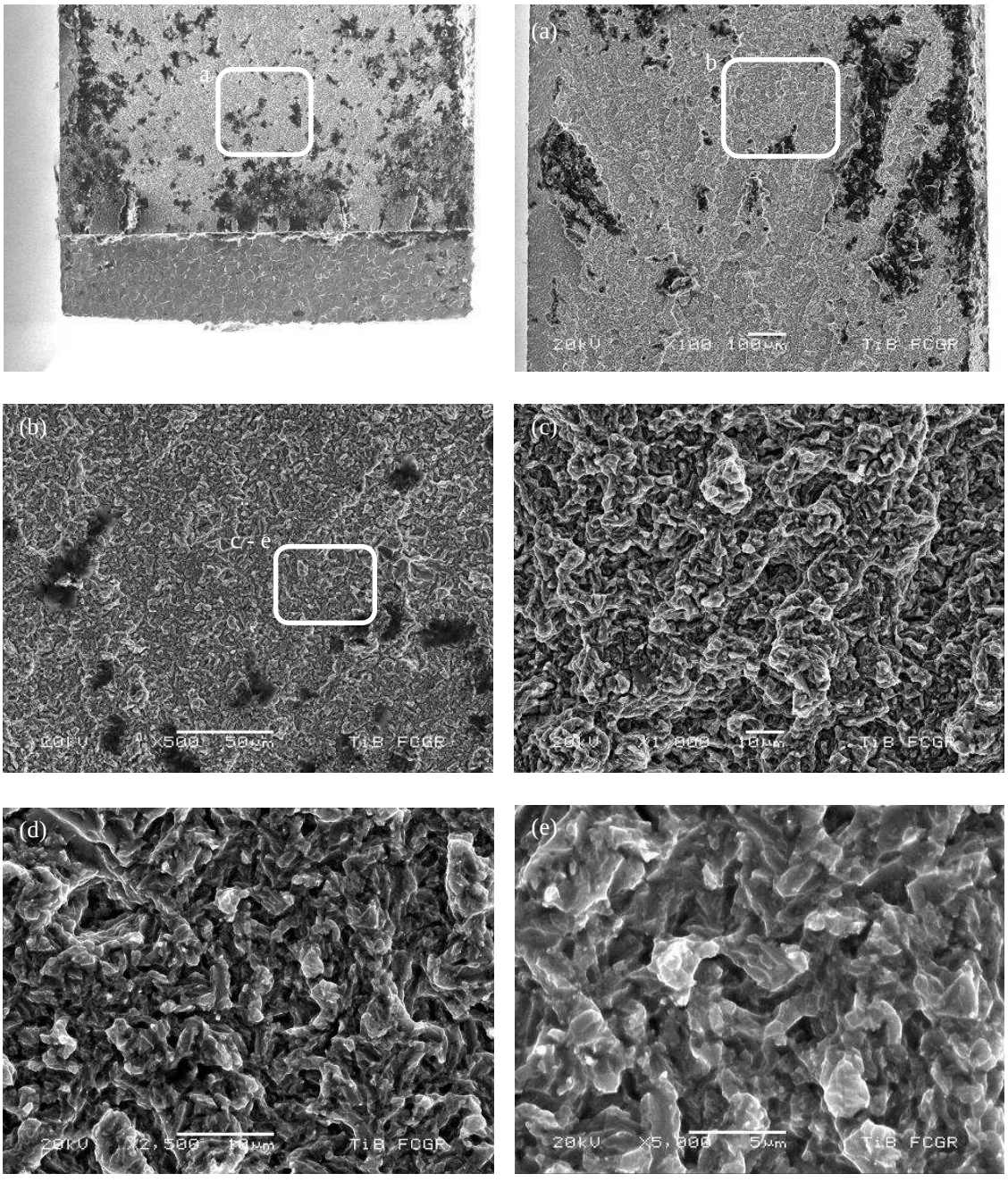

Figure 4.16. Micrographs of crack growth fracture surfaces of consolidated and heat-treated Ti-0.8B produced using the Armstrong process.

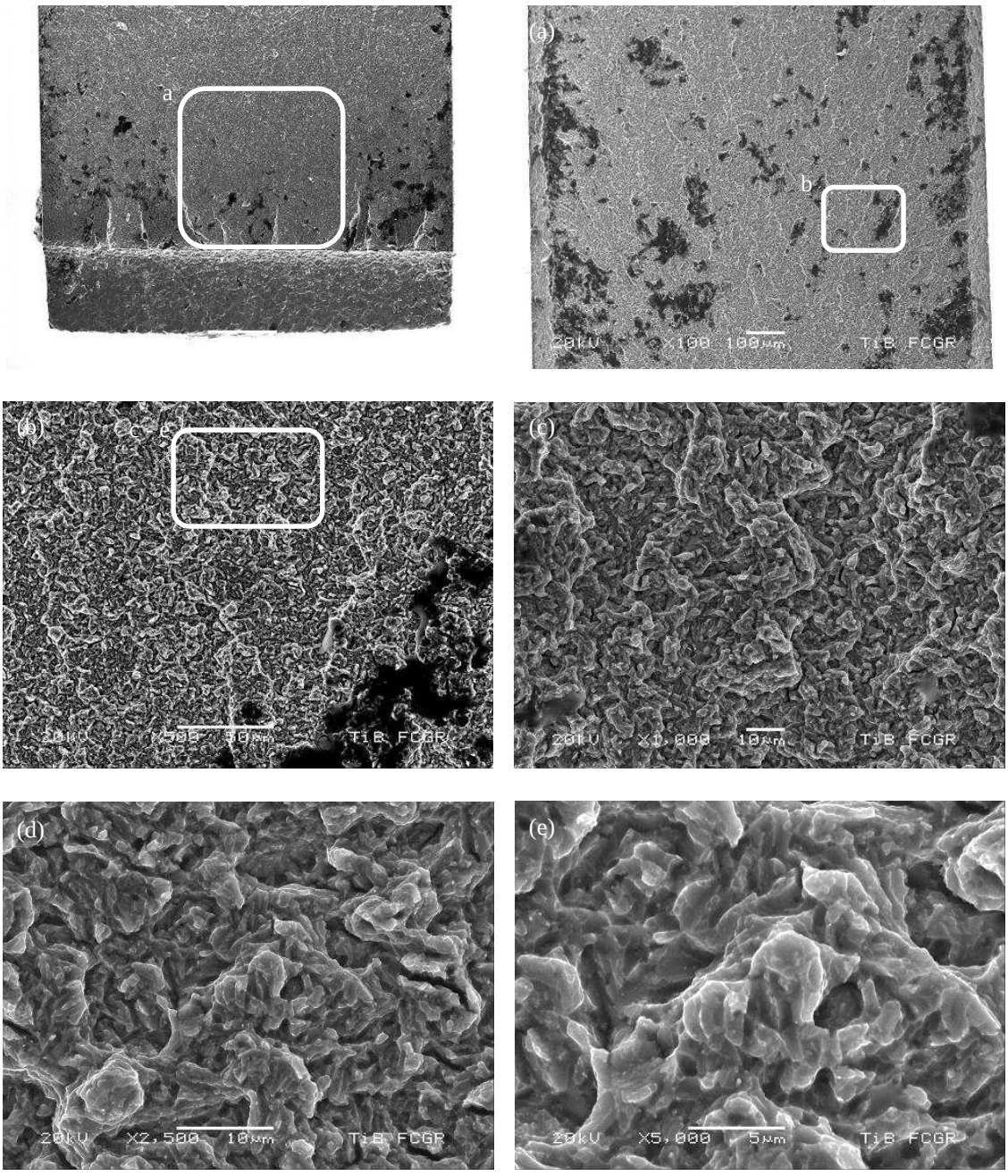

Figure 4.17. Micrographs of crack growth fracture surfaces of consolidated and heat-treated Ti-0.9B produced using the Armstrong process.

fracture surfaces are dirt/stains from handling of the specimens. The crack propagation mode was consistent with that of the notched fatigue test specimens.

4.3.4 Compression Testing

The consolidated and heat-treated CP-Ti, Ti-0.8B and Ti-0.9B material was compressed to examine the deformation structure. The dislocation density, slip character and dislocation interaction with TiB particles were examined in the CP-Ti, Ti-0.8B and Ti-0.9B material.

4.3.4.1 Transmission Electron Microscopy (TEM)

The CP-Ti material had severe deformation in the α grains and α lath substructure as shown in Figure 4.18. The dislocations were observed to be in both the α grains and α lath substructure, but no slip across the boundaries was observed. Dislocation analysis was completed using several diffraction conditions. The dislocations were observed to have $\vec{a}$ and $\vec{c}$ type slip character and wavy in appearance. Based on the published literature and morphology of the dislocations, they are most likely $\vec{a}$ and $\vec{c} + \vec{a}$ type. No planar slip was observed in the CP-Ti material.

The T-0.8B and Ti-0.9B materials had severe deformation in the α grains as shown in Figure 4.19 and 4.20, respectively. The dislocations were observed to be in the α grains, but no slip across the boundaries was observed. Dislocation analysis was completed using several diffraction conditions. The dislocations were observed to have $\vec{a}$ and $\vec{c} + \vec{a}$ type slip character and wavy in appearance. As with the CP-Ti material, the

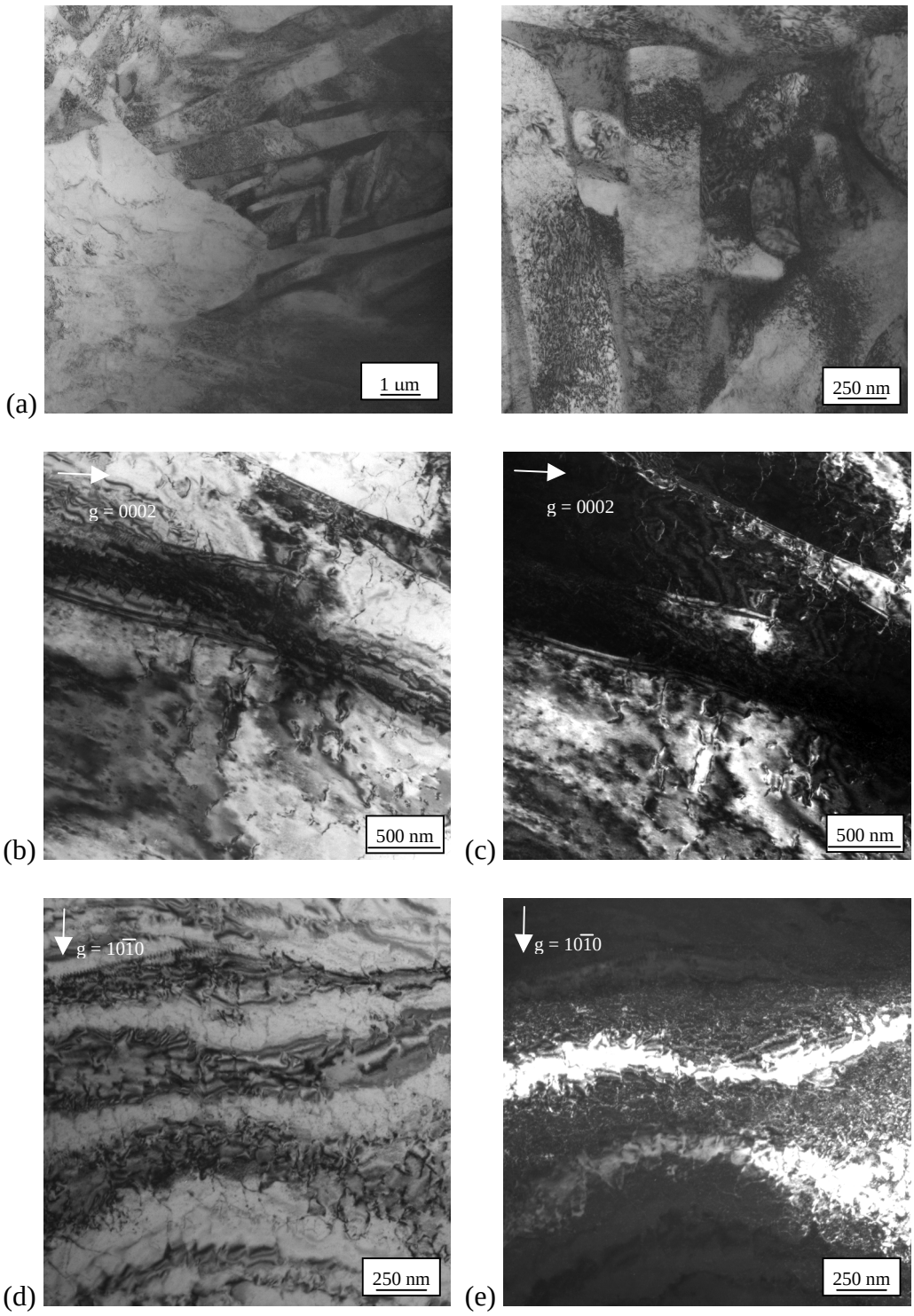

Figure 4.18. Transmission electron micrographs of consolidated and heat-treated commercially pure (CP) titanium produced using the Armstrong process after compression testing. (a) Overall dislocation structure of consolidated and heat-treated CP-Ti. g = 0002: (b) bright field, (c) dark field; g=10$\bar{1}$0: (d) bright field, (e) dark field.

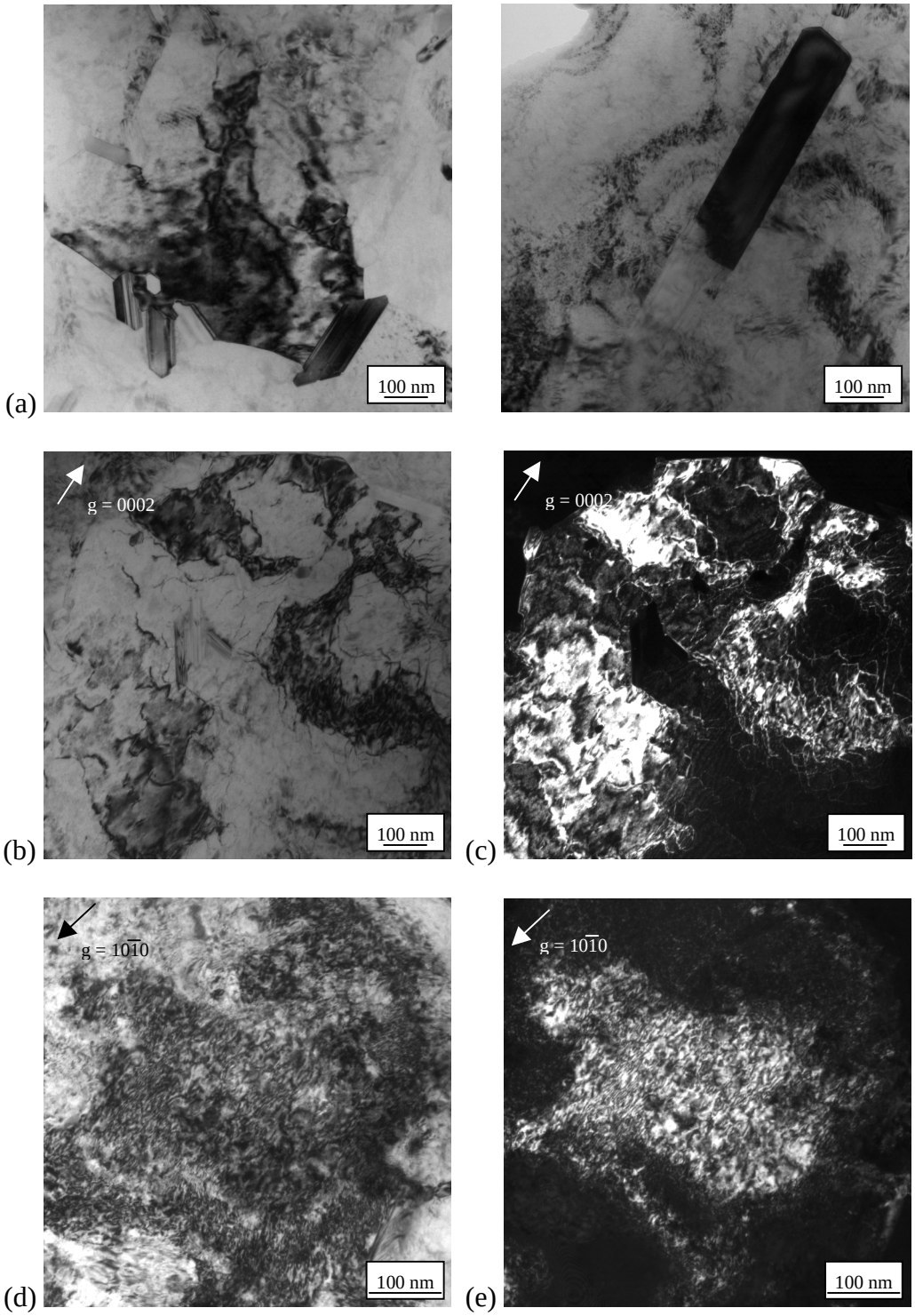

Figure 4.19. Transmission electron micrographs of consolidated and heat-treated Ti-0.8B produced using the Armstrong process after compression testing. (a) Overall dislocation structure of consolidated and heat-treated Ti-0.8B. g = 0002: (b) bright field, (c) weak beam; g=10$\bar{1}$0: (d) bright field, (e) dark field.

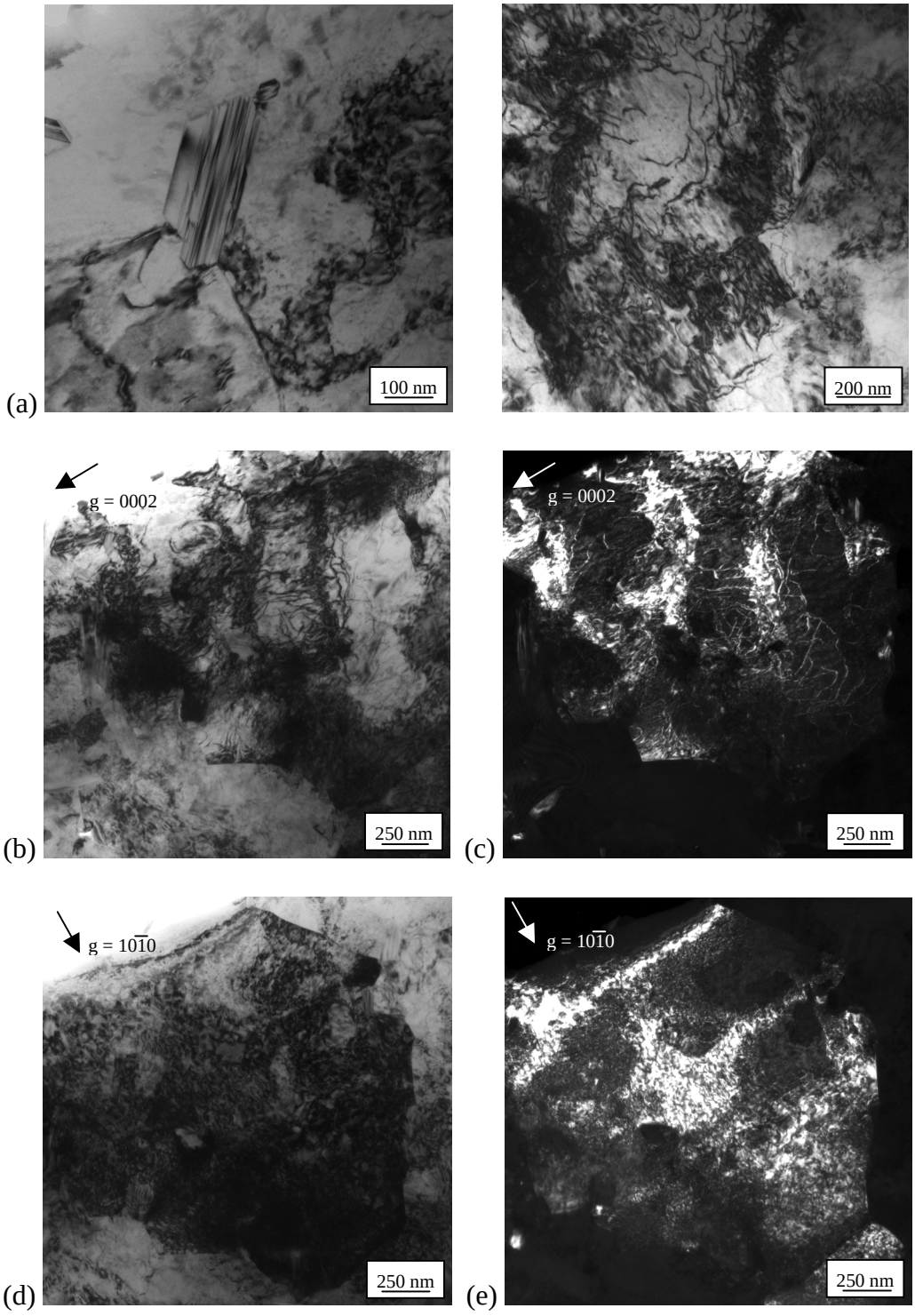

Figure 4.20. Transmission electron micrographs of consolidated and heat-treated Ti-0.9B produced using the Armstrong process after compression testing. (a) Overall dislocation structure of consolidated and heat-treated Ti-0.9B. g = 0002: (b) bright field, (c) dark field; g=10$\bar{1}$0: (d) bright field, (e) dark field.

dislocations are most likely $\vec{a}$ and $\vec{c}$ + $\vec{a}$ type. No planar slip was observed in either the Ti-0.8B and Ti-0.9B material. The TiB showed no dislocation structure but did have planar faults from the formation of the borides (Figures 4.19 and 4.20). In addition, there were no observations of the TiB being fractured or cut by dislocations slipping through the borides. There were several dislocation loops observed only within the α grains and not near TiB particles.

4.4 Discussion

Commercially pure (CP) titanium alloys are limited in the amount of strengthening that can be obtained due to the chemistry and lack of response to heat treatment. The main methods for strengthening CP-Ti alloys are dependant on the input chemistry, amount of plastic deformation applied to the material, and grain size of the material. These three factors directly affect the final microstructure and subsequently the final properties of the material. The chemistry provides solid solution strengthening including interstitial strengthening with the addition of oxygen, nitrogen, and carbon. Plastic deformation from cold and hot working operations including rolling, isothermal forging and extrusion refine the α grain size and produce texture or preferred crystallographic orientations in the α grains. The limited ability to strengthen these alloys is the main reason why these alloys are generally used in applications where factors such as corrosion resistance and weldability are more important than high strength.

The addition of boron to CP-Ti has been shown to produce a dispersion of titanium borides, TiB, that provide additional strengthening above and beyond that from solid solution and grain size.[4-9,12,14,15,17-19,22] Figure 4.21 – 4.23 shows the 0.2% yield

strength, ultimate tensile strength, and % elongation as a function of volume percent TiB for various titanium alloys with boron. The plots show how the tensile properties are also a function of the base titanium alloy and the process used to produce the material. In addition, the Ti-0.8B and Ti-0.9B tensile properties are also plotted in these figures. The Ti-0.8B and Ti-0.9B produced from Armstrong powder shows a higher strength and elongation than Ti-B alloys produced using other methods. In addition, the Ti-B material showed similar strengths as that of other titanium alloys with boron added, but with lower elongation. The lower elongation is a result of the base titanium alloys having lower levels of oxygen in comparison to the material in this study, and some of the alloys used for comparison have a considerable amount of ductility due to the additional phases present. For example, Panda and Ravi Chandran[23] have shown that for β titanium alloys with boron, the TiB increases the strength of the alloy while the β phase provides ductility that would not be present in CP-Ti alloys. This is not unexpected as the β phase is usually more ductile than the α phase in titanium alloys. It should be noted, the processing method also plays a role in the amount of ductility that will be present in an alloy as the amount of work induced into the material could potentially reduce the ductility of the alloy. In addition to volume fraction of TiB, the morphology, distribution and possible alignment are factors that need to be taken into account when comparing titanium alloys with boron produced using different methods.

In contrast to the amount of research completed on tensile properties, the fatigue properties of titanium alloys with boron are not well documented including no published work on fatigue crack growth. The most likely reason for this is the quantity of titanium

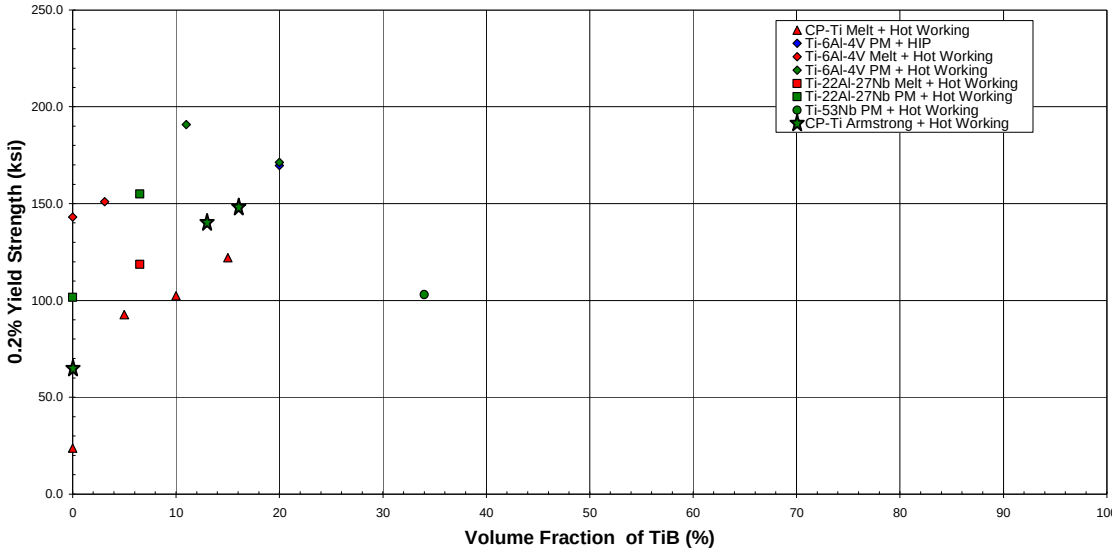

Figure 4.21. 0.2% yield strength as a function of volume percent TiB for various titanium alloys with boron added produced using various processes.[22]

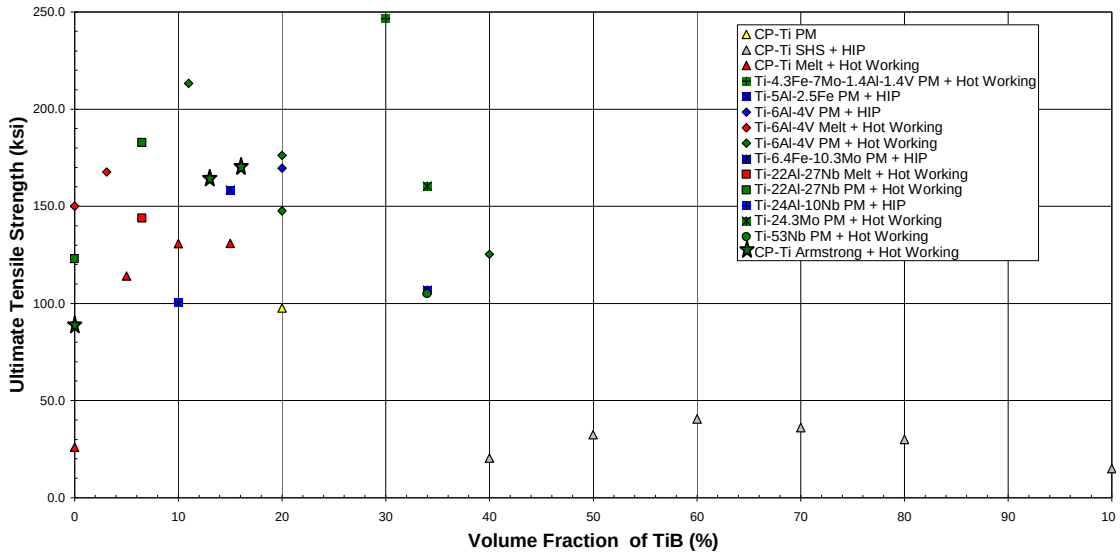

Figure 4.22. Ultimate tensile strength as a function of volume percent TiB for various titanium alloys with boron added produced using various processes.[22]

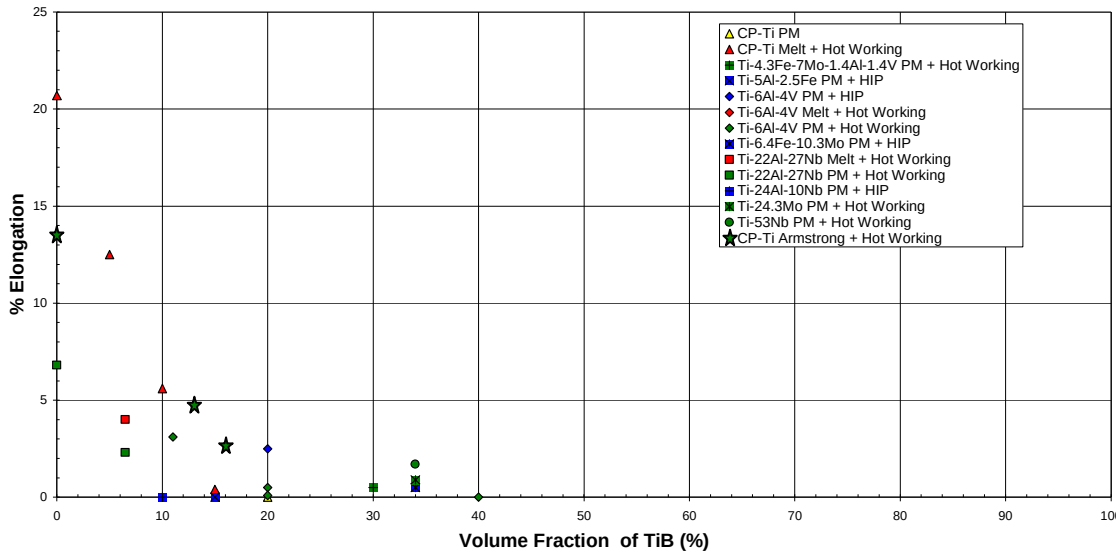

Figure 4.23. Elongation as a function of volume percent TiB for various titanium alloys with boron added produced using various processes.[22]

material produced with boron is not great enough to complete this testing. The use of notched fatigue testing in this work was because the cleanliness of the material was in question due to post-production handling issues. The concentrated fatigue strength at 10^7 cycles was determined to be 51 ksi (352 MPa) and 71 ksi (490 MPa) for Ti-0.8B and Ti-0.9B material, respectively. The K_t due to the notch was 1.7, therefore the unconcentrated fatigue strength at 10^7 cycles was 30 ksi (207 MPa) and 42 ksi (290 MPa) for Ti-0.8B and Ti-0.9B material, respectively. Saito et al.[24-27] observed that the addition of boron to Ti-6Al-4V and Ti-4.3Fe-6.8Mo-1.4Al-1.4V increased the fatigue strength at 10^7 cycles when tested at an R ratio of 0.1. The addition of boron to Ti-6Al-4V provided an increase of ~22 ksi (~152 MPa) in comparison to Ti-6Al-4V without boron. The alloy Ti-4.3Fe-6.8Mo-1.4Al-1.4V with boron additions was reported to have a fatigue strength of 152 ksi (1048 MPa) while no fatigue strength was reported for this alloy without boron. The addition of boron to CP-Ti doubled the fatigue strength between the Armstrong product and conventional Grade 4 CP-Ti (increase of ~40 ksi (~275 MPa)). The doubling of the fatigue strength and difference in fatigue strengths of the base titanium alloy with and without boron was significantly greater than that of the published alloyed Ti-B material data.

Although there have been numerous published reports on the influence of boron additions on the mechanical properties of titanium alloys, the detailed amount of individual contributions to strengthening has not been thoroughly analyzed. In each of the published studies, the total strengthening has been attributed to the boron additions. Several factors have not been taken into account including the chemistry, grain size, and TiB morphology and distribution. There is a lot of interaction between these factors that

needs to be taken into account to understand the true strengthening from the addition of boron. These factors will be examined for the CP-Ti, Ti-0.8B and Ti-0.9B material to determine the amount of strengthening due to the chemistry, grain size, TiB, and the use of the Armstrong process (including the HIP, extrusion and heat treatment).

4.4.1 Solid Solution Strengthening

The Armstrong powder was consolidated and heat-treated to create CP-Ti material with a target composition of Grade 4 CP-Ti. As shown in Table 4.2, the oxygen concentrations are equivalent to 0.25 wt.% in the CP-Ti. This and the low iron make the material more similar to Grade 2 rather than Grade 4 CP-Ti. The Ti-B material had oxygen levels higher than that of Grade 4 CP-Ti with concentrations at 0.62 – 0.67 wt.% and the iron was still very low. Oxygen is an important solid solution strengthening addition of the α phase in these alloys. At concentrations of oxygen above about 0.25 wt.% in an α alloy, the slip character has been reported to transition from wavy to planar.[28,29] Based on these observations, strengthening from the addition of oxygen to α titanium is accompanied by a transition in slip character. Welsch et al.[30] and Weissmann and Shrier[31] have proposed that this transition is connected to short-range ordering of oxygen in the α lattice. Therefore, the CP-Ti and Ti-B material would be expected to have planar slip but this was not observed in any of the material (Figures 4.19 – 4.21). Both the CP-Ti and Ti-B material exhibited wavy slip and the dislocations were most likely $\vec{a}$ and $\vec{c} + \vec{a}$ in character (mainly the former).

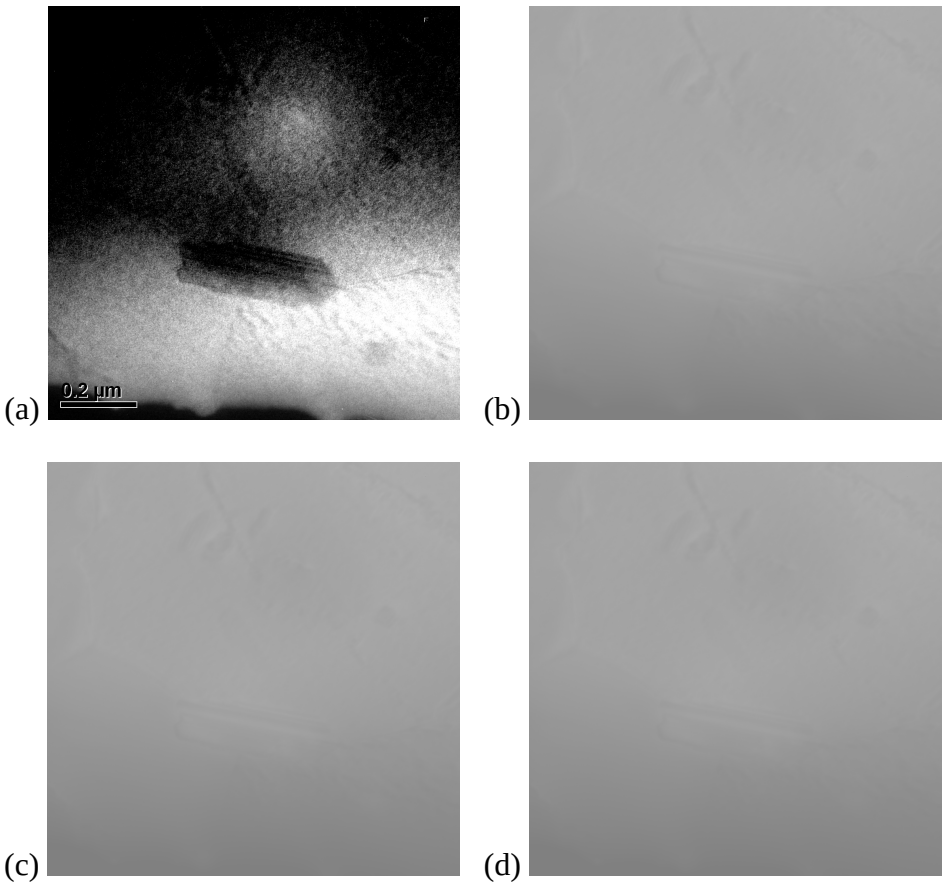

Figure 4.24. Gatan image filtering transmission electron (FTEM) micrographs of consolidated and heat-treated Ti-B material produced using the Armstrong process showing local concentration of oxygen. (a) Oxygen concentration map - white contrast shows where each element is more concentrated; (b) Pre-edge 1 map; (c) Pre-edge 2 map; (d) Post-edge map.

	CP-Ti	Ti-0.8wt.%B	Ti-0.9wt.%B
Predicted UTS (ksi)	41.3	47.1	50.8
Actual UTS (ksi)	88.5	164.0	170.5
Predicted 0.2% YS (ksi)	28.3	34.1	36.3
Actual 0.2% YS (ksi)	65.3	140.5	148.0
Predicted % EL	55.0	45.0	41.0
Actual % EL	13.5	4.7	2.7
Predicted % RA	85.0	77.0	75.0
Actual % RA	16.0	5.8	2.9

Table 4.2. Tensile properties expected for Armstrong produced commercially pure (CP) titanium, Ti-0.8B and Ti-0.9B material using tensile vs. oxygen equivalencies results from Ouchi et al.'s work.

The absence of planar slip could possibly be explained by the local concentration of oxygen in the matrix being less than 0.25 wt.% and a large concentration of oxygen in the TiB. Gatan image filtering transmission electron (FTEM) analysis was completed on the Ti-B material to determine where most of the oxygen was situated. Figure 4.24 shows the oxygen concentration is equivalent to or greater in the α titanium matrix as compared to the TiB. Therefore, the lack of planar slip is not attributable to oxygen segregation in the TiB.

The lack of planar slip also can be attributed to the reduced slip length due to the fine α grain size. The short slip lengths do not allow for dislocations to pile up as the back stress builds up quickly not allowing dislocation sources to continue to create dislocations on the same slip plane. For sources to stay active, cross-slip must occur thus the presence of wavy slip character.

The extent to which the Armstrong product is strengthened due to the addition of interstitial elements was evaluated using the following relationship derived by Jaffee [32]:

$$\{O\} = O + 2N + 2/3C \text{ (all elements in wt.\%)} \qquad [4.12]$$

The equivalent oxygen content relationship was derived in an attempt to quantify the individual contributions of the elements oxygen, nitrogen and carbon to solid solution strengthening in CP-Ti and Ti-B material. The oxygen equivalence for the CP-Ti, Ti-0.8B and Ti-0.9B material was 0.28, 0.63 and 0.69 wt.%, respectively. Ouchi et al.[33] reported tensile test results for CP-Ti material with large ranges of oxygen, nitrogen and carbon concentrations. Table 4.2 shows the tensile properties that would be expected for the CP-Ti and Ti-B material using the oxygen equivalencies calculated from the regression analysis work of Ouchi et al. These calculated tensile results do not agree with

the actual results. The actual 0.2% yield strength and ultimate tensile strength are still larger than that of the calculated values while the elongation and reduction in area are lower than calculated. The grain size of the material in Ouchi et al.'s work ranged from ~25 – 45 μm, which is typical of conventional CP-Ti. The grain size in the CP-Ti and Ti-B material is unusually fine at ~5 μm and ~1.5 - 2 μm, respectively. The differences between calculated and actual yield strengths indicate there are other strengthening mechanisms that need to be taken into account to fully understand the tensile results, including grain size and dispersion strengthening.

The fatigue strength at 10^7 cycles is strongly dependent on the interstitial content of the CP-Ti material as it is with yield strength.[34-40] As the oxygen equivalence is increased, the yield strength and fatigue strength increases. These results were expected based on the good correlation between the high cycle fatigue strength and yield strength in titanium alloys. However, a strong relationship between the fatigue strength of CP-Ti material with respect to oxygen equivalency has not been developed as it has for tensile properties. Therefore, the increase in fatigue strength due to the oxygen equivalence level is not able to be determined. The fatigue crack growth rate of Ti-B material was faster in comparison to published results of CP-Ti fatigue crack growth.[21] Robinson and Beevers[41] observed that at room temperature, the fatigue crack growth rate is essentially independent of the interstitial content in the range from 0.2 - 0.9 wt.% oxygen. Therefore, the increase in crack growth rate observed in the Ti-B material is not expected to be due to the higher oxygen concentrations.

4.4.2 Grain Size Strengthening

The Armstrong powder was consolidated and heat-treated to create CP-Ti material that was HIPed, extruded and then annealed. The α grain size was ~5 μm, ~2 μm, and ~1.5 μm for the CP-Ti, Ti-0.8B and Ti-0.9B material, respectively. The resulting α grain sizes were significantly finer than the maximum 45 μm by ASM standards for Grade 2 and Grade 4 CP-Ti. Since all the processing steps were the same between the CP-Ti and Ti-B material, the fine α grain size in the CP-Ti showed that the Armstrong aggregate powder produces a fine grain size in the consolidated and heat-treated material. The addition of boron to the titanium material further refines the microstructure as has been observed by several authors[1,2,4-10,14]. It appears though, that the materials with or without boron show recrystallized grain size forming finer than typical α grains in conventionally produced titanium alloys. This is most likely due to the large number of nuclei in the CP-Ti and Ti-B powder produced using the Armstrong process with fine recrystallized grains formed during the consolidated and heat-treated as discussed in Chapter 3.

The finer α grain size in the CP-Ti and Ti-B material will provide strengthening above that in typical Grade 2 and Grade 4 CP-Ti, in accordance with the Hall-Petch relationship[42,43]. This relationship was used to determine the amount of strengthening obtained from a finer α grain size. It should be noted that the friction stress (σ_i) increases significantly with interstitial content while the locking parameter (k_y) is relatively independent of the interstitial levels. Using published values for the friction stress and locking parameter for the oxygen equivalent levels of the CP-Ti and Ti-B material, the

	CP-Ti	Ti-0.8wt.%B	Ti-0.9wt.%B
Oxygen Equivalence Predited 0.2% YS (ksi)	28.3	34.1	36.3
Hall-Petch/Grain Size Predicted 0.2% YS (ksi)	36.3	78.0	81.5
Total Predicted 0.2% YS (ksi)	64.6	112.1	117.8
Actual 0.2% YS (ksi)	65.3	140.5	148.0

Table 4.3. Predicted 0.2% yield strength properties using oxygen equivalencies and the Hall-Petch relationship and oxygen equivalencies for Armstrong produced commercially pure (CP) titanium, Ti-0.8B and Ti-0.9B material.

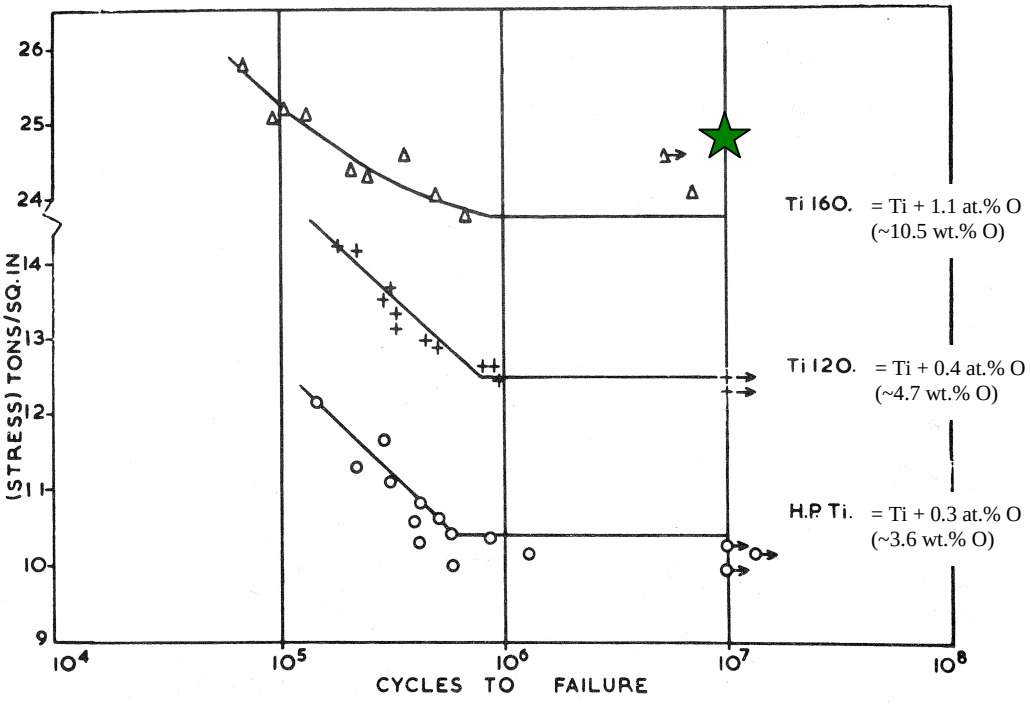

Figure 4.25. Fatigue strengthening for constant grain size (32 μm) in conventional commercially pure (CP) titanium material.[35] Green star shows fatigue strength for Ti-B material with grain size of 1.5 – 2.0 μm and lower oxygen levels.

expected yield strengths were calculated and are shown in Table 4.3. Since the effects of grain size and interstitial concentrations on strength are essentially additive[11], the calculated yield strengths from the oxygen equivalency and Hall-Petch relationships were added to determine the overall calculated yield strength. This is shown in Table 4.3 as well as the actual yield strengths obtained. The results in Table 4.3 show that the calculated and actual yield strengths are essentially the same for the CP-Ti material, which suggests that the strengthening mechanisms are interstitial solid solution and grain size. The Ti-B material, however, still has a significant difference between the calculated and actual yield strengths. Therefore, there are additional strengthening mechanism(s) that still need to be explained.

The α grain size strongly affects the fatigue strength at 10^7 cycles of CP-Ti material.[34-40] As the grain size is decreased, the fatigue strength increases. An example of the amount of fatigue strengthening obtained from grain size is shown in Figure 4.25. However, as with oxygen equivalence a strong relationship between the fatigue strength of CP-Ti material with respect to α grain size has not been developed as it has for tensile properties. The fatigue strengths for the Ti-B material are shown with work from Turner and Roberts[35] in which they tested CP-Ti at three different oxygen equivalencies but all with an α grain size of 32 μm. As shown in Figure 4.25, the Ti-B material had oxygen equivalencies between 0.63 – 0.69 wt%, which is significantly less than the maximum in the plot of ~10.5 wt.% from Turner and Roberts, yet the fatigue strengths were slightly higher. These results were expected since there is a good correlation between yield strength and high cycle fatigue. In addition, the yield strength is dependant on oxygen equivalency and grain size. Therefore, as the oxygen equivalence is increased and/or

grain size decreased the yield strength increases and subsequently the fatigue strength increases.

As mentioned previously, the fatigue crack growth rate of Ti-B material was faster in comparison to published results. In addition to examining the effect of interstitial content on the fatigue crack growth rate of CP-Ti at room temperature, Robinson and Beevers[41] examined the effect of α grain size on crack growth rate with R-ratio equal to 0.35. As expected, the fatigue crack growth rate was observed to decrease by an order of magnitude upon increasing the α grain size from 23 - 80 μm. The crack propagation at low R-ratios is dependent on several factors including crack front geometry and crack closure. The finer α grain size provides for a less torturous crack path and thus an increased crack growth rate. In addition, the fracture surface becomes rougher as the slip length (i.e. grain size) is increased which increases the crack closure factor. The finer α grain size results in a decreased effect from crack closure and thus faster crack growth rates. Therefore, the increase in crack growth rate observed in the Ti-B material is most likely a result of the finer α grain size from processing in addition to possibly the presence of TiB. Also, since the material is so much finer in comparison to the material in Robinson and Beevers work, it is difficult to compare results of each study.

4.4.3 Dispersion Strengthening

Solid solution and grain size strengthening have been credited with ~80% of the total strength of the Ti-B material. The remaining 20% of this strength is believed to be mostly due to the presence of the TiB as a strengthening phase. The rod-shaped TiB

provide the dispersion strengthening while the TiB stringers are believed not to provide any additional strengthening. The fine dispersion of TiB acts as barriers impeding the motion of dislocations through the α titanium matrix. The motion of the dislocations will be impeded thus producing a large amount of strain hardening of the material as the dislocations either bypass or cut through the TiB particles. With every dislocation bypassing the TiB particles, a dislocation loop will be left around the particles. As the number of loops left around the particles increases, the particle spacing decreases thus increasing the amount of strain hardening. Fractography of failed tensile, fatigue, and crack growth test specimens, and transmission electron microscopy (TEM) of compression test specimens show no evidence of the TiB being fractured or cut by dislocations. This is consistent with having a good strengthening phase that is hard to shear: (1) TiB has a significantly higher modulus (see Table 4.1) than the α titanium matrix; (2) no documented evidence of coherency between the matrix and TiB; and (3) the TiB is a compound that impedes dislocations from slipping within the TiB and across the α titanium to TiB interface.

The observations are consistent with the strengthening due to the presence of TiB and the dislocations having to bypass the TiB. As mentioned from the previous section, estimates of the amount of strengthening due to the fine dispersion of the TiB can be estimated using the Orowan equation[44]. This relationship was used but the results were not consistent with actual results when published values of the shear modulus and burgers vectors were used. The dispersoid spacing required to account for the remaining amount of yield strength is not consistent with that in the Ti-B material. This is believed to be partially due to the morphology of the TiB. The rod-shape of the TiB makes it more

difficult for the dislocations to bypass the TiB and thus providing for additional strengthening[45] over that estimated by the Orowan relationship which is based on spherical particles. There also was not a homogeneous and uniform distribution of the TiB in the material. The Orowan relationship assumes a homogeneous and uniform distribution of the reinforcement phase.

The presence of the TiB strongly affects the fatigue strength at 10^7 cycles of CP-Ti material. The TiB is believed to provide additional resistance to fatigue crack initiation but not crack propagation.[26,46-48] The initiation of all fatigue cracks were observed at or just sub-surface in the notch root not near any TiB. The TiB has been proposed to provide resistance to crack propagation by bridging the crack(s) by Srivatsan et al.[46] for Ti-6Al-4V with boron and Li et al.[47] for CP-Ti with 10 vol.% of TiB. These published results are not consistent with the results of the current Ti-B study. Fractography and TEM analysis showed no evidence of TiB cracking or debonding from the α titanium matrix. The Ti-B material had a faster crack growth rate than conventional CP-Ti material most likely due to the finer α grain size and presence of TiB. Both the Ti-0.8B and Ti-0.9B have an α grain size of ~1.5 - 2.0 μm, which is much finer than conventional material. However, the resistance to crack growth is less in the Ti-0.9B material than in the Ti-0.8B material suggesting the boron does not bridge the crack reducing crack growth rates.

4.5 Conclusions

The Armstrong process was used to produce commercially pure (CP) titanium, Ti-0.8B and Ti-0.9B powder that was HIPed, extruded and annealed in order to understand the effect of boron additions on the mechanical properties of the final product. The

tensile, notched fatigue and fatigue crack growth properties of CP-Ti and Ti-B material were characterized. The Ti-B material showed an increase in tensile strength and fatigue strength in comparison to CP-Ti material. However, the Ti-B material also showed a reduction in ductility and crack growth resistance. When compared to published results for other titanium alloys containing boron, the Ti-B material was equivalent to or higher in 0.2% yield strength and ultimate tensile strength while maintaining higher ductility and similar fatigue strengths at 10^7 cycles.

The strengthening mechanisms for the CP-Ti and Ti-B material were examined. The oxygen equivalency of the CP-Ti and Ti-B material was determined and used to calculate the expected tensile properties. The higher levels of oxygen and other interstitial elements have been suggested by others to provide strengthening through short range ordering of the α titanium matrix. In addition, the Hall-Petch relationship was used to calculate the expected yield strength of the CP-Ti and Ti-B material. The addition of boron produced a finer α grain size that provided additional strengthening over that of the already fine α grains for the CP-Ti material. When these results were combined, it predicted the yield strength of the CP-Ti material and was within 20% of the Ti-B material. The unaccounted 20% of the yield strength is most likely from the presence of the TiB. The rod shaped TiB provide dispersion strengthening in addition to the solid solution and grain size strengthening through impeding dislocation motion and causing dislocation cross-slip and bypassing of the TiB.

The fatigue strength increased as well due to the increased resistance to crack initiation from the refined α grain size (shorter slip lengths), and the presence of TiB. The

increased fatigue crack growth was attributed to the refined α grain size providing a less tortuous path and reduced effects of crack closure from fracture roughness, and observation as boron additions were increased the resistance to crack growth reduced.

4.6 References

1. Yolton, C.F. *JOM.* **56(5).** 2004. pp. 56.
2. Tamirisakandala, S., Bhat, R.B., Ravi, V.A., Miracle, D.B. *JOM.* **56(5).** 2004. pp. 60.
3. Saito, Takashi. *JOM.* **56(5).** 2004. pp. 33.
4. Abkowitz, S., Abkowitz, S.M., Fisher, H., Schwartz, P. J. *JOM.* **56(5).** 2004. pp. 37.
5. Ravi Chandran, K.S., Panda, K.B., Sahay, S.S. *JOM.* **56(5).** 2004. pp. 42.
6. Kumari, S., Eswara Prasad, N., Ravi Chandran, K.S., Malakondaiah, G. *JOM.* **56(5).** 2004. pp. 51.
7. Hanusiak, W., Yolton, C.F., Fields, J., Hammond, V., Grabow, R. *JOM.* **56(5).** 2004. pp. 49.
8. Ravi Chandran, K.S., Miracle, D.B. *JOM.* **56(5).** 2004. pp. 32.
9. Banerjee, R., Genc, A., Collins, P.C., Fraser, H.L. *Met. and Mater. Trans.* **35A.** 2004. pp. 2143.
10. Banerjee, R., Collins, P.C., Genc, A., Fraser, H.L. *Mater. Sci. Eng. A.* **A358.** 2003. pp. 343.
11. Leutjering, G. Williams, J.C. **Titanium (Engineering Materials and Processes).** *Springer-Verlag Publishing*. 2003.
12. Fan, Z., Chandrasekaran, L., Ward-Close, C.M., Miodownik, P. *Scripta Met.* **32(6).** 1995. pp. 833.
13. Saito, T., Furuta, T., Takamiya, H. *Titanium '95: Science and Technology.* 1995. pp. 2763.
14. Yolton, C.F., Moll, J.H. *Titanium '95: Science and Technology.* 1996. pp. 2755.

15. Tsang, H.T., Chao, C.G., Ma, C.Y. *Acta. Met.* **37(9).** 1997. pp. 1359.

16. Zhang, X., Lu, W., Zhang, D., Wu, R., Bian, Y., Fang, P..*Acta. Met.* **41(1).** 1999. pp. 39.

17. Godfrey, T.M.T., Wisbey, A., Goodwin, P.S., Bagnall, K., Ward-Close, C.M. *Mater. Sci. Eng. A.* **A282.** 2000. pp. 240.

18. Dubey, S., Lederich, R.J., Soboyejo, W.O. *Metall. Trans. A* **28.** 1997.

19. Philliber, J.A., Dary, F.C., Zok, F.W., Levi, C.G., Blenkinsop, P.A. *Titanium '95: Science and Technology.* 1995. pp. 2714.

20. Reed-Hill, R. **Physical Metallurgy Principles.** *PWS Publishing Company.* 1991.

21. Adib, A.M.L., Baptista, C.A.R.P. *Materials Science and Engineering A.* **452-453.** 2007. pp. 321.

22. Morsi, K., Patel, V.V. *Journal of Materials Science.* **42.** 2007. pp. 2037.

23. Panda K.B., Ravi Chandran, K.S. *Metall. Mater. Trans. A.* **34(6).** 2003. pp. 1371.

24. Saito, T., Takamiya, H ., Furuta, T. *Titanium '95: Science and Technology.* 1995. pp. 2859.

25. Saito, T., Furuta, T., Takamiya, H. *Titanium '95: Science and Technology.* 1995. pp. 2763.

26. Saito, T., Takamiya, H ., Furuta, T. *Mat. Sci. & Eng. A.* **A243.** 1998. pp. 273.

27. Saito, T., Furuta, F., Yamaguchi, Y. **Recent Advances In Titanium Metal Matrix Composites.** *TMS Warrendale, PA.* 1995. pp. 33.

28. Paton, N.E., Williams, J.C., Rauscher, G.P. *Titanium Science and Technology.* 1973. pp. 1049.

29. Williams, J.C., Sommer, A.W., Tung, P.P. *Metall. Trans. A.* **3(11).** 1972. pp. 2979.

30. Welsch, G., Leutjering, G., Gazioglu, K., Bunk, W. *Metall. Trans.* **8A.** 1977. pp. 169.

31. Weissmann, S., Shrier, A. **The Science, Technology and Application of Titanium.** *Pergamon Press, Oxford*. 1970. pp. 441.

32. Jaffe, R.I. **Titanium '80, Science and Technology. Vol. 4.** 1980. pp. 1665.

33. Ouchi, C., Iizumi, H., Mitao, S. *Materials Science and Engineering.* **A243.** 1998. pp. 186.

34. Jaffee, R.I., Campbell, I.E. *Met. Prog.* **55.** 1949. pp.356.

35. Turner, N.G., Roberts, W.T. *Trans. AIME.* **242.** 1968. pp. 1223.

36. Lipsitt, H.A., Wang, D.Y. *Trans. AIME.* **221.** 1961. pp. 918.

37. Turner, N.G., Roberts, W.T. *Journal of Less-Common Met.* **16.** 1968. pp. 37.

38. Beevers, C.J., Robinson, J.L. *Journal of Less-Common Met.* **17.** 1969. pp. 345.

39. Golland, D.I., Beevers, C.J. *Met. Sci. Journal.* **5.** 1971. pp.174.

40. Golland, D.I., Beevers, C.J. *Journal of Less-Common Met.* **23.** 1971. pp. 174.

41. Robinson, J.L., Beevers, C.J. *Titanium Science and Technology.* 1973. pp. 1245.

42. Hall, E.O. *Proceedings of the Physical Society*. London B64. 1951. pp. 747.

43. Petch, N.J. *Journal of the Iron and Steel Institute*. London 174. 1953. pp. 25.

44. Orowan, E. *Discussion in "Symposium on Internal Stresses"*. London. 1947. pp. 451.

45. Kelly, P.M. *Scripta. Metall.* **6.** 1972. pp. 647.

46. Srivatsan, T.S., Soboyejo, W.O., Lederich, R.J. **Recent Advances In Titanium Metal Matrix Composites.** *TMS Warrendale, PA.* 1995. pp. 225.

47. Li, B.S., Shang, J.L., Fu, H.Z. *Materials Science and Engineer A.* **383(2).** 2004. pp. 316.

48. Feng, H., Zhou, Y., Jia D., Meng, Q. *Computer Science Technology.* **64(16).** 2004. pp. 2495.

CHAPTER 5

SUMMARY AND RECOMMENDED FUTURE WORK

5.1 Summary and Conclusions

The Armstrong process is a vapor phase method for producing titanium and titanium alloys from metal chlorides. The product of the Armstrong process is an irregular powder. This process was used to produce commercially pure (CP) titanium, Ti-0.8 wt.%B and Ti-0.9 wt.%B powder. It should be noted that the Ti-0.8B and Ti-0.9B powders originated from the first boron containing experimental runs of the Armstrong process. The resulting three materials studied here are termed CP-Ti, Ti-0.8B and Ti-0.9B. Samples of the powder were characterized. The powder was HIPed, extruded and annealed in order to understand the effect of using the Armstrong process to produce the starting material and boron additions on the microstructure and mechanical properties of the final product. The following are the conclusions from this work.

5.1.1 CP-Ti, Ti-0.8B and Ti-0.9B Powder Produced Using The Armstrong Process

- CP-Ti, Ti-0.8B and Ti-0.9B powder morphology was analogous to titanium sponge in that it was friable with an irregular shaped aggregate, and rough, porous appearance.

Ti-B powder was finer in size than that of CP-Ti powder. No microstructural features were observed for either the CP-Ti or the Ti-B powder, but x-ray diffraction (XRD) or transmission electron microscopy (TEM) was not performed to validate whether α grains were present in the as-received powder and not observable using scanning electron microscopy (SEM). The powder is most likely in a metastable form with the boron in solution with titanium, and TiB being formed during consolidation.

- The chemical reactions involved in formation of the CP-Ti and Ti-B alloyed powder using the Armstrong process is analogous to those of the Kroll and Hunter processes. Because the powder is formed directly from the vapor phase, the likelihood of a more uniform distribution of second phases, i.e. TiB, is more attractive.
- The Ti-B powder was found to have higher levels of oxygen, carbon, and iron than CP-Ti powder. Sodium and chlorine were lower in Ti-B powder as compared to CP-Ti powder. The reduced amount of sodium and chlorine provides for a cleaner and better quality powder such that there is an absence of porosity in the final product.

5.1.2 Microstructure Characterization of Consolidated and Heat-Treated CP-Ti, Ti-0.8B and Ti-0.9B Powder

- The microstructures of the consolidated and heat-treated CP-Ti and Ti-B material was analogous to that observed by other processes used to create CP-Ti and Ti-B alloys. The CP-Ti material had α (HCP) grains and the Ti-B material had α (HCP) grains and TiB (orthorhombic) particles dispersed throughout the material. The CP-Ti material had a fine α grain size (~5.0 μm) elongated in the extrusion direction along

with an α lath substructure, which has not been observed in published literature. The Ti-B material had a finer α grain size than CP-Ti (~2.0 μm for Ti-0.8B;~1.5 μm for Ti-0.9B) and had rod shaped TiB at α grain boundaries and within the α grains, blocky TiB at α grain boundaries and TiB stringers randomly distributed.

- The morphologies and non-uniform distribution of the TiB was attributed to the limited diffusion of boron in titanium and the orthorhombic structure of the TiB, and the crystallographic restrictions and relationships between the α phase and TiB precipitates. The TiB particles located at α/α grain boundaries were observed to be coarser and in some cases blocky due to easier diffusion rates of boron along the grain boundaries and less of a crystallographic restriction on the TiB at the grain boundaries. The TiB particles within the α grains were finer than the grain boundary TiB due to the limited diffusion rates of boron in titanium and the crystallographic restrictions with the grains.
- The chemistry and amount of plastic deformation from working of CP-Ti, Ti-0.8B and Ti-0.9B material, as with other non-heat treatable grade titanium alloys, determines the microstructure (principally grain size) and subsequently the properties of the final product. Therefore, the spacing of the TiB dispersoids could not be altered using heat treatment. This is similar to other materials made by mechanical alloying of powder. However, the TiB is formed directly from the powder and not during mechanical alloying which reduces the PM processing cost.

5.1.3 Mechanical Properties of Consolidated and Heat-Treated CP-Ti, Ti-0.8B and Ti-0.9B Powder

- The CP-Ti material with boron showed an increase in tensile strength, fatigue strength and crack growth rate with a reduction in ductility in comparison to CP-Ti. CP-Ti and Ti-B alloys were equivalent to or higher in yield and ultimate tensile strengths than typical CP-Ti and Ti-B alloys, while maintaining a higher ductility and similar fatigue strengths at 10^7 cycles in comparison to published results of other Ti-B alloys.
- The operative strengthening mechanisms for the CP-Ti and Ti-B material studied were solid solution (from oxygen, nitrogen and carbon), grain size, and dispersion (from fine TiB particles) strengthening.
    - The oxygen equivalency of the CP-Ti and Ti-B material was calculated from an accepted relationship (equation 4.1). This was used in conjunction with a relationship reported by Ouchi et al. to calculate the expected tensile properties of the three materials.
    - The Hall-Petch relationship was used to calculate the expected yield strength of the three materials. The boron containing alloys had a finer grain size that provided additional strengthening compared to the already fine α grain size of the CP-Ti. When these two results were combined, it predicted the yield strength of the CP-Ti material was within 20% of the Ti-B material.
    - The unaccounted portion of the yield strength is most likely to be from the presence of the TiB. The rod shaped TiB provides dispersion strengthening

through impeding dislocation motion and causing dislocation cross-slip and bypassing of the TiB. Additional strengthening could be obtained if the distribution of the TiB was more uniform and had a smaller spacing.

- The fatigue strength is believed to have increased as well due to the increased resistance to crack initiation from the refined grain size (shorter slip lengths). The increased fatigue crack growth was attributed to the refined grain size providing a less tortuous path and less of a crack closure effect along with the presence of the TiB.

5.2 Recommended Future Work

Commercially pure (CP) titanium alloys are largely produced as a flat rolled product with some applications produced from castings or forgings. There are few if any powder metallurgy (PM) products produced using the various grades of CP-Ti, as the cost to benefit relation is too low. The Armstrong process could change this ratio by lowering the cost to produce CP-Ti from inexpensive powder. In addition, this process could also allow for the introduction of novel titanium alloys, which are not producible using conventional ingot metallurgy methods. The following additional questions/issues are recommended for future work based on the results and conclusions of this study:

- A review of all the processes used to create titanium alloys containing boron show there is no published work on producing these alloys from a vapor to a solid (powder in this case) with a supersaturated solution of boron. Therefore, further work is required to fully understand how the microstructure develops in Ti-B alloys made from the vapor phase to the solid phase.

- The TiB observed in this study is believed to have precipitated out of the α phase upon consolidation using HIP and extrusion. The only other reference to the TiB precipitating out of the α phase was when the LENS™ process was used and nano-TiB was observed. All other methods to produce titanium alloys with boron have reported the boron precipitating out of the liquid phase with the α and/or β phase(s) nucleating on the TiB. The microstructural development of the TiB precipitating from the α phase needs further work to fully understand the mechanisms of formation including crystallographic relationships between the TiB and α phase.
- The chemistry of the consolidated and heat-treated Ti-0.8B and Ti-0.9B material was found to have high levels of oxygen. The CP-Ti material had an oxygen concentration similar to that of typical Grade 2 CP-Ti material. The high levels of oxygen and other minor elements of the powder are a concern as subsequent handling and processing needs to minimize the introduction of oxygen, and other minor elements, as they will reduce the mechanical properties.
- Powder handling and cleanliness are a couple of the main factors governing the quality of PM alloys. Contamination from foreign particles may lead to a substantial loss of properties, in particular fatigue strength. This is a major concern for titanium alloys as inclusions are not currently an issue in commercial materials produced using hearth melting and/or vacuum arc melting. Therefore, the downstream PM processing will have to be controlled and the effects of various consolidation methods need to be better understood before any PM process can be used in production.

- It would be useful to understand the nature and circumstances leading to the formation of an α lath substructure in the CP-Ti material. This was an unexpected observation with current study.
- In addition to the α lath substructure, the regions of material that were originally thought to be TiB stringers should be fully characterized. The present study showed titanium in these regions, but lean in boron. The lack of boron in these regions is most likely due to non-uniform chemical distribution in the powder. As with the α lath substructure, there was a low volume fraction of these areas in the material and most likely had to no effect on tensile properties. It is likely these regions will affect the minimum values of fatigue strength generated for specific applications. It is believed that these areas were formed during the consolidation of the material, but the nature and circumstances leading to the formation of these regions needs further work.

MASTER LIST OF REFERENCES

1. Abkowitz, S. *Powder Metallurgy of Titanium Alloys.* 1980.

2. Abkowitz, S., Abkowitz, S.M., Fisher, H., Schwartz, P.J. *JOM.* **56(5).** 2004. pp. 37.

3. Adams, R.T., Rosenberg, H.W. **Titanium and Titanium Alloys—Scientific and Technological Aspects.** *Plenum Press Publishing.* 1982. pp. 127.

4. Adib, A.M.L., Baptista, C.A.R.P. *Materials Science and Engineering A.* **452-453.** 2007. pp. 321.

5. Albrecht, J., Leutjering, G. Nicolai, H-P., Liesner, C. **Fatigue 2002**, *EMAS, Warley, UK.* 2002. pp. 2085.

6. Andersen, P.J., Eloff, P.C. *Powder Metallurgy of Titanium Alloys.* 1980.

7. Anderson, R.P., Armstrong, D.R., Jacobsen, L.E. **Filter cake treatment apparatus and method.** *U.S. Patent Office.* Patent No. 2005284824 A1. 2005.

8. Anderson, R.P., Armstrong, D.R., Jacobsen, L.E. **System and method of producing metals and alloys.** *U.S. Patent Office.* Patent No. 2006107790 A1. 2006.

9. Anderson, R.P., Ernst, W., Jacobsen, L., Kogut, D., Steed, J.M. **Cost-Affordable Titanium: A Symposium Dedicated to Professor Harvey Flower as held at the 2004 TMS Annual Meeting.** 2004. pp. 121.

10. Anderson, R.P., Jacobsen, L.E. **Separation system of metal powder from slurry and process.** *U.S. Patent Office.* Patent No. 2006086435 A1. 2006.

11. Armstrong, D.R., Anderson, R.P., Jacobsen, L.E. **Filter extraction mechanism.** *U.S. Patent Office.* Patent No. 2005225014 A1. 2005.

12. Armstrong, D.R., Anderson, R.P., Jacobsen, L.E. **Method and apparatus for controlling the size of powder produced by the Armstrong Process.** *U.S. Patent Office.* Patent No. 2004079196 A1. 2004.

13. Armstrong, D.R., Anderson, R.P., Jacobsen, L.E. **Method and apparatus for controlling the size of powder produced by the Armstrong Process.** *U.S. Patent Office.* Patent No. 2005081682 A1. 2005.

14. Armstrong, D.R., Anderson, R.P., Jacobsen, L.E. **Preparation of alloys by the armstrong method.** *U.S. Patent Office.* Patent No. 2004079197 A1. 2004.

15. Armstrong, D.R., Anderson, R.P., Jacobsen, L.E. **Preparation of alloys by the armstrong method.** *U.S. Patent Office.* Patent No. 2006150769 A1. 2006.

16. Armstrong, D.R., Borys, S.S., Anderson, R.P. **Ceramics and method of producing ceramics.** *U.S. Patent Office.* Patent No. 6,861,038. 2005.

17. Armstrong, D.R., Borys, S.S., Anderson, R.P. **Elemental material and alloy.** *U.S. Patent Office.* Patent No. 2002148327 A1. 2002.

18. Armstrong, D.R., Borys, S.S., Anderson, R.P. **Elemental material and alloy.** *U.S. Patent Office.* Patent No. 2002152844 A1. 2002.

19. Armstrong, D.R., Borys, S.S., Anderson, R.P. **Method of Making Metals and Other Elements.** *U.S. Patent Office.* Patent No. 5,779,761. 1998.

20. Armstrong, D.R., Borys, S.S., Anderson, R.P. **Method of Making Metals and Other Elements from the Halide Vapor of the Metal.** *U.S. Patent Office.* Patent No. 5,958,106. 1999.

21. Armstrong, D.R., Borys, S.S., Anderson, R.P. **Method of Making Metals and Other Elements from the Halide Vapor of the Metal.** *U.S. Patent Office.* Patent No. 6,409,797 B2. 2002.

22. Armstrong, D.R., Borys, S.S., Anderson, R.P. **Method of making metals and other elements from the halide vapor of the metal.** *U.S. Patent Office.* Patent No. 2002005090 A1. 2002.

23. Axelbaum, R.L., Bates, S.E., Buhro, W.E., Frey, C.A., Kelton, K.F., Lawton, S.A., Rosen, L.J., Sastry, S.M.L. *Nanostructured Materials.* **2.** 1993. pp. 139.

24. Axelbaum, R.L., DuFaux, D.P., Frey, C.A., Kelton, K.F., Lawton, S.A., Rosen, L.J., Sastry, S.M.L. *Journal of Materials Research.* **11(4).** 1996. pp. 948.

25. Axelbaum, R.L., DuFaux, D.P., Frey, C.A., Sastry, S.M.L. *Metallurgical and Materials Transactions.* **B28.** 1997. pp. 1199.

26. Banerjee, R., Collins, P.C., Genc, A., Fraser, H.L. *Mater. Sci. Eng. A.* **A358.** 2003. pp. 343.

27. Banerjee, R., Collins, P.C., Genc, A., Tiley, J. Fraser, H.L. *Titanium Science and Technology '03*. Munich. 2004. pp. 2547.

28. Banerjee, R., Genc, A., Collins, P.C., Fraser, H.L. *Met. and Mater. Trans.* **35A.** 2004. pp. 2143.

29. Barth, W.J., Field, A.L. *Metal Progr.* **64.** 1953. pp. 74.

30. Beevers, C.J., Robinson, J.L. *Journal of Less-Common Met.* **17.** 1969. pp. 345.

31. Benish, A.J., Sathaye, A., Nash, P., Anderson, R., Zwitter, T. **International Conference on Powder Metallurgy & Particulate Materials.** 2005. pp. 61.

32. Blackburn, M.J., Williams, J.C. *Trans. ASM*. **62.** 1969. pp. 398.

33. Blenkinsop, P.A. *Titanium '95: Science and Technology.* The University Press, Cambridge, UK. 1996. pp. 1.

34. Borradaile, J.B., Jeal, R.H. *Titanium Science and Technology*. 1984. pp. 141.

35. Boyer, R., Welsch, G., Collings, E.W. **ASM Materials Properties Handbook: Titanium Alloys.** *ASM International, Materials Park, OH.* 1994.

36. Boyer, R.R. **Beta Titanium Alloys in the 1990s.** *TMS Warrendale, USA.* 1993. pp. 335.

37. Boyer, R.R. **Beta Titanium Alloys.** *Societe Francaise de Metallurgie et de Materiaux, Paris, France.* 1994. pp. 253.

38. Boyer, R.R. *Mat. Sci. & Eng. A*. **(A213).** 1996. pp. 103.

39. Boyer, R.R. *Titanium '95: Science and Technology.* The University Press, Cambridge, UK. 1996. pp. 41.

40. Breme, J. *6th World Conference on Titanium.* Les Editions de Physique, Les Ulis, France. 1988. pp. 57.

41. Breme, J., Biehl, V., Wack, T. Eisenbarth, E. *Titanium '99: Science and Technology.* St. Petersburg, Russia. 2000. pp.1187.

42. Brice, C.A., Schwendner, K.I., Mahaffey, D.W., Moore, E.H., Fraser, H.I. **Proceedings of the Solid Freeform Fabrication.** 1999. pp. 369.

43. Brooks, J., Robino, C., Headley, T., Goods, S., Griffith, M. **Proceedings of the Solid Freeform Fabrication.** 1999. pp. 375.

44. Brunette, D.M., Tengvail, P., Textor, M., Thomsen, M. **Titanium in Medicine.** *Springer-Verlag, Berlin, Germany.* 2001.

45. Burgers, W.G. *Physica 1*. 1934. pp. 561.

46. Cadle, R.D. **Particle Size: Theory and Industrial Applications.** *Reinhold Publishing.* 1965.

47. Carneiro Ueta, M.C., Fracote, C.A., Rodrigues Henriques, V.A., Alencastro Graca, M.L., Alves Cairo, C.A. *Materials Science Forum.* **498-499.** 2005. pp. 211.

48. Chen, L., Gu, Y., Qian, Y. Shi, L., Yang, Z., Ma, J. *Materials Research Bulletin.* **39.** 2004. pp. 609.

49. Coble, R.L. *Journal of Applied Physics.* **32.** 1961. pp. 789.

50. Crowley, G. *Advanced Materials & Processes.* **161(11).** 2003. pp. 25.

51. Decker, B.F., Kasper, R. *Acta Crystallogr.* **7.** 1954. pp. 77.

52. Dubey, S., Lederich, R.J., Soboyejo, W.O. *Metall. Trans. A* **28.** 1997.

53. Dulis, E.J., Chandhok, V.K., Froes, F.H., Clark, L.P. *Proceedings of the 10th National SAMPE Technical Conference*. 1978. pp.316.

54. Eylon, D., Kerr, W.R. *STP 645: Fractography in Failure Analysis.* 1978. pp. 235.

55. F. Cardarelli, "A Method for Electrowinning of Titanium Metal or Alloy from Titanium Oxide Containing Compound in the Liquid State", WO 03/046258 A2, June 5 2003.

56. Fan, Z., Chandrasekaran, L., Ward-Close, C.M., Miodownik, P. *Scripta Met.* **32(6).** 1995. pp. 833.

57. Fan, Z., Guo Z.X., Cantor, B. *Composites.* **28A.** 1997. pp. 131.

58. Fan, Z., Miodownik, P. *Acta Metall.* **44.** 1995. pp. 93.

59. Fan, Z., Niu, H.J., Miodownik, A.P., Saito, T., Cantor, B. *Key Engineering Materials.* **127-131.** 1997. pp. 423.

60. Fanning, J.C. *Titanium '95: Science and Technology.* The University Press, Cambridge, UK. 1996. pp. 1800.

61. Feng, H.B., Jia, D.C., Zhou, Y., Huo, J. *Materials Science and Technology.* **20.** 2004. pp. 1205.

62. Finlay, W.L., Snyder, J.A. *Trans. AIME.* **188.** 1950. pp. 277.

63. Friedrich, H., Kiese, J., Haldenwanger, H-G., Stich, A. *Proceedings of the 10th World Conference on Titanium.* Wiley-VCH, Weinheim, Germany. 2003.

64. Froes, F.H. **Non-Aerospace Applications of Titanium.** *TMS Warrendale, USA.* 1998. pp. 317.

65. Froes, F.H., Allen, P.G., Niinomi, M. **Non-Aerospace Applications of Titanium.** *TMS Warrendale, USA.* 1998. pp. 3.

66. Froes, F.H., Eylon, D. **Titanium Technology: Present Status and Future Trends.** 1985. pp. 49.

67. Froes, F.H., Suryanarayana, C. **Powder Processing of Titanium Alloys.** 1993. pp. 223.

68. Fujita, T., Agawa, A., Ouchi, C., Tajima, H. *Materials Science and Engineering.* **A213.** 1996. pp. 148.

69. Fuwa, A. Takaya, S. *JOM*. **57(10).** 2005. pp.56.

70. Garriott, R.E., Thellman, E.L. *Proceedings of the 1976 International Powder Metallurgy Conference.* 1976.

71. Gerdemann, S.J. *Advanced Materials & Processes.* July 2001. pp. 41.

72. Gerdemann, S.J., Alman, D.E. **International Conference on Powder Metallurgy & Particulate Materials.** 2000. pp. 12.41.

73. Giantta; M.V. **2003 Hamburg Titanium Conference: Vol. 1.** 2003. pp. 237.

74. Godfrey, T.M.T., Wisbey, A., Goodwin, P.S., Bagnall, K., Ward-Close, C.M. *Mater. Sci. Eng. A.* **A282.** 2000. pp. 240.

75. Golland, D.I., Beevers, C.J. *Journal of Less-Common Met.* **23.** 1971. pp. 174.

76. Golland, D.I., Beevers, C.J. *Met. Sci. Journal.* **5.** 1971. pp.174.

77. Goodwin, P.S., Wisbey, A., Ubhi, H.S., Kulikowski, Z., Gasson, P., Ward-Close, C.M. *Titanium '95: Science and Technology.* 1995. pp. 2874.

78. Hall, E.O. *Proceedings of the Physical Society*. London B64. 1951. pp. 747.

79. Hansen, D., Rusin, R.P., Teng, M.H., Johnson, D.L. *J. Amer. Chem. Soc.* **75.** 1992. pp. 1129.

80. Hanusiak, W., Yolton, C.F., Fields, J., Hammond, V., Grabow, R. *JOM.* **56(5).** 2004. pp. 49.

81. Helm D. **Fatigue Behavior of Titanium Alloys.** *TMS Warrendale, USA. 1999.* pp. 291.

82. Hirschhorn, J.S. **Introduction to Powder Metallurgy.** *American Powder Metallurgy Institute.* 1976.

83. Hirth, J.P. *Metall. Trans*. **3.** 1972. pp. 3047.

84. Hirth, J.P., Balluffi, R.W. *Acta Met.* **21.** 1973. pp. 929.

85. Hosonuma, M., Shimamune, T. *6th World Conference on Titanium.* Les Editions de Physique, Les Ulis, France. 1988. pp. 495.

86. Hu, D., Johnson, T.P., Loretto, M.H. **Advances In Powder Metallurgy and Particulate Materials.** *MPFI.* 1995. pp. 109.

87. Hunter M.A. *J. Amer. Chem. Soc.* **32**. 1910. pp. 330.

88. Hyman, M.E., McCullough, C., Valencia, J.J., Levi, C.G., Mehrabian, R. *Metall. Trans.* **22A.** 1991. pp. 1647.

89. Irani, R.R., Callis, C.F. **Particle Size: Measurement, Intrepretation and Application.** *Wiley Publishing.* 1963.

90. Jackson, M., Dring., K. *Materials Science and Technology.* **22(8).** 2006. pp. 881.

91. Jacobsen, L.. *Advanced Materials & Processes.* **160(8).** 2002. pp. 25.

92. Jacobsen, L.E., Benish, A.J. **Titanium alloy.** *U.S. Patent Office.* Patent No. 2007017319 A1. 2007.

93. Jacobsen, L.E., Benish, A.J. **Titanium boride.** *U.S. Patent Office.* Patent No. 2007079908 A1. 2007.

94. Jaffe, R.I. *Progr. Metal Phys.* **7.** 1958. pp. 65.

95. Jaffe, R.I. *Titanium '80, Science and Technology.* **Vol. 4.** 1980. pp. 1665.

96. Jaffe, R.I. **Titanium Steam Turbine Blading.** *Pergamon Press, New York, USA.* 1999.

97. Jaffe, R.I., Campbell, I.E. *Trans. AIME.* **185.** 1949. pp. 646.

98. Jaffee, R.I., Campbell, I.E. *Met. Prog.* **55.** 1949. pp.356.

99. Jones, I.P., Hutchinson, W.B. *Acta Met.* **29.** 1981. pp. 951.

100. Kang, S-K.L., Jung, Y-L. *Acta Materialia.* **52.** 2004. pp. 4573.

101. Kao, W.H. *AFML Contract F33615-77-C-5173, Semi-annual Report.* 1979.

102. Kao, W.H., Orsborn, L.M. *Powder Metallurgy of Titanium Alloys.* 1980.

103. Keicher, D.M., Miller, W.D. *Metal Powder Report.* **53.** 1998. pp. 26.

104. Kelly, P.M. *Scripta. Metall.* **6.** 1972. pp. 647.

105. Kobayashi, M., Funami, K., Suzuki, S., Ouchi, C. *Materials Science & Engineering.* **A243.** 1998. pp. 279.

106. Koike, J. Shimoyama, Y., Fujii, H., Maruyama, K. *Scripta Materialia.* **39.** 1998. pp. 1009.

107. Kroll W. J. *Trans El. Soc.* **78**. 1940. pp. 35.

108. Kumari, S., Eswara Prasad, N., Ravi Chandran, K.S., Malakondaiah, G. *JOM.* **56(5).** 2004. pp. 51.

109. Lavender, C.A., Carpenter, J.A. **2004 Annual Progress Report for Automotive Lightweighting Materials.** 2005.

110. Leutjering, G. Williams, J.C. **Titanium (Engineering Materials and Processes).** *Springer-Verlag Publishing*. 2003.

111. Li, B.S., Shang, J.L., Fu, H.Z. *Materials Science and Engineer A.* **383(2).** 2004. pp. 316.

112. Lin, F.S., Starke, E.A. Chakrabortty, S.B., Gylser, A. *Metall. Trans. A.* **15A.** 1984. pp. 1229.

113. Lipsitt, H.A., Wang, D.Y. *Trans. AIME.* **221.** 1961. pp. 918.

114. Liu, Y., Chen, L.F., Tang, H.P., Liu, C.T., Liu, B., Huang, B.Y. *Materials Science and Engineering.* **A418.** 2006. pp. 25.

115. Leutjering, G., Weissmann, S. *Acta. Met.* **18.** 1970. pp. 785.

116. Miller, J.A., Brodi, G. *AFML-TR-79-4028.* 1979.

117. Mills, M.J., Hou, D.H., Suri, S., Viswanathan, G.B. *Boundaries and Interfaces in Materials*. TMS Warrendale, PA. 1998. pp. 295.

118. Miska, K. *Materials Engineering.* **79-80.** 1974. pp. 61.

119. Morsi, K., Patel, V.V. *Journal of Materials Science.* **42.** 2007. pp. 2037.

120. Moxson, V., Froes, F.H. *JOM.* **52(5).** 2000. pp. 24.

121. Nagesh, CH.R.V.S., Sridhar Rao, CH., Ballal, N.B., Krishna Rao, P. *Metallurgical and Materials Transactions B.* **35B.** 2004. pp. 65.

122. Newkirk, J.B., Geisler, A.H. *Acta Met. 1*. 1953. pp. 370.

123. Niinomi, M., Kuroda, D., Fukunaga, K., Fukui, H., Kato, Y., Yashiro, T., Suzuki, A., Hasegawa, J. *Titanium '99: Science and Technology.* St. Petersburg, Russia. 2000. pp.1195.

124. Ogurtsov, S.V. **Titanium and Titanium Alloys—Scientific and Technological Aspects.** *Plenum Press Publishing.* 1982. pp. 41.

125. Okabe, H.T., Waseda, Y. *JOM.* **49(6).** 1997. pp. 28.

126. Orowan, E. *Discussion in "Symposium on Internal Stresses"*. London. 1947. pp. 451.

127. Ouchi, C., Iizumi, H., Mitao, S. *Materials Science and Engineering.* **A243.** 1998. pp. 186.

128. Panda K.B., Ravi Chandran, K.S. *Metall. Mater. Trans. A.* **34(6).** 2003. pp. 1371.

129. Partridge, P.G. *Met. Rev.* **12.** 1967. pp.169.

130. Paton, N.E., Backofen, W.A. *Metall. Trans. 1*. 1970. pp. 2839.

131. Paton, N.E., Baggerly, R.G., Williams, J.C. Rockwell Report. 1976.

132. Paton, N.E., Williams, J.C. *2nd International Conference on the Strength of Metals and Alloys*. 1970. pp. 108.

133. Paton, N.E., Williams, J.C., Rauscher, G.P. *Titanium Science and Technology.* 1973. pp. 1049.

134. Petch, N.J. *Journal of the Iron and Steel Institute*. London 174. 1953. pp. 25.

135. Petrunko, A.N., Galitsky, N.V., Pampooshko, N.A., Denisov, S.I., Andeev, A.E. **Titanium and Titanium Alloys—Scientific and Technological Aspects.** *Plenum Press Publishing.* 1982. pp. 101.

136. Philliber, J.A., Dary, F.C., Zok, F.W., Levi, C.G. **Recent Advances In Titanium Metal Matrix Composites.** *TMS Warrendale, PA.* 1995. pp. 213.

137. Philliber, J.A., Dary, F.C., Zok, F.W., Levi, C.G., Blenkinsop, P.A. *Titanium '95: Science and Technology.* 1995. pp. 2714.

138. Radhakrishna Bhat, B.V., Subramanyam J., Bhanu Prasad, V.V. *Materials Science & Engineering A.* **325(1-2).** 2002. pp. 126.

139. Radhakrishna Bhat, R.V., Tamirisakandala, S., Miracle, D. *Journal of Materials Engineering and Performance.* **13(6).** pp. 653.

140. Radhakrishna Bhat, R.V., Tamirisakandala, S., Miracle, D. *Metallurgical and Materials Transactions A.* **36(3).** 2005. pp. 845.

141. Ravi Chandran, K.S., Miracle, D.B. *JOM.* **56(5).** 2004. pp. 32.

142. Ravi Chandran, K.S., Panda, K.B., Sahay, S.S. *JOM.* **56(5).** 2004. pp. 42.

143. Reed-Hill, R. **Physical Metallurgy Principles.** *PWS Publishing Company.* 1991.

144. Reznichenko, V.A. **Titanium and Titanium Alloys—Scientific and Technological Aspects.** *Plenum Press Publishing.* 1982. pp. 63.

145. Rivard, J.D.K., Blue, C.A., Harper, D.C., Kiggans, J.O., Menchhofer, P.A., Mayotte, J.R., Jacobsen, L., Kogut, D. *JOM.* **57(11).** 2005. pp. 58.

146. Robinson, J.L., Beevers, C.J. *Titanium Science and Technology.* 1973. pp. 1245.

147. Sahay, S.S., Ravichandran, K.S., Atri, R., Chen, B., Rubin, J. *Journal of Materials Research.* **14(11).** 1999. pp. 4214.

148. Saito, T., Furuta, F., Yamaguchi, Y. **Recent Advances In Titanium Metal Matrix Composites.** *TMS Warrendale, PA.* 1995. pp. 33.

149. Saito, T., Furuta, T., Takamiya, H. *Titanium '95: Science and Technology.* 1995. pp. 2763.

150. Saito, T., Takamiya, H ., Furuta, T. *Mat. Sci. & Eng. A.* **A243.** 1998. pp. 273.

151. Saito, T., Takamiya, H ., Furuta, T. *Titanium '95: Science and Technology.* 1995. pp. 2859.

152. Saito, Takashi. *JOM.* **56(5).** 2004. pp. 33.

153. Sakurai, K., Itabashi, Y., Komatsu, A. *Titanium '80: Science and Technology.* AIME, Warrendale, USA. 1980. pp. 299.

154. Sastry, S.M.L., Peng, T.C., O'Neal, J.E. *5th International Conference on Titanium.* Munich. 1984. pp. 397.

155. Savage, S.J, Froes, F.H. **Titanium Technology: Present Status and Future Trends.** 1985. pp. 60.

156. Schmid, Z.E. *Elektrochem.* **37.** 1931. pp. 447.

157. Schutz, R.W., Thomas, D.E. **Corrosion, Metals Handbook, 9th Edition, Volume 13.** *ASM Metals Park, USA.* 1987. pp. 669.

158. Shigeta, M., Watanabe, T. **Bulletin of the Research Laboratory for Nuclear Reactors. Volume 28(I/II).** 2004. pp. 108.

159. Shira, C., Froes, F.H. **Non-Aerospace Applications of Titanium.** *TMS Warrendale, USA.* 1998. pp. 331.

160. Simbi, D.J., Scully, J.C. *Materials Letters.* **26.** 1996. pp. 35.

161. Snow, D.B., Breinan, E.M., Kear, B.H. *Superalloys.* **189.** 1980. pp. 1980.

162. Soboyelo, W.O., Lederich, R.J., Sastry, S.M.L. *Acta Metall.* **42(8).** 1994. pp. 2579.

163. Sommer, C., Peacock, D. *Titanium '95: Science and Technology.* The University Press, Cambridge, UK. 1996. pp. 1836.

164. Srivatsan, T.S., Soboyejo, W.O., Lederich, R.J. **Recent Advances In Titanium Metal Matrix Composites.** *TMS Warrendale, PA.* 1995. pp. 225.

165. Steffens, K.L., Zachariah, M.R., DuFaux, D.P., Axelbaum, R.L. *Chemical Materials.* **8.** 1996. pp. 1871.

166. Su, H., Jouhnson, D.L. *J. Amer. Chem. Soc.* **79.** 1996. pp. 3211.

167. Suri, S., Viswanathan, G.B., Neeraj, T., Hou, D.H., Mills, M.J. *Acta Mater.* **47.** 1999. pp.1019.

168. Suryanarayana, C., Froes, F.H., Rowe, R.G. *International Materials Reviews.* **36(3).** 1991.

169. Suzuki, R.O. **2003 Hamburg Titanium Conference: Vol. 1.** 2003. pp. 245.

170. Tamirisakandala, S., Bhat, R.B., Ravi, V.A., Miracle, D.B. *JOM.* **56(5).** 2004. pp. 60.

171. Terlinde, G. **PhD Thesis.** *Ruhr-University Bochum.* 1978.

172. Terlinde, G., Luetjering, G. *Metall. Trans. A.* **13(7).** 1982. pp. 1283.

173. Thompson, A.M., Harmer, M.P. *J. Amer. Chem. Soc.* **76.** 1993. pp. 2248.

174. Tsang, H.T., Chao, C.G., Ma, C.Y. *Scripta. Met.* **37(9).** 1997. pp. 1359.

175. Turner, N.G., Roberts, W.T. *Journal of Less-Common Met.* **16.** 1968. pp. 37.

176. Turner, N.G., Roberts, W.T. *Trans. AIME.* **242.** 1968. pp. 1223.

177. Wang, K., Gustavson, L., Dumbleton, J. *Titanium '92: Science and Technology*. TMS Warrendale, USA. 1993. pp. 2697.

178. Wartman, F.S., Baker, D.H., Nettle, J.R., Homme, V.F. *J. Electrochem. Soc.* **101.** 1954. pp. 507.

179. Wei, W.F., Liu, Y., Tang, H.P., Huang, B.Y. *Powder Metallurgy.* **46.** 2003. pp. 246.

180. Weissmann, S., Shrier, A. **The Science, Technology and Application of Titanium.** *Pergamon Press, Oxford*. 1970. pp. 441.

181. Welsch, G., Leutjering, G., Gazioglu, K., Bunk, W. *Metall. Trans*. **8A.** 1977. pp. 169.

182. Williams, J.C., Baggerly, R.G., Paton, N.E. *Metall. Trans. A* **33.** 2002. pp. 837.

183. Williams, J.C., Blackburn, M.J. **Order Alloys**. *Claitors Press.* 1970. pp. 425.

184. Williams, J.C., Leutjering, G. *Titanium Science and Technology*. 1984. pp. 671.

185. Williams, J.C., Starke, E.A. **1982 ASM Seminar: Deformation, Processing, and Structure.** 1982. p. 284.

186. Williams, J.C., Sommer, A.W., Tung, P.P. *Metall. Trans. A.* **3(11).** 1972. pp. 2979.

187. Williams, J.C., Thompson, A.W., Rhodes, C.G., Chestnutt, J.C. *Titanium and Titanium Alloys*. 1982. pp. 467.

188. Yinjiang W., Qingwen, D. **Metal Powder Design and Fabrication For Laser Forming. Titanium Alloy Powders & Development For Automotive Parts (I).** 2002.

189. Yinjiang W., Qingwen, D. **Study of Motive Hydrogenate/Dehydrogenate. Titanium Alloy Powders & Development For Automotive Parts (I).** 2002.

190. Yolton, C.F. *JOM.* **56(5).** 2004. pp. 56.

191. Yolton, C.F., Moll, J.H. *Titanium '95: Science and Technology.* 1996. pp. 2755.

192. Yoo, H.M. *Metall. Trans. A.* **12A.** 1981. pp. 409.

193. Zhang, X., Lu, W., Zhang, D., Wu, R., Bian, Y., Fang, P. *Scripta. Met.* **41(1).** 1999. pp. 39.

194. Zhao, F., Fan, Y. *Titanium '95: Science and Technology.* 1996. pp. 2688.

195. Zhao, J., Harmer, M.P. *Philos. Mag. Letters.* **63.** 1991. pp. 7.